1-1-2017

Biofidelity Assessment Of 6-Year-Old Anthropometric Test Devices (atds) And Scaling Laws In Lateral Impact

Jennifer Yaek
Wayne State University,

BIOFIDELITY ASSESSMENT OF 6-YEAR-OLD ANTHROPOMETRIC TEST DEVICES (ATDs) AND SCALING LAWS IN LATERAL IMPACT

by

JENNIFER L. YAEK

DISSERTATION

Submitted to the Graduate School

of Wayne State University,

Detroit, Michigan

in partial fulfillment of the requirements

for the degree of

DOCTOR OF PHILOSOPHY

2017

MAJOR: BIOMEDICAL ENGINEERING

Approved By:

_____

Advisor Date

_____

Advisor

_____

_____

_____

_____

DEDICATION

Dedicated to:

my parents, Edward and Edwina Gebauer

&

my husband, Jonathan, and sons, Derek and Curtis

To my mom and dad, thank you from the bottom of my heart for all your love, support, encouragement, and all you have done for me in order for me to be where I am today. I have always been humbled and gracious for the hard work ethic you engrained in me and for pushing me to always do my best. You inspired me and made me believe I could do anything I set my mind to, and for that I am forever grateful. Although you are no longer here physically on this Earth, you are with me in love, strength, and spirit each and every moment of my days.

To you, Ed and Winnie – I am Finally a Doctor ☺

To Jonathan, Derek, and Curtis, I am most humbly and graciously indebted. Thank you from the bottom of my heart for putting your lives on hold, sacrificing, and giving up so very much in the past 7 ½ years. You have been a constant source of unconditional love, patience, understanding, encouragement, and support, that without, this doctoral study would have truly been unattainable. You inspire me, motivate me, and outright make me be the best I can be each and every day. I am truly blessed to have you in my life!

Never Give Up On Your Dreams!

ACKNOWLEDGMENTS

"Appreciation is a wonderful thing. It makes what is excellent in others belong to us as well."

-Voltaire

I would like to take this opportunity to thank, individually, all those who have assisted me in one way or another with my doctoral studies at Wayne State University. First, I would like to genuinely thank my advisors, Dr. John M. Cavanaugh and Dr. Steve W. Rouhana, for affording me the opportunity to work under their mentorship and accomplish my PhD research. Their profound insight, kindness, immense support, and encouragement throughout the workings and preparation of my dissertation are most graciously acknowledged and appreciated. I consider myself very fortunate to be able to work with such knowledgeable patient, understanding, and compassionate advisors.

I would also like to express my sincere thanks and gratitude to Dr. Paul C. Begeman, Dr. John H. Bolte, and Dr. King H. Yang, for kindly accepting to serve on my doctoral dissertation committee. Their insightful recommendations during the course of this dissertation effort are greatly appreciated.

I would like to graciously thank Dr. Gerry Hish, our clinical veterinarian, and his staff at Wayne State University's Laboratory Animal Resources for their amazing care of the swine utilized in this study as well as their patience, insight, dedication, technical and medical assistance, and overall efforts in the preparation and completion of the numerous tests performed. I would also like to thank Dr. Chaoyang Chen for taking time out of his busy schedule to assist with the gross dissections of the test specimens.

I would also like to graciously thank my research assistants, Christopher Andrecovich and Matthew Diehl, for their patience, dedication, technical assistance, and overall efforts in the preparation and completion of the numerous tests performed. Their support was instrumental to the overall project success.

I am extremely thankful to Ford Motor Company for its funding through its URP (University Research Program) and support of this dissertation research. I am also tremendously thankful to TRL (Transport Research Laboratories) for use of its Q6 ATD, Transport Canada for use of its Q6s prototype ATD, the ORSP (Occupant Safety Research Partnership) Committee for its time in verifying the ISO biofidelity ratings, Humanetics for their insight regarding dummy design, and Dr. Richard Kent for providing the swine necropsy data acquired during his research studies.

I am tremendously thankful and grateful to my dear friends and colleagues Michael Holcomb, Garry Bahling, Dr. Jim Raddin, Dr. Tom McNish, Tim Fleming, and Dr. Mark Edwards for encouraging me to do what I thought was unattainable, and for providing constant support in this extraordinary endeavor. Thank you all for continuing to push me to always do my best and be at my best.

My heartfelt thanks and gratitude to all of my family, extended family, and friends for their patience, understanding, love, and support. I couldn't do this without you. Finally, please forgive me if I left anyone out. It would have been impossible to complete this without everyone's love and support. Thank you all!

TABLE OF CONTENTS

LIST OF TABLES

LIST OF FIGURES

CHAPTER 1 - INTRODUCTION

1.1 – Background and Significance

Much effort has been put forth over the past many years to improve motor vehicle child safety such as improved child restraint systems, enhanced vehicle safety designs and implementations, child safety awareness programs, and legislation. Despite these efforts, in the United States during the year 2012, an average of 3 occupants, ages 14 and younger, were killed and 462 injured every day in all motor vehicle crashes (National Highway Traffic Safety Administration [NHTSA], 2014A). This equates to 1,095 deaths and 168,630 child injuries in motor vehicle crashes per year. As of 2013, the leading cause of death for children ages 1 to 14 was unintentional injury accidents (CDC, 2015). Just over 4,000 child fatalities for ages 1-4 and just over 5,300 child fatalities for ages 5-14 were reported by the CDC in 2013 for all causes of death. Motor vehicle crashes (MVCs) were the cause of 425 of the 4,000 fatalities for children ages 1-4 and 910 of the 5,300 fatalities for children ages 5-14 (10.0 percent and 17.0 percent, respectively) (CDC, 2015).

A study published by the National Center for Statistics and Analysis (NCSA) in 2002 analyzed fatality and injuries to children under the age of 8 involved in a motor vehicle traffic crash based on various impact characteristics, including impact direction (Starnes, 2002). Data was analyzed from the National Automotive Sampling System (NASS), General Estimating System (GES), Fatality Analysis Reporting System (FARS) and the NASS Crashworthiness Data System (CDS) databases for years 1991 through 2000. Fatality rates were determined using the U.S. Census Bureau's population data and the Federal Highway Administration's (FHWA) vehicle miles traveled (VMT) data

(Starnes, 2002). FARS data specific to lateral impact was broken down into age groups (Age<1, Ages 1-3, Ages 4-8), seating position with regard to impact point (near-side, middle, far-side), and restraint use (Child Safety Seat, Lap and/or Shoulder Belt, None Used, Other/Unknown). For the Age<1 age group seated in the second row, 56% of side impact fatalities were on the near side, 25% were in the middle seat, and 19% were on the far side of the vehicle. Among the child occupants less than 1-year-old seated in the second row, 65% of side impact fatalities were children seated in a child safety seat and 25% were unrestrained. For the 1 through 3-year-old age group seated in the second row, 56% of side impact fatalities were on the near side, 22% were in the middle seat, and 22% were on the far side of the vehicle. Among the child occupants, ages 1 through 3, seated in the second row, 61% of fatalities were near side impacts with children seated in a child safety seat or lap and/or shoulder belt and 21% were restrained child far side impact fatalities. Unrestrained 1 through 3-year-old occupants in the second row involved in a side impact accounted for 27% of fatalities in the near side seat, 43% of fatalities in the middle seat, and 33% of fatalities in the far side seat. For the 4 through 8-year-old age group seated in the second row, 60% of side impact fatalities were on the near side, 18% were in the middle seat, and 22% were on the far side of the vehicle. Among the child occupants ages 4 through 8 seated in the second row, 68% of fatalities were near side impacts with children seated in a child safety seat or lap and/or shoulder belt and 20% were restrained child far side impact fatalities. 63% of unrestrained 4 through 8-year-old child fatalities in a second row side impact were located in the middle seat position (Starnes, 2002). Based on this study, it was concluded that the number of side impact fatalities involving children seated on the struck side (near side) was 2.6 times

greater than the number of side impact fatalities for children seated on the opposite side (far side) of the vehicle. In addition, it was determined that the frequency of near side impact fatalities was consistent over all age groups studied (Starnes, 2002).

A study published by NHTSA in 2010 analyzed incapacitating injury rates of children under the age of 8 involved in a motor vehicle traffic crash utilizing the NASS and GES databases for years 1998 through 2008, as well as the National Trauma Data Bank-National Sample Project (NTDB-NSP) for years 2003 through 2007 (Hanna, 2010). According to this study, approximately 27.0 % of child passengers, age 0 to 7, were involved in lateral impact motor vehicle crashes. Of all impact directions and age groups analyzed, lateral impact had the highest rate of incapacitating injuries for children age 4 to 7 (Hanna, 2010). When considering NASS-GES data, estimated incident rates of incapacitating injuries for children in vehicles impacted in any direction, the incident rate for unrestrained children in a laterally impacted motor vehicle was found to be 21% versus children who were lap and shoulder belted (4.5%), or children restrained in a safety seat (3.3%) (Hanna, 2010).

High injury and fatality rates have prompted research in child side impact protection. Sherwood et al. (2003) performed an in-depth analysis of 92 child vehicle collision fatalities obtained from the FARS database and the police departments that investigated these collisions. Of these 92 fatalities, 37 were from a side impact collision, 17 of the 37 fatalities were determined to be unsurvivable, and 14 were considered potentially survivable. Of these 14 potentially survivable side impact collisions, all were near side impacts with intrusion occurring at the child's seating position, and six of these cases, which had known injury data, documented head trauma as the fatality mechanism.

Orechowski et al. (2003) analyzed data, from 1991 to 2002, for restrained children ages 0 to 14 who were admitted to a Level I pediatric trauma center due to crash injuries through the National Highway Traffic Safety Administration (NHTSA) sponsored Crash Injury Research and Engineering Network (CIREN). Side impact crash data was compared to frontal impact crash data as well as to the NASS database. Case vehicles with a Principal Direction of Force (PDOF) of 45 to 135 degrees (1:30 to 4:30 as designated on a clock with 12:00 being straight forward on the vehicle) or 225 to 315 degrees (7:30 to 10:30) were designated as side impacts. It was concluded that compared to frontal collisions, side impact crashes produced 2.5 times greater risk of an AIS 2+ head injury, 3.7 times greater risk of AIS 2+ cervical spine injury, and 4.0 times greater risk of AIS 2+ thoracic injury to children 0 to 14 years of age. Children in frontal impacts were found to be at greater risk of AIS 2+ abdominal and lumbar spine injuries than in side impact collisions.

Howard et al. (2004) studied the injury mechanism of children in side impact collisions. This study focused, first, on the investigation of trauma-based collisions (collisions where occupants ended up in trauma center) and, second, on seating position and injury using the National Highway Traffic Safety Administration's Fatality Analysis Reporting System (FARS) and the National Automotive Sampling System Crashworthiness Data System (NASS-CDS) databases. The trauma-based collisions included 0 to 12-year-olds in a motor vehicle collision with a lateral PDOF plus or minus 45 degrees. Seating positions were grouped as near-side, far-side, or center. The FARS database files included years 1995 to 2000. Through their trauma-based collision study, it was determined that near-side child occupants were the most severely injured, with

principal injuries occurring at the head, brain, and neck, typically accompanied by thoracic, abdominal, pelvic girdle, and limb injuries. The analyses illustrated that children restrained on the near side of the impact were significantly more likely to be severely injured or killed than those seated in the center seat. The primary mechanism of injury was determined to be contact with the vehicle interior which could occur with or without significant intrusion.

Viano and Paranteau (2008) analyzed field accident data for 0 to 7 year old restrained and unrestrained occupants of a vehicle's second row in the FARS and NASS-CDS databases covering years 1991 to 2005 for fatality risk based on seating position and PDOF. PDOF designations were defined by the following impact types as frontal impacts (impact location GAD1="F" and no rollover, rollover $\leq$ 0), side impacts (impact location GAD1="L" or "R" and no rollover, rollover $\leq$ 0), and rear impacts (impact location GAD1="B" and no rollover, rollover $\leq$ 0). Injury severity was defined using the Maximum Abbreviated Injury Scale (MAIS). MAIS ranges from MAIS 0 to 9 and denotes assessment of life-threatening injuries at the time of first medical evaluation, but not resulting long-term injuries, and is designated as MAIS = 0 for an uninjured occupant, MAIS = 1-2 for minor to moderate injury, MAIS = 3-6 for serious to unsurvivable injuries, and MAIS = 7-9 for missing or unknown injuries. An accident was also considered fatal if the occupant died from injuries within three days of the accident. The variable "TREATMNT=1" was used to identify fatality and was incorporated with the serious to unsurvivable MAIS 3-6 coding as MAIS3+F. Risk of serious to fatal injury was determined by taking the ratio of the MAIS3+F to MAIS0+F data. It was determined that 30.9% of serious to fatal child second row injuries (MAIS 3+F) were caused by side impact. Location of the occupant

relative to collision forces and intrusion were found to play a role in increased injury risk.

Recent research has focused on the relative effectiveness of restraints for children seated in belt-positioning booster seats compared to those using seatbelts only with respect to injury risk reduction in side impacts. Arbogast et al. (2005) studied data from the Partners for Child Passenger Safety (PCPS) program from 1998 through 2004. Qualifying data included vehicle model years 1990 or newer, involved in a crash with at least one child occupant ≤ 15 years of age, regardless of restraint use, and rear row child occupants weighing 30 to 80 pounds. Direction of first impact was defined through a series of questions by telephone survey of the vehicle's insured person regarding vehicle parts involved in the first collision. Lateral impact crashes were defined by vehicle parts involved in the first collision located along the vehicle's lateral plane. Crash severity was defined through telephone survey by driver reported intrusion into the occupant compartment. Injury severity was defined through survey question response, classified by body region and Abbreviated Injury Scale (AIS-1990) severity score. All injuries with an AIS score of 2 or greater defined "injuries" for the study. Based on the reviewed data, relative risk of injury in side impact was analyzed for children ages 4 to 8, restrained in a belt-positioning booster seat compared to those restrained by seatbelts. Based on this study, a 58% risk reduction of injury was observed for children ages 4 to 8 restrained by a seatbelt in a belt-positioning booster seat compared to those in seat belts only. The largest injury reduction benefit was found at the head and face as well as a pattern of injuries to the abdomen and spine known as seat belt syndrome (SBS).

Arbogast et al. (2009), used the same PCPS data source as utilized in their 2005 study, but they extended their analysis based on a more comprehensive dataset which

included years 2005 to 2007. The analysis looked at unadjusted and adjusted relative risk of injury for child occupants by seating row. Linear regression modelling was performed to determine the unadjusted and adjusted relative risk. Adjusted data included child restraint use (CRS, seatbelt, unrestrained), age of driver (<25 years and 25+years), vehicle model year, and initial direction of impact (frontal, right side, left side, rear, and other/unknown). Analyses were performed using the whole study sample year range as well as grouped by model year 1998 to 2002 versus 2003 to 2007. Based on the study results, it was determined that children seated in booster seats in a side impact fared better than when restrained by seat belts only, with injury reduction observed in 68% of near side impacts and 82% of far side impacts.

In 2011, NHTSA published their Biomechanics Research Plan for 2011 to 2015. NHTSA's plan included research in the advancement of both front and side impact child dummies (NHTSA, 2011). Most recently, in January of 2014, NHTSA proposed an upgrade to the Federal Motor Vehicle Safety Standard for child restraint systems (FMVSS 213). This proposed upgrade included a side impact test utilizing a Q3s child dummy for assessing car seats sold in the United States, designed for children weighing up to 40 pounds. The goal of the proposed upgrade to FMVSS 213 was to work toward making sure child passengers are protected in side impacts (NHTSA, 2014B).

Research has shown assessment and development of child side impact dummies is necessary. Customarily, adult ATDs have been validated using Post Mortem Human Subject (PMHS) data. Due to the paucity of pediatric PMHS tests, biofidelity targets for children have been scaled down from adult response data (Irwin and Mertz 1997). One issue that has been raised regarding scaling from adult data to a child is that children are

not just small adults. From a biomechanical perspective, there are not only changes with regard to growth in body proportions and skeletal structure but also with tissue and bone properties (Franklyn, 2007; Wenger and Pring, 2005). For instance, the cortex of young bones tends to be more porous, flexible, and less likely to fracture than adult bones (Wenger and Pring, 2005). These research findings and others like them indicate the need for further child safety research, particularly in lateral impacts, and the assessment and development of more advanced child side impact dummies (anthropometric test devices (ATDs)).

1.2 – A Brief Review of Anthropometric Test Devices (ATDs)

Occupant safety and injury risk during motor vehicle collisions (MVC) are evaluated using anthropomorphic test devices (ATDs). ATDs are intended to represent the geometrical size and biofidelic response of a human being during a MVC event. The ATDs are used in government regulated and experimental MVC testing that can be as severe as real world MVCs, necessitating that ATDs be robust and durable enough to withstand many demanding impact tests while still being able to produce repeatable responses. The most frequently used family of ATDs in the United States, particularly for frontal impact testing, is the Hybrid III. The Hybrid III family includes the 50th percentile midsize male, the 95th percentile large male, the 5th percentile female, as well as a series of child ATDs. The Hybrid III child ATDs, which were developed in the 1990s, include the 3-year-old, 6-year-old, and 10-year-old.

Another family of child dummies, the Q-series child dummies, were developed in Europe in the late 1990s in order to meet the demands of European government regulated MVC testing, taking into account the deceleration profile of modern day

vehicles. The Q-series family of child dummies include the new-born (Q0), the 12-month (Q1), the 18-month (Q1.5), three-year-old (Q3), and six-year-old (Q6) dummies (EEVC, 2014). There are currently three 6-year-old ATDs: the HIII and the more current Q6, both of which are designed primarily for frontal impact testing, and the Q6s, which is a prototype side impact dummy.

1.3 – A Brief Overview of 6-Year-Old Pediatric ATD Design

The Hybrid III 6-year-old ATD was designed in 1993. Representative dimensions of the HIII 6-year-old ATD were based on information available at the time for size and weight of children in the United States, and interpolated, as necessary, to estimate these data to the desired age (Irwin and Mertz, 1997). Table 1.3.1 contains characteristic anthropometric measurement comparisons of the 50th percentile mid-sized adult human male and 6-year-old human child based on data provided in Irwin and Mertz (1997) and used for scaling purposes. Total body mass for the HIII 6-year-old ATD was also obtained from the anthropometric studies. In addition, body mass segments for the HIII 6-year-old ATD were defined based on a Masterbody Form cast of the 6-year-old child (Irwin and Mertz, 1997). Table 1.3.2 contains body segment mass comparisons of the HIII 50th percentile mid-sized adult male ATD and HIII 6-year-old ATD used for scaling purposes. The elastic bending moduli of bone for the 6-year-old and adult were acquired from published research on the parietal bone (Irwin and Mertz, 1997). Table 1.3.3 contains elastic bending moduli of bone comparisons for the 50th percentile mid-sized adult male and 6-year-old child used to establish scaling techniques.

Table 1.3.1 Irwin and Mertz (1997) Characteristic Dimensions Comparison

Dimension Description	6-Year-Old	50th Percentile Mid-sized Male
Standing Height (mm)	1168	1751
Erect Sitting Height (mm)	635	907
Shoulder Breadth (mm)	290	465
Shoulder to Elbow (mm)	234	366
Chest Depth (mm)	143	229
Chest Breadth (mm)	194	311
Waist Breadth (mm)	168	314
Hip Breadth (seated) (mm)	230	368

Table 1.3.2 Irwin and Mertz (1997) HIII ATD Body Segment Masses

Body Segment	HIII 6-Year-Old	HIII 50th Percentile Mid-sized Male
Torso (kg)	10.76	40.23
Upper Extremities (kg)	1.98	8.53
Lower Extremities (kg)	4.28	23.36
Total Body Mass (kg)	20.91	78.20

Table 1.3.3 Irwin and Mertz (1997) Elastic Bending Moduli of Bone for Children and Adults

Dimension Description	6-Year-Old	50th Percentile Mid-sized Male
Elastic Modulus (GPa)	6.6	9.9

The biofidelity requirements of the HIII 6-year-old ATD, in both front and side impact, were obtained by scaling the biomechanical response corridors of the HIII 50th percentile mid-sized adult male ATD using size and material properties (Irwin and Mertz, 1997; Irwin et al., 2002).

The Q6 ATD was designed in 1999. The anthropometry of the Q6 ATD is based on child anthropometric measurements from a database entitled the CANDAT (Child Anthropometric DATabase) which combined child anthropometry data from the United States, Europe, and Japan (EEVC, 2014). Table 1.2.4 contains characteristic anthropometric measurements for the Q6 ATD. Table 1.2.5 contains body segment masses for the Q6 ATD (Q6 User Manual 2012). Elastic bending modulus of bone used to develop the HIII 6-year-old ATD was also used in the development of the Q6 ATD. Measurements and body mass segments for the Q6s ATD are similar to the Q6 ATD.

Table 1.3.4 Q6 User Manual (2012) Characteristic Dimensions

Dimension Description	Q6/Q6s
Standing Height (mm)	1143
Sitting Height – with head tilted forward (mm)	601
Shoulder Breadth (mm)	305
Shoulder to Elbow (mm)	--
Chest Depth (mm)	141
Chest Breadth (mm)	--
Waist Breadth (mm)	--
Hip Breadth (mm)	223

Table 1.3.5 (Q6 User Manual 2012) Q6 ATD Body Segment Masses

Body Segment	Q6/Q6s
Torso (kg)	9.07
Upper Extremities (kg)	2.49
Lower Extremities (kg)	6.90
Total Body Mass (kg)	22.90

Images of the three 6-year-old ATDs are provided in Figure 1.3.1, below.

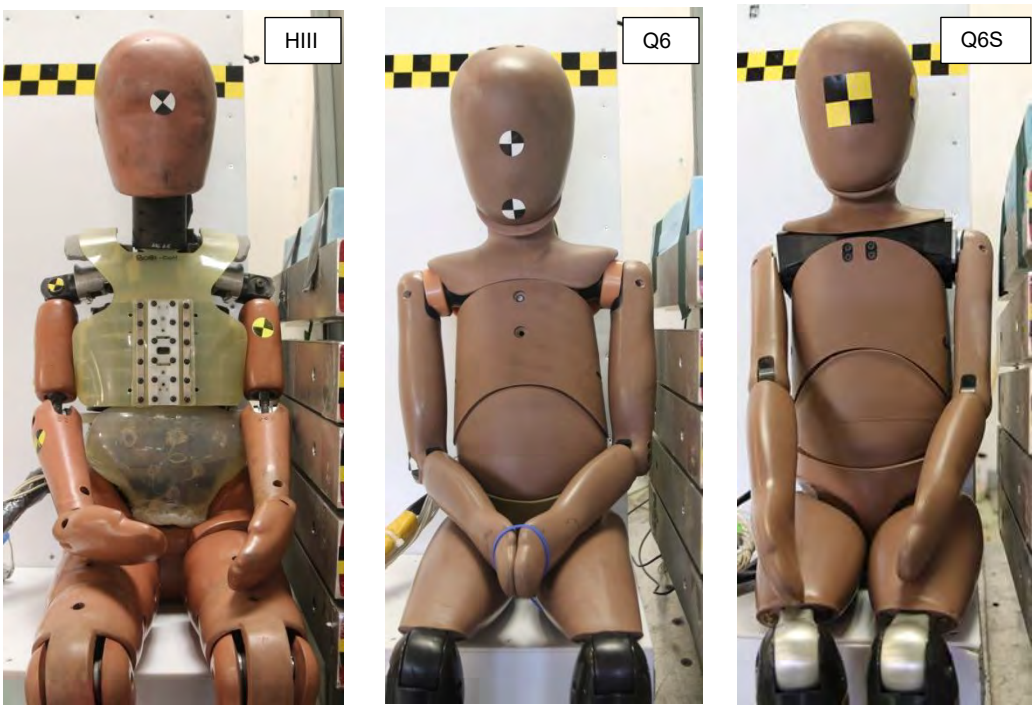

Figure 1.3.1 6-Year-Old ATDs

Research and development of the 6-year-old side impact ATD (Q6s) has stalled over the past several years. According to NHTSA's Biomechanics Research Plan 2011 to2015, any assessment of the Q6s, which is currently a prototype, would follow the lead of the Q3s ATD, currently in production. Regarding changes to hardware, design, and potential development of the Q6s, it is several years behind the Q3s (NHTSA, 2011). In

January of 2014, NHTSA proposed an amendment to the Federal Motor Vehicle Safety Standard (FMVSS) No. 213, “Child restraint systems”. In this proposed amendment, it documents that there is currently no side impact dummy representative of children larger than the Q3s that can reasonably test CRSs to the dynamic side impact requirements proposed in the amended FMVSS 213 standard (NHTSA 2014B).

Scarceness of pediatric postmortem human subjects (pediatric PMHS) has yielded very limited information regarding pediatric biomechanical behavior and injury level assessments for child ATD development. Lack of pediatric PMHS biomechanical research has necessitated researchers to generate biofidelity requirements and injury assessment reference values (IARVs) for pediatric ATDs based on geometric and material property scaling of 50th percentile adult male PMHS data. Scaling from adult to child assumes, however, geometric and material property similarities between the two, which requires validation data that is lacking due to the deficiency of pediatric PMHS resources. Lack of proper validation raises some doubt among researchers regarding scaling law validity. For instance, Franklyn (2007) postulates that mature adult skeletal bones and pediatric skeletal bones differ greatly in geometry as well as physical properties, and thus a child is not just a scaled down adult.

1.4 – A Brief Overview of the Anatomical and Physiological Differences between Human, Adults, and Children

Geometric differences in body proportions and skeletal structure of immature children compared to mature adults are greatest during a child’s infancy stage and decrease as the child develops into an adult. As a child grows to maturity, there is a continual increase in height and weight, although not at a constant rate. Along with

change in stature is a gradual increase in seated height, body widths, and body circumferences (Franklyn, 2007; Frick, 2005). At age 6, body proportions are about 20% head and neck, 35% torso, and 45% lower extremities, whereas, a midsized adult male's body proportions are more like 13% head and neck, 40% torso, and 47% lower extremities, as shown in Figure 1.4.1 below (Frick, 2005).

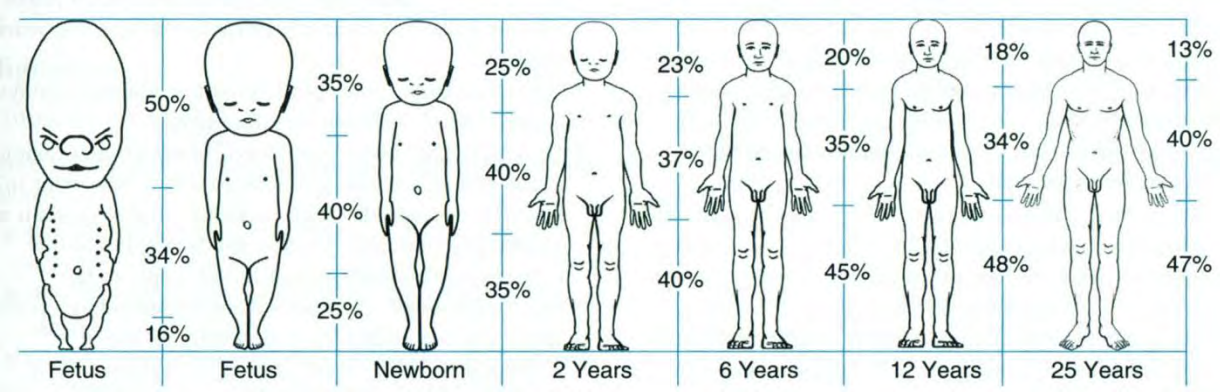

Figure 1.4.1 Body Proportion Change with Growth (Frick, 2005)

From a biomechanical perspective, there are not only changes with growth in body proportions and skeletal structure but with tissue and bone properties (Franklyn, 2007; Wenger and Pring, 2005). For instance, the cortex of young bones tends to be more porous, flexible, and less likely to fracture than adult bones (Wenger and Pring, 2005).

The human shoulder (pectoral girdle) consists of an anterior clavicle and a posterior scapula that articulate at the acromioclavicular joint. The medial end of the clavicle articulates with the manubrium, and the scapula articulates with the proximal end of the humerus at the glenohumeral joint, as illustrated in Figure 1.4.2, below (Scheuer and Black, 2004).

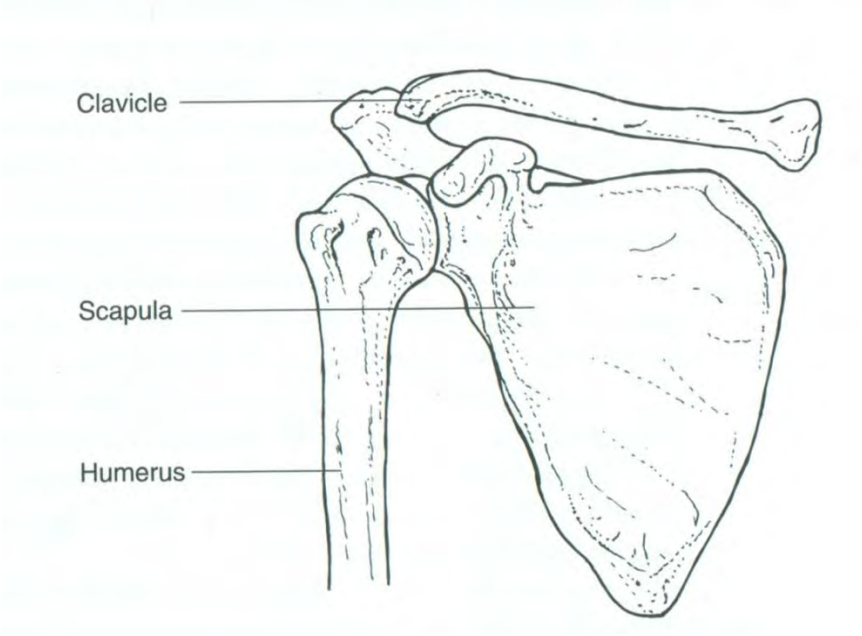

Figure 1.4.2 Bones of the Shoulder (Pectoral Girdle) (Scheuer and Black, 2004)

The only joint between the shoulder and the axial skeleton is located at the medial end of the clavicle, at the manubrium. The clavicle serves as a strut to brace and support the upper limb to the thorax, whereas the scapula serves as a site of maximum mobility, being held in place by muscles and ligaments only. The primary function of the shoulder is to increase upper limb movement (Scheuer and Black, 2004). The clavicle is a long bone, derived from a shaft, or primary center of ossification, and medial and lateral articular surfaces which develop from secondary ossification centers. The clavicle's primary ossification center appears sometime between weeks 5 and 6 of fetal development with fusion occurring at roughly week 7. By week 11 of fetal development, the clavicle takes on its adult "S" shape. Ossification begins in the epiphyseal cartilage of the medial clavicle end at roughly 13-14 years of age, and fusion to the diaphysis does not occur until typically 10 years after initial formation. Although literature varies somewhat as to whether a lateral epiphysis is generated, if and when it is, it tends to be a temporary structure that forms around ages 19 to 20 with fusion occurring months after formation (Scheuer and Black,

2004). Fetal clavicle growth occurs at a relatively linear rate until term where it reaches a length of approximately 40-41 mm (Scheuer and Black, 2004). Rate of clavicle growth has been shown to be similar between genders from birth to approximately age 12, growing at an average of 8.4 mm per year. After age 12, clavicle growth rate tends to be lower for females compared to males. By age 18, the average clavicle length for females is approximately 149.2 mm $\pm$ 12.3 mm and 161.3 $\pm$ 10.8 mm for males (McGraw et al., 2009). The primary ossification center of the scapula appears during approximately weeks 7 and 8 of fetal growth. Although the main body of the scapula has taken on its adult morphology by prenatal growth weeks 12 to 14, most of it's at least 7 secondary ossification centers appear and fuse sometime after age 8, with exception to the coracoid. The coracoid begins ossification around 1 year of age and is recognized as a separate ossification center at approximately age 3 (Scheuer and Black, 2004).

The human thoracic region spans from the base of the neck, superiorly, to the diaphragm, inferiorly. It consists of the rib cage and its underlying organs. The rib cage is composed of 12 pairs of ribs in combination with the sternum anteriorly and the vertebrae of the spinal column posteriorly. Ribs 1 through 7 (superior ribs) directly attach, in combination with cartilaginous attachment, to the sternum. Ribs 8 through 10 (central or false ribs) attach to the sternum through a much longer, stronger cartilaginous attachment. Ribs 11 and 12 (inferior or floating ribs) have no anterior connection. Intercostal muscles are located between the ribs and assist in respiration. The lungs are located within the rib cage with the left lung consisting of two lobes and the right lung consisting of three lobes. The mediastinum, located in the central chest region, encloses the heart and its associated vessels, the thymus, esophagus, and trachea. The diaphragm separates the

thoracic and abdominal cavities. Primary ossification centers are present for all sternebra except the xiphoid process age 1. Sternebra begin to ossify and fuse by age 4, with epiphysis appearing and beginning to fuse by age 11. All rib ossification centers are present by birth with the appearance of epiphyses and subsequent fusion of the epiphyses occurring at approximately age 12. During childhood, the rib cage gradually ossifies from cartilage, causing the ribs to become more rigid. At approximate ages 2 and 3, a corresponding change in the shape of the chest occurs wherein the pediatric chest becomes more oblique (Scheuer and Black, 2004). The anterior of the ribs become more inferior, creating a downward sloping of the ribs from posterior to anterior. These structural aspects of the thorax are not accounted for in current child ATD designs which have resulted from fixed scaling techniques down from the midsize male ATD.

The abdominal cavity ranges from the diaphragm to the pelvic basin and includes the internal organs within this region. The abdominal cavity organs consist of both solid organs and hollow organs. The major solid organs are fluid-filled vessels and include the liver, spleen, and kidneys. The major hollow organs include the small and large intestines, stomach, and bladder.

The human pelvic region (pelvic girdle) consists of two hip bones comprised of three main bones: the ilium, the ischium, and the pubis which come together to form the acetabulum. The two hip bones are attached at the pubic symphysis anteriorly and at the sacrum posteriorly, as illustrated in Figure 1.4.3 (Moore and Agur, 2007), below.

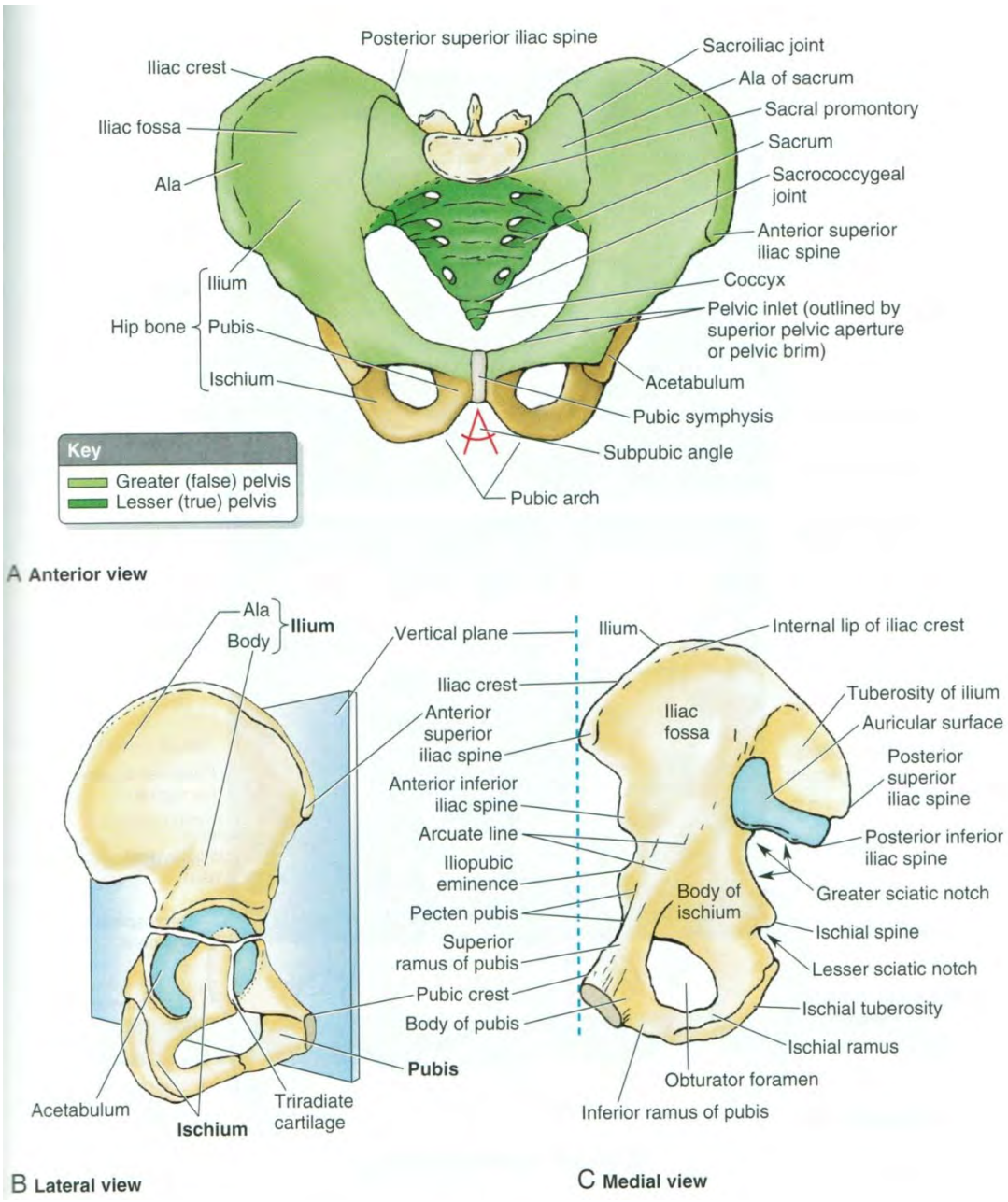

Figure 1.4.3 Bones of the Pelvis (Pelvic Girdle) (Moore and Agur, 2007)

These bones are loosely connected by cartilaginous tissue and fuse at different pediatric growth stages. Starting between ages 5 and 8, fusion of the ischiopubic rami occurs. At roughly age 11 to 15 in females and 14 to 17 in males, the triradiate cartilage of the acetabulum fuses. Additional growth and fusion of the pelvic girdle continues into early adulthood (Scheuer and Black, 2004; Yoganandan et al., 2015).

The sacroiliac joint, the bilateral joint connecting the sacrum and the illiums, is comprised of fibrocartilage on the iliac surface and hyaline cartilage on the sacral surface during all stages of embryonic development (Scheuer and Black, 2004). The epiphysis of the sacroiliac joint develops from several isolated ossification locations that eventually combine to form a thin sheet of bone which covers the articular surface. The epiphysis appears generally around age 15 to 16 and fuses by age 18 or older (Scheuer and Black, 2004).

Because the pediatric pelvis is more cartilaginous in nature compared to the adult pelvis, it allows for more energy absorption during impact and results in less bony fractures. Pelvic fractures tend to be extremely rare in children under 7 to 8 years of age, whereas isolated pubic rami fractures tend to occur in children ages 8 to 14. Multiple pelvic bone fractures, similar to those found in adults, tend to be visible in post-pubescent adolescents (Yoganandan et al., 2015).

1.5 – A Brief Overview of Human Subject Research Related to Structural Response Data of the Pediatric Shoulder, Thorax, Abdomen, and Pelvis Regions

As of this date, the author is unaware of any pediatric PMHS shoulder testing. However, whole thoracic region impact testing of pediatric PMHS was performed by Ouyang et al. (2006). Two age groups were used in the research study, a younger group consisting of four subjects aged 2 to 4 years and an older group of five subjects aged 5 to 12 years. Testing was performed with a pneumatic impactor device actuated by a predetermined air pressure and predetermined velocity of just below 6.7 m/s. The pediatric PMHS used in this particular thoracic impact testing were previously used that same day in another series of abdominal impact tests, resulting in some potential compromise of the thoracic

test results. Two different impactors were used in order to accommodate for the difference in stature of the two groups. The younger PMHS group subjects were impacted with a 50 mm diameter, 2.5 kg mass impactor, and the older PMHS group subjects were impacted with a 75 mm diameter, 3.5 kg impactor. Neither of the impactors used in the Ouyang et al. (2006) study corresponded with impactors used for ATD thorax frontal impact biofidelity corridor testing, which uses a 92 mm diameter, 1.2 kg pendulum for the 3-year-old response corridor testing, a 102 mm diameter 2.9 kg pendulum for the 6-year-old response corridor testing, and a 121 mm 6.89 kg pendulum for the 10-year-old response corridor testing. Testing was performed in the anterior-posterior (AP) plane with the impactor striking the anterior thorax of the pediatric PMHS. Testing was performed without arterial pressurization and with the lungs collapsed. Test subjects were suspended in the seated position on a sheet of Teflon with their arms extended forward. The head was positioned upright using a cervical collar and tape. Test subjects were instrumented with a sternal accelerometer, a tri-axial accelerometer secured to the fourth thoracic vertebrae (T4), an accelerometer attached to the third lumbar vertebrae (L3), and a contour chest band. The impactor was backed with a load cell and data was adjusted for impactor mass. Each test subject was impacted only once in order to easily identify hard or soft tissue injuries (Ouyang et al. 2006). A significant difference was reported in average peak impact force for the old and young groups, and chest deformation results were found to correlate well with injury for the younger group versus the older group. In addition, pediatric PMHS sternal impact stiffness values were determined to be 60-75 N/mm (Ouyang et al. 2006).

Whole abdomen pediatric PMHS testing has been performed by Kallieris et al.

(1976) and Kent et al. (2009). Kallieris et al. (1976) performed abdominal region dynamic load testing of 4 unembalmed pediatric PMHS ages 2 to 11 years. The pediatric PMHS were seated in a standard Volkswagen front seat, which was secured to the Heidelberg deceleration sled, and restrained by a lap belt around a semi-cylindrically shaped safety table (abdominal impact shield), which maintained the abdominal region during impact. Tests were conducted at impact velocities of 30 kph and 40 kph. A trapezoidal deceleration pulse shape was utilized for the testing resulting in 18 to 23 g's of deceleration. Testing resulted in muscular hemorrhages and intervertebral disk and ligament hemorrhages, but no internal organ injuries. Kent et al. (2009) tested the abdominal region of a seven-year-old PMHS utilizing a 50-mm-wide polyethylene fiber-reinforced composite belt. A table-top test rig with a hydraulic master-slave cylinder arrangement linking a high-speed material testing machine was utilized for the test runs. The belt was attached directly to the slave cylinder pistons by steel cables that passed through channels cut in the center of the hardware supporting the specimen. Plywood sheets were also present to adjust the specimen's height on the table in order to attain appropriate belt angles off its shoulder and pelvis. Both upper and lower abdominal region testing was performed in an anterior-posterior (AP) load direction. For the upper abdominal test series, the belt was positioned 70 mm superior to the umbilicus while for the lower abdominal test series, the belt was centered over the umbilicus. For the lower abdomen test, a quasi-static (20 mm/s) rise up to a 46-mm displacement of the piston was performed. Following the quasi-static test, a dynamic ramp-and-hold test to the same peak displacement was performed using a peak abdominal displacement rate of approximately 1.6 m/s and held for 60 seconds. During the hold time, force relaxation

was measured to observe transient behavior of the abdomen. A similar test was executed for the upper abdomen but to 38-mm peak displacement. Maximum abdominal penetration ranged from 33 to 39 mm with corresponding peak posterior reaction forces ranging from 1,655 N during the quasi-static testing to 5,352 N at the end of the dynamic loading, and peak penetration rates of 2.2 to 2.3 m/s during the ramp-hold testing.

Ouyang et al. (2003), performed lateral impact testing with a flat free-mass pneumatic impact device to the greater trochanter and iliac wing of 12 pediatric PMHS, ages 2 to 12. Test subjects were placed in a seated position on a test table with the right side of the pelvis facing the flat impacting plate surface, which weighed 3.24 kg, measured 180 mm in height by 140 mm in width, and was backed by a load cell. Test subjects were positioned such that the buttocks were in full contact with the test table, their left pelvis was firmly positioned against a support fixture, and the torso and head were attached via tape to a support boom. Subjects' legs were aligned freely at a right angle to the direction of impact. Impact speeds ranged from 7.0 to 9.1 m/s. Impactor mass compensated force versus pelvic deflection were reported. The Ouyang et al. (2003) study provides the only lateral impact experimental testing of the human pediatric pelvis, to this author's knowledge, to date. No reported pelvic injuries were found in any of the pediatric test subjects even though pelvic compression levels recorded were over 50%. In contrast, adult pelvic response in similar tests generated a 25% risk of injury at approximately 30% compression.

1.6 – Statement of the Problem and Specific Aims

There is a clear need for the biofidelic assessment of the 6-year-old ATDs in lateral impact in order to further develop the design and biofidelity of these ATDs for future child

safety research and child occupant protection in side impacts. Of the known pediatric PMHS research relative to structural response data for the shoulder, thorax, abdomen, and pelvis, as described previously, the only body region to have been tested in the lateral direction was the pelvis by Ouyang et al. (2003). Due to the scarcity of pediatric PMHS impact testing, specifically in the lateral direction, alternative means of obtaining relevant data for pediatric models, need to be considered. Other options include scaling from adult data and the use of animal models.

The main objective of this dissertation is to systematically assess the current mechanical behavior and biofidelity of the 6-year-old ATDs in lateral impact, evaluate the geometric and material properties of appropriately age and torso proportioned porcine surrogates, and verify current scaling laws in order to generate biofidelity requirements and injury assessment reference values (IARVs) through research and testing of appropriately age-torso-proportioned surrogates.

Specific Aim 1: Perform a literature review on the epidemiology of injury patterns of 4 to10-year-old children in lateral and oblique vehicle collisions. Also, perform a field data analysis of injury patterns and sources in lateral impact crashes. This specific aim investigates the main injury patterns and injury sources for children in rear seat lateral impact using the National Automotive Sampling System-Crashworthiness Data System (NASS-CDS) and Crash Injury Research Engineering Network (CIREN) databases. The criteria for the review would include occupant age, occupant seating location, impact force direction, restraint use, injury location (by body region), injury level, and injury source.

Specific Aim 2: Assess the design and biofidelity of the current 6-year-old HIII

(with Ford in-house abdominal insert), Q6, and Q6s prototype anthropometric test dummies (ATD) in lateral impact loading. The biofidelity performance in lateral impact for the three ATDs will be assessed against the scaled biofidelity targets published in Irwin et al. (2002), the abdominal biofidelity target suggested in van Ratingen et al. (1997), and the biofidelity targets published in Rhule et al. (2013). Regional and overall biofidelity rankings for each of the three ATDs will be performed using both the ISO 9790 Biofidelity Rating System (ISO/TR 9790, 1999) and the National Highway Traffic Safety Administration's (NHTSA) External Biofidelity Ranking System (BRS) (Rhule et al., 2013). This specific aim is to understand the existing mechanical behavior of the current 6-year-old ATDs in lateral impact and determine the body regions of the 6-year-old ATDs requiring further research and development. The complete assessment will include:

Shoulder: (1) ISO pendulum test, (1) ISO WSU rigid sled test

Thorax: (1) ISO pendulum test, (2) ISO drop tests, (1) ISO WSU rigid sled test

Abdomen: (2) ISO drop tests, (1) van Ratingen pendulum test, (1) ISO WSU rigid sled test

Pelvis: (2) ISO drop tests, (1) ISO pendulum test, (1) ISO WSU rigid sled test

Specific Aim 3: Lateral pendulum impact testing of appropriate age and size cadaveric porcine surrogates (to be determined based on necropsy and regression analysis developed in Kent et al. (2006)) of 3-year-old, 6-year-old, 10-year-old, and 50th percentile male equivalent thorax and abdomen regions will be performed and data will be compared to scaled human response corridors. Due to the paucity of pediatric PMHS, cadaveric pigs will be used for this portion of the testing and analysis. Shoulder and pelvis testing will be deleted from the test matrix due to the dissimilarity between the swine and

human shoulder and pelvis. Sub-aims include the following:

1. Test the porcine surrogate equivalents (PSE) (3 tests per condition) based on the same scaled lateral impact assessment test methodology used in ISOTR9790 and van Rantingen for the thorax and abdomen as used for the biofidelity assessment of the 6-year-old ATDs.
2. Measure and quantify erect sitting height, upper torso mass, lower torso mass, and whole body mass for the determined 3-year-old, 6-year-old, 10-year-old, and 50th adult male PSE in order to establish the same test normalization scaling parameters as performed in Mertz (1984) and Irwin et al. (2002) for the porcine thorax and abdomen.
3. Assess and compare the impact response of the porcine surrogate torso and abdomen data results to the established ISO TR9790 age specific human scaled lateral impact response corridors and van Ratingen scaled corridors for the thorax and abdomen body regions.

Specific Aim 4: Perform analysis and testing to generate rib segment elastic bending modulus for the determined 3-year-old, 6-year-old, 10-year-old, and 50th adult male PSE in order to establish the same test scaling parameters as performed in Mertz (1984) and Irwin et al. (2002) for the porcine thorax and abdomen.

Specific Aim 5: Develop test response ratios for force, deflection, acceleration, and time for the 3-year-old, 6-year-old, 10-year-old, and 50th adult male PSE from lateral pendulum impact of the thorax and abdomen. The response ratios developed for the PSE will then be compared to the already established human response ratios. Using the determined porcine response ratios, 50th adult male PSE response corridors for lateral

pendulum impact of the thorax and abdomen will be scaled to the 10-year-old, 6-year-old, and 3-year-old PSE. PSE impact response test data will be compared to the response corridors scaled from the 50th male PSE to assess scaling laws and determine if any correlation exists.

CHAPTER 2 - EPIDEMIOLOGY OF INJURY PATTERNS FOR 4 TO 10-YEAR-OLDS IN LATERAL AND OBLIQUE IMPACTS: A SURVEY OF THE NASS-CDS DATABASE FROM 1991 TO 2014 AND CIREN DATABASE FROM 1996 TO 2014 (SPECIFIC AIM 1)

2.1 – Background

Epidemiology is the study of the distribution and determinants of health-related states or events in specified populations (Last, 2001). With regard to the pediatric population involved in vehicle collision side impacts, epidemiologic data can be used to identify specific injury producing conditions and offer possible safety technology effectiveness through population-based estimates.

Much of the past epidemiologic work regarding child injury in lateral and oblique vehicle impacts has focused on quantifying the relative risk of child occupants among seating positions in side impact crashes. A study published by the National Center for Statistics and Analysis (NCSA) in 2002 analyzed fatality and injuries to children under the age of 8 involved in a motor vehicle traffic crash based on various impact characteristics, including impact direction (Starnes, 2002). Based on this study, it was concluded that the number of side impact fatalities involving children seated on the struck side (near side) is 2.6 times greater than the number of side impact fatalities for children seated on the opposite side (far side) of the vehicle. In addition, it was determined that the frequency of near side impact fatalities is consistent over all age groups studied (Age<1, Ages 1-3, Ages 4-8) (Starnes, 2002).

A study published by NHTSA in 2010 analyzed incapacitating injury rates of children under the age of 8 involved in a motor vehicle traffic crash (Hanna, 2010). According to this study, approximately 27.0% of child passengers ages 0 to 7, involved in a motor vehicle crash, are involved in a lateral impact. Of all impact directions and age

groups analyzed, lateral impact has the highest rate of incapacitating injuries for children ages 4 to 7 (Hanna, 2010). The incidence rate for children unrestrained in a motor vehicle involved in a lateral impact was found to be 21% versus 4.5% of children who were lap and shoulder belted, or 3.3% of children restrained in a safety seat (Hanna, 2010).

Howard et al. (2004) determined that child occupants in near-side impacts were the most severely injured, with principal injuries occurring at the head, brain, and neck, typically accompanied by thoracic, abdominal, pelvic girdle, and limb injuries. It was also determined that children restrained on the near side of the impact were significantly more likely to be severely injured or killed than those seated in the center seat. The primary mechanism of injury was determined to be contact with the vehicle interior which could occur with or without significant intrusion (Howard et al., 2004).

Viano and Paranteau (2008) attributed higher fatality rates to children located on the near side of right-sided impact crashes than the nearside of left-sided impact crashes for vehicles making a left turn across traffic. The study determined these types of crashes likely result in side crashes of increased severity (Viano and Paranteau, 2008).

Epidemiologic research has also focused on the relative effectiveness of belt-positioning booster seats compared to seatbelts with regard to injury risk reduction in side impacts. Arbogast et al. (2005) observed a 58% risk reduction of injury for children ages 4 to 8 seated in a belt-positioning booster seat compared to those in seat belts. The largest injury reduction benefit was found at the head and face as well as a pattern of injuries to the abdomen and spine known as seat belt syndrome (SBS). Arbogast et al. (2009), using the same but more comprehensive dataset, determined that children seated in booster seats in a side impact benefited most, with injury reduction experienced in 68%

of near side impacts and 82% in far side impacts. No difference in side impact effectiveness was discovered in the study for belt-positioning booster restrained children seated in backless boosters versus high back boosters.

Epidemiological studies have analyzed mechanisms of injury for children seated in child restraints and seatbelts in side impact crashes. For instance, Sherwood et al. (2003) analyzed 14 fatal side impact collisions of children restrained in child seats. Six of the fourteen fatalities had sufficient injury data. Of these six, head trauma was found to be the cause of the fatality. In addition, for all the fatalities studied, intrusion was present at the child's seat location. In the European-based CREST project, as presented in Lesire et al. (2001), cases in which 168 restrained children were involved in severe side impact crashes were analyzed. The head was found to be the body region most severely injured in 62% of the cases with cervical spine injuries being rare; however, when they were found to have occurred, they often led to fatality. In addition, this study documented severe chest and abdomen injuries predominantly when the child was restrained in either a booster seat or using the seat belt. Maltese et al. (2007) analyzed 24 cases involving seatbelt restrained children ages 4 to 15 in side impact and documented that the majority of head and face impacts were with both the vehicle's interior structures and the impacting vehicle. In addition, these impact points were found to be horizontally within the rear half of the window opening and vertically from the center of the window down to the window sill.

Fractured pelvis injuries tend to be common in adults with respect to side impact crashes, but have been found to be more infrequent in the pediatric population due to cartilaginous connection of the pelvic bones and increased elasticity of the symphysis

pubis and sacroiliac joints (Arbogast et al., 2002; Silber and Flynn, 2002). Arbogast et al. (2002) found that prepubescent children experienced isolated pubic rami fractures; however, post-pubescent children experienced more adult-like multiple fractures of the pelvic ring. Multiple fractures of the pelvic ring is an injury pattern directly associated with the ossification of the cartilage linkages of the three pelvic bones during puberty.

2.2 – Methods

The objective of this specific aim is to perform a field data analysis using the National Automotive Sampling System-Crashworthiness Data System (NASS-CDS) and Crash Injury Research Engineering Network (CIREN) field databases to investigate injury patterns to 4 to 10-year-olds in lateral and oblique impacts as well as analyze the main injury patterns and sources of injury to children in rear seat, lateral impacts based on the most current data.

DATA – In this analysis, occupant injury data will be taken from the NASS-CDS database, which is retained by the NCSA for crashes between years 1991 and 2014. Commercially available software SAS (SAS Institute, Cary, NC) was used to retrieve the raw data and translate it into Excel (Microsoft, Redmond, WA) which was used for data analysis. In addition, occupant injury data was taken from the CIREN database, which is also retained by the NCSA, for crashes between 1996 and 2014. Occupant injury data is not available from the CIREN database prior to 1996. Results from this study could potentially be helpful in the design of pediatric ATDs, child restraints, or vehicles. Results from this study might also be used to investigate lateral impact pediatric injury mechanisms.

INJURY DEFINITION – Abbreviated Injury Scale (AIS) 2005 - Update 2008

(AAAM, Des Plaines, IL) was used to determine specific injuries and injury severities. Injury distributions were examined by body region as specified in the AIS dictionary (Head, Face, Neck, Thorax, Abdomen and Pelvis, Spine, Upper Extremity, Lower Extremity, and Other Trauma). Injury distributions were examined by AIS severity coding and the Maximum AIS (MAIS) for multiply-injured patients based on the following AIS defined injury severity rankings:

AIS CODE	DESCRIPTION
1	MINOR
2	MODERATE
3	SERIOUS
4	SEVERE
5	CRITICAL
6	MAXIMAL (CURRENTLY UNTREATABLE)
9	UNKNOWN

CRITERIA – Children ages 4 to 10 were examined in this study. All occupant seating locations were investigated. Seating positions were designated by row, and reported for the purposes of the study as either near side (seat location nearest the impacted side of the vehicle), middle, or far side (seat location opposite the impacted side of the vehicle). The study focused on side impacts with a Principal Direction of Force (PDOF) between 2:00 and 4:00 as well as between 8:00 and 10:00, with 12:00 representing straight ahead on the vehicle. Child restraint use was also analyzed. Restraint use was documented only as restrained or unrestrained and not whether the restraint was being used properly. Injury

distribution by injury severity (MAIS), MAIS by body region (head, face, neck, thorax, abdomen and pelvic contents, spine, upper extremity, lower extremity, and other trauma), and source of injury by age were documented. There were many injury source descriptions provided in the NASS-CDS database. In order to simplify the analysis of the data, the following eighteen key descriptors were used: seat, back support; vehicle interior; other noncontact; flying glass; child seat; roof/convertible top; pillar structure; belt restraint/buckle; window frame; glass; ground; air bag; other vehicle; other occupants; loose object; vehicle hardware; fire; and unknown. The NASS-CDS documented injury sources were designated to the most closely related descriptor possible.

OTHER ISSUES FOR DATA ANALYSIS – Since the aim of this study is to identify the most common injury patterns and sources, only unweighted data was analyzed. Weighting factors were not used since they are based on the number of vehicles on the road and were therefore not suitable to evaluate individual injuries.

According to the Federal Register, Federal Motor Vehicle Safety Standard 214 was amended in 1990 in order to include a dynamic side impact test requirement to improve vehicle crashworthiness involved in vehicle-to-vehicle and vehicle-to-barrier side impact collisions. This dynamic crash test focused on thoracic protection in side impact and was phased in for passenger cars beginning in 1993 and extended to Light Truck Vehicles (LTVs) with a Gross Vehicle Weight Rating (GVWR) of 2,722 kg (6,000 lb) or less manufactured on or after September 1, 1998 (NHTSA (2004)). In 1995, Mercedes installed the first side impact air bags

into its E-class model vehicles (NHTSA (2004)), and by September of 1998, when the FMVSS 214 dynamic side impact crash test was phased in, side impact air bags were either standard or optional equipment on 16.9 percent of all passenger and LTVs (IIHS HLDI (2017)). With new dynamic side impact regulations implemented by 1998, modification of side structures of vehicles would expect to change to accommodate the advancement of safety features in side impact. An additional analysis regarding occupant injury severity and body region injured for model year vehicles prior to 1998 was performed separate from model years 1998 to 2014.

2.3 – Results

A total of 2,039 child occupants, ages 4 through 10, were extracted from the NASS-CDS database for all vehicle accident scenarios. In addition, a total of 98 child occupants, age 4 through 10, were extracted from the CIREN database for all vehicle accident scenarios. Based on the above-mentioned selection criteria, a total of 810 child occupants (39.7% of total) from the NASS-CDS data and 25 child occupants (25.5% of total) from the CIREN database, involved in side and oblique impacts, were extracted for the current study.

NASS-CDS Database

A fairly even age distribution was noted for the 810 occupants extracted from the NASS-CDS database who were involved in side and oblique impacts, as shown in Table 2.3.1, below.

Table 2.3.1 Age Distribution of Child Occupants in Side Impacts Extracted from the NASS-CDS Database from 1991 through 2014

Occupant Age	Count	Percent of Total
4 years	111	13.7%
5 years	120	14.8%
6 years	114	14.1%
7 years	129	15.9%
8 years	106	13.1%
9 years	115	14.2%
10 years	115	14.2%
TOTAL	810	100.0%

Vehicle seat positions are typically designated by a numbering system as illustrated in Figure 2.3.1, below. As seen in Table 2.3.2, the majority, or 86.9% (701 of 810) of the child occupants involved in a side impact, extracted from the NASS-CDS database, were documented as being seated in either the front row right position (194 (24.0%) Seating Location 3), the second row left position (214 (26.4%) Seating Location 4), the second row middle (91 (11.2%) Seating Location 5), or the second row right position (205 (25.3%) Seating Location 6). Of the 194 child occupants documented as seated in seat location 3, 22 (11.3%) were 4-years-olds, 29 (14.9%) were 5-year-olds, 24 (12.4%) were 6-year-olds, 35 (18.0%) were 7-year-olds, 22 (11.3%) were 8-year-olds, 28 (14.4%) were 9-year-olds, and 34 (17.5%) were 10-year-olds.

Of the 810 NASS-CDS occupants studied, only 72 (8.9%) were documented as using a child restraint system (CRS), 473 (57.3%) were documented as being restrained to some extent, 162 (19.6%) were documented as being unrestrained, and 103 (12.5%) were documented as unknown regarding restraint use.

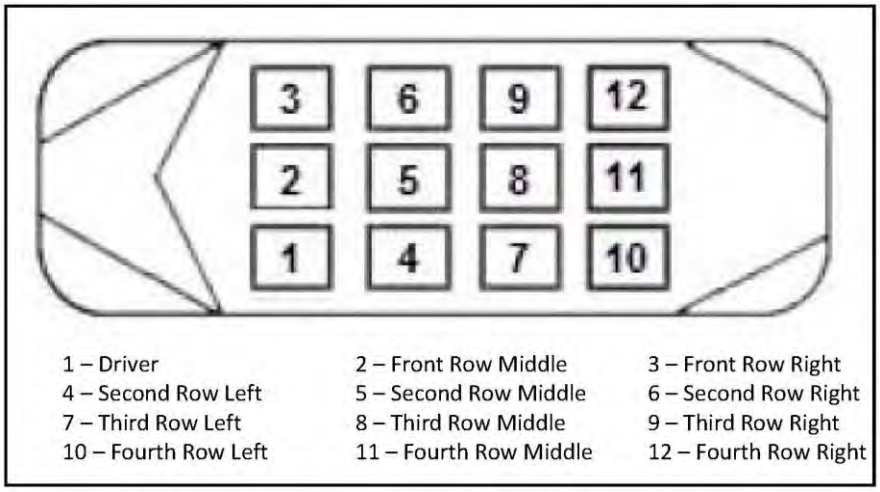

Figure 2.3.2 Vehicle Seat Position Designation Diagram

Table 2.3.2 Age Designated Seating Positions of Child Occupants in Side Impacts Extracted from the NASS-CDS Database from 1991 through 2014

Seat Position	Count	Percent of Total
2	7	0.9%
3	194	24.0%
4	214	26.4%
5	91	11.2%
6	205	25.3%
7	19	2.3%
8	7	0.9%
9	29	3.6%
10	0	0.0%
11	0	0.0%
12	1	0.1%
unknown	43	5.3%
TOTAL	810	100.0%

When broken down by side impact Principal Direction of Force (PDOF), 291 (35.9%) of the 810 child occupants experienced impact forces from the 2 o'clock (2:00) direction, 127 (15.7%) experienced the impact from the 3 o'clock (3:00) direction, 17 (2.1%) experienced impact from the 4 o'clock (4:00) direction, 8 (1.0%) experienced

impact from the 8 o'clock (8:00) direction, 108 (13.3%) experienced impact from the 9 o'clock (9:00) direction, and 259 (32.0%) experienced impact from the 10 o'clock (10:00) direction. This side impact force direction distribution for the 810 child occupants is illustrated in Figure 2.3.2 for reference below.

Based on seat location relative to PDOF, 361 (44.6%) of the child occupants were documented as near side occupants to the location of impact, 312 (38.5%) were documented as far side occupants, 98 (12.1%) were documented as middle seat occupants, and 39 (4.8%) were documented as having an unknown seating location relative to impact.

Maximum injury severity distribution, based on the AIS scale chart designated previously and regardless of vehicle model year for the 810 child occupants was documented with respect to side impact (Table 2.3.3). Of the 810 child occupants involved in side impact, 1 (0.1%) of the child occupants was documented as receiving Maximum AIS (or MAIS) 0 injuries, 585 (72.2%) were documented with MAIS 1 injuries, 103 (12.7%) were documented with MAIS 2 injuries, 66 (8.1%) were designated with MAIS 3 injuries, 14 (1.7%) were documented with MAIS 4 injuries, 25 (3.1%) were documented with MAIS 5 injuries, 9 (1.1%) were documented with MAIS 6 injuries, and 7 (0.9%) were documented with MAIS 9 injuries.

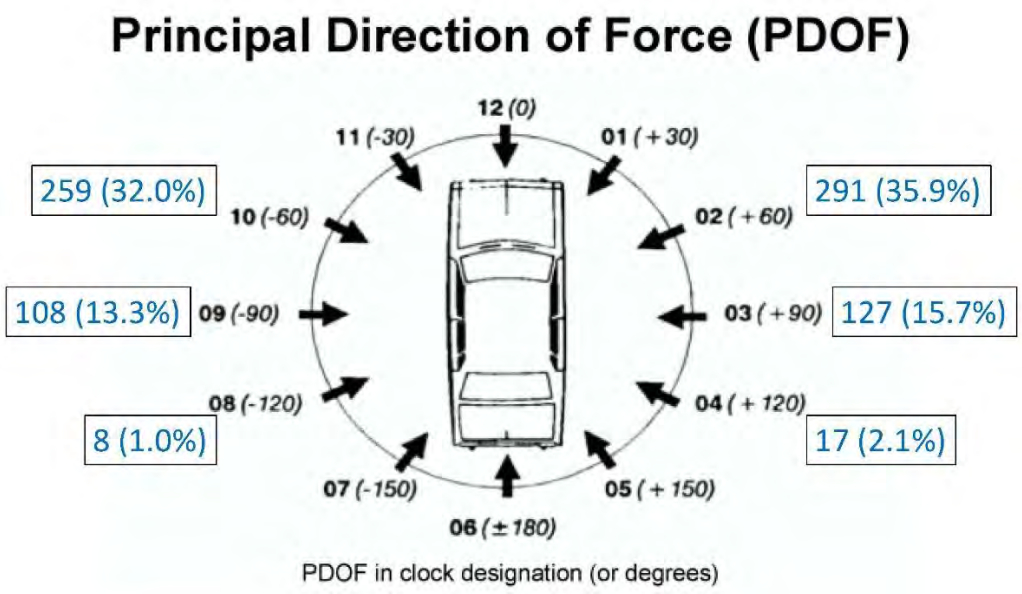

Figure 2.3.3 NASS-CDS Database Side Impact PDOF Distribution

Table 2.3.3 MAIS Distribution for Child Occupants in Side Impacts Extracted from the NASS-CDS Database from 1991 through 2014

MAIS	Count	Percent of Total
0	1	0.1%
1	585	72.2%
2	103	12.7%
3	66	8.1%
4	14	1.7%
5	25	3.1%
6	9	1.1%
9	7	0.9%
TOTAL	810	100.0%

Of the 810 child occupants, 555 (68.5%) were involved in side impact in vehicles manufactured prior to 1998, and 255 (31.5%) were involved in side impacts in vehicles manufactured from 1998 to 2014. Of the child occupants involved in side impacts in pre-1998 year manufactured vehicles, 392 (70. 6%) received MAIS 1 level injuries, 77 (13.8%) received MAIS 2 injuries, 52 (9.4%) received MAIS 3 injuries, 5 (0.9%) received MAIS 4

injuries, 18 (3.2%) received MAIS 5 injuries, 6 (1.1%) received MAIS 6 injuries, and 3 (0.5%) received MAIS 9 injuries. More simply, 70.6% of child occupants involved in side impact in pre-1998 manufactured vehicles experienced MAIS 1 (minor) injuries and the remaining 29.4% experienced MAIS2+ (moderate or greater) injuries.

Of the child occupants involved in side impacts in 1998 year manufactured vehicles or later, 1 (0.4%) received MAIS 0 injuries, 194 (76.0%) received MAIS 1 level injuries, 25 (9.8%) received MAIS 2 injuries, 14 (5.5%) received MAIS 3 injuries, 7 (2.7%) received MAIS 4 injuries, 7 (2.7%) received MAIS 5 injuries, 3 (1.2%) received MAIS 6 injuries, and 2 (0.8%) received MAIS 9 injuries. More simply, 76.4% of child occupants involved in side impact in vehicles manufactured from 1998 to 2014 experienced either no or minor injuries and the remaining 23.6% experienced MAIS2+ (moderate or greater) injuries.

Tables 2.3.4 and 2.3.5 illustrate MAIS injury by age and the vehicle manufacture year ranges described above, respectively. Note that one 10-year-old child occupant riding in a vehicle manufactured from 1998 to 2014 received an MAIS 0 injury severity rating in addition to the data presented in Table 2.3.5, below.

Table 2.3.4 Distribution of Child Occupants in Side Impacts by Age and MAIS for Vehicles Manufactured Before 1998 - NASS-CDS Database from 1991-2014

	MAIS 1		MAIS 2		MAIS 3		MAIS 4-6,9		
Occupant Age	Count	Percent of Total	Count	Percent of Total	Count	Percent of Total	Count	Percent of Total	*TOTAL*
4-Year-Old Occupants	53	13.5%	16	20.8%	7	13.5%	7	20.6%	83
5-Year-Old Occupants	62	15.8%	13	16.9%	5	9.6%	6	17.6%	86
6-Year-Old Occupants	59	15.1%	8	10.4%	8	15.4%	3	8.8%	78
7-Year-Old Occupants	67	17.1%	6	7.8%	11	21.2%	6	17.6%	90
8-Year-Old Occupants	53	13.5%	12	15.6%	6	11.5%	4	11.8%	75
9-Year-Old Occupants	62	15.8%	7	9.1%	7	13.5%	1	2.9%	77
10-Year-Old Occupants	36	9.2%	15	19.5%	8	15.4%	7	20.6%	66
TOTAL	392	100.0%	77	100.0%	52	100.0%	34	100.0%	555

Table 2.3.5 Distribution of Child Occupants in Side Impacts by Age and MAIS for Vehicles Manufactured from 1998 to 2014 - NASS-CDS Database from 1991-2014

	MAIS 1		MAIS 2		MAIS 3		MAIS 4-6,9		
Occupant Age	Count	Percent of Total	Count	Percent of Total	Count	Percent of Total	Count	Percent of Total	TOTAL
4-Year-Old Occupants	22	11.3%	2	8.0%	0	0.0%	4	19.0%	28
5-Year-Old Occupants	25	12.9%	2	8.0%	2	14.3%	5	23.8%	34
6-Year-Old Occupants	29	14.9%	4	16.0%	2	14.3%	1	4.8%	36
7-Year-Old Occupants	29	14.9%	5	20.0%	1	7.1%	4	19.0%	39
8-Year-Old Occupants	19	9.8%	4	16.0%	3	21.4%	5	23.8%	31
9-Year-Old Occupants	33	17.0%	2	8.0%	3	21.4%	0	0.0%	38
10-Year-Old Occupants	37	19.1%	6	24.0%	3	21.4%	2	9.5%	48
TOTAL	194	100.0%	25	100.0%	14	100.0%	21	100.0%	254

The distribution of injury severity with respect to body region for the 810 child occupants is provided in Table 2.3.6, below.

Table 2.3.6 Injured Body Region Distribution of Child Occupants in Side Impacts - NASS-CDS Database from 1991-2014

Injured Body Regions	Count	Percent of Total
Face	196	24.2%
Head	206	25.4%
Upper Extremities	90	11.1%
Lower Extremities	106	13.1%
Neck	59	7.3%
Thorax	55	6.8%
Abdomen and Pelvic Contents	70	8.6%
Spine	18	2.2%
Other Trauma	10	1.2%
TOTAL	810	100.0%

The head (209 (25.4%)), followed closely by the face (196 (24.2%)), were documented as the most injured body regions for child occupants in side impact. The lower extremities (106 (13.1%)) and upper extremities (90 (11.1%)) were the next most injured body regions. The thorax (55 (6.8%)) and abdomen and pelvic contents (70 (8.6%)) were also identified as frequently injured body regions with respect to child occupants in side impact. Injury severity relative to body region was further evaluated by age as well as by vehicle manufacture year range for the 810 child occupants. Since

MAIS 4-6 and MAIS 9 constituted only 6.3% of the injury severities for all child occupants in side impact, these injury severity levels were combined for this portion of the study. Table 2.3.7 represents the injured body regions of the child occupants by age and MAIS in vehicles manufactured prior to 1998 involved in side impact, and Table 2.3.8 illustrates the injured body regions of the child occupants by age and MAIS in vehicles manufactured from 1998 to 2014 involved in side impact.

Table 2.3.7 Injured Body Region Distribution by Age and MAIS of Child Occupants in Side Impacts involving Vehicles Manufactured Prior to 1998 - NASS-CDS Database from 1991-2014

4-Year-Old Occupants	MAIS 1		MAIS 2		MAIS 3		MAIS 4-6,9	
Injured Body Regions	Count	Percent of Total	Count	Percent of Total	Count	Percent of Total	Count	Percent of Total
Face	22	41.5%	4	25.0%	0	0.0%	0	0.0%
Head	11	20.8%	2	12.5%	1	14.3%	3	42.9%
Upper Extremities	6	11.3%	3	18.8%	1	14.3%	0	0.0%
Lower Extremities	3	5.7%	2	12.5%	2	28.6%	1	14.3%
Neck	4	7.5%	0	0.0%	0	0.0%	0	0.0%
Thorax	1	1.9%	2	12.5%	2	28.6%	1	14.3%
Abdomen	3	5.7%	3	18.8%	1	14.3%	0	0.0%
Spine	2	3.8%	0	0.0%	0	0.0%	1	14.3%
Other Trauma	1	1.9%	0	0.0%	0	0.0%	1	14.3%
TOTAL	53	100.0%	16	100.0%	7	100.0%	7	100.0%

5-Year-Old Occupants	MAIS 1		MAIS 2		MAIS 3		MAIS 4-6,9	
Injured Body Regions	Count	Percent of Total	Count	Percent of Total	Count	Percent of Total	Count	Percent of Total
Face	22	35.5%	0	0.0%	0	0.0%	0	0.0%
Head	13	21.0%	10	76.9%	1	20.0%	4	66.7%
Upper Extremities	6	9.7%	1	7.7%	1	20.0%	0	0.0%
Lower Extremities	9	14.5%	2	15.4%	2	40.0%	0	0.0%
Neck	2	3.2%	0	0.0%	0	0.0%	2	33.3%
Thorax	3	4.8%	0	0.0%	1	20.0%	0	0.0%
Abdomen	6	9.7%	0	0.0%	0	0.0%	0	0.0%
Spine	1	1.6%	0	0.0%	0	0.0%	0	0.0%
Other Trauma	0	0.0%	0	0.0%	0	0.0%	0	0.0%
TOTAL	62	100.0%	13	100.0%	5	100.0%	6	100.0%

6-Year-Old Occupants	MAIS 1		MAIS 2		MAIS 3		MAIS 4-6,9	
Injured Body Regions	Count	Percent of Total	Count	Percent of Total	Count	Percent of Total	Count	Percent of Total
Face	25	42.4%	1	12.5%	2	25.0%	0	0.0%
Head	15	25.4%	3	37.5%	1	12.5%	2	66.7%
Upper Extremities	5	8.5%	3	37.5%	0	0.0%	0	0.0%
Lower Extremities	4	6.8%	0	0.0%	3	37.5%	0	0.0%
Neck	2	3.4%	0	0.0%	0	0.0%	0	0.0%
Thorax	0	0.0%	0	0.0%	2	25.0%	1	33.3%
Abdomen	7	11.9%	1	12.5%	0	0.0%	0	0.0%
Spine	0	0.0%	0	0.0%	0	0.0%	0	0.0%
Other Trauma	1	1.7%	0	0.0%	0	0.0%	0	0.0%
TOTAL	59	100.0%	8	100.0%	8	100.0%	3	100.0%

7-Year-Old Occupants	MAIS 1		MAIS 2		MAIS 3		MAIS 4-6,9	
Injured Body Regions	Count	Percent of Total	Count	Percent of Total	Count	Percent of Total	Count	Percent of Total
Face	15	22.4%	0	0.0%	0	0.0%	0	0.0%
Head	11	16.4%	2	33.3%	5	45.5%	4	66.7%
Upper Extremities	7	10.4%	2	33.3%	0	0.0%	0	0.0%
Lower Extremities	14	20.9%	0	0.0%	2	18.2%	0	0.0%
Neck	7	10.4%	0	0.0%	0	0.0%	1	16.7%
Thorax	3	4.5%	1	16.7%	3	27.3%	0	0.0%
Abdomen	8	11.9%	1	16.7%	1	9.1%	1	16.7%
Spine	2	3.0%	0	0.0%	0	0.0%	0	0.0%
Other Trauma	0	0.0%	0	0.0%	0	0.0%	0	0.0%
TOTAL	67	100.0%	6	100.0%	11	100.0%	6	100.0%

8-Year-Old Occupants	MAIS 1		MAIS 2		MAIS 3		MAIS 4-6,9	
Injured Body Regions	Count	Percent of Total	Count	Percent of Total	Count	Percent of Total	Count	Percent of Total
Face	22	41.5%	0	0.0%	0	0.0%	0	0.0%
Head	9	17.0%	7	58.3%	1	16.7%	4	100.0%
Upper Extremities	6	11.3%	2	16.7%	2	33.3%	0	0.0%
Lower Extremities	4	7.5%	1	8.3%	1	16.7%	0	0.0%
Neck	2	3.8%	0	0.0%	0	0.0%	0	0.0%
Thorax	4	7.5%	1	8.3%	2	33.3%	0	0.0%
Abdomen	3	5.7%	1	8.3%	0	0.0%	0	0.0%
Spine	1	1.9%	0	0.0%	0	0.0%	0	0.0%
Other Trauma	2	3.8%	0	0.0%	0	0.0%	0	0.0%
TOTAL	53	100.0%	12	100.0%	6	100.0%	4	100.0%

9-Year-Old Occupants	MAIS 1		MAIS 2		MAIS 3		MAIS 4-6,9	
Injured Body Regions	Count	Percent of Total	Count	Percent of Total	Count	Percent of Total	Count	Percent of Total
Face	19	30.6%	1	14.3%	0	0.0%	0	0.0%
Head	15	24.2%	4	57.1%	2	28.6%	1	100.0%
Upper Extremities	5	8.1%	0	0.0%	1	14.3%	0	0.0%
Lower Extremities	10	16.1%	1	14.3%	0	0.0%	0	0.0%
Neck	6	9.7%	0	0.0%	0	0.0%	0	0.0%
Thorax	1	1.6%	1	14.3%	3	42.9%	0	0.0%
Abdomen	5	8.1%	0	0.0%	1	14.3%	0	0.0%
Spine	1	1.6%	0	0.0%	0	0.0%	0	0.0%
Other Trauma	0	0.0%	0	0.0%	0	0.0%	0	0.0%
TOTAL	62	100.0%	7	100.0%	7	100.0%	1	100.0%

10-Year-Old Occupants	MAIS 1		MAIS 2		MAIS 3		MAIS 4-6,9	
Injured Body Regions	Count	Percent of Total	Count	Percent of Total	Count	Percent of Total	Count	Percent of Total
Face	9	25.0%	0	0.0%	1	12.5%	0	0.0%
Head	7	19.4%	7	46.7%	1	12.5%	7	100.0%
Upper Extremities	6	16.7%	2	13.3%	0	0.0%	0	0.0%
Lower Extremities	6	16.7%	4	26.7%	2	25.0%	0	0.0%
Neck	4	11.1%	0	0.0%	0	0.0%	0	0.0%
Thorax	2	5.6%	0	0.0%	3	37.5%	0	0.0%
Abdomen	0	0.0%	2	13.3%	1	12.5%	0	0.0%
Spine	0	0.0%	0	0.0%	0	0.0%	0	0.0%
Other Trauma	2	5.6%	0	0.0%	0	0.0%	0	0.0%
TOTAL	36	100.0%	15	100.0%	8	100.0%	7	100.0%

Table 2.3.8 Injured Body Region Distribution by Age and MAIS of Child Occupants in Side Impacts involving Vehicles Manufactured From 1998 to 2014 - NASS-CDS Database from 1991-2014

4-Year-Old Occupants	MAIS 1		MAIS 2		MAIS 3		MAIS 4-6,9	
Injured Body Regions	Count	Percent of Total	Count	Percent of Total	Count	Percent of Total	Count	Percent of Total
Face	6	27.3%	0	0.0%	0	0.0%	0	0.0%
Head	2	9.1%	2	100.0%	0	0.0%	4	100.0%
Upper Extremities	2	9.1%	0	0.0%	0	0.0%	0	0.0%
Lower Extremities	4	18.2%	0	0.0%	0	0.0%	0	0.0%
Neck	5	22.7%	0	0.0%	0	0.0%	0	0.0%
Thorax	2	9.1%	0	0.0%	0	0.0%	0	0.0%
Abdomen	0	0.0%	0	0.0%	0	0.0%	0	0.0%
Spine	1	4.5%	0	0.0%	0	0.0%	0	0.0%
Other Trauma	0	0.0%	0	0.0%	0	0.0%	0	0.0%
TOTAL	22	100.0%	2	100.0%	0	0.0%	4	100.0%

5-Year-Old Occupants	MAIS 1		MAIS 2		MAIS 3		MAIS 4-6,9	
Injured Body Regions	Count	Percent of Total	Count	Percent of Total	Count	Percent of Total	Count	Percent of Total
Face	9	36.0%	0	0.0%	0	0.0%	0	0.0%
Head	5	20.0%	1	50.0%	1	50.0%	1	20.0%
Upper Extremities	3	12.0%	0	0.0%	1	50.0%	0	0.0%
Lower Extremities	3	12.0%	0	0.0%	0	0.0%	0	0.0%
Neck	4	16.0%	0	0.0%	0	0.0%	1	20.0%
Thorax	0	0.0%	0	0.0%	0	0.0%	2	40.0%
Abdomen	1	4.0%	1	50.0%	0	0.0%	1	20.0%
Spine	0	0.0%	0	0.0%	0	0.0%	0	0.0%
Other Trauma	0	0.0%	0	0.0%	0	0.0%	0	0.0%
TOTAL	25	100.0%	2	100.0%	2	100.0%	5	100.0%

6-Year-Old Occupants	MAIS 1		MAIS 2		MAIS 3		MAIS 4-6,9	
Injured Body Regions	Count	Percent of Total	Count	Percent of Total	Count	Percent of Total	Count	Percent of Total
Face	8	27.6%	0	0.0%	0	0.0%	0	0.0%
Head	1	3.4%	4	100.0%	0	0.0%	1	100.0%
Upper Extremities	4	13.8%	0	0.0%	0	0.0%	0	0.0%
Lower Extremities	5	17.2%	0	0.0%	2	100.0%	0	0.0%
Neck	3	10.3%	0	0.0%	0	0.0%	0	0.0%
Thorax	4	13.8%	0	0.0%	0	0.0%	0	0.0%
Abdomen	3	10.3%	0	0.0%	0	0.0%	0	0.0%
Spine	1	3.4%	0	0.0%	0	0.0%	0	0.0%
Other Trauma	0	0.0%	0	0.0%	0	0.0%	0	0.0%
TOTAL	29	100.0%	4	100.0%	2	100.0%	1	100.0%

7-Year-Old Occupants	MAIS 1		MAIS 2		MAIS 3		MAIS 4-6,9	
Injured Body Regions	Count	Percent of Total	Count	Percent of Total	Count	Percent of Total	Count	Percent of Total
Face	9	31.0%	1	20.0%	0	0.0%	0	0.0%
Head	5	17.2%	1	20.0%	1	100.0%	2	50.0%
Upper Extremities	4	13.8%	1	20.0%	0	0.0%	0	0.0%
Lower Extremities	1	3.4%	0	0.0%	0	0.0%	0	0.0%
Neck	4	13.8%	0	0.0%	0	0.0%	0	0.0%
Thorax	1	3.4%	0	0.0%	0	0.0%	1	25.0%
Abdomen	3	10.3%	2	40.0%	0	0.0%	1	25.0%
Spine	1	3.4%	0	0.0%	0	0.0%	0	0.0%
Other Trauma	1	3.4%	0	0.0%	0	0.0%	0	0.0%
TOTAL	29	100.0%	5	100.0%	1	100.0%	4	100.0%

8-Year-Old Occupants	MAIS 1		MAIS 2		MAIS 3		MAIS 4-6,9	
Injured Body Regions	Count	Percent of Total	Count	Percent of Total	Count	Percent of Total	Count	Percent of Total
Face	4	21.1%	0	0.0%	1	33.3%	0	0.0%
Head	1	5.3%	2	50.0%	0	0.0%	3	60.0%
Upper Extremities	5	26.3%	0	0.0%	0	0.0%	0	0.0%
Lower Extremities	4	21.1%	0	0.0%	1	33.3%	0	0.0%
Neck	1	5.3%	0	0.0%	0	0.0%	1	20.0%
Thorax	4	21.1%	1	25.0%	1	33.3%	0	0.0%
Abdomen	0	0.0%	1	25.0%	0	0.0%	1	20.0%
Spine	0	0.0%	0	0.0%	0	0.0%	0	0.0%
Other Trauma	0	0.0%	0	0.0%	0	0.0%	0	0.0%
TOTAL	19	100.0%	4	100.0%	3	100.0%	5	100.0%

9-Year-Old Occupants	MAIS 1		MAIS 2		MAIS 3		MAIS 4-6,9	
Injured Body Regions	Count	Percent of Total	Count	Percent of Total	Count	Percent of Total	Count	Percent of Total
Face	9	27.3%	0	0.0%	0	0.0%	0	0.0%
Head	7	21.2%	1	50.0%	1	33.3%	0	0.0%
Upper Extremities	4	12.1%	0	0.0%	0	0.0%	0	0.0%
Lower Extremities	2	6.1%	0	0.0%	1	33.3%	0	0.0%
Neck	5	15.2%	0	0.0%	1	33.3%	0	0.0%
Thorax	1	3.0%	0	0.0%	0	0.0%	0	0.0%
Abdomen	2	6.1%	1	50.0%	0	0.0%	0	0.0%
Spine	3	9.1%	0	0.0%	0	0.0%	0	0.0%
Other Trauma	0	0.0%	0	0.0%	0	0.0%	0	0.0%
TOTAL	33	100.0%	2	100.0%	3	100.0%	0	0.0%

10-Year-Old Occupants	MAIS 1		MAIS 2		MAIS 3		MAIS 4-6,9	
Injured Body Regions	Count	Percent of Total	Count	Percent of Total	Count	Percent of Total	Count	Percent of Total
Face	7	18.9%	0	0.0%	0	0.0%	0	0.0%
Head	3	8.1%	1	16.7%	2	66.7%	1	50.0%
Upper Extremities	7	18.9%	0	0.0%	0	0.0%	0	0.0%
Lower Extremities	6	16.2%	3	50.0%	1	33.3%	0	0.0%
Neck	4	10.8%	0	0.0%	0	0.0%	0	0.0%
Thorax	0	0.0%	1	16.7%	0	0.0%	0	0.0%
Abdomen	6	16.2%	1	16.7%	0	0.0%	0	0.0%
Spine	4	10.8%	0	0.0%	0	0.0%	0	0.0%
Other Trauma	0	0.0%	0	0.0%	0	0.0%	1	50.0%
TOTAL	37	100.0%	6	100.0%	3	100.0%	2	100.0%

Source of injury was documented with respect to side impact for the 810 child occupants. The three primary sources of injury documented for all 810 child occupants involved in side impact were the vehicle's interior (205 (25.3%)), the seat, back support (130 (16.0%)), and the belt restraint/buckle (110 (13.6%)), respectively. The three primary injury sources for child occupants involved in side impacts in pre 1998 manufactured vehicles were similar to the primary injury sources found regardless of vehicle manufacture year. For the 555 child occupants involved in side impacts in pre 1998 manufactured vehicles, the primary injury sources were the vehicle's interior (158 (28.5%)), the seat, back support (97 (17.5%)), and the belt restraint/buckle (60 (10.8%)),

respectively. It should be noted that during an oblique lateral impact, as collision forces change the velocity of the struck vehicle, the occupant of the vehicle will continue to travel at its pre-collision velocity. The discrepancy between the velocity of the struck vehicle and the velocity of the occupant produces occupant movement both laterally and longitudinally relative to the vehicle interior. This movement of the occupant continues until arrested via the restraints, if worn, or the vehicle's interior, if seat restraints are not worn. It is this forward motion of the occupant into the seatbelt restraint system that provides possibility for injury. Although seat restraints tend to reduce injury, they don't prevent any injury from occurring. (Rouhana and Foster, 1985).

For the 255 child occupants involved in side impacts in vehicles manufactured from 1998 to 2014, the primary injury sources were found to be the belt restraint/buckle (52 (19.6%)), the vehicle's interior (47 (18.4%)), and the seat, back support (33 (12.9%)), respectively.

Table 2.3.9 represents the injury source for child occupants involved in side impact by age in vehicles manufactured prior to 1998. The primary injury source for child occupants of all ages studied who were involved in a side impact in a vehicle manufactured prior to 1998 was the vehicle's interior. The second primary injury source for the child occupants of vehicles manufactured prior to 1998 involved in side impacts was the seat, back support, except for the 7-year-old age level. At the 7-year-old age level, belt restraint/buckle was the second primary injury source documented, and the seat, back support was documented as the third primary injury source. The third primary injury source for all other child occupant age levels involved in side impact in pre-1998 manufactured vehicles was documented as either belt restraint/buckle or flying.

It should be noted that any injury source documented as “ground” was verified from actual NASS case references as being from an occupant that was ejected due to impact forces and not ground contact due to rollover, as rollovers were omitted from this study.

Table 2.3.9 Injury Source Distribution by Age of Child Occupants in Side Impacts involving Vehicles Manufactured Prior to 1998 - NASS-CDS Database from 1991-2014

	4-Year-Old Occupants		5-Year-Old Occupants		6-Year-Old Occupants		7-Year-Old Occupants		8-Year-Old Occupants		9-Year-Old Occupants		10-Year-Old Occupants			
Injury Source	Count	Percent of Total	Count	Percent of Total	Count	Percent of Total	Count	Percent of Total	Count	Percent of Total	Count	Percent of Total	Count	Percent of Total	TOTAL	Percent of Total
Seat, Back Support	10	12.0%	13	15.1%	16	20.5%	12	13.3%	18	24.0%	17	22.1%	11	16.7%	97	17.5%
Interior	33	39.8%	24	27.9%	24	30.8%	22	24.4%	21	28.0%	18	23.4%	16	24.2%	158	28.5%
Other Noncontact	4	4.8%	4	4.7%	2	2.6%	6	6.7%	1	1.3%	7	9.1%	4	6.1%	28	5.0%
Flying Glass	8	9.6%	4	4.7%	4	5.1%	5	5.6%	8	10.7%	4	5.2%	6	9.1%	39	7.0%
Child Seat	6	7.2%	2	2.3%	2	2.6%	0	0.0%	0	0.0%	1	1.3%	0	0.0%	11	2.0%
Roof/Convertible Top	1	1.2%	1	1.2%	0	0.0%	1	1.1%	0	0.0%	1	1.3%	1	1.5%	5	0.9%
Pillar Structure	4	4.8%	3	3.5%	5	6.4%	4	4.4%	4	5.3%	1	1.3%	2	3.0%	23	4.1%
Belt Restraint/Buckle	7	8.4%	10	11.6%	6	7.7%	16	17.8%	6	8.0%	9	11.7%	6	9.1%	60	10.8%
Window Frame	1	1.2%	0	0.0%	1	1.3%	1	1.1%	0	0.0%	1	1.3%	1	1.5%	5	0.9%
Glass	1	1.2%	3	3.5%	1	1.3%	6	6.7%	2	2.7%	7	9.1%	5	7.6%	25	4.5%
Ground	1	1.2%	4	4.7%	4	5.1%	0	0.0%	1	1.3%	2	2.6%	3	4.5%	15	2.7%
Air Bag	1	1.2%	0	0.0%	0	0.0%	0	0.0%	1	1.3%	0	0.0%	2	3.0%	4	0.7%
Other Vehicle	0	0.0%	0	0.0%	0	0.0%	0	0.0%	0	0.0%	1	1.3%	1	1.5%	2	0.4%
Other Occupants	1	1.2%	8	9.3%	5	6.4%	8	8.9%	4	5.3%	3	3.9%	0	0.0%	29	5.2%
Loose Object	0	0.0%	1	1.2%	2	2.6%	1	1.1%	1	1.3%	0	0.0%	0	0.0%	5	0.9%
Unknown	4	4.8%	4	4.7%	4	5.1%	4	4.4%	8	10.7%	4	5.2%	4	6.1%	32	5.8%
Hardware	0	0.0%	5	5.8%	2	2.6%	4	4.4%	0	0.0%	1	1.3%	4	6.1%	16	2.9%
Fire	1	1.2%	0	0.0%	0	0.0%	0	0.0%	0	0.0%	0	0.0%	0	0.0%	1	0.2%
TOTAL	83	100.0%	86	100.0%	78	100.0%	90	100.0%	75	100.0%	77	100.0%	66	100.0%	555	100.0%

Table 2.3.10, below, illustrates the injury sources for child occupants involved in side impact by age in vehicles manufactured from 1998 to 2014. For the 4-year-olds, the top two primary injury sources were documented as the child seat and pillar structure, respectively. The seat, back support and the belt restraint/buckle were both documented as the third primary injury source for 4-year-olds involved in side impacts in vehicles manufactured from 1998 to 2014. The top two injury sources for child occupants aged, 8, 9 and 10, in side impacts involving vehicles manufactured from 1998 to 2014 were found to be vehicle’s interior and the belt restraint/buckle. The third primary injury source for the 8-year-old was the pillar structure while the seat/back support was the third primary injury source for the 9 and 10-year-olds. For 6 and 7-year-olds involved in side impacts in vehicles manufactured from 1998 to 2014, the top three injury sources were found to

be belt restraint/buckle, vehicle interior, and seat, back support. The top three injury sources for 5-year-old child occupants in side impacts involving vehicles manufactured from 1998 to 2014 were found to be the pillar structure, belt restraint/buckle, and other occupants.

Table 2.3.10 Injury Source Distribution by Age of Child Occupants in Side Impacts involving Vehicles Manufactured from 1998 to 2014 - NASS-CDS Database from 1991-2014

	4-Year-Old Occupants		5-Year-Old Occupants		6-Year-Old Occupants		7-Year-Old Occupants		8-Year-Old Occupants		9-Year-Old Occupants		10-Year-Old Occupants			
Injury Source	Count	Percent of Total	Count	Percent of Total	Count	Percent of Total	Count	Percent of Total	Count	Percent of Total	Count	Percent of Total	Count	Percent of Total	TOTAL	Percent of Total
Seat, Back Support	4	14.3%	1	2.9%	7	19.4%	4	10.3%	3	9.7%	7	18.4%	7	14.3%	33	12.9%
Interior	1	3.6%	3	8.8%	6	16.7%	7	17.9%	9	29.0%	8	21.1%	13	26.5%	47	18.4%
Other Noncontact	2	7.1%	1	2.9%	2	5.6%	1	2.6%	1	3.2%	3	7.9%	1	2.0%	11	4.3%
Flying Glass	1	3.6%	2	5.9%	3	8.3%	3	7.7%	1	3.2%	2	5.3%	2	4.1%	14	5.5%
Child Seat	7	25.0%	2	5.9%	1	2.8%	0	0.0%	0	0.0%	1	2.6%	0	0.0%	11	4.3%
Roof/Convertible Top	0	0.0%	1	2.9%	0	0.0%	0	0.0%	2	6.5%	0	0.0%	1	2.0%	4	1.6%
Pillar Structure	5	17.9%	7	20.6%	2	5.6%	3	7.7%	4	12.9%	2	5.3%	0	0.0%	23	9.0%
Belt Restraint/Buckle	4	14.3%	5	14.7%	8	22.2%	10	25.6%	5	16.1%	8	21.1%	10	20.4%	50	19.6%
Window Frame	0	0.0%	0	0.0%	0	0.0%	2	5.1%	0	0.0%	1	2.6%	0	0.0%	3	1.2%
Glass	0	0.0%	0	0.0%	2	5.6%	1	2.6%	0	0.0%	1	2.6%	2	4.1%	6	2.4%
Ground	0	0.0%	2	5.9%	0	0.0%	2	5.1%	1	3.2%	0	0.0%	2	4.1%	7	2.7%
Air Bag	0	0.0%	1	2.9%	0	0.0%	0	0.0%	0	0.0%	1	2.6%	0	0.0%	2	0.8%
Other Vehicle	1	3.6%	0	0.0%	0	0.0%	0	0.0%	0	0.0%	0	0.0%	0	0.0%	1	0.4%
Other Occupants	1	3.6%	4	11.8%	0	0.0%	1	2.6%	2	6.5%	2	5.3%	1	2.0%	11	4.3%
Loose Object	0	0.0%	1	2.9%	1	2.8%	1	2.6%	1	3.2%	0	0.0%	0	0.0%	4	1.6%
Unknown	2	7.1%	2	5.9%	1	2.8%	1	2.6%	1	3.2%	2	5.3%	2	4.1%	11	4.3%
Hardware	0	0.0%	2	5.9%	3	8.3%	3	7.7%	1	3.2%	0	0.0%	7	14.3%	16	6.3%
Fire	0	0.0%	0	0.0%	0	0.0%	0	0.0%	0	0.0%	0	0.0%	1	2.0%	1	0.4%
TOTAL	28	100.0%	34	100.0%	36	100.0%	39	100.0%	31	100.0%	38	100.0%	49	100.0%	255	100.0%

CIREN Database

A fairly even age distribution of child occupants in side impact was also noted for the 25 child occupants extracted from the CIREN database, except the number of 5 and 8-year-olds. From the child occupants involved in side impact extracted from CIREN database, there was only one 5-year-old and eight 8-year-olds documented, as illustrated in Table 2.3.11, below.

Table 2.3.11 Age Distribution for Child Occupants in Side Impacts Extracted from the CIREN Database from 1996 through 2014

Occupant Age	Count	Percent of Total
4 years	3	12.0%
5 years	1	4.0%
6 years	4	16.0%
7 years	3	12.0%
8 years	8	32.0%
9 years	3	12.0%
10 years	3	12.0%
TOTAL	25	100.0%

Using the designated seat position numbering system previously illustrated in Figure 2.3.1 for the 25 child occupants involved in a side impact extracted from the CIREN database, the majority, or 72.0% (18 of 25), of the child occupants extracted from the CIREN database were documented as being seated in either the second row right position (10 (40.0%) Seating Location 6) or second row left position (8 (32.0%) Seating Location 4), respectively (Table 2.3.12). The remaining 7 child occupants were documented as sitting in the front row right (3 (12.0%) Seating Location 3) and second row middle (4 (16.0%) Seating Location 5).

Table 2.3.102 Age Distribution for Child Occupants in Side Impacts Extracted from the CIREN Database from 1996 through 2014

Seating Location	Count	Percent of Total
2	0	0.0%
3	3	12.0%
4	8	32.0%
5	4	16.0%
6	10	40.0%
TOTAL	25	100.0%

Of the 25 CIREN database child occupants involved in side impact studied, only 5

(20.0%) were documented as using a child restraint system (CRS), 19 (76.0%) were documented as being restrained to some extent, and only 1 child occupant was documented as being unrestrained.

When broken down by side impact PDOF, 10 (40.0%) of the 25 child occupants experienced the impact force from the 2 o'clock direction, 2 (8.0%) experienced impact from the 4 o'clock direction, 7 (28.0%) experienced impact from the 9 o'clock direction, and 6 (24.0%) experienced impact from the 10 o'clock direction. Side impact direction distribution for the 25 child occupants involved in side impact extracted from the CIREN database is illustrated in Figure 2.3.3 for reference below. Based on seat location relative to PDOF, 7 (28.0%) of the child occupants were documented as near side occupants to the location of impact, 14 (56.0%) were documented as far side occupants, and 4 (16.0%) were documented as middle seat occupants relative to impact.

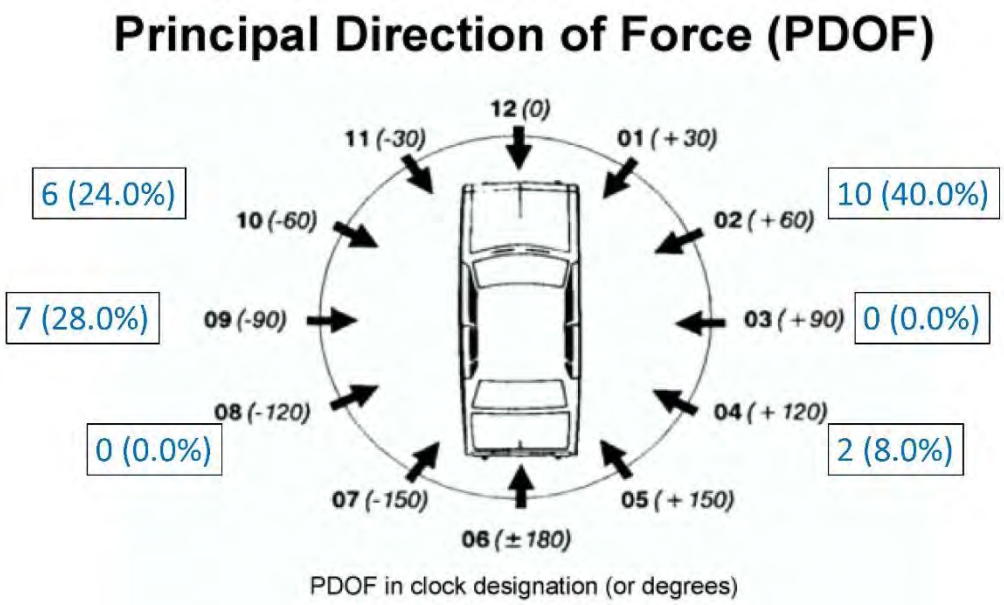

Figure 2.3.4 CIREN Database Side Impact PDOF Distribution

Maximum injury severity distribution for the 25 child occupants was documented

with respect to side impact (Table 2.3.13). Of the 25 child occupants, 7 (28.0%) of the child occupants were documented as receiving MAIS 0 injuries, 8 (32.0%) were documented with MAIS 1 injuries, 2 (8.0%) were documented with MAIS 2 injuries, 5 (20.0%) were designated with MAIS 3 injuries, 2 (8.0%) were documented with MAIS 4 injuries, and 1 (4.0%) were documented with MAIS 9 injuries. There were no documented MAIS 5 or 6 injuries.

Table 2.3.11 MAIS Distribution of Child Occupants in Side Impacts Extracted from the CIREN Database from 1996 through 2014

MAIS	Count	Percent of Total
0	7	28.0%
1	8	32.0%
2	2	8.0%
3	5	20.0%
4	2	8.0%
5	0	0.0%
6	0	0.0%
9	1	4.0%
TOTAL	25	100.0%

All 25 child occupants extracted from the CIREN database involved in side impact collisions were in vehicles manufactured from 1998 or newer, therefore, there was no need to perform a separate analysis based on vehicle manufacture year for this database. Table 2.3.14 shows MAIS distribution broken down by age for the child occupants studied. Of the three 4-year-olds included in the study, two were documented with MAIS 0 injuries and one was documented with MAIS 1 injuries. The only 5-year-old included in the study was documented as having no injuries. Of the four 6-year-olds included in the study, one was documented with MAIS 0 injuries, one was documented with MAIS 1 injuries, one was documented with MAIS 2 injuries, and one was documented with MAIS 4 injuries. Of the three 7-year-olds included in the study, one was documented with MAIS 1 injuries,

one with MAIS 2 injuries, and one with MAIS 3 injuries. Of the eight 8-year-olds included in the study, two were documented with MAIS 0 injuries, two with MAIS 1 injuries, one with MAIS 2 injuries, two with MAIS 3 injuries, and one with MAIS 9 injuries. Of the three 9-year-olds included in the study, one was documented with MAIS 0 injuries, one with MAIS 1 injuries, and one with MAIS 3 injuries. Of the three 10-year-olds included in the study, two were documented with MAIS 1 injuries and one with MAIS 4 injuries.

Table 2.3.12 Distribution of Child Occupants in Side Impacts by Age and MAIS for Vehicles Manufactured from 1998 to 2014 - CIREN Database Years 1996-2014

	MAIS 0		MAIS 1		MAIS 2		MAIS 3		MAIS 4-6,9		
Occupant Age	Count	Percent of Total	Count	Percent of Total	Count	Percent of Total	Count	Percent of Total	Count	Percent of Total	TOTAL
4-Year-Old Occupants	2	28.6%	1	12.5%	0	0.0%	0	0.0%	0	0.0%	3
5-Year-Old Occupants	1	14.3%	0	0.0%	0	0.0%	0	0.0%	0	0.0%	1
6-Year-Old Occupants	1	14.3%	1	12.5%	0	0.0%	1	20.0%	1	33.3%	4
7-Year-Old Occupants	0	0.0%	1	12.5%	1	50.0%	1	20.0%	0	0.0%	3
8-Year-Old Occupants	2	28.6%	2	25.0%	1	50.0%	2	40.0%	1	33.3%	8
9-Year-Old Occupants	1	14.3%	1	12.5%	0	0.0%	1	20.0%	0	0.0%	3
10-Year-Old Occupants	0	0.0%	2	25.0%	0	0.0%	0	0.0%	1	33.3%	3
TOTAL	7	100.0%	8	100.0%	2	100.0%	5	100.0%	3	100.0%	25

Details involving injured body regions and injury sources were not documented in the CIREN database for occupants that were not considered case study occupants. The majority of the child occupants extracted from the CIREN database were not case study occupants, and therefore, injured body regions and injury source were not analyzed based on this database source for the current study.

2.4 – Discussion

The current epidemiological study was aimed at providing relevant information regarding the level of injury severity, most injured body region, and injury source in the pediatric population during lateral and oblique impacts. Although the number of cases in some categories are relatively small and unyielding of any statistical significance, tendencies have been observed that prove to be helpful for the stated goal.

Based on the data analyzed in the current study, the majority of child occupants

(51.1% from the NASS database and 72.0% from the CIREN database) , ages 4 to 10, involved in side or oblique impacts were seated in either the second row left or second row right seating positions (seating locations 4 or 6). This is most likely due to the increased awareness for the need for child safety in motor vehicles beginning in the mid-1990's, when vehicle's began to have frontal airbags as standard equipment, as well as the establishment of seatbelt and child safety laws requiring child occupants to be restrained in seating positions aft of the first row of a vehicle. Interestingly, following the two second row outboard seating positions, the next most populated seating location by child occupants in side and oblique impacts, documented in the NASS database, was the front row right seating position at 23.9% (seating location 3). Of the 197 (23.9%) child occupants in the NASS-CDS database documented as seated in seat location 3, 22 (11.2%) were 4-years-olds, 29 (14.7%) were 5-year-olds, 24 (12.2%) were 6-year-olds, 35 (17.8%) were 7-year-olds, 22 (11.2%) were 8-year-olds, 28 (14.2%) were 9-year-olds, and 37 (18.7%) were 10-year-olds. Three out of the 25 child occupants studied from the CIREN database, or 12.0%, were documented as sitting in seat location 3 and were 9 to 10 years of age.

It has been shown by the data analyzed in the current study that the majority of side and oblique impacts occurred in either the 2 o'clock (37.2% - NASS-CDS; 40.0% - CIREN) or 10 o'clock (31.4% - NASS; 24.0%-CIREN) PDOF directions. The majority (67.9%) of lateral and oblique impacts occurred at a PDOF equal to either 10 or 2 o'clock, indicating that most of the struck vehicles had some significant forward velocity. These findings are consistent with Rouhana and Foster (1985) who documented in their study that nearly three-quarters (74%) of lateral impacts had a PDOF equal to 10, 11, 1, or 2

o'clock.

Child occupants were fairly evenly distributed in the NASS-CDS database as either far side (38.2%) or near side (45.2%) occupants in side and oblique impacts, with near side occupants being slightly more prevalent. The majority of child occupants in the CIREN database were documented as far side (56.0%) compared to the near side (28.0%) occupants.

The majority (68.2%) of child occupants involved in side and oblique impacts extracted from the NASS-CDS database were reported as being restrained to some extent; however, only 10.2% of those reported as restrained were identified as using a child seat. Of the 84 child occupants documented as using a child seat, only 6 (7.1%) were reported as being in the age range of 8 to 10. The remaining 78 (92.9%) child occupants reported as using child seats included 32 (38.1%) 4-year-olds, 20 (23.8%) 5-year-olds, 15 (17.9%) 6-year-olds, and 11 (13.1%) 7-year-olds. A decrease in child seat use was expected with age; however, lack of child seat use does not mean the child occupant was necessarily ready to be out of a child seat based on government recommendations.

The large majority of MAIS injuries to child occupants in side and oblique impacts identified in both databases (73.5% - NASS; 60.0% - CIREN) were reported as having either MAIS 0 or 1 level injuries (none to minor), and the remaining 26.5% of child occupants identified in the NASS-CDS database and 40.0% of child occupants identified in the CIREN database were documented as having MAIS 2+ injuries. Neither age nor vehicle manufacture year seemed to play a factor in terms of the distribution of minor

(MAIS 1) injuries in the current study. There does appear to be a higher number of MAIS2+ injuries in vehicles manufactured prior to 1998 than in vehicles manufactured from 1998 to 2014 which could potentially be related to advanced side impact safety technologies implemented into the newer model vehicles but more research is needed for verification.

According to the study performed by Hanna (2010), approximately 27.0% of child passengers ages 0 to 7 were involved in side impact motor vehicle crashes. Although the current study considered children ages 4 through 10, the rate of child occupants involved in side motor vehicle crashes is consistent with the CIREN database analysis (25.5%) but somewhat lower than the NASS-CDS database distribution (40.2%). The incidence rate for children unrestrained in a motor vehicle in a lateral impact in the Hanna (2010) study was found to be 21% compared to 31.8% based on the NASS-CDS database for the current study. The higher rate of unrestrained occupants in the current study, based on the NASS-CDS, may be due to the older age range analyzed in the current study and the expectation that older children will put their own restraint on versus infants studied in Hanna (2010) who cannot. Only 1 child was reported as being unrestrained out of 25 child occupants in side and oblique impacts in the CIREN database. Any comparison of the rate of restraint use from this database should be cautioned due to the relatively low number of child occupants from this database meeting the current study's criteria.

The vast majority of injuries identified in the current study using the NASS-CDS database (49.2%) occurred at the head and face regions of child occupants involved in side and oblique impacts. These findings are consistent with Lesire et al. (2001) in which

the head was found to be the body region most severely injured. Upper and lower extremities were also identified as being regions of the body frequently injured (11.2% and 13.3% of the total injuries, respectively). Thorax (6.7%) and abdomen (8.8%) body regions were likewise recognized as significant injury locations in side and oblique vehicle impacts for child occupants. Upon further detailed review of the data, again, the majority of MAIS injuries to the thorax and abdomen were MAIS 2 or less and appeared not to be affected by age of the child occupant or vehicle manufacture year. There appeared to be a higher number of thorax and abdominal MAIS3+ injuries in vehicles manufactured prior to 1998 (23 total) than in vehicles manufactured from 1998 to 2014 (7 total) which could potentially be related to advanced side impact safety technologies implemented into the newer model vehicles but more research is needed for verification.

The main sources of injury for child occupants in side and oblique impacts were reported in the NASS-CDS database as vehicle interior, seat, back support, and belt restraint/buckle. For vehicles manufactured prior to 1998, the primary sources of injury were vehicle interior, seat, back support, belt restraint/buckle, and flying glass. For vehicles manufactured from 1998 to 2014, primary injury sources included vehicle interior, seat, back support, belt restraint/buckle, pillar structure, and for the 4-year-olds, child seat. When considering only thorax and abdomen body regions, the primary sources of injury were documented as the vehicle interior or the belt restraint/buckle.

The above findings in the current study are consistent with Maltese et al. (2007) who documented that the majority of head and face impacts were with the vehicle's interior structures.

2.5 – Conclusions

Several main conclusions were drawn from this epidemiological study:

1) Age did not seem to have an effect on injury severity, body region injured, or injury source in side and oblique impacts for minor injuries.
2) Vehicle manufacture year did not seem to have an effect on injury severity, body region injured, or injury source in side and oblique impacts.
3) The majority of side and oblique impacts occurred in either the 2 o'clock or 10 o'clock PDOF directions.
4) The majority of child occupants, age 4 through 10, involved in side and oblique impacts were reported as being restrained to some extent; however, only a small percentage of those reported as restrained were identified as using a child seat.
5) The vast majority of MAIS injuries to child occupants in side and oblique impacts were reported to be either MAIS 0 or 1 level injuries (none to minor).
6) The main sources of injury for child occupants in side and oblique impacts were reported in the NASS-CDS database as vehicle interior, seat, back support, and belt restraint/buckle.
7) The vast majority of injuries identified in the current study, using the NASS-CDS database, occurred at the head and face regions (49.2%) of child occupants involved in side and oblique impacts. Upper and lower extremities were also identified as being regions of the body frequently injured (11.2% and 13.3% of the total injuries, respectively). Thorax (6.7%) and abdomen (8.8%) body regions were likewise recognized as significant injury locations in side and oblique vehicle impacts for child occupants.

8) There appears to be a higher number of thorax and abdominal MAIS3+ injuries in vehicles manufactured prior to 1998 than in vehicles manufactured from 1998 to 2014 which could be due to advanced side impact safety technologies implemented into the newer model vehicles.
9) When considering only thorax and abdomen body regions, the primary sources of injury were documented as the vehicle interior or the belt restraint/buckle. During an oblique lateral impact, as collision forces change the velocity of the struck vehicle, the occupant of the vehicle will continue to travel at its pre-collision velocity. The discrepancy between the velocity of the struck vehicle and the velocity of the occupant produces occupant movement both laterally and longitudinally relative to the vehicle interior. This movement of the occupant continues until arrested via the restraints, if worn, or the vehicle's interior, if seat restraints are not worn. It is this forward motion of the occupant into the seatbelt restraint system that provides possibility for injury. In vehicle safety research, ATD biofidelity, and the ATD thorax, abdomen, and pelvis anthropometry need to be accurate in order to generate injury patterns observed in real world collisions.
10) Based on the current epidemiological study performed, in order to continue to advance child safety technologies and protect child occupants in lateral vehicle impacts, more innovative and biofidelic child anthropometric test devices (ATDs) need to be designed.

CHAPTER 3 - BIOFIDELIC ASSESSMENT OF THE 6-YEAR-OLD ATDs IN LATERAL IMPACT (SPECIFIC AIM 2)

3.1 – Background

In 2011, NHTSA published their Biomechanics Research Plan for 2011-2015. NHTSA's plan included research in the advancement of both front and side impact child dummies (NHTSA, 2011). Most recently, in January of 2014, NHTSA proposed an upgrade to the Federal Motor Vehicle Safety Standard for child restraint systems (FMVSS 213). This proposed upgrade includes a side impact test utilizing a Q3s child dummy for assessing car seats sold in the United States, designed for children weighing up to 40 pounds. The goal of the proposed upgrade to FMVSS 213 is to work toward making sure child passengers are protected in side impacts (NHTSA, 2014B).

Research has shown a need for assessment and development of child side impact dummies. Customarily, the biofidelity of adult ATDs has been assessed using PMHS data. Due to paucity of pediatric PMHS tests, biofidelity targets for children have been scaled from adult response data. Irwin and Mertz (1997) derived seven different length scale factors, four different mass scale factors, as well as a scale factor for the elastic bending modulus of bone to scale adult response data to the child utilizing the best available child anthropometry and bone property studies at the time. One issue with scaling from an adult to a child is that children are not just small adults. From a biomechanical perspective, there are not only changes with growth in body proportions and skeletal structure but with tissue and bone properties (Franklyn et al. 2007; Wenger and Pring, 2005). For instance, the cortex of young bones tends to be more porous and flexible than adult bones (Wenger and Pring, 2005).

The purpose of the current study is to provide performance results for the biofidelity of the 6-year-old anthropometric test dummies' (HIII (with Ford-designed abdomen insert described in Rouhana (2006) and Elhagediab et al. (2006) and UMTRI-designed pelvis described in Klinich et al. (2010)), Q6, and Q6s) shoulder, thorax, abdomen, and pelvis regions in lateral impact. According to Humanetics Innovation Solutions (a manufacturer of the HIII and Q-series dummies), there are currently two 6-year-old ATDs, the HIII and the recently developed Q6, both of which are designed primarily for frontal impact testing. The Q6s is a prototype lateral impact dummy. The prototype Q6s is built on the platform of the Q6 but the neck, shoulders, thorax, and hip joints have been modified to improve durability and biofidelity in lateral impact. The Q6s also has additional measurement channels.

3.2 – Methods

The objective of this specific aim was to assess the design and biofidelity of the current 6-year-old HIII (with Ford in-house abdominal insert), Q6, and Q6s prototype anthropometric test dummies (ATD) in lateral loading. The biofidelity performance in lateral impact for the three ATDs was assessed against the scaled biofidelity targets published in Irwin et al. (2002), the abdominal biofidelity target suggested in van Ratingen et al. (1997), and the biofidelity targets published in Rhule et al. (2013). Regional and overall biofidelity rankings for each of the three ATDs were performed using both the ISO 9790 Biofidelity Rating System (ISO/TR 9790 1999) and the National Highway Traffic Safety Administration's (NHTSA) External Biofidelity Ranking System (BRS) (Rhule et al., 2013). This specific aim provided an understanding of the current mechanical behavior of the current 6-year-old ATDs in lateral impact and to determine the body regions of the

6-year-old ATDs requiring further research and development. The complete assessment included (Table 3.2.1):

Shoulder: (1) ISO pendulum test, (1) ISO WSU rigid sled test

Thorax: (1) ISO pendulum test, (2) ISO drop tests, (1) ISO WSU rigid sled test

Abdomen: (1) van Ratingen pendulum test, (1) ISO drop test, (1) ISO WSU rigid sled test

Pelvis: (1) ISO pendulum test, (2) ISO drop tests, (1) ISO WSU rigid sled test

Table 3.2.1 ATD Biofidelity Assessment in Lateral Impact Test Matrix

	Pendulum Tests	Drop Tests		Sled Tests
Shoulder	ISO Shoulder Test 1 2.9 kg mass 4.5 m/s impact			6.8 m/s WSU sled
Thorax	ISO ThoraxTest 1 2.9 kg mass 4.3 m/s impact	ISO Thorax Test 3 1 m drop - Rigid	0.5 m drop - Rigid	ISO Thorax Test 5 6.8 m/s - WSU sled
Abdomen	van Ratingen 2.9 kg mass 4.8 m/s impact	ISO Abdomen Test 1 1 m drop - Rigid Armrest		ISO Abdomen Test 3 6.8 m/s - WSU sled
Pelvis	ISO Pelvis Test 1 3.89 kg mass 6 m/s impact	ISO Pelvis Test 3 0.5 m drop - Rigid	ISO Pelvis Test 4 1 m drop - Rigid	ISO Pelvis Test 10 6.8 m/s - WSU sled

A series of lateral impact pendulum tests, vertical drop tests, and WSU 6.8 m/s rigid sled tests were performed using the 6-year-old ATDs. Since the Q6s is still a prototype and the opportunity to compare all three ATDs is rare, testing in the current study was conducted to establish whole body and component level responses, and higher level testing such as the 6.7 m/s thorax pendulum impact test, 10.0 m/s pelvis pendulum impact test, 2-meter drop test, and 8.9 m/s sled test were omitted to maintain ATD integrity throughout the entire test sequence. This would provide a better understanding of the overall biofidelity performance of these dummies to aid in their future design and

performance. Component level testing (pendulum tests) was conducted in order to analyze the individual body region responses of each dummy. Rigid sled and drop tests were conducted in order to assess individual body region responses of each dummy as well as whole dummy response and kinematics. The protocols for the above described tests were based on the procedures detailed in ISO/TR 9790 (1999) and scaled for the 6-year-old using Irwin et al. (2002). The abdomen used in the 6-year-old HIII ATD for the current analysis is the Ford-designed abdomen, which is a fluid-filled compressible silicone abdominal insert that sits in the space between the bottom of the rib cage and the modified pelvis structure described in Klinich et al. (2010). The three ATDs tested were instrumented with tri-axial accelerometers attached to mounting blocks at the head center of gravity (CG), T1 and T12 levels of the thoracic spine, the middle rib (at the equivalent HIII 6-year-old ATD rib 3-4 location), and lumbar spine. The accelerometers mounted in the lateral impact direction were Endevco 7264-2000TZ (2000 G) piezoresistive accelerometers. The accelerometers mounted in the longitudinal and vertical directions were Measurement Specialties 64C-0200-360T (200 G) piezoresistive accelerometers. The T1, T12, and lumbar spine tri-axial accelerometer mount blocks were attached to the posterior side of each dummy's spine box for consistent accelerometer readings. An IR-TRACC™ linear transducer (Humanetics Innovative Solutions, Plymouth, MI; Rouhana et al., (1998)) was installed laterally in each dummy's rib cage, to measure rib deflection relative to the spine in a left side impact at the equivalent HIII 6-year-old rib 3-4 location. Six-channel load cell force and moment sensors (Humanetics) were installed and data was recorded at the upper neck, lower neck, and pelvis in the Q6 and Q6s ATDs and at the upper neck in the HIII ATD. All

sensors were connected to a TDAS data acquisition system (Diversified Technical Systems (DTS), Seal Beach, CA), and data was collected at a sampling rate of 10,000 Hz. The impact events were captured at 1,000 frames per second by a high-speed video camera (Kodak 2k). Three replicate runs were performed for each of the tests.

The data collected was filtered using the SAE J211 Recommended Practice (2003), aligned using the methodology described in Donnelly and Moorhouse (2012), and compared for each body region tested (shoulder, thorax, abdomen, and pelvis). The biofidelity performance in lateral impact for the three ATDs was assessed against the scaled biofidelity targets published in Irwin et al. (2002), abdominal biofidelity target suggested in van Ratingen et al. (1997), and biofidelity targets described in Rhule et al. (2013). Body region and overall biofidelity rating scores were determined for each of the three 6-year-old ATDs tested using both the ISO 9790 Biofidelity Rating System (1999) and NHTSA's External Biofidelity Ranking System (BRS) (Rhule et al., 2013).

Pendulum Tests

A flat-faced, rigid, aluminum probe was fabricated for use in the shoulder, thorax, and abdomen lateral impact pendulum tests. The impacting surface had a diameter of 88.9 millimeters with a 12.7-millimeter edge radius. This is slightly smaller than the diameter for the thorax impactor face (106 millimeters) and shoulder impactor face (97 millimeters) specified in Irwin and Mertz (2010) based on scaling techniques. The pendulum probe size used in the current study was chosen because it is the size of the impacting probe used to calibrate the Q6 in side impact (Q6 User Manual, 2012), to reduce testing complexity, and because it also provided a geometric fit (impact of the thorax only without bridging to other body regions of the ATD) to the side of all three

tested dummies. The pendulum mass was 2.9 kilograms which was consistent with the pendulum mass specified by Irwin et al (2002) for the 6-year-old. A uniaxial accelerometer was mounted on the rear of the pendulum. The pendulum impact force was obtained by multiplying the pendulum mass by the recorded acceleration data.

A flat-faced, rigid, aluminum pendulum probe was fabricated for use in the pelvis lateral impact pendulum tests. The impacting surface had a 76.2-millimeter diameter with a 12.7-millimeter edge radius. The diameter was based on a similar method used by Carlson et al. (2007) to scale the pelvis probe for the 50th-percentile male side impact dummy to the Q3s. In the current study the probe scaling was done to the 6-year-old dummy age level, which is slightly smaller in diameter than the impactor face (84 millimeters) specified in Irwin and Mertz (2010). When the geometric arc of the 50th percentile male ATD impact probe (which is the salad bowl impact face) is applied to the smaller diameter impactor face for the 6-year-old the curvature is almost non-existent and would result in only minimal, if any, differences in the force response compared to a flat-faced impactor. It was decided, based on this rationale, to use a flat-faced impactor for the pelvic pendulum impact testing. The pendulum mass was 3.89 kilograms, consistent with the pendulum impactor mass specified in Irwin et al. (2002). A uniaxial accelerometer was mounted on the rear of the pendulum. The pendulum impact force was obtained by multiplying the mass and acceleration data.

The ATDs were seated on two sheets of 3.2-millimeter thick mechanical grade Teflon™ for all pendulum tests. The ATDs were impacted on their left side. The ATDs were rotated to an oblique 60-degree angle from anterior-posterior for the abdominal pendulum impact tests in accordance with testing performed by van Rantingen et al. (1997) and

scaled abdominal impact response corridors developed in that study based on the oblique abdominal impact testing proposed in Viano (1989A). An optical sensor speed trap was used to verify pendulum speed just prior to impact.

Vertical Drop Tests

A vertical drop fixture was fabricated, allowing the ATD to drop freely, using a flat metal frame structure, chains, and a two-stage "quick release" device. The "quick release" device utilized a stage 1 - manual "quick release" and stage 2 - hybrid electromagnets (Kanetec USA Corp., Bensenville, IL). Two separate rigid aluminum load plate surfaces (12-inch by 12-inch thorax load plate, 8-inch by 12-inch pelvis load plate) and a wooden armrest load surface were fabricated as specified in ISO 9790 Abdomen Impact Response Requirement 1 (1999) for impact of the dummy torso, pelvis, and abdomen, respectively. The armrest was designed as specified and was not scaled down to the 6-year-old because it was interpreted to be representative of a simulated armrest, impacted in a vehicle side impact environment. No size was specified in the ISO 9790 Abdomen Impact Response Requirement 1 (1999) for the thorax and pelvis load plates. Load plate sizes for the current study were chosen based on the anthropometries of the 6-year-old dummies and the ability to obtain complete and accurate contact of the dummy thorax and pelvis regions. Ten 4,448-Newton (1,000-pound) capacity load cells (Transducer Techniques, Temecula, CA) were used to acquire dummy impact force loads (four mounted under each torso and pelvis load plate and 2 mounted under the wooden armrest). The ATD was positioned based on ISO 9790 specifications (1999).

Drop distances from the ATD to the impact surface were 1.0-meter and 0.5-meters, respectively. The wooden armrest was removed for the 0.5-meter drop test per ISO 9790

test requirements. The ATDs used were on loan, and therefore, in an effort not to damage them, the ISO 9790 2.0 meter drop test was excluded from the current study.

WSU 6.8 m/s Rigid Sled Test

A bench and impact wall based on the WSU design documented in Cavanaugh et al. (1990) were scaled from the 50th-percentile male anthropometry sled setup to a size appropriate for the 6-year-old. Five impact beams were used and the locations were scaled to target the shoulder, thorax, abdomen, and pelvis (iliac crest and greater trochanter region). The bench and wall were fixed on the WSU HyGe sled. Two 4,448-Newton (1,000-pound) capacity load cells were installed on the back of the impacted side of each of the five impact beams. Lateral impact force data was acquired at each beam level, consistent with previously specified body regions during impact. Each ATD was seated at a distance from the rigid impacting wall to allow the sled to achieve a constant impact speed of 6.8 m/s relative to the wall before impact occurred.

Data Post Processing and Analysis

Pendulum impact force, load cell data, and ATD lateral acceleration and force data were analyzed. Sensor data were filtered according to the SAE J211-1 Recommended Practice except for the thorax and abdomen pendulum mass accelerometers which were filtered using the FIR 100 filters per ISO 9790.

ISO 9790 biofidelity rating system analysis

The data from replicate runs were aligned using the optimized phase cross-correlation methodology described in Donnelly and Moorhouse (2012). In order to assess the repeatability of the dummy test parameter responses, a single value peak response Percent Coefficient of Variation (%CV), as defined in Moorhouse (2013), was calculated

for each of the aligned test data sets for each of the dummies. The data was aligned at time zero based on initial contact between the dummy and the contact surface. Time zero was determined using synchronized test video and data. Sensor data for each body region (shoulder, thorax, abdomen, and pelvis) were compared among the three ATDs. The biofidelity performance for the three ATDs in lateral impact was assessed against the scaled biofidelity targets published in Irwin et al. (2002). Regional body biofidelity ratings, B_i, for the four body regions tested, were calculated using Eq. (1) (ISO/TR9790, 1999) below:

$$B_i = \frac{\sum_{j=1,2,\ldots m} V_{i,j}\left(\sum_{k=1,2,\ldots n} W_{i,j,k} R_{i,j,k} \Big/ \sum_{k=1,2,\ldots n} W_{i,j,k}\right)}{\sum_{j=1,2,\ldots m} V_{i,j}} \quad (1)$$

where:

$V_{i,j}$ = The weighting factor for each test condition for a given body region

$W_{i,j,k}$ = The weighting factor for each response measurement for which a requirement is given

$R_{i,j,k}$ = The rating of how well a given response meets its requirements

i = The subscript denoting the body region

j = The subscript denoting the test condition for a given body region i

k = The subscript denoting the response measurement for a given test condition, j, and body region, i.

Values for weighting factors, $V_{i,j}$ and $W_{i,j,k}$, were determined through a poll of the ISO/TC22/SC12/WG5 experts and were provided in the ISO 9790 Technical Report (1999). The ratings, $R_{i,j,k}$, were determined through evaluation of the response data by

me and the United States Council for Automotive Research, LLC (USCAR)/Occupant Safety Research Partnership (OSRP) Q-Series ATD Task Group and the assigned $R_{i,j,k}$ values outlined in the ISO 9790 Technical Report as:

$R_{i,j,k}$ = 10 if response meets requirement

$R_{i,j,k}$ = 5 if response is outside requirement,

but lies within one corridor width of requirement

$R_{i,j,k}$ = 0 if neither of the above is met.

Once regional body biofidelity ratings were determined, an overall biofidelity rating, B, was calculated for each of the three tested 6-year-old ATDs using Eq. (2) (ISO/TR9790, 1999) below:

$$B = \frac{\sum_{i=1,2,\ldots m} U_i B_i}{\sum_{i=1,2,\ldots m} U_i} \qquad (2)$$

where:

B=The overall biofidelity rating with a value of 0 (poorest) to 10 (best), and

U_i=The weighting factor for each body region (which was given in ISO 9790).

Based on the ISO 9790 Technical Report, five classifications indicate the ATD's degree of biofidelity. The WG5 experts specified the ATD's biofidelity rating be greater than a value of 2.6 to be suitable for assessing side impact occupant protection. The ISO 9790 Technical Report (1999) degree of biofidelity classifications are described as follows:

Excellent Biofidelity:	$8.6 \leq B < 10.0$
Good Biofidelity:	$6.5 \leq B < 8.6$
Fair Biofidelity:	$4.4 \leq B < 6.5$
Marginal Biofidelity:	$2.6 \leq B < 4.4$
Poor Biofidelity:	$0.0 \leq B < 2.6$

NHTSA biofidelity ranking system (BRS) analysis

External biofidelity of the tested ATDs was analyzed using the BRS method, which included impact force response data. An internal biofidelity analysis was not performed for this study since it would be comprised of only the thorax acceleration and deflection response data. Biofidelity response targets for this analysis were generated using the approach described in Rhule et al. (2013). Since 6-year-old PMHS response data were not available to develop response targets, the upper and lower response corridors from ISO 9790 response data were scaled to a 6-year-old and used to generate a mean biofidelity response curve. The mean biofidelity response curve was then used to develop +/- one standard deviation biofidelity response targets for each of the tests.

Replicate runs for each of the tests were aligned using the optimized phase cross-correlation methodology described in Donnelly and Moorhouse (2012), producing a mean response curve for each ATD for each test. The mean response curves for each of the ATDs for each test was then phase-minimized with the mean biofidelity response curve by using cross-correlation to determine the phase-shift, or lag, which minimizes the squared difference between the mean ATD response curve and the mean biofidelity

response curve. Each ATD mean response curve was then shifted toward the mean biofidelity target response curve by the lag amount (Rhule et al., 2013).

Using this phase-minimized data, the Shape and Magnitude Response Comparison Value (SM Value) and Phase Response Comparison Value (P Value) were calculated. The SM value (or $\sqrt{R}$), is calculated by taking the square root of R. The value R (or DCV/CCV), is the ratio of the cumulative variance between the ATD response and the mean biofidelity response curve (DCV), over the cumulative variance between the mean biofidelity response curve and the mean plus one standard deviation biofidelity curve (CCV). The calculated SM value represents the difference between the ATD's response and the mean biofidelity target response in multiples of standard deviation (Rhule et. al., 2002, 2013). The P value is calculated by taking the ratio of the ATD's phase lag and a standard acceptable lag. The standard acceptable lag is determined by shifting the mean biofidelity response curve with respect to itself and calculating the lag between the shifted and unshifted mean biofidelity response curves such that $\sqrt{R} = 1$. For P values less than 1.0, the ATD's phasing is within tolerance of the one standard deviation of the mean biofidelity response target curve, and if the P value is greater than 1, the ATD's phasing is multiples of standard deviation outside of the mean biofidelity response target curve (Rhule et al., 2013).

SM and P values were determined for each response channel measured and the root mean square (RMS) of these two values was calculated to produce the total biofidelity quality for each response channel. Each response channel RMS value for a given test condition was then averaged to produce an average biofidelity ranking for that test condition. Each body region biofidelity ranking was determined by averaging its test

condition ranks. The overall biofidelity ranking for each ATD was determined by averaging its tested body region rankings (Rhule et. al., 2013). The lower the external biofidelity ranking, the more closely the ATD would tend to respond like a PMHS. According to Rhule et al. (2013), an external biofidelity ranking less than 2.0 would correspond to a dummy response that is as similar to a PMHS as it would be to another human subject.

van Ratingen abdomen pendulum impact biofidelity target assessment

Since ISO 9790 does not include abdomen pendulum impact tests as part of its biofidelity rating assessment, results from the abdomen pendulum tests were visually compared and assessed with respect to abdominal biofidelity targets suggested and published in van Ratingen et al. (1997). These test results were, however, used in the BRS ratings of the three ATDs as one of the external impact tests performed on the abdomen region since the BRS rating system does not define specific tests for analysis but generally refers to pendulum impact testing, drop tests, and sled tests. Figure 3.2.1 illustrates the NHTSA external BRS methodology for this particular study.

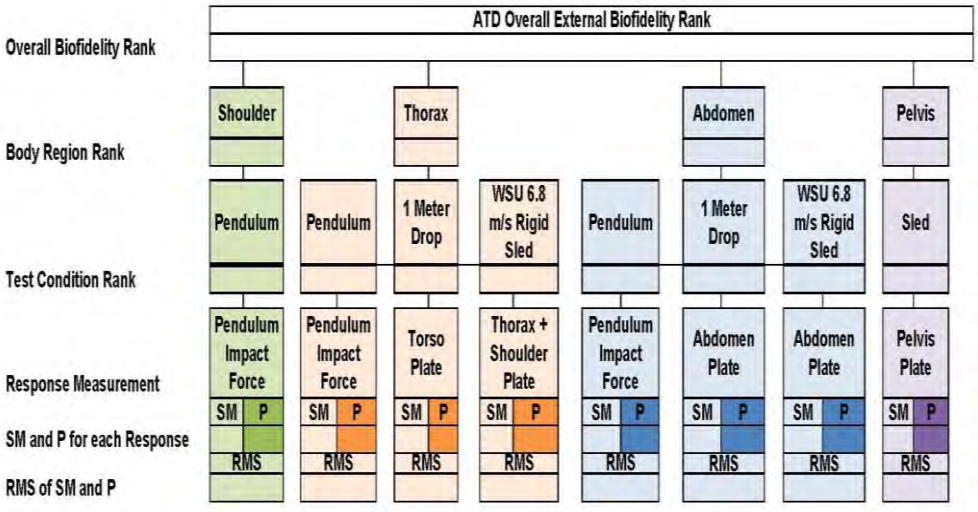

Figure 3.2.5 BRS Calculation Flow Chart for ATD External Biofidelity Ranking

3.3 – Results

Shoulder, thorax, abdomen, and pelvis response data for the three dummies tested were compared to the response requirements described in the ISO/TR9790 Technical Report, as scaled to the 6-year-old in Irwin et al. (2002), and to the biofidelity response targets determined from Rhule et al. (2013). Pendulum impact abdominal response data for the three tested ATDs were compared to the response corridor suggested in van Ratingen et al. (1997).

An example of the response requirement data comparisons for both the ISO 9790 biofidelity rating analysis and the BRS are shown for the shoulder pendulum impact test in Figure 3.3.1. All other ISO 9790, BRS biofidelity, and van Ratingen biofidelity response comparison graphs for the three ATDs tested, along with a summary table of tests per body region, are provided in the Appendix A.

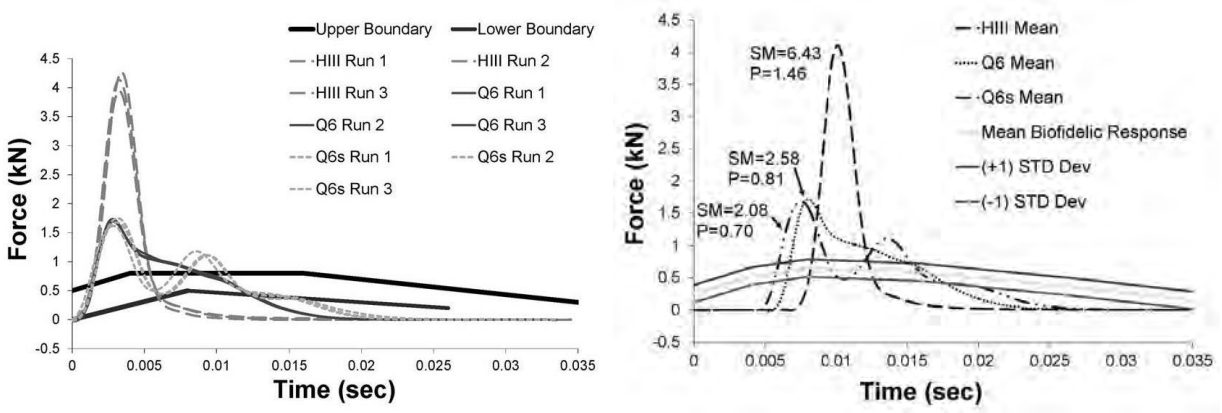

Figure 3.3.1 ISO 9790 Biofidelity Analysis (Left Plot) and BRS Analysis (Right Plot), Respectively, of ISO 9790 4.5 m/s Lateral Impact to Shoulder

ISO 9790 analysis regional and overall biofidelity ratings for each of the three tested 6-year-old ATDs are provided in Table 3.3.1. Values for the HIII 6-year-old biofidelity ratings for all four of its tested body regions were less than 2.6. The HIII 6-year-

old would be considered inappropriate, based on the ISO 9790 WG5 experts specification that the ATD's biofidelity rating be higher than a value of 2.6, for assessing side impact occupant protection. Based on the ISO 9790 biofidelity rating system, the Q6 and Q6s were determined to have marginal biofidelity at the shoulder (Q6 rating = 2.86; Q6s rating = 3.57) and abdomen (Q6 rating = 4.17; Q6s rating = 4.35). The Q6s resulted in a good ISO lateral impact biofidelity rating of the thorax (Q6s rating = 6.75), whereas the Q6 was found to have a fair biofidelity rating (Q6 rating = 6.19). The HIII dummy would be considered unsuitable and the Q-series dummies would be considered marginal for assessing side impact occupant protection based on their overall ISO biofidelity ratings (HIII rating = 0.56; Q6 rating = 3.53; Q6s rating = 3.87), according to the ISO 9790 WG5 experts specification.

Table 3.3.1 ISO 9790 Analysis Regional and Overall Biofidelity Ratings

Results – ISO 9790 Biofidelity Rating of 6 yo ATDs in Lateral Impact

BODY REGION	HIII	Q6	Q6s
Shoulder	0.00	2.86	3.57
Thorax	0.75	6.19	6.75
Abdomen	1.25	4.17	4.35
Pelvis	0.00	0.00	0.00
Total Biofidelity Rating	0.56	3.53	3.87

Overall Rating

8.6 ≤ B≤ 10.0	Excellent Biofidelity
6.5 ≤ B≤ 8.6	Good Biofidelity
4.4 ≤ B≤ 6.5	Fair Biofidelity
2.6 ≤ B≤ 4.4	Marginal Biofidelity
0.0 ≤ B≤ 2.6	Unacceptable Biofidelity

BRS rankings for the three tested ATDs are provided in Table 3.3.2. According to the BRS external biofidelity ranking (Rhule et al., 2013), values less than 2.0 correspond to a dummy response that is as similar to a PMHS as it would be to another human subject (or a dummy response that is within two cumulative standard deviations of the mean PMHS response data). Based on the BRS ranking system, all three 6-year-old ATDs were found to have a highest biofidelity ranking at the pelvis (HIII ranking = 4.97, Q6 ranking = 5.06, Q6s ranking = 5.33), which indicates less than PMHS-like qualities.

Table 3.3.2 BRS Analysis Regional and Overall Biofidelity Rankings

Results - NHTSA External Biofidelity Rank

BODY REGION	HIII	Q6	Q6s
Shoulder	6.51	2.70	2.19
Thorax	2.92	1.64	2.10
Abdomen	3.39	2.97	3.13
Pelvis	4.97	5.06	5.33
Overall External Biofidelity Ranking	4.45	3.09	3.19

Overall Rating

Lower External Biofidelity Ranking indicates a more biofidelic ATD

External Biofidelity Rank of B<2.0 can be considered to respond as much like a PMHS as would another human subject

The shoulder and thorax of the HIII also resulted in less than PMHS-like rankings (HIII shoulder ranking = 6.51; HIII thorax ranking = 2.92). The shoulder for the Q6 and Q6s (Q6 ranking = 2.70; Q6s ranking = 2.19) were within one standard deviation of NHTSA's 2.0 level, with the Q6s performing more PMHS-like than the Q6. The BRS lateral impact biofidelity ranking for the abdomen region of all three ATDs performed with less than PMHS-like response qualities (HIII ranking = 3.39, Q6s ranking = 3.13, Q6 ranking

= 2.97). The lateral impact biofidelity ranking for the Q6 thorax (Q6 ranking =1.64) fell within the BRS guidelines l while the Q6s thorax (Q6s ranking = 2.10) was 0.1 standard deviations above the BRS biofidelity response 2.0 level. All three 6-year-old ATDs were above the BRS external biofidelity 2.0 level in overall biofidelity rankings (HIII ranking = 4.45; Q6 ranking = 3.09; Q6s ranking = 3.19), indicating a dummy response is less than mean PMHS-like qualities by more than three cumulative standard deviations.

3.4 – Discussion

The biofidelity results presented in this paper were obtained to better understand how the mechanical response of each dummy compared to biofidelity response corridors. These corridors were based on those for the 50th-percentile male but were scaled to the size and material properties of a 6-year-old child. This assessment will help further develop the biofidelity of child ATDs for future safety research especially with respect to side impacts.

The Hybrid III ATDs are frontal impact dummies and were never designed for side impact testing. In addition, **the Q6 is a frontal impact dummy**, although it was originally intended to be an omni-directional ATD. Nevertheless, it was deemed worthwhile to include the Q6 and 6-year-old HIII dummies because comparing the responses and design differences of the three ATDs could help lead to better design of child side impact dummies.

Shoulder Design and Biofidelity

The biofidelity of the ATD shoulder, one of the first regions contacted in lateral impact, is very important. The shoulder of the HIII dummy consists of a metal yoke which is attached to the clavicles. The motion of the entire assembly is controlled by various

pivots and rubber and urethane components. The Q6 dummies' shoulder consists of a more human-like ball-and-socket joint simulating the glenohumeral joint. Molded and compressible rubber and other components attach the joint to the sternum and spine, allowing for better load transfer. Figure 3.4.1 depicts the design differences in the three 6-year-old ATD shoulders from a rear view.

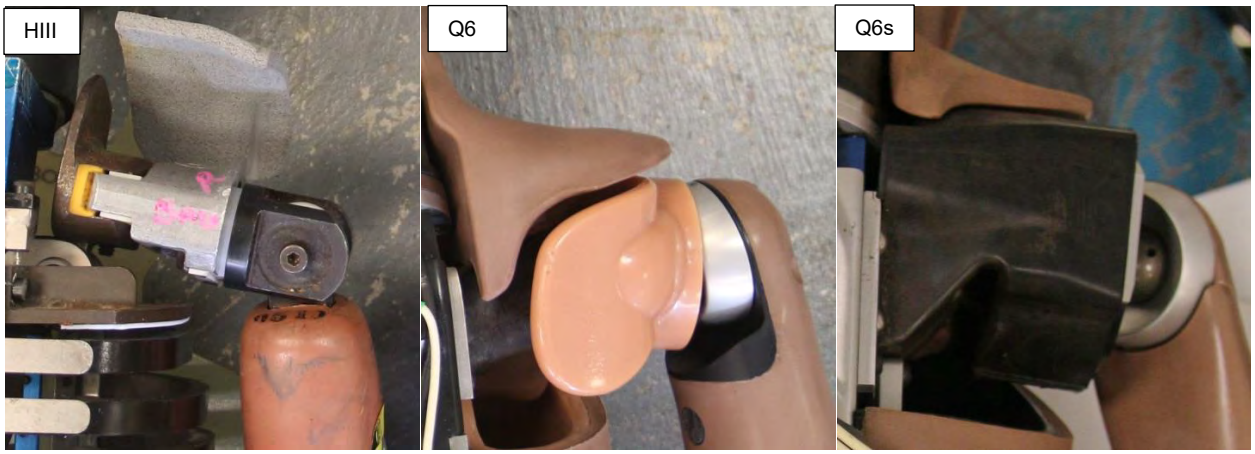

Figure 3.4.1 Visual Comparison of 6-Year-Old ATDs Shoulder Design - Rear View

The shoulders of the Q6 and Q6s are more biofidelic in design for lateral impact than the HIII 6-year-old shoulder. The Q6s shoulder design had the best biofidelity ranking or PMHS-like qualities in this region with a 3.57 ISO rating and a 2.19 BRS ranking. The Q6 followed with an ISO rating of 2.86 and a BRS ranking of 2.70. The Hybrid III had an ISO rating of 0.0 and had a 6.52 BRS rank. Because the shoulder is typically the first region struck in side impact, its design and biofidelity are crucial in order to properly characterize dummy kinetics and kinematics during the impact sequence. Recent efforts have been made by Suntay et al. (2011) to quantify pediatric shoulders stiffness. Ita et al. (2014) then compared this data to the Q3s ATD. Although the lack of child impact response data and representative animal surrogates make it difficult to advance the

design of the pediatric shoulder region in lateral impact, efforts should continue to be made to advance research in this area.

Thorax Design and Biofidelity

The thorax of the 6-year-old HIII is comprised of an aluminum thoracic spine box with six individual ribs of spring steel and polymer-based damping materials. The Q6 and Q6s dummies' thorax consist of an aluminum thoracic spine box and a single, deformable, more child-like shaped synthetic composite or a PVC outer skin layer bonded to a urethane rib cage, respectively (Q6 User Manual, 2012; Q3s User Manual, 2012). The Q6s rib cage is reinforced by a steel insert, and the corners of its rib cage are redesigned compared to the Q6 rib cage in order to avoid stress concentrations and improve fatigue resistance (Q3s User Manual, 2012). Figure 3.4.2 illustrates a comparison of the thorax design of three 6-year-old ATDs from a frontal view.

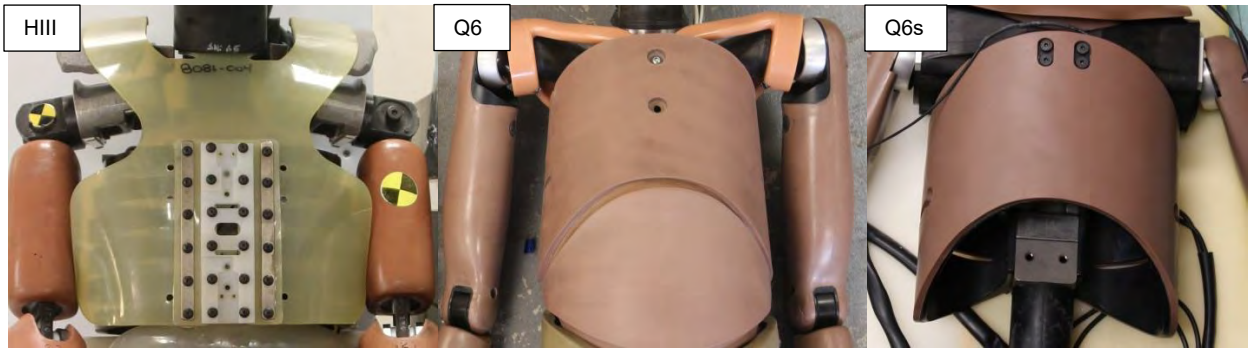

Figure 3.4.2 Visual Comparison of 6-Year-Old ATDs Thorax Design - Frontal View

The updated ribcage design of the Q series ATDs provides better lateral compliance as illustrated in the thorax test results of this study. The Q6s performed closer to the response corridors and therefore resulted in a better biofidelity rating or PMHS-like qualities (6.75 ISO rating and 1.69 BRS ranking) than the Q6 (6.19 ISO rating and 2.02 BRS ranking) and HIII 6-year-old (0.75 ISO rating and 3.38 BRS ranking) based on both

rating systems analyzed. To the best of the author's knowledge, Seacrist et al. (2014) is currently the only other known study to analyze all three 6-year-old ATDs in lateral impact. Their study utilizes a different test methodology and outcome metrics than the current study. The 6-year-old ATDs were subjected to low speed lateral and oblique sled tests. The whole-body kinematics and responses of the ATDs were compared to those of human volunteer's ages 6 to 11 years old subjected to similar sled tests. Despite the differences in test methodology and outcome metrics, Seacrist et al. (2014) concluded that the Q6s ATD more closely matched the pediatric human volunteer belt-to-torso interaction and kinematics compared to the Q6 or HIII. These findings appear to match well with the more biofidelic or PMHS-like qualities observed in the Q6s in lateral impact of the thorax compared to the Q6 or HIII dummies during the current study.

Abdomen Design and Biofidelity

The abdomen used in the 6-year-old HIII for the current analysis is the Ford-designed abdomen, which is a fluid-filled compressible silicone abdominal insert that sits in the space between the bottom of the rib cage and the pelvis structure. The Q6 and Q6s both possess a foam covered by plastic skin abdomen that sits in the space between the rib cage and the pelvic structure. Figure 3.4.3 shows a comparison of the abdomen design of all three 6-year-old ATDs from a frontal view.

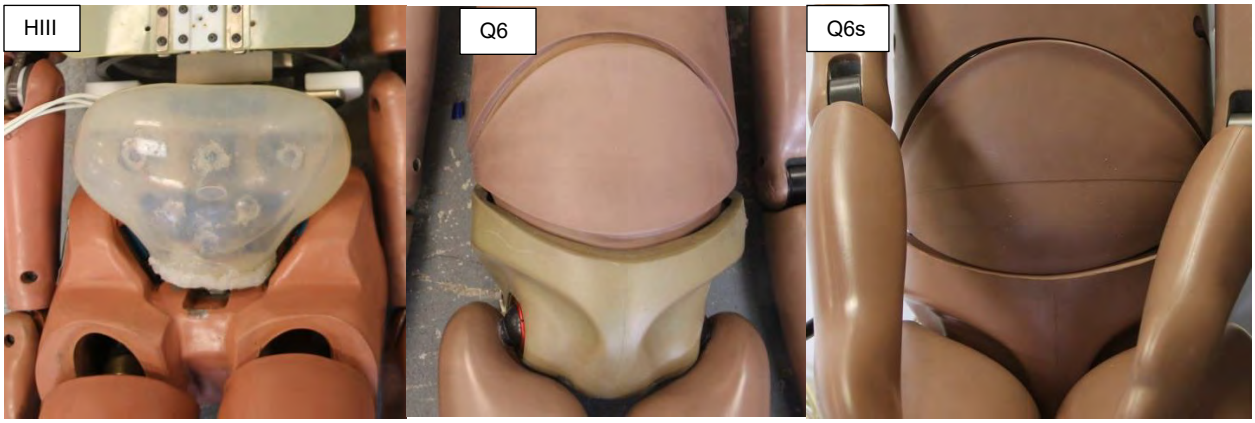

Figure 3.4.3 Visual Comparison of 6-Year-Old ATDs Abdomen Design - Frontal View

The current study showed that the abdomen test results of the Q6 and Q6s follow the ISO response corridor requirements relatively closely in the drop tests and sled tests performed. The Q6s abdomen performed closer to the ISO 9790 response corridors and therefore resulted in a better ISO biofidelity rating (4.35 ISO rating - fair) than the Q6 abdomen (4.17 ISO rating- marginal). The HIII Ford-designed abdomen received a 1.25 ISO rating which is considered biofidelically unacceptable. The Q6 resulted in a better BRS biofidelity ranking (2.97 BRS ranking) for the abdomen region than the Q6s (3.13 BRS ranking). The HIII Ford-designed abdomen region was rated a 3.38 using the BRS ranking system. Based on the BRS ranking system, all three ATDs were determined to have less than PMHS-like qualities. The more PMHS-like quality ranking the HIII Ford-designed abdomen received using the BRS ranking system versus the unacceptable biofidelic ranking the HIII Ford-designed abdomen received using the ISO ranking method may be a function of the difference in methodology between the two rating systems analyzed. In addition, differences in response seen with the HIII Ford-designed abdomen compared to the Q-series dummies abdomens may be a function of the differences in the Q6 and Q6s abdomen and rib design, the fact that the Q6 upper arm is longer than the HIII and covers or shields this area to a certain extent (even though the arms were brought

forward as if to have the hands resting on the dummy's lap) during the drop and sled impact tests, or a combination of factors. The HIII 6-year-old Ford-designed abdomen, however, appeared to perform closer to the pendulum response corridor requirements than the other dummies' abdomens. The arm is moved out of the way for the pendulum impact and therefore exposes more of the HIII abdomen itself based on the nature of its abdomen and rib design.

The wooden armrest load surface used in the 1.0-meter vertical drop tests in the current study was not scaled down to the 6-year-old because it was interpreted by the author to be representative of a simulated armrest impacted in a vehicle side impact environment (as described in ISO 9790 Abdomen Impact Response Requirement 1 (1999)). To more directly assess the child ATD's abdomen impact response, the simulated armrest (offset impact surface) should be scaled in future vertical drop testing as described in Irwin et al. (2010).

Pelvis Design and Biofidelity

The pelvis can also be the location of first contact in a side impact; therefore, pelvis design also plays a large role in the ATD's overall lateral impact response and biofidelity. The 6-year-old HIII has a welded aluminum human-shaped pelvis casting with optional biaxial load cells on each ilium. The pelvis is covered by vinyl skin over urethane foam and molded into a seated position. The HIII 6-year-old's hip contains ball-jointed femur assemblies located within the pelvis casting in the lower torso which act as hip joints, allowing for hip joint rotation. A shaft located on the end of the femur attaches to the ball-jointed femur assembly in order to connect the HIII's femur to its pelvis. (HIII 6-Year-Old User Manual, 2009). The Q6 and Q6s pelves are comprised of a similar pelvis casting

which sits inside a foam pelvic flesh. The Q6 and Q6s have ball-and-socket hip joint assemblies such that the ball attached to the upper legs can fit into the socket openings on the left and right sides of the pelvis casting. The hip joint socket of the Q6s is constructed to allow for some inward deflection of the hip joint (Carlson et al, 2007). Figure 3.4.4 shows a comparison of the pelvis design of three 6-year-old ATDs from an oblique view.

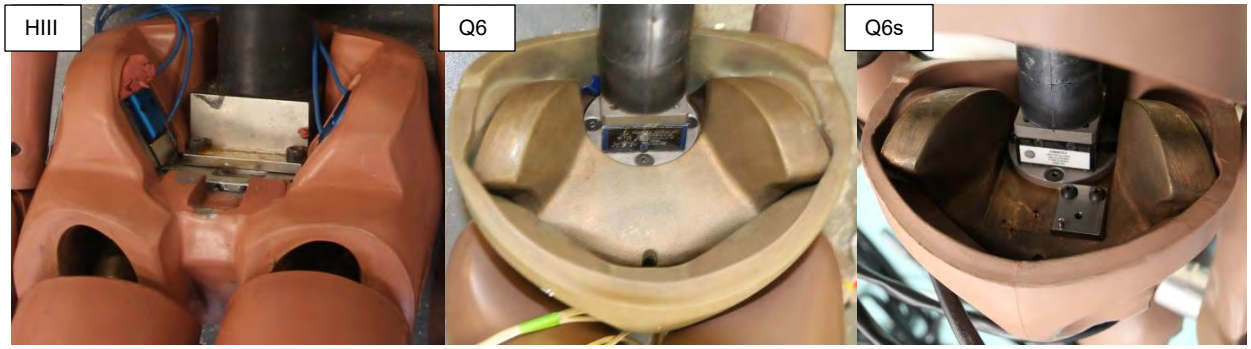

Figure 3.4.4 Visual Comparison of 6-Year-Old ATDs Pelvis Design - Oblique View

Like the shoulder, lack of child impact response data and representative animal surrogates make it difficult to advance the design of this body region in lateral impact. However, efforts should be made to continue to advance research in this area in order to properly characterize dummy kinetics and kinematics during lateral impact. The pelvis yielded the lowest biofidelity rating of all body regions using both rating systems. All ATDs scored a zero ISO biofidelity rating for the pelvis. The HIII did have a better BRS biofidelity ranking (4.97 BRS ranking) for the pelvis than the Q-series ATDs (5.06 BRS ranking for Q6 and 5.33 BRS ranking for Q6s). This can most probably be attributed to the more stable seated pelvis design of the HIII compared to the compressible ball-in-socket joints of the Q-series ATDs.

3.5 – Conclusions

In lateral impact, overall, all three ATDs were found to be more biofidelic in the thorax and abdomen than the shoulder and pelvis, with the pelvis being the least biofidelic of all four tested body regions. With respect to the BRS external ranking, none of the three tested 6-year-old ATDs had an overall ranking of 2.0 or less. Based on this ranking system, none of the three ATDs have PMHS-like response qualities. With respect to the ISO biofidelity rating, the HIII dummy would be considered unsuitable and the Q-series dummies would be considered marginal for assessing side impact occupant protection. Further ATD development with respect to the thorax, abdomen, shoulder, and pelvis is clearly necessary to advance the biofidelity and usefulness of child ATDs in lateral impact occupant safety research. With the shoulder and pelvis being the first body regions contacted in lateral impact, future research to advance the biofidelity of these body regions should be a main focus as they tend to take the brunt of the force and shield more vulnerable body regions such as the thorax and abdomen. Testing performed by Tylko et al. (2009) exemplify this with results from a Q3s ATD in near side vehicle-to-vehicle impacts showing highest accelerations experienced at the hip, followed by the chest, and then the head. Recent efforts have been made toward advancing knowledge of pediatric shoulder response; however, efforts should also be made to advance pediatric pelvis response in order to enhance pediatric ATD full body response in lateral impact.

CHAPTER 4 – LATERAL IMPACT ASSESSMENT AND COMPARISON OF APPROPRIATE AGE AND SIZE TORSO CADAVERIC PORCINE SURROGATES FOR FORMATION OF SURROGATE RESPONSE CORRIDOR SCALING RELATIONSHIP (SPECIFIC AIM 3)

4.1 – A Review of the Use of Surrogate Scaling Techniques in Research

Due to a paucity of pediatric PMHS for use in testing over history, researchers have had to consider other avenues to help establish response corridors for child crash test dummy design and development. Response corridor development is central to establishing ATD response similar to that of humans. Normalization and scaling of response data has been an indirect technique to establish pediatric response biofidelity corridors for crash test dummy design and development, both through scaling of adult PMHS data and animal surrogate test data to the pediatric level. Normalization of data can be described as the method by which measured impact responses from individual specimen tests with variable characteristics are brought into a standard. Scaling, particularly in impact biomechanics, can be used as a process to convert normalized response data from one standard group to another; for example, mid-size male lateral impact response corridor data to the pediatric population. (Petitjean et. al, 2015).

Normalization and scaling techniques have been used for many years to establish response corridors from a standard group of data, using both human and animal surrogates.

For instance, Reed et al. (2001) performed an analysis of already existing child anthropometry databases to develop reference dimensions for the 6-year-old child for an Occupant Classification ATD (OCATD). Data included, among others, stature, weight, erect sitting height, shoulder breadth, shoulder-elbow length, chest breadth, waist breadth, and hip breadth. Comparison of the database data analyzed in the Reed et al.

(2001) study for use to develop the OCATD to that of the data used as scaling parameters in Irwin and Mertz (1997) is presented in Table 4.1.1 below.

Table 4.1.1 Irwin and Mertz (1997)/Reed et al. (2001) Characteristic Dimensions Comparison

Dimension Description	6-Year-Old (Irwin and Mertz, 1997)	6-Year-Old (Reed et al., 2001)
Standing Height (mm)	1168	1193
Erect Sitting Height (mm)	635	653
Shoulder Breadth (mm)	290	294
Shoulder to Elbow (mm)	234	243
Chest Depth (mm)	143	--
Chest Breadth (mm)	194	188
Waist Breadth (mm)	168	194
Hip Breadth (seated) (mm)	230	227

Eppinger (1976), in evaluating PMHS thoracic impact data from several different sources, used a basic linear normalization approach (labeled a “scaling approach” by the authors) which assumed linear relationships between the central constraints of length, mass, and time as well as equal density and modulus of elasticity between the mass and its reference (dummy).

Mertz (1984) derived an impulse-momentum normalization technique for specific body regions based on segment characteristics and type of impact test. This approach used mass and stiffness ratios along with assumptions of lumped mass and spring models. Mertz et al. (1989) established scaling criteria for the 5th percentile female and

95th percentile male Hybrid III ATDs from the 50th percentile male Hybrid III ATD, who's biofidelity was based on dynamic responses relative to PMHS and limited volunteer data (Foster et al., 1977). Geometric and mass scale factors were used to scale the Hybrid III 50th percentile male design drawings and biomechanical impact response requirements to the corresponding target design size for preservation of scaled biofidelity response in each ATD design (Mertz et al., 1989). Irwin and Mertz (1997) used the scaling techniques from Mertz (1984, 1989) to develop biomechanical frontal impact response corridors for the HIII 3-year-old and 6-year-old child dummies and the Child Restraint Air Bag Interaction (CRABI) child dummies representing the 6-month, 12-month, and 18-month child. In 2002, these similar scaling techniques were used to develop guidelines for assessing the biofidelity of dummies of all ages and sizes in side impact (Irwin et al., 2002).

Pintar et al. (2000) developed scaling factors as a percentage of adult properties to help develop neck strength characteristics of children using data collected regarding both nondestructive bending and tensile stiffness of individual functional spinal units from a caprine (goat) model. Ching et al. (2001) used cadaveric baboon (*Papio anubis*) spines to study the outcome of spinal development on tensile mechanics of isolated cervical functional spinal units. A skeletal maturation index based on computed tomographic (CT) assessment was used to scale animal surrogate age to human age equivalence. Luck et al. (2008) studied eighteen pediatric PMHS osteoligamentous head-neck complexes in tension based on an age range of 20 weeks to 14 years. Findings in this study were used to assess animal surrogate cervical spine age-property scaling relationships to the prediction of human pediatric response.

Porcine have been used as a surrogate for human adults in a number of past studies (Gogler et al., 1977, Viano et al., 1989B, Viano et al., 1989C, Miller, 1989, Rouhana et al., 1989).

Prasad and Daniel (1984) used piglets as surrogates to children to develop preliminary head, neck, and torso injury tolerance data for the child surrogates and compare it to a 3-year-old child test dummy. A subjective anatomical comparison between the piglet and human's major organs were made with respect to injury potential. It was determined that the piglet's thoracic-abdominal organ masses were similar to those of a 3-year-old child; however, initial sternal deflection would increase intra-thoracic volume in the piglet, whereas it would decrease intra-thoracic volume in the child based on the difference in their rib cage design. The piglet was also found to have a larger abdomen and a longer, more rigid ribcage, which would in effect better guard the liver and spleen from injury compared to a child. For each piglet test, a similar test was run using a 3-year-old child dummy in an attempt to associate dummy response with animal injury. Engineering judgment was used to determine validity of response parameters.

Kent et al. (2006) performed an anatomically focused necropsy study of 25 swine, aged from birth to maturity, in order to develop a properly sized and aged porcine surrogate model for the human 6-year-old. The study established human anatomy and organ mass age trends. Eight thoracoabdominal anatomical parameters were quantified for the human 6-year-old and used as targets to identify the porcine surrogate model that best characterized the 6-year-old human with respect to overall size through an optimization solution technique. These parameters included liver mass, kidney mass, lung mass, sitting height, waist breadth, waist to superior sternum measurement, waist

depth, and trunk mass. The data collected for the Kent et al. (2006) 6-year-old swine to human optimization study are provided in Table 5.1.2, below. Once a proper pig model was determined, this surrogate was tested to determine abdominal response characteristic of the swine through seatbelt loading. Although this comparison was made direct to the 6-year-old in the Kent et al. (2006) study, no attempt was made to establish biomechanical response data for any other age equivalent porcine model to human relationship. Kent et al. (2009) and Lamp et al. (2010) compared 6-year-old PMHS thoracic and abdominal belt loading to the Kent et al. (2006) previously developed 6-year-old porcine model to determine the efficacy of the porcine surrogate model in predicting human response.

Table 4.1.2 Kent et al. (2006) Parameter Values and Sources Used for Porcine Model to 6-Year-Old Human Optimization

Parameter	Value used to represent 6-year-old human	Primary data source	Secondary data sources referenced for consistency
Liver mass	660 g	Stocker and Dehner (2002), average of male and female	None
Kidney mass	133 g (both)		
Lung mass	328 g (both)		
Sitting height, supine (measurement 16 in Figure 4)	64.5 cm	Anthrokids, average of male and female	Arbogast et al. (2005), Hybrid III
Waist breadth (measurement 67 in Figure 4)	18.5 cm		GEBOD
Waist to superior sternum (see Figure 4)	25.4 cm		None
Waist depth	15.1 cm	GEBOD	Arbogast et al. (2005), Hybrid III
Trunk mass	11.8 kg	Anthrokids for whole-body mass, with ratio of whole-body to trunk mass based on GEBOD	Arbogast et al. (2005) and Hybrid III for whole-body mass.

4.2 – Swine Thoracic and Abdominal Anatomy

The pig's thoracic region spans from the base of the neck, superiorly (cranially), to the diaphragm, inferiorly (caudally). It consists of the rib cage (thoracic vertebrae, ribs and sternum) and its underlying organs (primarily the heart and lungs). Pigs typically have 14 or 15 pairs of ribs, but have been found to vary anywhere from 13 to 17 pairs of ribs. Like humans, the first 7 pairs of ribs attach to the sternum via shorter expanses of cartilage (Sack, 1982). The pig's thoracic skeleton is illustrated in Figure 4.2.1 (Sack, 1982), below.

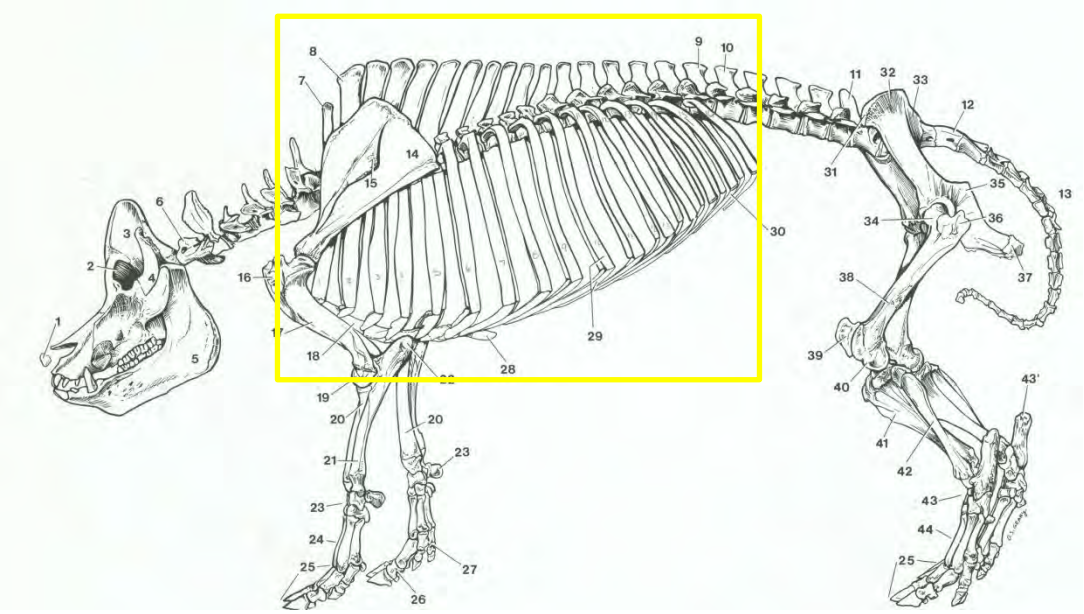

Figure 4.2.1 Swine Thoracic Skeleton Identified by Yellow Box (Sack, 1982)

The heart typically extends from the 2nd to the 5th ribs, occupies somewhat more than the anterior (ventral) half of the thoracic space, and like many other mammals, lies more to the left of the median plane (Sack, 1982). Porcine lungs are located within the rib cage, similar to humans; however, where the human left lung consists of two lobes and the right lung three lobes, the pig left lung consists of three lobes and the right lung consists of four lobes (Sack, 1982). Figures 4.2.2 and 4.2.3, below, show the location of the heart and lungs within the rib cage of the swine and

humans, respectively, for comparison.

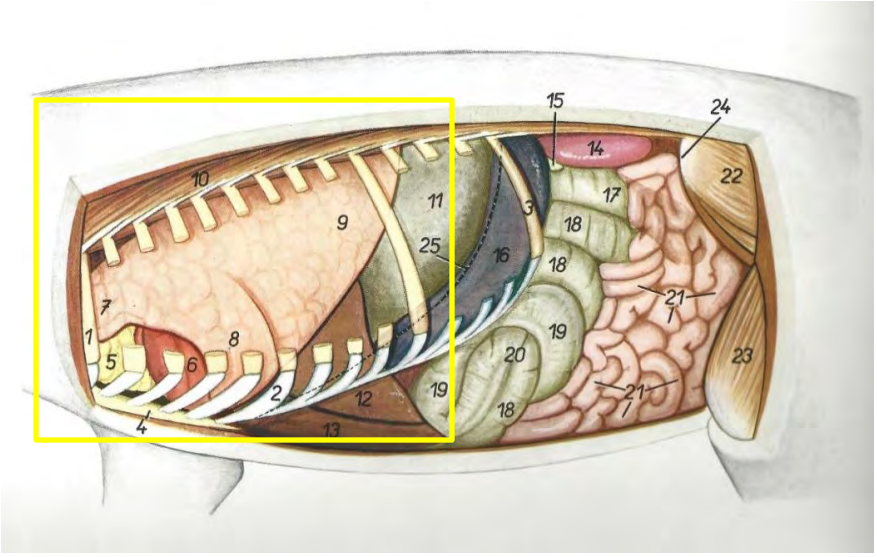

Figure 4.2.2 Swine Anatomy (Heart and Lungs Highlighted by Yellow Box) ("Atlas of Topographical Anatomy of the Domestic Animals – Volume 1" by Peter Popesko, W.B.Saunders Company, Philadelphia, 1977, Figure 96, Page 100.)

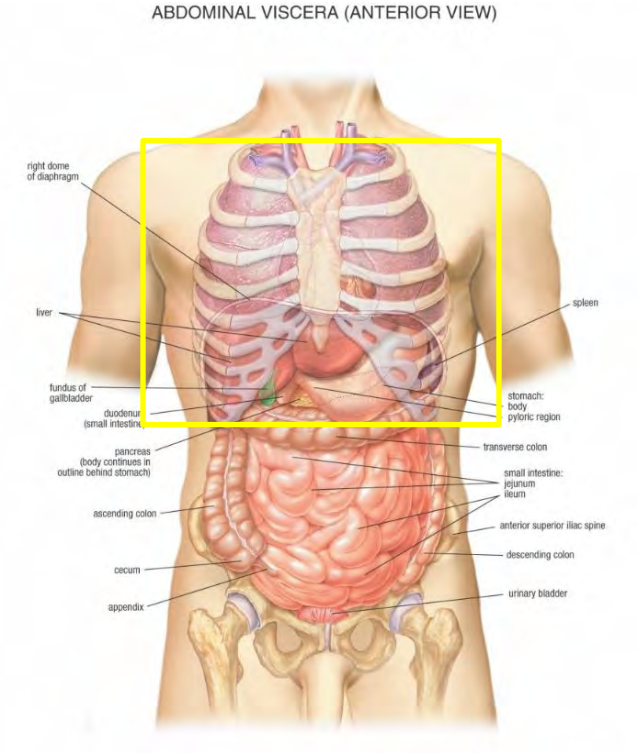

Figure 4.2.3 Human Anatomy (Heart and Lungs Highlighted by Yellow Box) (https://anatomyclass123.com/diagram-of-bones-of-thorax/diagram-of-bones-of-thorax-anatomy-of-chest-and-abdomen-human-anatomy-library/)

The pig's abdominal cavity extends from the diaphragm to the pelvis. Major abdominal organs include the liver, stomach, spleen, intestines, pancreas, and kidneys. The porcine liver is positioned inferior (caudal) to the diaphragm, and consists of five lobes, as opposed to a human liver which has four lobes. The porcine liver is covered by the ribs except anteriorly (ventrally) and extends further inferiorly (caudally) on the right than the left (Sack, 1982). The porcine stomach is in contact with the liver and diaphragm superiorly (cranially) and in contact with the spleen to the left, the intestines anteriorly (ventrally), and the pancreas posteriorly (dorsally) (Sack, 1982). The porcine spleen is long and narrow, as compared to the oval-shaped spleen of the human, and is located between the stomach and the intestines (Sack, 1982). As observed in Figures 4.2.2 and 4.2.3 above, the general location of the major abdominal organs are similar in the swine and human.

Any animal model has accompanying limitations in terms of its ability to represent human response. There are also associated limitations with respect to scaling animal models to reflect human response due to variances in size and species. Scaling techniques have been developed in past research with respect to the cervical spine. However, there is no research known to this author that establishes scaling of animal surrogate thorax and abdomen lateral impact response data to the human adult and pediatric thorax and abdomen.

4.3 – Methods

In order to provide additional response corridor research data for pediatric ATD biofidelity enhancement, development of a scaling relationship using animal surrogate test data to apply to the pediatric level is very valuable. For this reason, lateral pendulum

impact testing of appropriate age and size torso cadaveric porcine surrogates of human 3-year-old, 6-year-old, 10-year-old, and 50th percentile male equivalent were performed in order to compare the actual swine test data to already established human response corridors scaled from the 50th percentile human male to the pediatric level. Equivalent human 3, 6, and 10-year-old as well as the 50th percentile adult male ages were chosen based on already established ATDs and human pendulum lateral impact response corridors at these age levels.

Porcine Surrogate Size Determination

The methodology proposed by Kent et al. (2006), based on a necropsy and regression analysis involving specific anthropometry and organ masses, including supine seated height, waist to superior sternum dimension, abdominal breadth, abdominal depth, kidney mass, liver mass, lung mass, and trunk mass for both pigs and humans was used in this study in an attempt to determine appropriate age and size domestic swine (*sus scrofa domesticus)* surrogates, equivalent to a human 3-year-old, 6-year-old, 10-year-old and 50th percentile male for the thorax and abdomen regions. The human 3-year-old, 6-year-old, and 10-year-old data and similar data for 25 pigs, ages 14 days to 429 days with whole body mass ranging from 4 kg to 101 kg, were already collected by Kent et al. (2006) in their research and was utilized in the current study. Similar data was then collected in the current study for the 50th percentile human male. Data for the 50th percentile human male trunk weight was determined using the weight of the upper and lower torso assemblies for the Hybrid III 50th percentile male ATD (HIII 50th Male User Manual, 2012). Whole body mass and supine seated height for the 50th percentile human male were also taken from the Hybrid III 50th percentile male ATD (HIII 50th Male User Manual, 2012).

Organ masses for the 50th percentile human male were obtained from Molina and DiMaio (2012), while the waist to superior sternum, chest depth, chest breadth, and abdominal breadth measurements for the 50th percentile human male were taken from the Anthropometry and Biomechanics section of the National Aeronautics and Space Administration (NASA) Space Flight Human-Systems Standard Volume 1 (NASA-STD-3000, 1995). The abdominal depth measurement for the 50th percentile human male was taken from Kodak's Ergonomic Design for People at Work, 2nd Edition (Chengular et al., 2004). The chest breadth and chest depth measurements for the 3-year-old, 6-year-old, and 10-year-old were taken from Reed et al. (2005). Tables 4.3.1 and 4.3.2, below, provide the specific human and porcine anthropometry and organ masses obtained and used for the current study, respectively.

Table 4.3.1 Specific Human Anthropometry and Organ Masses

Subject	3-year-old human (similar measurements)	6-year-old human (similar measurements)	10-year-old human (similar measurements)	50th percentile male human (similar measurements)
Whole-body mass (kg)	14.1	21	33.1	77.7
Supine seated height (cm)	58.1	64.5	73.3	94.2
Waist to superior sternum (cm)	23.1	25.4	29.7	40.9
Abdominal depth (umbilicus) (cm)	13.9	15.1	16.7	23.1
Abdominal breadth (deepest) (cm)	16.1	18.3	21.9	35.8
Chest depth (cm)	15.9	18.5	22	25
Chest breadth (cm)	16	19.7	23.9	33.2
Liver mass (g)	552	660	901	1561
Right kidney mass (g)	50.35	66	88.25	129
Left kidney mass (g)	51.7	67	89.9	137
Lungs (both) mass (g)	118.27	328	233.15	840
Trunk mass (kg)	6.00	11.82	16.85	40.23

Table 4.3.2 Specific Porcine Anthropometry and Organ Masses (Kent et.al. (2006))

Subject	04-P-10	04-P-11	04-P-12	04-P-13	04-P-14	04-P-15	04-P-16
Age when studied (days)	82	91	46	117	62	134	129
Whole-body mass (kg)	13.5	30.3	13	32.8	19.1	47	39.3
Top of head to tail base ("sitting" height) (cm)	65.8	84.5	66	84.7	73.5	97	88.5
Cranial end of sternum to umbilicus (cm)	28.5	40	31	39	34	43	41
Abdominal depth (umbilicus) (cm)	11.7	15.6	11	17.7	15	23.5	19.1
Abdominal breadth (deepest) (cm)	20.3	27	21.1	27	24.5	28.7	28.8
Liver mass (g)	472.7	879.2	552.8	958	870.6	1350	1100
Right kidney mass (g)	30.4	75.6	42.3	77.2	58.5	115.6	92.9
Left kidney mass (g)	41.9	75.4	36.6	82.2	66.4	113.9	94.8
Lungs (both) mass (g)	184.9	290.7	303.1	295.3	327.8	544	405.4
Trunk mass (kg)	6.82	17.02	7.55	20.46	11.93	28.44	23.62

Subject	04-P-17	04-P-18	04-P-19	04-P-20	04-P-21	04-P-22
Age when studied (days)	89	14	162	28	33	429
Whole-body mass (kg)	27	3.75	101.2	5.6	6.2	69.4
Top of head to tail base ("sitting" height) (cm)	82	42.1	120	48.2	49	128
Cranial end of sternum to umbilicus (cm)	37	17	52	21	20	53
Abdominal depth (umbilicus) (cm)	17.5	9.1	29.5	8.5	9	19.5
Abdominal breadth (deepest) (cm)	27	12.1	41	14.1	15.7	30
Liver mass (g)	1045.1	130	3160	173.5	218.3	1878.9
Right kidney mass (g)	81	16	284.3	18.3	22.4	175.7
Left kidney mass (g)	82	16.5	257	18.6	22.8	179
Lungs (both) mass (g)	499.6	91.2	631.8	92.2	78.4	560.6
Trunk mass (kg)	16.82	2.044	64.78	3.25	3.33	41.52

Subject	04-P-23	04-P-24	04-P-25	04-P-26	04-P-27	04-P-28
Age when studied (days)	40	116	48	49	55	61
Whole-body mass (kg)	8.6	47.5	11.5	11	13.4	14.5
Top of head to tail base ("sitting" height) (cm)	55.5	99	61.5	62.5	64	69
Cranial end of sternum to umbilicus (cm)	23	45	27.5	26.3	26	29
Abdominal depth (umbilicus) (cm)	10.75	18.5	11.5	11	12.8	12.5
Abdominal breadth (deepest) (cm)	18.5	30.2	19.51	20	21.7	20
Liver mass (g)	304.9	1490	484	353.1	606.6	475.3
Right kidney mass (g)	26.1	154.7	39.3	36.5	50.7	53.9
Left kidney mass (g)	26.1	147.2	43.4	37.6	46.1	50.8
Lungs (both) mass (g)	93.7	580.1	137.8	120.1	164.6	170.8
Trunk mass (kg)	4.93	28.63	6.76	6.24	8.12	8.31

Subject	04-P-29	04-P-30	04-P-31	04-P-32	04-P-33	04-P-34
Age when studied (days)	211	76	82	132	89	97
Whole-body mass (kg)	96	14.5	16.1	73.4	21.2	19.7
Top of head to tail base ("sitting" height) (cm)	126	68.5	68	115	75	72.6
Cranial end of sternum to umbilicus (cm)	60	29	31.5	50	33	31.1
Abdominal depth (umbilicus) (cm)	27.5	12.5	13.9	25	15	14
Abdominal breadth (deepest) (cm)	38.5	19.9	21.7	34	23.5	22.6
Liver mass (g)	2850	495	508.1	1910	700.3	746.2
Right kidney mass (g)	194.4	47.2	48	173.1	62.9	62.7
Left kidney mass (g)	156.9	44.5	49.2	175.9	70.1	68.9
Lungs (both) mass (g)	779	174	164.9	652.2	219.1	189
Trunk mass (kg)	63.76	8.4	10.20	51.17	14.37	12.09

The data provided in Tables 4.3.1 and 4.3.2 were used in the multiple linear

regression model established in Kent et al. (2006) in which two functions defining the series of characteristics, listed above, were utilized. These two functions include i = 1..5 external parameters (f^1_i) and j = 1..3 organ masses ((f^2_j). The values for each of the parameters for each pig were defined as a percentage of the human target (3-year-old, 6-year-old, 10-year-old, and 50th percentile male). An average percentage of the five external parameters were defined as f^1_{avg}, and the average percentage of the three organ parameters as f^2_{avg}. The coefficients for multiple linear regression equations were determined using an Add-In statistical analysis software called Analyse-It® for Microsoft Excel, version 4.80.2 (Analyse-It Software, Ltd., Leeds, United Kingdom). The multiple linear regression equations were then used to relate f^1_{avg} and f^2_{avg} to the swine age, (*a)* and mass (*m)*, through:

$$f^1_{avg} = g(a,m) \qquad \text{Eq. (1)}$$

$$f^2_{avg} = h(a,m) \qquad \text{Eq. (2)}$$

A second-order polynomial regression equation:

$$y = 0.0017x^2 + 0.1812x - 2.5239 \qquad \text{Eq. (3)}$$

developed in the Kent et al. (2006) study which defines the relationship between porcine age and whole body mass, as shown in Figure 4.3.1 below, was used as a constraining equation, in addition to a second constraining equation:

$$f^1_{avg} = f^2_{avg} = 100\% \qquad \text{Eq. (4)}$$

These equations were used to attempt to determine porcine age and mass that best represented the human target, while simultaneously minimizing errors in equations (1) and (2).

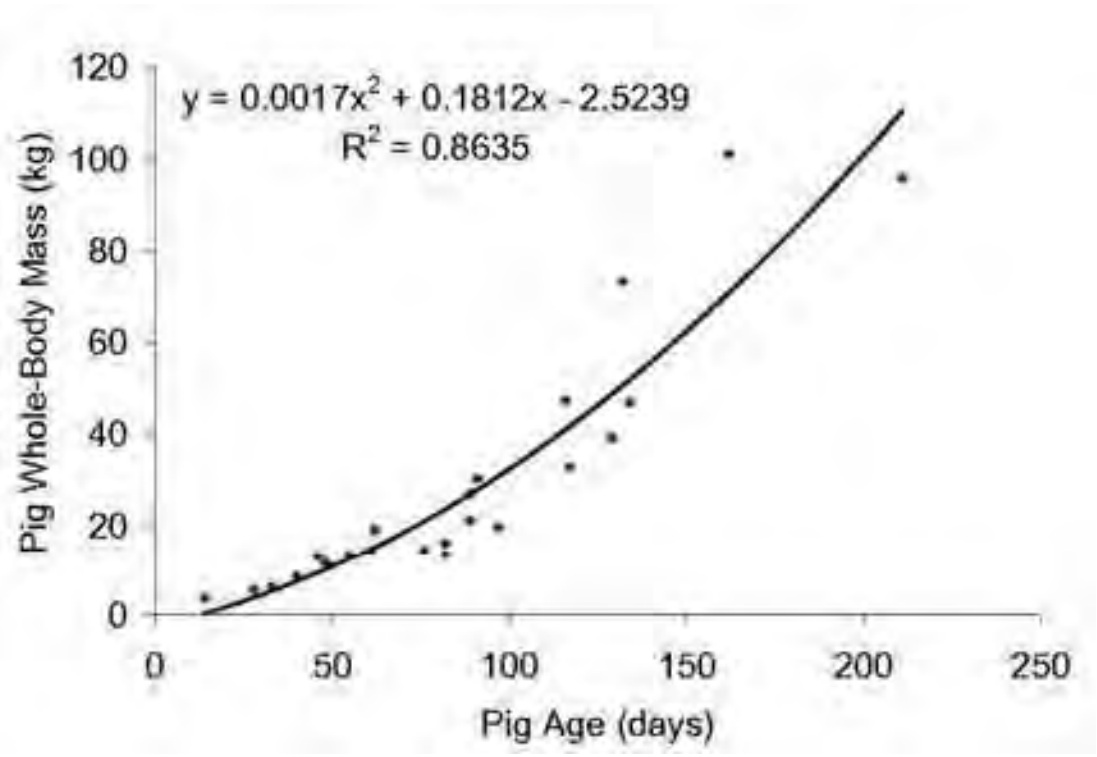

Figure 4.3.1 Relationship between Domestic Pig Age and Whole Body Mass Polynomial Regression Constraint Used by Kent et al. (2006)

The optimization was completed using a non-linear, Quasi-Newton solution scheme contained in the Minerr function in MathCAD, version 15 (Mathsoft, Cambridge, MA).

The multiple linear regression equations, as described above, used to identify the age (*a*) and whole-body mass (*m*) of the porcine surrogate equivalents (PSE), based on Kent et al. (2006) research, most representative as a model of the human 3-year-old, 6-year-old, 10 year-old, and 50th percentile human male thorax and abdomen were defined as:

PSE most representative as a model for the human 3-year-old:

$$f^1_{avg} = g(a,m) = 0.5907 + 0.002711a + 0.02987m = 1 \quad \text{Eq. (5)}$$

$$f^2_{avg} = h(a,m) = 0.389 + 0.0493m = 1 \quad \text{Eq. (6)}$$

$$m = -2.524 + 0.181a + 0.0017a^2 = 1 \quad \text{Eq. (7)}$$

PSE most representative as a model for the human 6-year-old:

$$f^1_{avg} = g(a,m) = 0.5361 + 0.002655a + 0.01789m = 1 \quad \text{Eq. (8)}$$

$$f^2_{avg} = h(a,m) = 0.2187 + 0.03255m = 1 \quad \text{Eq. (9)}$$

$$m = -2.524 + 0.181a + 0.0017a^2 = 1 \quad \text{Eq. (10)}$$

PSE most representative as a model for the human 10-year-old:

$$f^1_{avg} = g(a,m) = 0.4666 + 0.002349a + 0.01359m = 1 \quad \text{Eq. (11)}$$

$$f^2_{avg} = h(a,m) = 0.2109 + 0.02778m = 1 \quad \text{Eq. (12)}$$

$$m = -2.524 + 0.181a + 0.0017a^2 = 1 \quad \text{Eq. (13)}$$

PSE most representative as a model for the human 50th percentile male:

$$f^1_{avg} = g(a,m) = 0.3313 + 0.001735a + 0.007245m = 1 \quad \text{Eq. (14)}$$

$$f^2_{avg} = h(a,m) = 0.09721 + 0.01493m = 1 \quad \text{Eq. (15)}$$

$$m = -2.524 + 0.181a + 0.0017a^2 = 1 \quad \text{Eq. (16)}$$

The Kent et al. (2006) approach yielded the representative PSE whole-body mass and age, which are provided in Figure 4.3.2 and Table 4.3.3, respectively, below.

Comparison of the Kent et al. (2006) model determined PSE whole-body masses presented in Table 4.3.3 to the target age human whole body masses in Table 4.3.1 yields a 19.9% lower mass for the 3-year-old PSE relative to the 3-year-old human target mass, a 1.4% higher mass for the 6-year-old PSE relative to the 6-year-old human target mass, a 17.5% lower mass for the 10-year-old PSE relative to the 10-year-old human target mass, and a 23.2% lower mass for the 50th percentile male porcine equivalent relative to the 50th percentile human male target mass. Given the significant underestimation of determined PSE mass when compared to the human target masses for all age targets other than the 6-year-old equivalent, and the understanding that the Kent et al. (2006)

study was focused on the 6-year-old, it appears more work needs to be done to validate the Kent et al. (2006) model before using this approach to extrapolate outside of their research target 6-year-old equivalent range. In addition, it is acknowledged that swine growth can vary significantly with age and breed depending on how much they are fed over a given time span. Based on this finding, the human whole-body masses provided in Table 4.3.1 were the sole target parameter used to determine appropriate PSE for the human 3-year-old, 6-year-old, 10-year-old, and 50th percentile male in the current study.

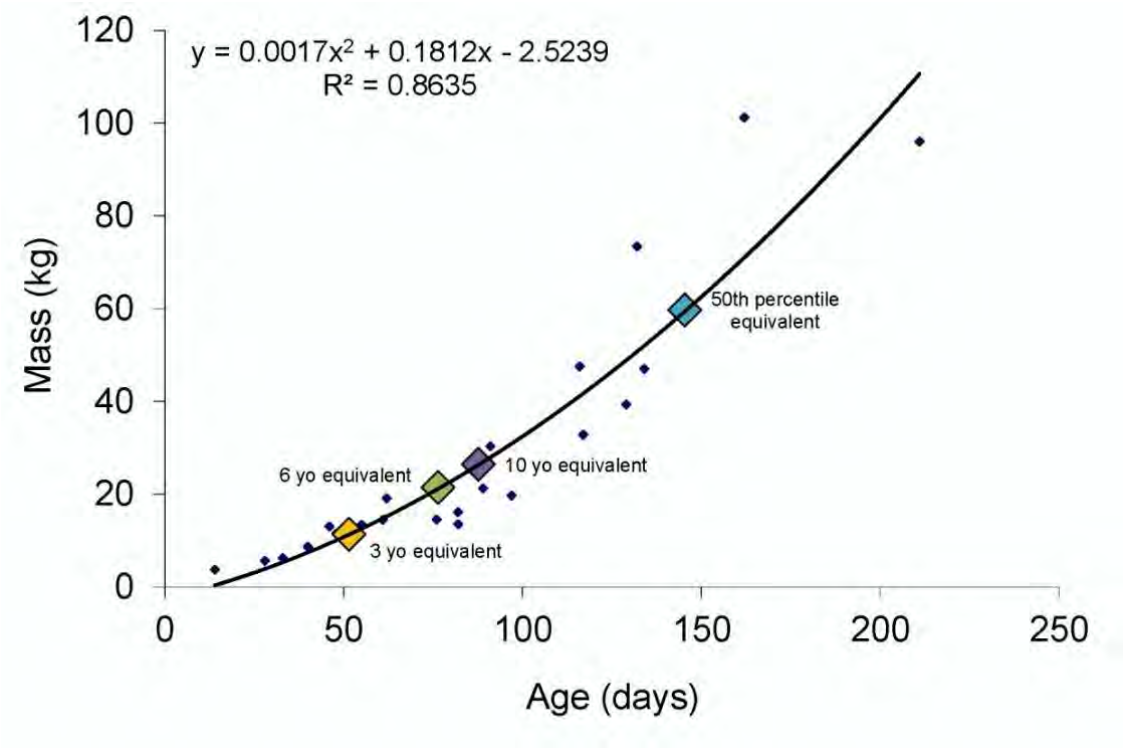

Figure 4.3.2 Domestic Pig Age and Whole Body Mass Polynomial Regression Constraint Used by Kent et al. (2006) with Determined Human- PSE

Table 4.3.3 PSE Whole-Body Mass and Age based on Kent et al. (2006) Model

Subject	Porcine Model Representative of 3-year-old human	Porcine Model Representative of 6-year-old human	Porcine Model Representative of 10-year-old human	Porcine Model Representative of 50th percentile male human
Whole-body mass (kg)	11.3	21.3	27.3	59.7
Age (days)	52	77	89	145

Surrogate female Hampshire/Yorkshire Cross domestic pigs were procured from Michigan State University based on the human target weights specified in Table 4.3.1. Approval from the Wayne State University's Institutional Animal Care and Use Committee (IACUC) was obtained prior to procurement of the PSE. Table 4.3.4, below, provides information regarding the procured PSE, including each individual PSE's whole-body mass and age when studied and percent difference ((+) under, (-) over) compared to the target human equivalent whole-body mass.

Average age of the procured PSE when studied was 50 days for the 3-year-old PSE, 76 days for the 6-year-old PSE, 82 days for the 10-year-old PSE, and 119 days for the 50th percentile male PSE.

Procured PSE were properly housed and cared for by Wayne State University's Division of Laboratory Animal Resources based on an approved IACUC protocol. Porcine surrogates were housed until their whole-body mass was as close to the target human whole-body mass as practical. Average whole-body mass of the procured PSE when studied was 13.6 kg for the 3-year-old, 21.3 kg for the 6-year-old, 30.9 kg for the 10-year-old, and 73.4 kg for the 50th percentile male. Average percent of subject PSE whole-body mass compared to target human whole-body mass was 3.9% under for the 3-year-old, 1.43% over for the 6-year-old, 6.75% under for the 10-year-old, and 5.02% under for the 50th percentile male.

Table 4.3.4 Procured PSE Information

Porcine Subject ID	Porcine Subject Ear Tag Number	Porcine Age When Studied (days)	Porcine Whole-Body Mass When Studied (kg)	Target Human Whole-Body Mass (kg)	% Difference Subject Porcine vs Target Human Whole-Body Mass
3-T1	14 2	50	13.9	14.1	1.42%
3-T2	11 1	53	13.1	14.1	7.09%
3-T3	11 3	50	13.1	14.1	7.09%
3-A1	11 4	48	14.1	14.1	0.00%
3-A2	11 2	49	13.7	14.1	2.84%
3-A3	13 2	51	13.4	14.1	4.96%
AVERAGE 3 YO		**50.2**	**13.6**	**14.1**	**3.90%**
6-T1	77 1	69	20.6	21	1.90%
6-T2	94 4	68	21.4	21	-1.90%
6-T3	84 1	68	21.8	21	-3.81%
6-A1	78 1	79	19.8	21	5.71%
6-A2	75 4	83	22	21	-4.76%
6-A3	88 1	88	22.2	21	-5.71%
AVERAGE 6 YO		**75.8**	**21.3**	**21.0**	**-1.43%**
10-T1	82 4	69	30.4	33.1	8.16%
10-T2	58 1	91	29.6	33.1	10.57%
10-T3	65 4	90	30.2	33.1	8.76%
10-A1	70 1	85	32.4	33.1	2.11%
10-A2	69 3	87	31.8	33.1	3.93%
10-A3	88 3	71	30.8	33.1	6.95%
AVERAGE 10 YO		**82.2**	**30.9**	**33.1**	**6.75%**
50-T1	15 6	122	74.8	77.7	3.73%
50-T2	10 6	119	77	77.7	0.90%
50-T3	25 21	118	74.8	77.7	3.73%
50-A1	47 2	115	72.2	77.7	7.08%
50-A2	44 1	115	74.4	77.7	4.25%
50-A3	10 4	120	69.6	77.7	10.42%
50-T4-A4	5 3	124	74.2	77.7	4.50%
50-T5-A5	43 5	121	74	77.7	4.76%
50-T6-A6	43 1	121	73.2	77.7	5.79%
AVERAGE 50th		**119.3**	**72.9**	**77.7**	**6.13%**

Porcine Surrogate Pendulum Lateral Impact Testing

A series of lateral impact thorax and abdomen pendulum testing of the appropriate whole-body mass cadaveric PSE (3-year-old, 6-year-old, 10-year-old, and 50th percentile male) were performed based on the same scaled lateral impact assessment test protocol used in ISO/TR 9790 (1999) and van Rantingen (1997) and as was used for the biofidelity assessment of the 6-year-old ATDs, discussed previously in Chapter 3. All porcine surrogates were properly disposed of after all testing was completed based on approved IACUC protocol.

Porcine surrogates tested were euthanized just prior to testing, based on the approved IACUC protocol. They were then instrumented, based on SAE J211-1 standard guidelines (2003), with tri-axial piezoresistive accelerometers attached to mount blocks, positioned at the PSE 1st thoracic vertebra (T1) spine location, the base of the thoracic vertebral spine (14th thoracic vertebra (T14) spine location for the Hampshire/Yorkshire pigs in the current study), and the base of the lumbar vertebral spine location (6th lumbar vertebra (L6) spine location for the Hampshire/Yorkshire pigs in the current study). The Hampshire/Yorkshire Cross porcine surrogates were viewed under a OEC (Orthopedic Equipment Company) 9600 C-Arm fluoroscope (Salt Lake City, Utah) prior to affixing accelerometer mount blocks to the specified spinal regions to verify that the breed of pig, indeed, had 14 thoracic vertebrae and 6 lumbar vertebrae. The fluoroscope was then used to verify that each of the accelerometer mount blocks were being secured to the proper vertebra. Once proper vertebra locations were verified, accelerometer mount blocks were secured to the 50th percentile male PSE vertebrae using stainless steel, square drive, coarse threaded deck screws – size #12 x 6-inch at the T1 vertebra location and size #12 x 5-inch at the T14 and L6 vertebrae locations. Accelerometer mount blocks were secured to the 10-year-old PSE vertebrae using stainless steel, square drive, coarse threaded deck screws – size #12 x 5-inch at the T1 vertebra location and size #10 x 4-inch at the T14 and L6 vertebrae locations. Accelerometer mount blocks were secured to the 6-year-old PSE vertebrae using stainless steel, square drive, coarse threaded deck screws size #10 x 4-inch at the T1 vertebra location and size #10 x 3-inch coarse thread wood screws at the T14 and L6 vertebrae locations. Accelerometer mount blocks were secured to the 3-year-old PSE vertebrae using stainless steel, coarse threaded wood

screws size #10 x 3 1/2-inch at the T1 vertebra location and size #10 x 3-inch coarse thread wood screws at the T14 and L6 vertebrae locations. An example of the verification process used for proper screw placement and accelerometer block mount securement are provided in Figure 4.3.3 through 4.3.5 for the 50th percentile male PSE T1, T14, and L6 locations, respectively. An overall view of the placement of the accelerometer block mount positions are shown in Figure 4.3.6 for reference.

The tri-axial accelerometer mount blocks were equipped with Endevco 7264-2000TZ (2000 G) piezoresistive accelerometers for lateral accelerations, and with Measurement Specialties 64C-0200-360T (200 G) piezoresistive accelerometers for longitudinal and vertical accelerations. T1, T14, and L6 spine tri-axial accelerometer mount blocks were attached to the posterior side of each pig spine for accelerometer readings consistent with ATD tested locations.

Figure 4.3.3 Fluoroscope Image of accelerometer block mount screw placement and securement at the T1 location for the 50th percentile male PSE

Figure 4.3.4 Fluoroscope Image of accelerometer block mount screw placement and securement at the T14 location for the 50th percentile male PSE

Figure 4.3.5 Fluoroscope Image of accelerometer block mount screw placement and securement at the L6 location for the 50th percentile PSE

Figure 4.3.6 Overall view of the placement of the accelerometer block mounts relative to each other for the 50th percentile male PSE

For the thorax lateral pendulum impact tests, porcine surrogates were instrumented to measure rib deflection. A trans-thoracic rod technique (Rouhana and Kroell, 1989) was used in which a 3.5-mm diameter carbon-fiber rod was pushed through an incision in the musculature and skin of the impacted side (left side) of the test swine specimen between ribs 6 and 7, maneuvered horizontally through its thoracic cavity at mid-thorax region, and pushed through an incision in the musculature and skin on the opposite, non-impacted side (right side). The positioning of the rod between ribs 6 and 7 was verified using the fluoroscope. A small aluminum mount bracket was fabricated in order to secure the impacted end of the rod and affix it through the use of small zip ties to the adjacent ribs (ribs 6 and 7). Images of the aluminum mount bracket for the trans-thoracic carbon fiber rod are provided in Figure 4.3.7, and as mounted and attached in a swine specimen in Figure 4.3.8, respectively.

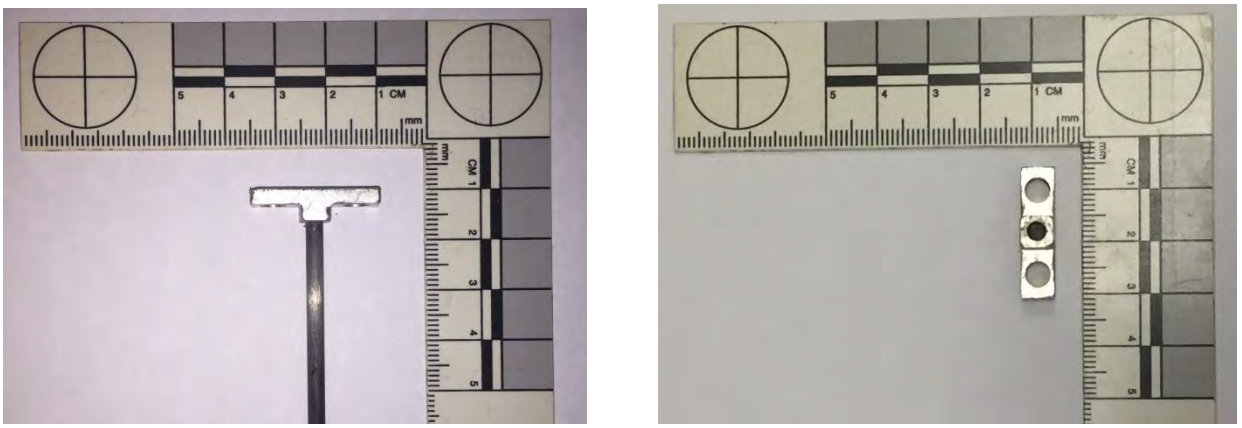

Figure 4.3.7 Fabricated aluminum mount bracket for rib deflection carbon fiber rod

The placement of the rod was chosen to allow the rod to lie in the horizontal plane (level), in the middle of the impacted thorax region, with the test specimen in a standing (upright) position. A photographic target was mounted to the non-impacted end of the rod. A fixed length secondary rod with attached photographic target was affixed in a similar fashion to ribs 6 and 7 of the non-impacted side of the test specimen with a similar mount bracket as in the impacted side in order to be able to track the deflection of the impacted ribs relative to the non-impacted ribs (Figure 4.3.9).

Figure 4.3.8 Aluminum mount bracket for rib deflection carbon fiber rod as affixed to impacted side (left side) ribs 6 and 7

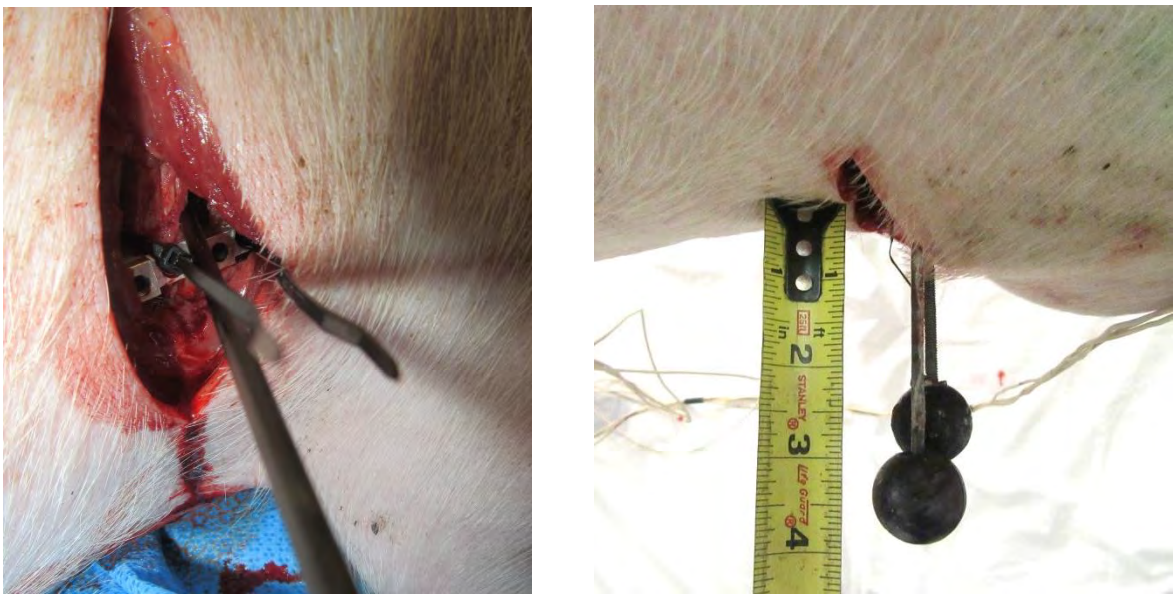

Figure 4.3.9 Aluminum mount bracket for rib deflection fixed rod as affixed to non-impacted side (right side) ribs 6 and 7 and photographic targets for rib deflection (impacted ribs relative to non-impacted ribs) measurement

Once the carbon fiber rod was placed and secured, the incision on the impacted side of the test specimen was closed using super glue. Photographic targets were also placed at T1 and T14 spine locations of the test specimens in order to track the impacted rib deflection relative to the spine. Motion of the moveable target (the target secured to the impacted rib side of the trans-thoracic rod) relative to the fixed target (the target secured to the non-impacted rib side of the test specimen) was tracked via a Redlake MotionXtra HG-100k high-speed camera positioned superiorly above the porcine surrogate at a frame rate of 2,500 frames per second to measure rib cage deflection as a function of time.

A stable fixture was fabricated using 80/20 t-slot aluminum structural components in order to position the tested swine specimens in a standing, upright orientation at the time of impact. Three separate segments of chain were used in combination with carabineer clips and turn buckles to hang the swine test specimens from the fixture at the

proper level and orientation relative to the impact pendulum mass.

For the pendulum impacts in which the pendulum mass impacted the mid-thorax region of the tested porcine ribs in a perpendicular impact orientation, the chains were passed through the pig's thick adipose tissue via incisions made bilaterally along the spinal region. The superior-most chain was positioned at the test specimen's cervical spine region, passing anterior to the nuchal ligament to provide support in holding up the head, neck, and shoulder region of the pig specimen. The second chain was positioned superior to the T14 tri-axial mount block, passing through the thick adipose tissue posterior to the spinal column to support the torso of the pig specimen. The inferior-most chain was positioned inferior to the L6 tri-axial mount block, passing through the thick adipose tissue posterior to the spinal column to support the rear hind quarter of the pig specimen. An inclinometer was used to verify the pig specimen's spine was level to the ground prior to impact. Figure 4.3.10 illustrates a pig test specimen in its pre-impact hanging orientation from the stable fixture and in proper position relative to the impacting pendulum mass for the thorax pendulum impact testing.

The swine specimens in the abdominal pendulum impact test were positioned at an oblique 60-degree angle from anterior-posterior, similar to the ATD testing, in accordance with testing performed by van Rantingen et al. (1997) and scaled abdominal impact response corridors developed in that study based on oblique abdominal impact testing proposed in Viano (1989A). The chains were used to position the swine specimen through incisions in the adipose tissue located further anterior on the specimen's left side compared to its right side. Chains were positioned superiorly and inferiorly similar to the chain positions in the thoracic pendulum impact test setup. The swine specimen was

positioned on the stable fixture such that the impacting face of the pendulum mass was positioned symmetrically inferior to the specimen's rib cage and superiorly to its bony pelvis. An inclinometer was used to verify the swine was oriented to the 60 degree anterior-posterior position and its spine was level to the ground prior to impact. Figure 4.3.11 illustrates a swine test specimen in its pre-impact hanging orientation from the stable fixture and in proper position relative to the impacting pendulum mass for the abdominal pendulum impact testing.

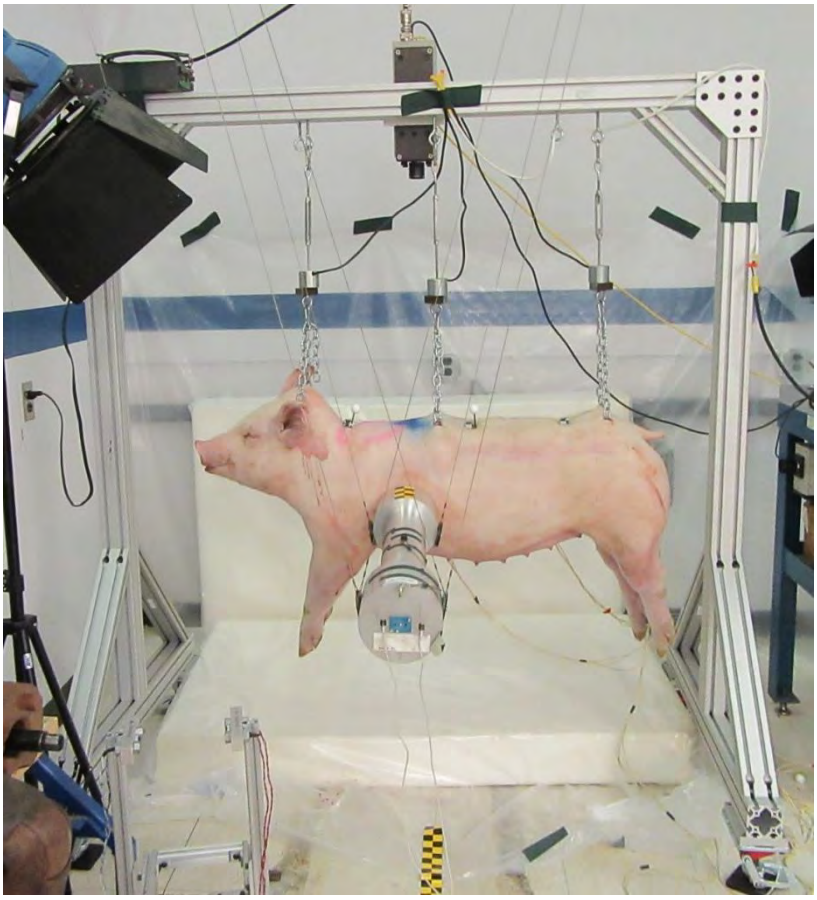

Figure 4.3.10 Thoracic Lateral Impact Test Setup with Swine Specimen in Proper Position Relative to Impacting Pendulum Mass

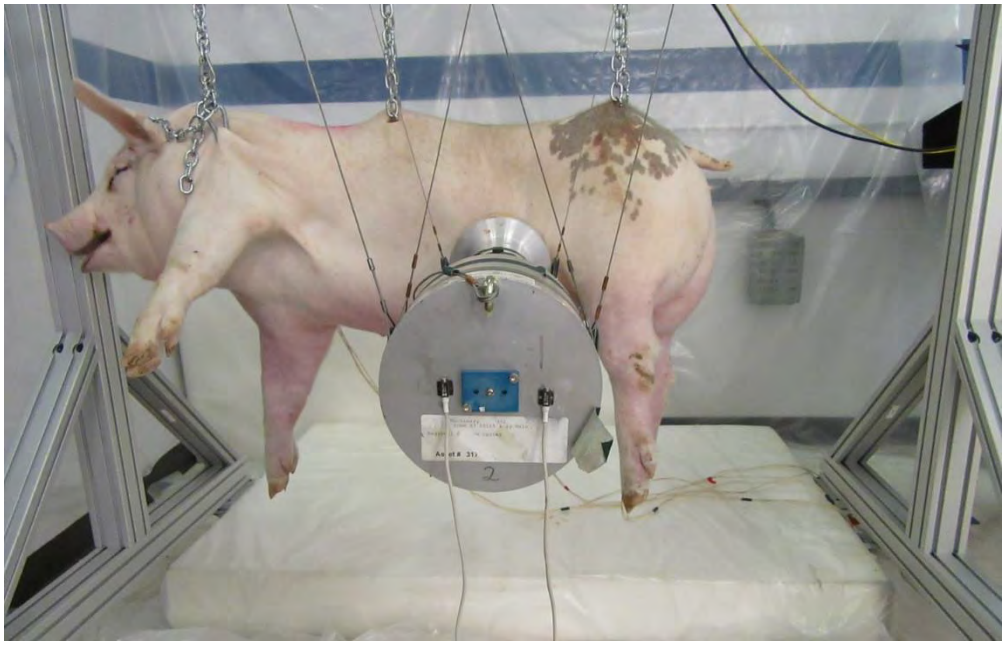

Figure 4.3.11 Abdominal Lateral Impact Test Setup with Swine Specimen in Proper Position Relative to Impacting Pendulum Mass

All pendulum impacting masses were fabricated for the current study except for the pendulum mass used with the 50th male PSE testing. The flat-faced, rigid aluminum pendulum mass used for the 50th percentile male ATD chest calibration tests (49CFR572.36 (1998)) was utilized in the 50th percentile male PSE lateral impact pendulum testing. This pendulum mass had a 152-millimeter (6-inch) diameter impacting surface with 12.7-millimeter (0.5-inch) edge radius and weighed 23.4 kilograms, consistent with the pendulum mass specified in Irwin et al. (2002) for the 50th percentile human male. The flat-faced, rigid, aluminum pendulum mass fabricated for use in the lateral pendulum impact testing during the 6-year-old ATD biofidelity testing, discussed in Chapter 3, was used for the 6-year-old PSE lateral impact pendulum testing. The flat-faced, rigid, aluminum pendulum mass fabricated for the 3-year-old PSE testing had a 70-millimeter (2.75-inch) diameter impacting surface with a 12.7-millimeter edge radius. Total pendulum mass was measured at 1.7 kilograms, consistent with the target

pendulum mass specified in Irwin et al. (2002) for the 3-year-old. The flat-faced, rigid, aluminum pendulum mass fabricated for the 10-year-old PSE testing was a 121-millimeter (4.75-inch) diameter impacting surface with a 12.7-millimeter edge radius. Total pendulum mass was 6.5 kilograms which was slightly less (5.6%) than the 6.89 kilogram pendulum mass specified as the target pendulum mass in Irwin et al. (2002) for the 10-year-old. The impacting pendulum's face diameters for the 3-year-old and 10-year-old pendulum probes were based on scaling ratios relative to the 89-millimeter (3.5-inch) pendulum probe used in Q6 lateral calibration testing (Q6 User Manual, 2012) and the 50th percentile male impactor probe. Pendulum impact force data was recorded through a uniaxial accelerometer mounted on the rear of the pendulum mass. A redundant uniaxial accelerometer was also mounted to the rear of the pendulum mass. Impact force was calculated by multiplying the pendulum mass by the recorded acceleration.

The target pendulum impact speed for the thoracic impact tests was 4.3 m/s, and the target pendulum impact speed for the abdominal impact tests was 4.8 m/s. A test table describing the various testing is provided in Table 4.3.5 below.

An optical sensor speed trap was used to verify pendulum speed just prior to impact. All sensors were connected to a TDAS data acquisition system, and data was collected at a sampling rate of 10,000 Hz. In addition to the superior mounted high speed camera mentioned previously, the impact events were captured at a rate of 1,000 frames per second by a second, lateral view high-speed video camera (Kodak EKTAPRO HG Imager, Model 2000). Three replicate runs, each with a different specimen, were performed for each of the tests in Table 4.3.5.

Table 4.3.5 Pendulum Impact Testing Matrix

	Pendulum Tests	
3-year-old equivalent	**ISO Thorax Test 1** 1.7 kg mass 4.3 m/s impact (3 Runs - 3 Porcine)	**van Rantingen Abdomen** 1.7 kg mass 4.8 m/s impact (3 Runs - 3 Porcine)
6-year-old equivalent	**ISO Thorax Test 1** 2.9 kg mass 4.3 m/s impact (3 Runs - 3 Porcine)	**van Rantingen Abdomen** 2.9 kg mass 4.8 m/s impact (3 Runs - 3 Porcine)
10-year-old equivalent	**ISO Thorax Test 1** 6.5 kg mass 4.3 m/s impact (3 Runs - 3 Porcine)	**van Rantingen Abdomen** 6.5 kg mass 4.8 m/s impact (3 Runs - 3 Porcine)
24-year-old equivalent (50th Male)	**ISO Thorax Test 1** 23.4 kg mass 4.3 m/s impact (3 Runs - 3 Porcine)	**van Rantingen Abdomen** 23.4 kg mass 4.8 m/s impact (3 Runs - 3 Porcine)

Gross dissection of the thoracic region for pigs involved in the thoracic impact tests and the abdominal region for the abdominal impact tests were performed to verify there were no broken ribs or internal tissue damage from the impacts.

The data collected was filtered using the SAE J211 standard (2003) and ISO/TR 9790 (1999) specifications. Since deflection data was not measured in the 6-year-old ATD biofidelity assessment, and therefore also not measured for the swine abdominal pendulum impacts, but measured using overall chest deflection in the thoracic pendulum impact tests, an effective stiffness normalization methodology was not feasible. The data, therefore, was normalized using the effective mass – characteristic length methodology described in Mertz (1984) and Irwin et al. (2002). The data was aligned using the

methodology described in Donnelly and Moorhouse (2012), and compared for each body region tested (thorax and abdomen).

Human Response Corridor Target Comparison to Porcine Surrogate Data

The impact response data collected from the porcine surrogate thorax and abdomen lateral impact pendulum tests were assessed against the scaled human thorax lateral impact response corridors from pendulum testing published in Irwin et al. (2002) and the scaled abdominal oblique impact response corridors from pendulum testing suggested in van Rantingen et al. (1997) for the 3-year-old, 6-year-old, 10-year-old, and 50th percentile human male. Impact response corridor guidelines for the thorax and abdomen are provided in Tables 4.3.6 and 4.3.7, respectively, below.

Table 4.3.6 Human Thorax Impact Response Corridor Guidelines

Human Thorax Impact Response Corridors - 4.3 m/s Pendulum Impact (Irwin et al. (2002))									
		3-Year-Old Struck by a 1.7 kg Pendulum		6-Year-Old Struck by a 2.9 kg Pendulum		10-Year-Old Struck by a 6.89 kg Pendulum		Mid Male Struck by a 23.4 kg Pendulum	
		Time (sec)	Force (kN)	Time (sec)	Force (kN)	Time (sec)	Force (kN)	Time (sec)	Force (kN)
Upper	A	0	0.3	0	0.5	0	0.8	0	1.7
Boundary	B	0.006	0.66	0.006	1.1	0.007	1.8	0.01	3.7
Coordinates	C	0.019	0.66	0.019	1.1	0.022	1.8	0.03	3.7
	D	0.028	0.36	0.028	0.6	0.032	1	0.045	2
Lower	E	0	0	0	0	0	0	0	0
Boundary	F	0.006	0.3	0.006	0.5	0.007	0.8	0.01	1.7
Coordinates	G	0.019	0.3	0.019	0.5	0.022	0.8	0.03	1.7
	H	0.025	0	0.025	0	0.029	0	0.04	0
		Time (sec)	T1 Acceleration (G)	Time (sec)	T1 Acceleration (G)	Time (sec)	T1 Acceleration (G)	Time (sec)	T1 Acceleration (G)
Upper	A	0	2	0	2	0	2	0	2
Boundary	B	0.009	14	0.009	16	0.011	18	0.015	15
Coordinates	C	0.031	0	0.031	0	0.036	0	0.05	0
Lower	D	0.004	0	0.004	0	0.004	0	0.006	0
Boundary	E	0.009	8	0.009	9	0.011	9	0.015	8
Coordinates	F	0.023	0	0.023	0	0.027	0	0.037	0

Table 4.3.7 Human Abdomen Impact Response Corridor Guidelines

Human Abdomen Impact Response Corridors - 4.8 m/s Pendulum Impact (van Rantingen et al. (1997))									
		3-Year-Old Struck by a 1.7 kg Pendulum		6-Year-Old Struck by a 2.9 kg Pendulum		10-Year-Old Struck by a 6.89 kg Pendulum		Mid Male Struck by a 23.4 kg Pendulum	
		Time (sec)	Force (kN)	Time (sec)	Force (kN)	Time (sec)	Force (kN)	Time (sec)	Force (kN)
Upper	A	0.000	0.0	0.000	0.0	0.000	0.0	0.00	0
Boundary	B	0.001	0.2	0.001	0.4	0.001	0.7	0.00	1.5
Coordinates	C	0.010	0.5	0.011	0.8	0.013	1.4	0.02	3
	D	0.018	0.5	0.019	0.8	0.022	1.4	0.03	3
	E	0.034	0.2	0.036	0.3	0.042	0.6	0.06	1.3
Lower	F	0.000	0.0	0.000	0.0	0.000	0.0	0.00	0
Boundary	G	0.015	0.2	0.016	0.4	0.019	0.7	0.03	1.5
Coordinates	H	0.022	0.2	0.024	0.4	0.028	0.7	0.04	1.5
	I	0.034	0.1	0.036	0.1	0.042	0.2	0.06	0.5
		Deflection (mm)	Force (kN)	Deflection (mm)	Force (kN)	Deflection (mm)	Force (kN)	Deflection (mm)	Force (kN)
Upper	A	0	0.0	0	0.0	0	0.0	0	0
Boundary	B	8	0.2	9	0.4	11	0.7	15	1.5
Coordinates	C	48	0.5	50	0.8	60	1.4	85	3
	D	84	0.5	89	0.8	105	1.4	150	3
Lower	E	0	0.0	0	0.0	0	0.0	0	0
Boundary	F	45	0.2	47	0.4	56	0.7	80	1.5
Coordinates	G	56	0.2	59	0.4	70	0.7	100	1.5

Peak mean pendulum impact force at each age level for the tested swine specimens was plotted against the peak value of pendulum impact force from the upper boundary of the human response corridor at each corresponding age level and used to determine if any correlation existed for this parameter with respect to age between pigs and humans. This was performed for both the thoracic and abdominal impact tests. Similarly, peak mean T1 acceleration at each age level for the thorax impact tested swine specimens was plotted against the peak value of T1 acceleration from the human response corridor upper boundary at each corresponding age level. This analysis was performed to determine if any correlation existed for T1 acceleration with respect to age between swine and humans. A Pearson's Correlation (r value) was calculated with respect to the above plotted comparison data in order to determine the strength of any linear correlation between the pigs test data relative to age and the human scaled impact response corridors. The closer the r value to $\pm$ 1, the stronger the correlation between

the data analyzed. In addition, an ANOVA (analysis of variance or p-value) test was performed on the data to determine if there is any statistical significance between human and swine impact response data relative to age. For the current study, a p-value less than 0.05 was considered statistically significant.

4.4 – Results

Gross dissection of the thoracic and abdominal regions for pigs involved in the thoracic and abdominal impact tests, respectively, were performed to verify there were no broken ribs or internal tissue damage from the impacts. Ribs 6 and 7 on the impacted side of the 50th percentile male PSE used in Test 37 were the only ribs determined to have fractured during all testing performed. No abdominal region internal bleeding or contusions were identified in any of the testing.

Pendulum impact thorax response data for the PSE tested were compared to the response requirements described in the ISO/TR9790 Technical Report, as scaled to the 3-year-old, 6-year-old, 10-year-old human from the 50th percentile human male in Irwin et al. (2002). Figures 4.4.1 and 4.4.2, respectively, illustrate the comparison of the 3-year-old PSE tested pendulum thorax impact force and T1 level accelerations with respect to time compared to the human scaled thorax response corridors for this age level. Figures 4.4.3 and 4.4.4, respectively, demonstrate the comparison of the 6-year-old PSE tested pendulum thorax impact force and T1 level accelerations with respect to time compared to the human scaled thorax response corridors for this age level. Figures 4.4.5 and 4.4.6, respectively, show the comparison of the 10-year-old PSE tested pendulum thorax impact force and T1 level accelerations with respect to time compared to the human scaled thorax response corridors for this age level, and Figures 4.4.7 and 4.4.8, respectively,

illustrate the comparison of the 50th male PSE tested pendulum thorax impact force and T1 level accelerations with respect to time compared to the human thorax response corridors.

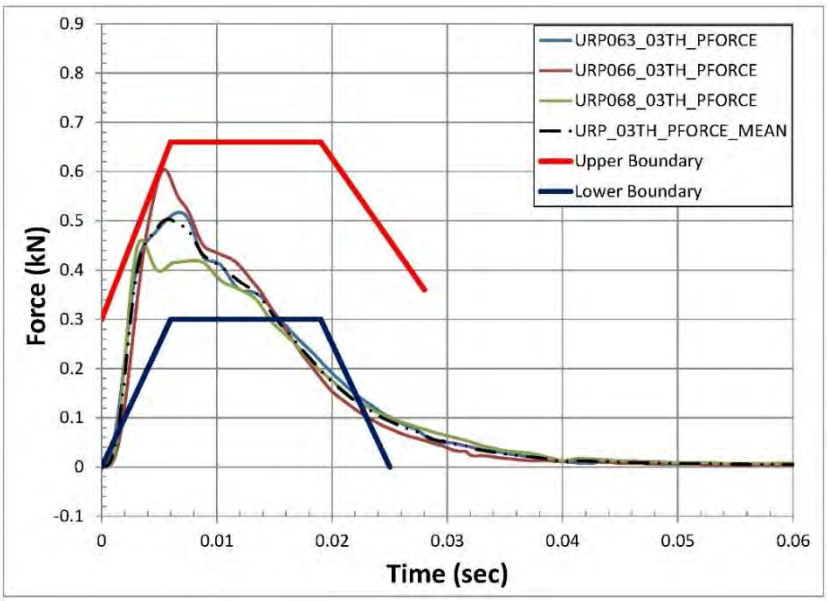

Figure 4.4.1 3-Year-Old PSE Pendulum Thorax Impact Force v Time Compared to ISO Scaled Human Thorax Impact Response Corridor

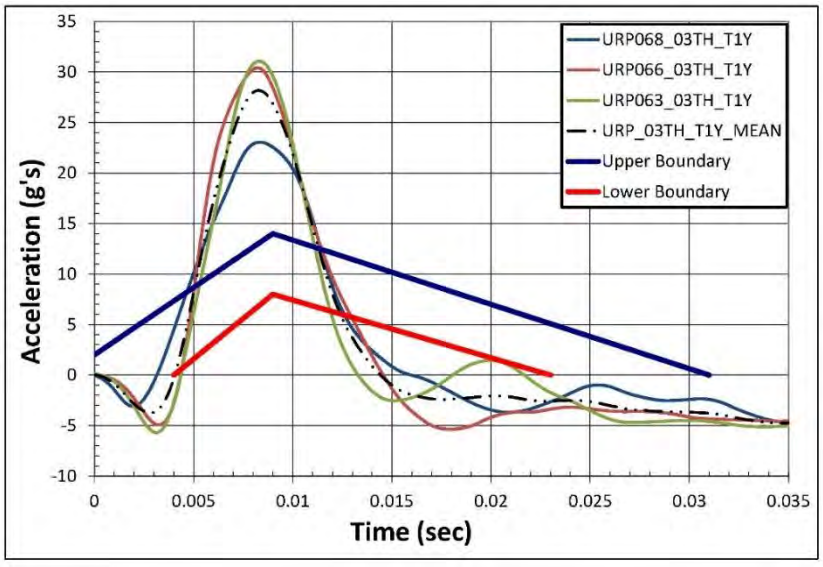

Figure 4.4.2 3-Year-Old PSE Pendulum Thorax Impact T1 Acceleration v Time Compared to ISO scaled Human Thorax Impact Response Corridor

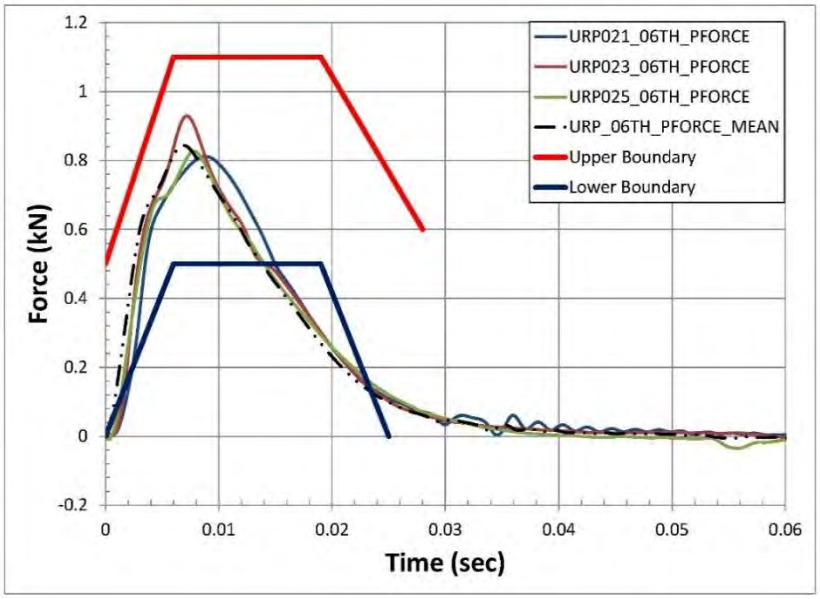

Figure 4.4.3 6-Year-Old PSE Pendulum Thorax Impact Force v Time Compared to ISO scaled Human Thorax Impact Response Corridor

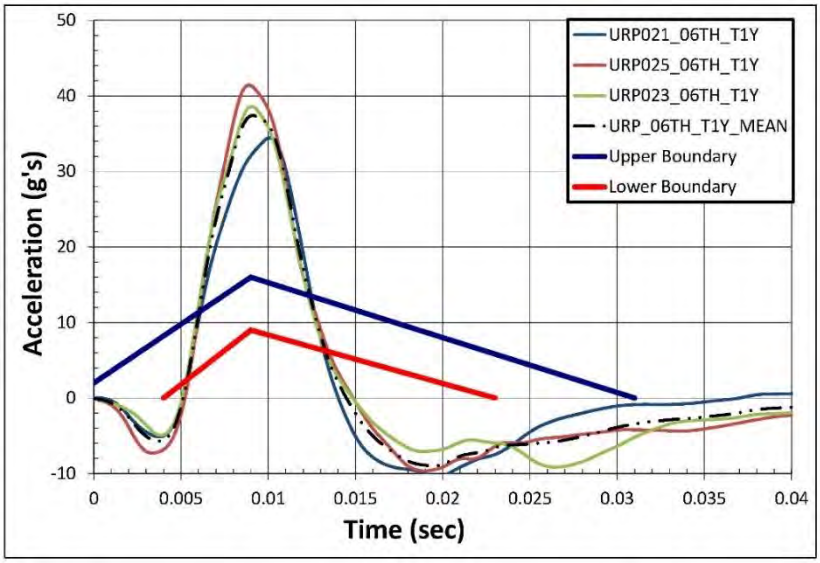

Figure 4.4.4 6-Year-Old PSE Pendulum Thorax Impact T1 Acceleration v Time Compared to ISO scaled Human Thorax Impact Response Corridor

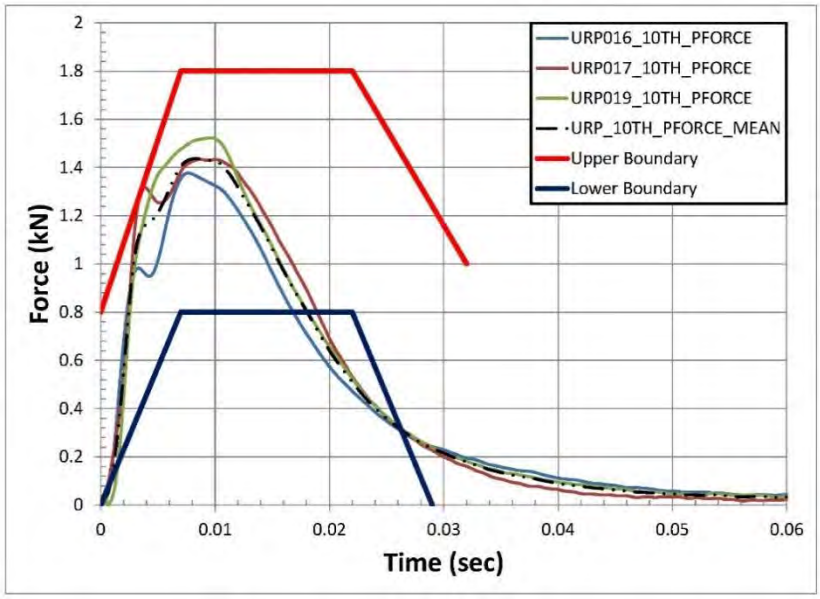

Figure 4.4.5 10-Year-Old PSE Pendulum Thorax Impact Force v Time Compared to ISO scaled Human Thorax Impact Response Corridor

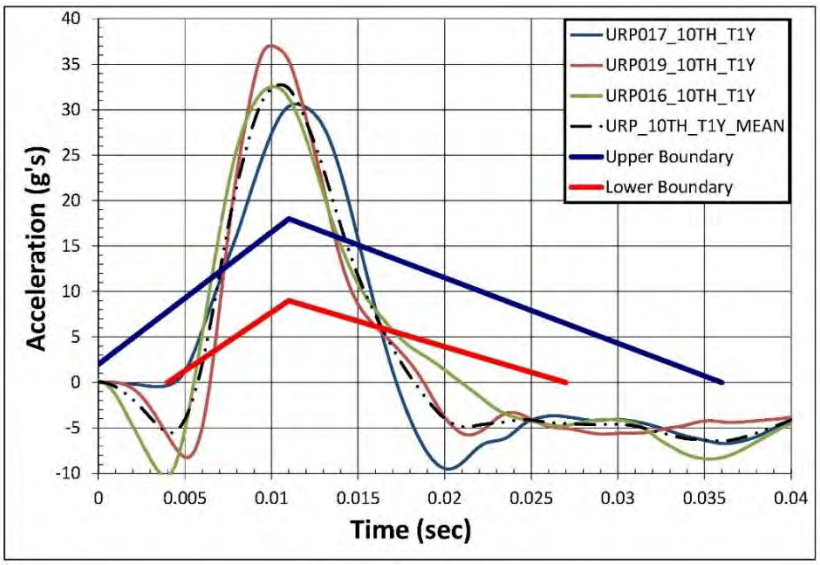

Figure 4.4.6 10-Year-Old PSE Pendulum Thorax Impact T1 Acceleration v Time Compared to ISO scaled Human Thorax Impact Response Corridor

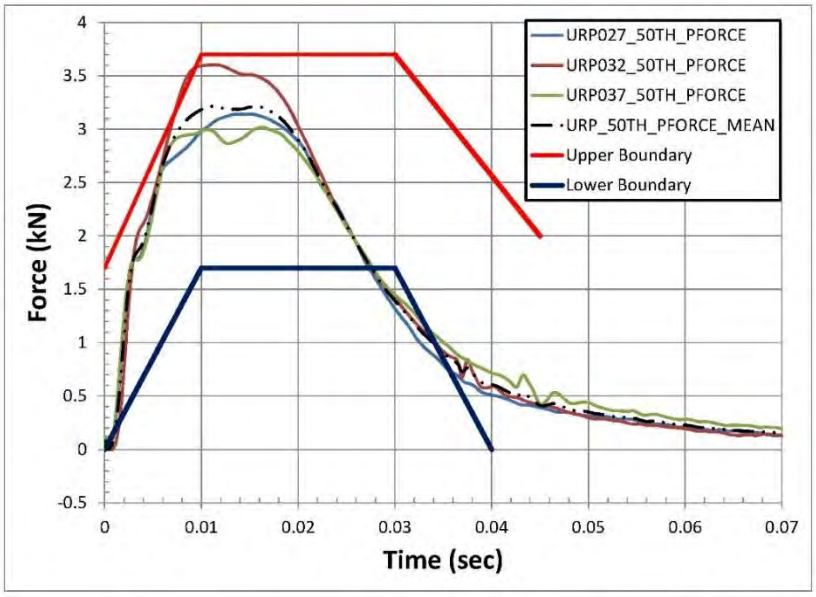

Figure 4.4.7 50th Male PSE Pendulum Thorax Impact Force v Time Compared to ISO scaled Human Thorax Impact Response Corridor

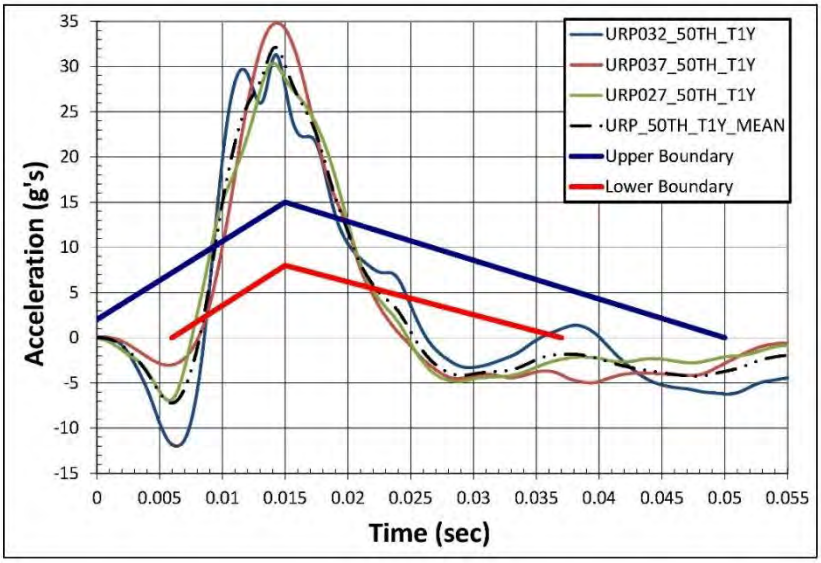

Figure 4.4.8 50th Male PSE Pendulum Thorax Impact T1 Acceleration v Time Compared to ISO scaled Human Thorax Impact Response Corridor

Pendulum impact abdominal response data for the PSE tested were compared to the abdominal response corridors suggested in van Ratingen et al. (1997), as scaled to the 3-year-old, 6-year-old, 10-year-old human from the 50th percentile human male.

Figures 4.4.9 through 4.4.12 illustrate the comparison of the 3-year-old, 6-year-old, 10-year-old, and 50th Male PSE tested pendulum abdominal impact force relative to time compared to the human scaled abdominal impact response corridors, respectively.

Based on the plotted data, a linear trend in PSE thoracic peak mean pendulum impact force compared to corresponding peak value response corridor upper boundary values was observed with increase in age, as illustrated in Figure 4.4.13. The Pearson's correlation R-value for this data was calculated to be 0.9994, which indicates a significantly strong linear correlation between the peak mean porcine thoracic pendulum impact force to scaled human peak impact response corridor force relative to age. In addition, the ANOVA p-value for the above data was calculated to be 0.0005, and therefore shows a statistical significance in human to porcine thoracic impact force response data relative to age.

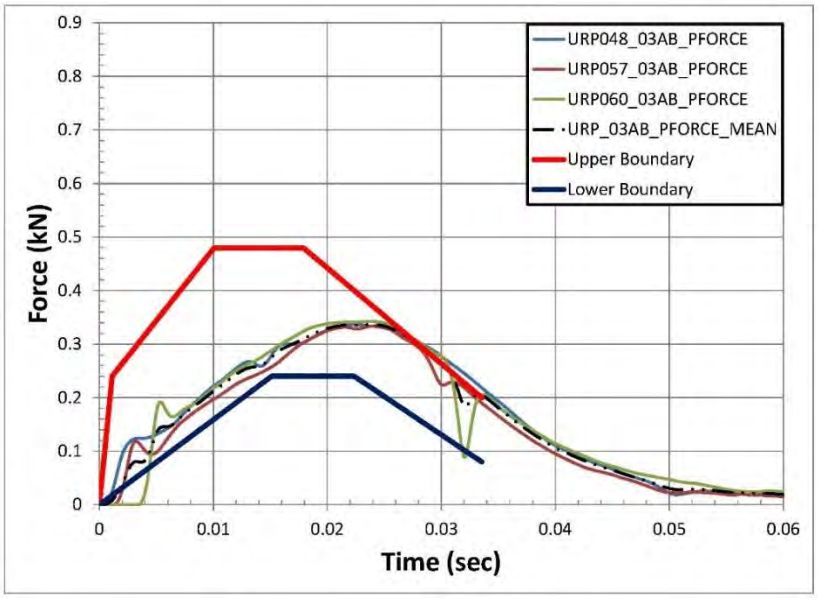

Figure 4.4.9 3-Year-Old PSE Pendulum Abdominal Impact Force v Time Compared to van Rantingen scaled Human Abdominal Impact Response Corridor

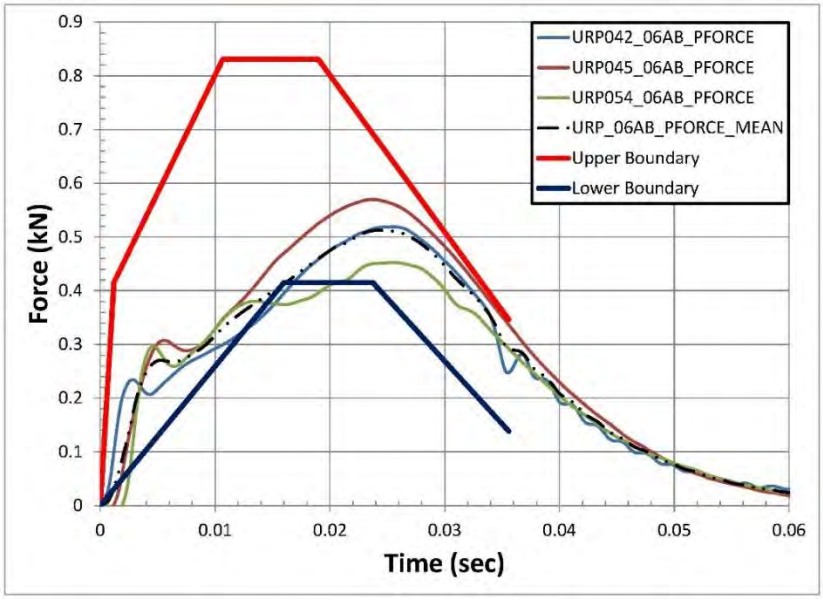

Figure 4.4.10 6-Year-Old PSE Pendulum Abdominal Impact Force v Time Compared to van Rantingen scaled Human Abdominal Impact Response Corridor

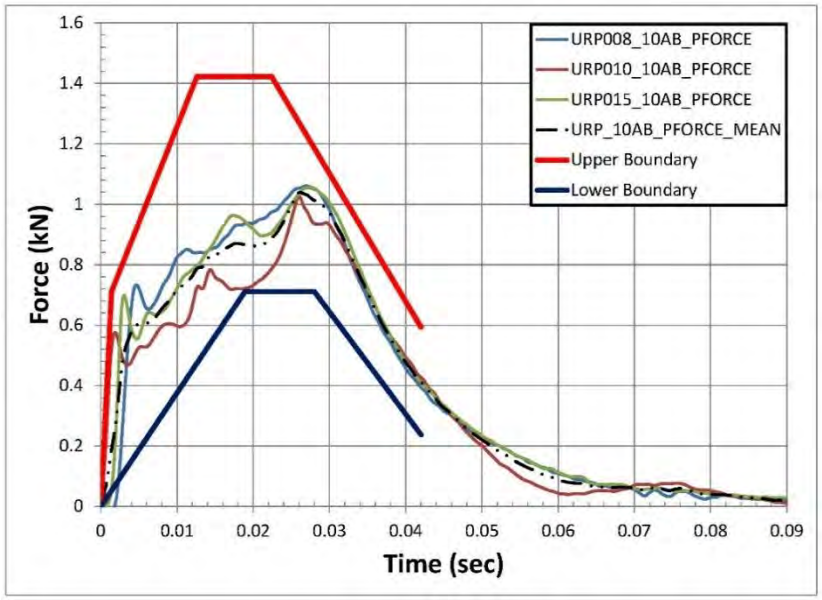

Figure 4.4.11 10-Year-Old PSE Pendulum Abdominal Impact Force v Time Compared to van Rantingen scaled Human Abdominal Impact Response Corridor

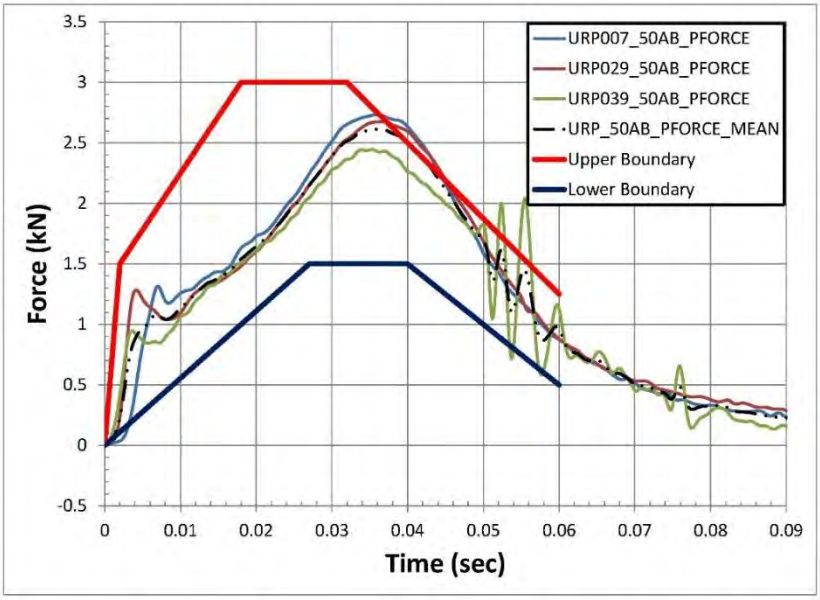

Figure 4.4.12 50th Male PSE Pendulum Abdominal Impact Force v Time Compared to van Rantingen scaled Human Abdominal Impact Response Corridor

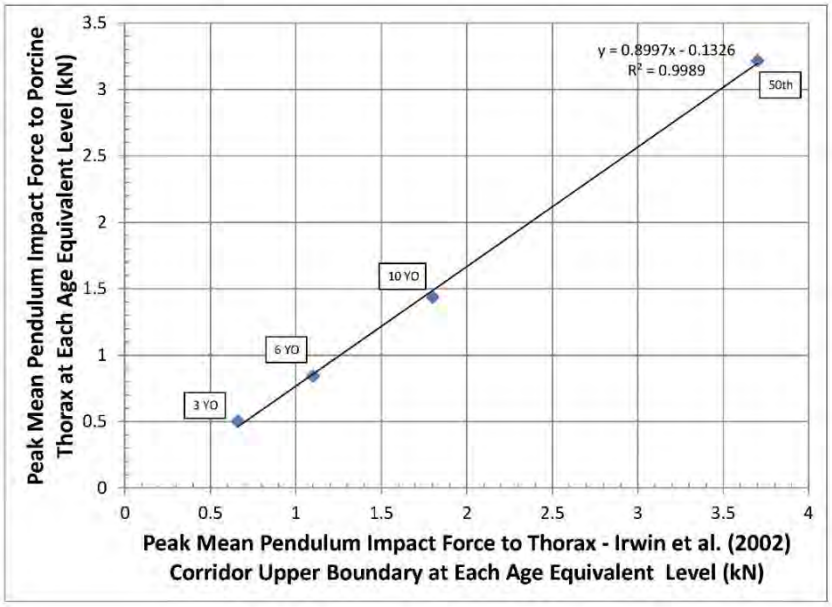

Figure 4.4.13 Correlation of Peak Mean PSE Thoracic Pendulum Impact Force to ISO Response Corridor Upper Boundary Values at Each Age Level

Based on the plotted data, a linear trend in PSE abdominal peak mean pendulum impact force compared to corresponding scaled human impact response corridor upper

boundary values is observed with increase in age, as shown in Figure 4.4.14, below. The Pearson's correlation R-value for this data was calculated to be 0.9964, which corresponds to a strong linear correlation between the peak mean porcine abdominal pendulum impact force to scaled human peak impact response corridor force relative to age. In addition, the ANOVA p-value for the data was calculated to be 0.0036, and therefore shows a statistical significance in human to porcine abdominal impact force response data relative to age.

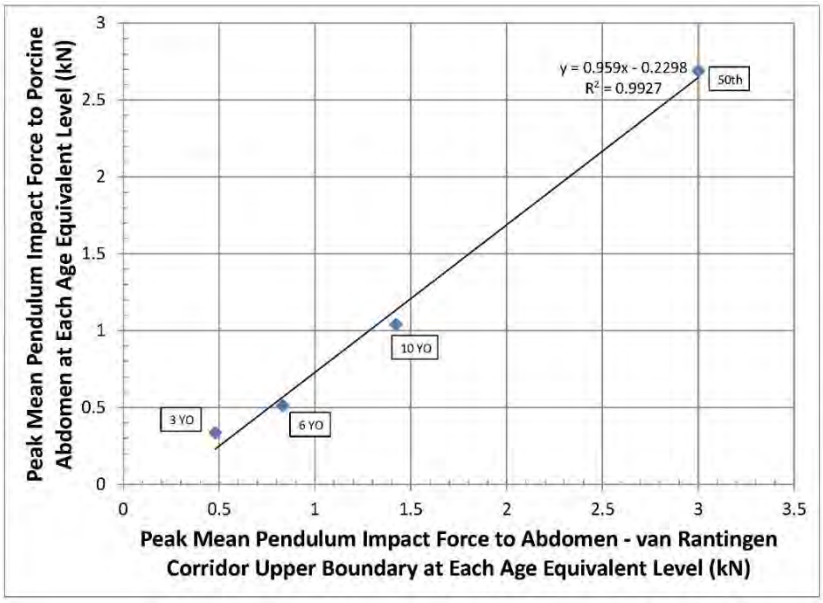

Figure 4.4.14 Correlation of Peak Mean PSE Abdominal Pendulum Impact Force to van Rantingen Response Corridor Upper Boundary Values at Each Age Level

Based on the plotted data, a decreasing second-order polynomial trend relative to age for the pendulum impact thoracic T1 accelerations compared to the corresponding scaled human upper response corridor peak values, as illustrated in Figure 4.4.15, below. The Pearson's correlation R-value for this data was calculated to be 0.4960, which corresponds to a weak linear correlation between the peak mean PSE thoracic pendulum impact T1 accelerations to scaled human peak impact response corridor T1 accelerations

relative to age. In addition, the ANOVA p-value for the data was calculated to be 0.5040, and therefore shows no statistical significance in human to porcine thoracic T1 impact acceleration response data relative to age.

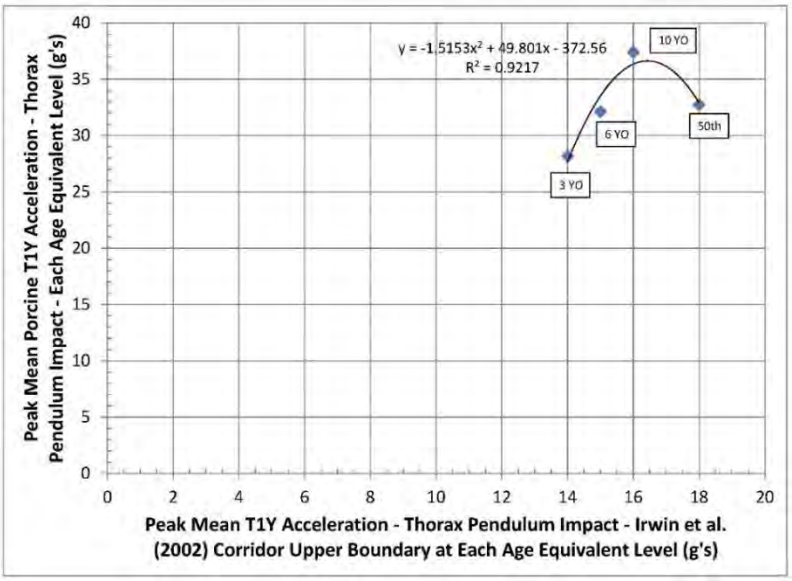

Figure 4.4.15 Correlation of PSE Peak Mean T1 Acceleration to ISO Response Corridor Upper Boundary Values at Each Age Level

4.5 – Discussion

Peak pendulum impact thorax T1 accelerations for all PSE tested, at all age equivalent levels were considerably higher in value than the corresponding scaled human upper response corridor boundaries. Peak PSE thorax T1 accelerations were 2.0 times greater at the 3-year-old age level, 2.3 times greater at the 6-year-old age level, 1.8 times greater at the 10-year-old age level, and 2.1 times greater at the 50th male age level than the human ISO upper boundary response corridors. Although magnitudes for the T1 accelerations were greater than the corresponding scaled human impact response corridors, peak accelerations appear to be consistent in time with the corresponding scaled human impact response corridor peak accelerations. In addition, thorax impact

pulse duration for all age level PSE T1 acceleration data is shorter than the corresponding human impact response corridors, and PSE thorax pendulum impact force pulse durations were less than the human impact response corridors by approximately 10 msec. Peak PSE thoracic pendulum impact force magnitudes essentially fell within the ISO scaled human impact response corridors for all ages.

The shorter impact pulse durations observed in the swine testing compared to the ISO human impact response corridors are due to the stiffer swine thorax compared to the human thorax at all age levels studied. Stiffness is how much an object will deform due to an applied force. Impact duration is a function of how long the impact force is applied before the two objects reach a common velocity and separate. The impact duration in this study, with a rigid impact pendulum probe, will be shorter if the struck object is more rigid and doesn't deform much, or longer if the struck object is yielding. Acceleration is the change in velocity over the change in time (impact pulse duration), and is, therefore, inversely proportional to the pulse duration. A shorter pulse duration will result in a higher acceleration whereas a longer pulse duration will result in a lower acceleration. Since force-deflection is not one of the included ISO impact response corridors, data plots are not provided and compared in this chapter but will be provided and discussed later in Chapter 6.

Peak PSE abdomen pendulum impact force magnitudes essentially fell within the ISO scaled human impact response corridors for all ages. The PSE abdominal pendulum impact force pulse durations tended to be within or slightly longer than the human impact response corridors.

The impulse, or duration over which an impacting force acts, can provide insight

into stiffness and relative response of the struck object, assuming the striking object is rigid and unyielding. Impulse response calculations were performed in the current study for the PSE force versus time impact data as well as for the corresponding average human impact response corridors for both the thorax and abdominal impacts. The corresponding PSE and human impulse response data was compared. Figure 4.5.1, below, shows the thorax impulse response data comparison for the PSE and human at all studied age levels. Figure 4.5.2 provides the abdominal impulse response data comparison for the PSE and humans at all age levels studied.

It can be seen from the thorax impulse response data graphs provided in Figure 4.5.1, above, that for all ages, impulse response of the swine is much higher in magnitude shorter in duration, and passes through zero sooner than the human impulse response. The time location where the impulse response curve passes through zero is where the maximum impact force occurs and a common velocity between the two impacting objects is achieved. Note that the more compliant porcine abdomen impulse response data in Figure 4.5.2 does not pass through zero until much later in time compared to the thorax. The porcine abdomen impact response data, is however, much higher in magnitude but typically longer in duration, passing through zero later in time than the human abdominal impulse response data. The impulse response data shows that the porcine thorax is stiffer than the human thorax, but the porcine abdomen tends to be as or slightly more compliant than the human abdomen. Based on the statistical analysis performed, there is a significant linear correlation with respect to peak impact pendulum force and age for porcine thoracic and abdominal test data compared to the peak ISO scaled human impact response corridors. The time (pulse) duration of the pendulum impact force is, however,

roughly 10 msec shorter for the PSE response data compared to the corresponding human thoracic impact response corridors. As for the thoracic T1 acceleration, no significant correlation was found with respect to the response data of PSE when compared to scaled human T1 acceleration response corridors.

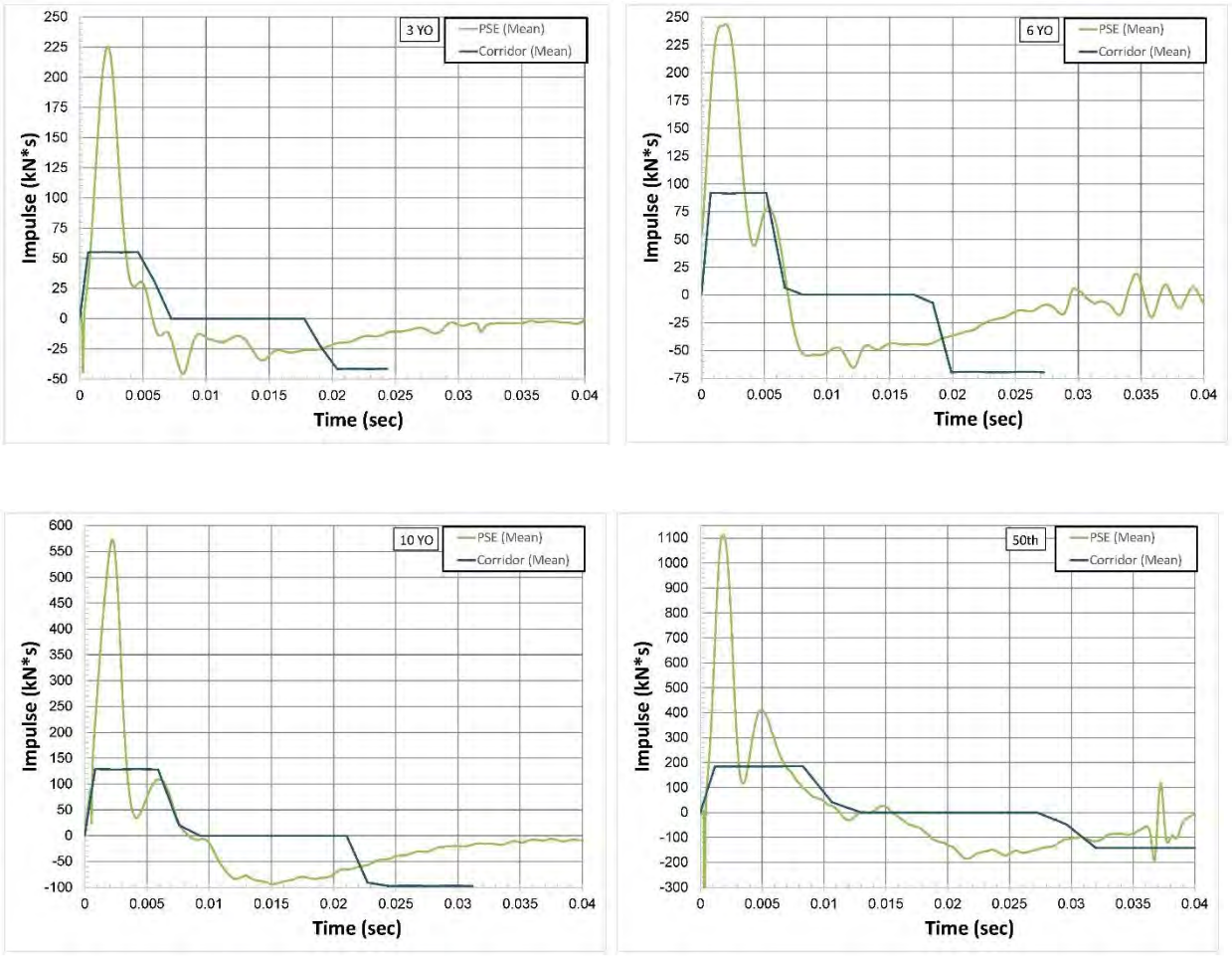

Figure 4.5.1 Thorax Impulse Response Data Comparison for the PSE and Human at all Studied Age Levels – 3-Year-Old (top left), 6-Year-Old (top right), 10-Year-Old (bottom left), 50th Male (bottom right)

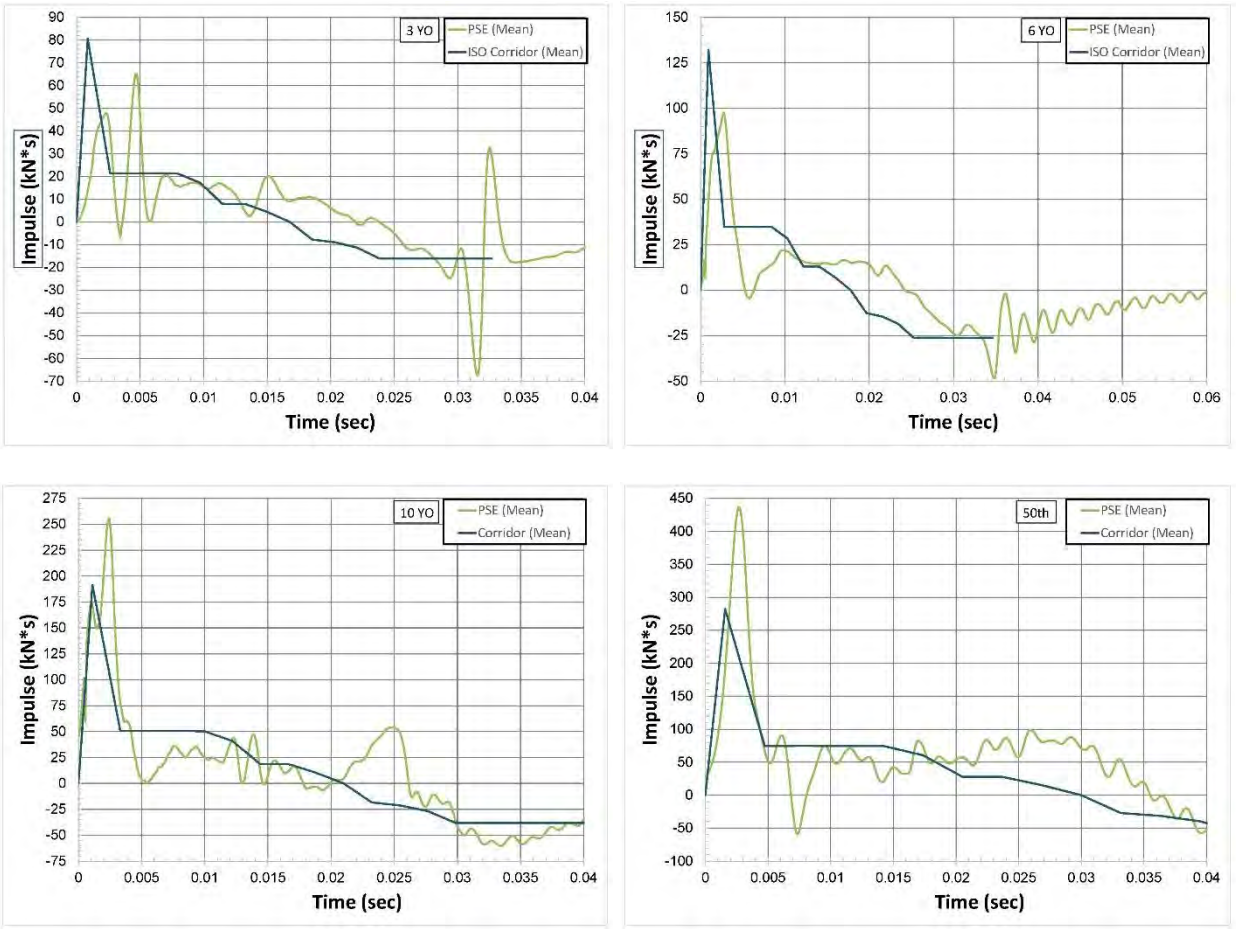

Figure 4.5.2 Abdominal Impulse Response Data Comparison for the PSE and Human at all Studied Age Levels – 3-Year-Old (top left), 6-Year-Old (top right), 10-Year-Old (bottom left), 50th Male (bottom right)

Viano et al. (1989B) performed lateral impact pendulum tests at various impacts speeds, using a 23.4 kg flat-faced pendulum impact mass, on unembalmed male and female human PMHS ranging in age from 29 to 75. Impacts were performed at the chest (including an impact speed of 4.3 m/s), abdomen (including an impact speed of 4.8 m/s), and pelvis levels. Figure 4.5.3, below, shows a comparison of the digitized pendulum impact force versus time thoracic data from the human PMHS in the Viano et al. (1989B) study with ISO human impact response corridors (top) compared directly to the current study 50th male PSE thoracic pendulum impact response data with corresponding ISO human impact response corridors (bottom).

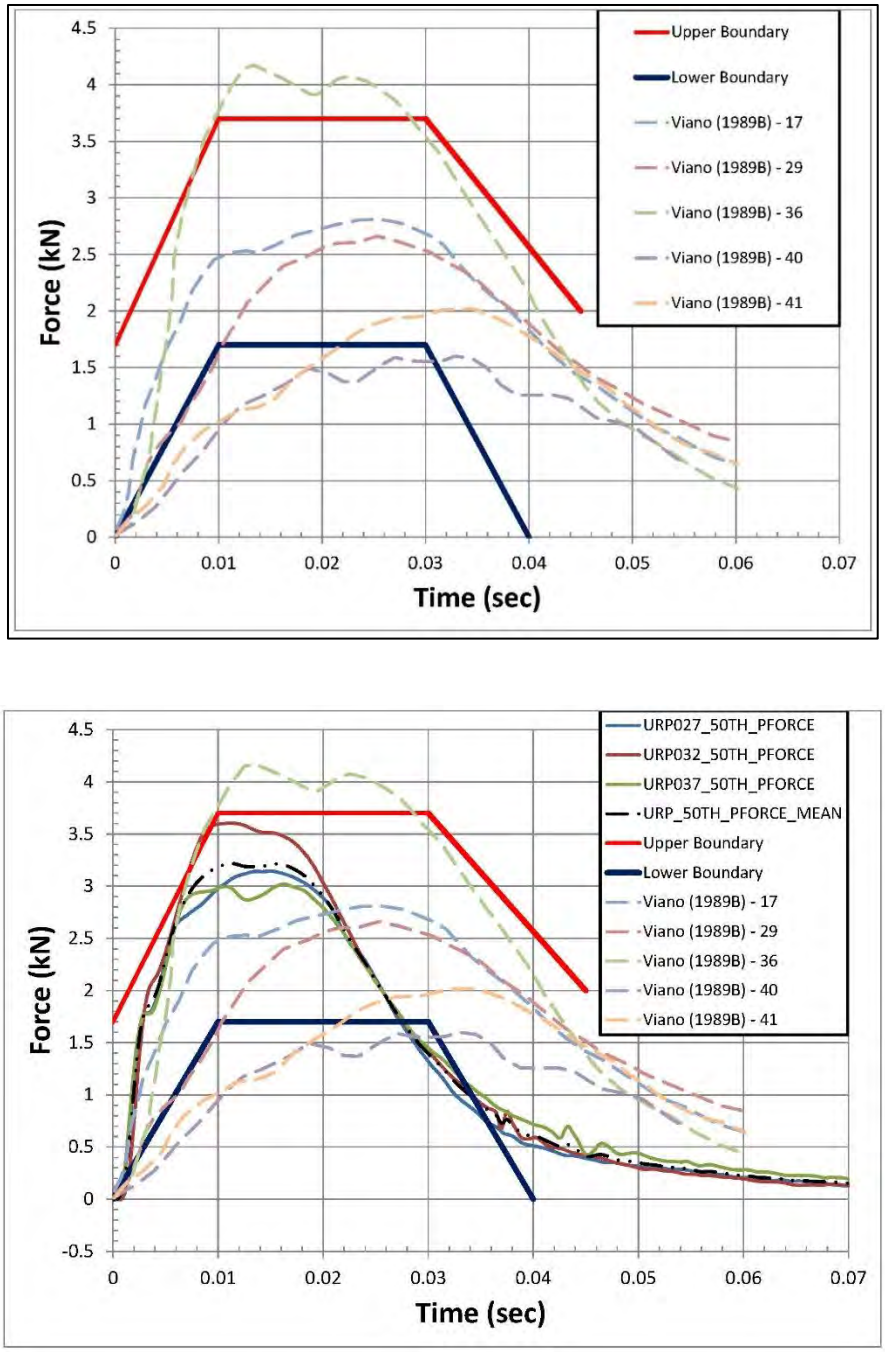

Figure 4.5.3 Comparison of Lateral Pendulum to Thoracic Impact Tests of Human PMHS (Viano et al. (1989B)) (top) to 50th Male PSE (4.3 m/s impact speed) (bottom)

This comparison clearly shows that the human PMHS data, except for test specimen #40, would fall within the 50th male human impact response corridors for both force magnitude and pulse duration. The 50th male PSE data is noticeably shorter in

pulse duration by roughly 10 msec and only slightly greater in force magnitude than the human data, which is consistent with the ISO impact response corridors.

Viano et al. (1989C) further performed lateral impact pendulum tests on anesthetized full-grown pigs at various impact speeds, including an impact speed of 4.3 m/s, using a 23.4 kg flat-faced pendulum impact mass, with the swine rotated 30-degrees so the point of impact of the pendulum was lateral on the thorax and upper abdomen. The lateral pendulum impact force versus time data for the Viano et al. (1989C) swine at the 4.3 m/s impact speed is provided in Figure 4.5.4, below, for reference.

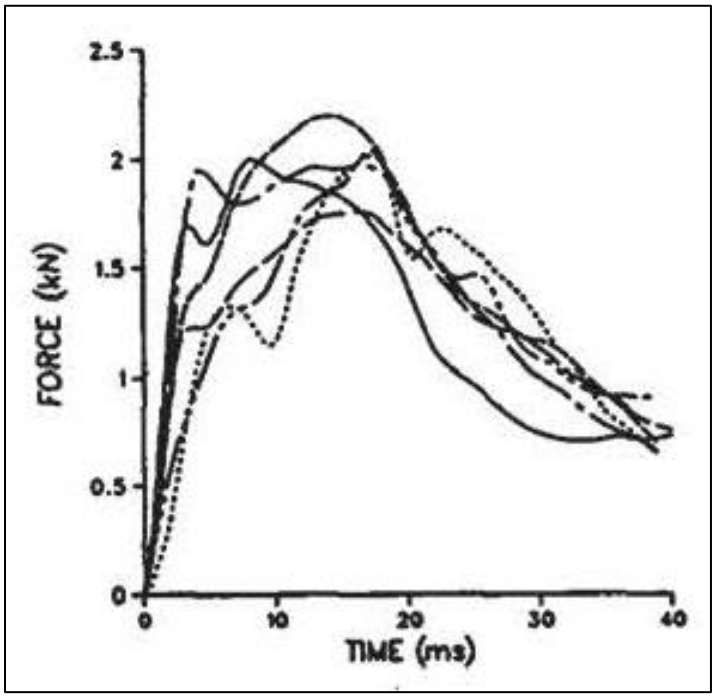

Figure 4.5.4 Lateral Pendulum to Thoracic/Abdominal Impact Tests of Full-Grown Pigs rotated 30 degrees (Viano et al. (1989C)) (4.3 m/s impact speed)

The pulse duration and pulse response shape of the porcine pendulum impact force response data provided in Figure 4.5.4 is similar to what was observed in the current study's thoracic lateral impact testing for the 50th male PSE (see bottom figure – Figure 4.5.3). The peak magnitude observed in the current study's thoracic impact pendulum

force data, however, is on the order of 1.5 times greater than what is observed in the Viano et al. (1989C) study (Figure 4.5.4 above). The magnitude difference in the porcine data is most probably due to the nature and location of the pendulum impact in the two studies. The current study positioned the thorax pendulum impact swine specimens in a standing, quadrupedal orientation, with the spine horizontal (parallel to the floor), and the impacting mass centered on the mid thorax region at the 6th and 7th rib position. The Viano et al. (1989C) study, on the other hand, positioned the swine specimens in a 30-degree rotated orientation so the point of impact of the pendulum was lateral on the thorax and upper abdomen. This overlap of the thorax and abdomen would tend to be more compliant in response, therefore resulting in a lower force compared to the pure thoracic structure impacted in the current study. It should be noted that Viano et al. (1989C) documented the reason for the 30-degree rotated impact orientation of the specimens was due to observed swine body deformation coupling with whole body rotation reaching 22-degrees at the time of peak compression which lead to an inaccurate body deformation analysis. Superior view high speed video of the thoracic impacts performed in the current study were reviewed and revealed no such whole body rotation prior to peak impact force. Again, this is most likely due to the difference in pendulum impact location on the swine specimens in the two studies.

Comparison of the current study's lateral abdominal impact data for the 50th male PSE to the digitized human PMHS abdomen impact data presented in the Viano et al. (1989B) study was also performed (Figure 4.5.5). The human PMHS data (top – Figure 4.5.5) and the 50th male PSE data (bottom figure) essentially fall within the human ISO impact response corridors in terms of force magnitude and pulse duration. The human

PMHS data and the 50th male PSE are similar in impact pulse shape, peak force magnitude, and pulse duration.

The overall findings of the current study are consistent with previous human and swine lateral pendulum impact testing. Porcine thoracic and abdominal impact response data for all equivalent age levels studied tend to follow the scaled human ISO and van Rantingen response corridors, respectively. The shorter thoracic pendulum impact force pulse duration, however, is observed in PSE relative to the human ISO impact response corridors for all equivalent ages studied. In addition, these studies as well as the current study, showed the adult PSE thorax tends to develop higher resistive forces sooner and doesn't compress as much as the adult human thorax in lateral impact. This is most likely due to the difference in shape of the swine and human thorax, with the swine rib cages tending to be thinner in breadth and longer in depth than the human rib cage (Sack, 1982). This can have an effect on the magnitude of lateral forces and accelerations documented in the current study. Adult human and porcine abdominal pendulum force impact data tend to be similar in pulse shape, magnitude, and pulse duration.

Since abdominal deflection was not measured in the 6-year-old ATD tests, it was not measured for the swine in the current study; however, analysis of the porcine abdominal force-deflection properties would be valuable in the development of ATD biofidelity design and should be considered in future studies.

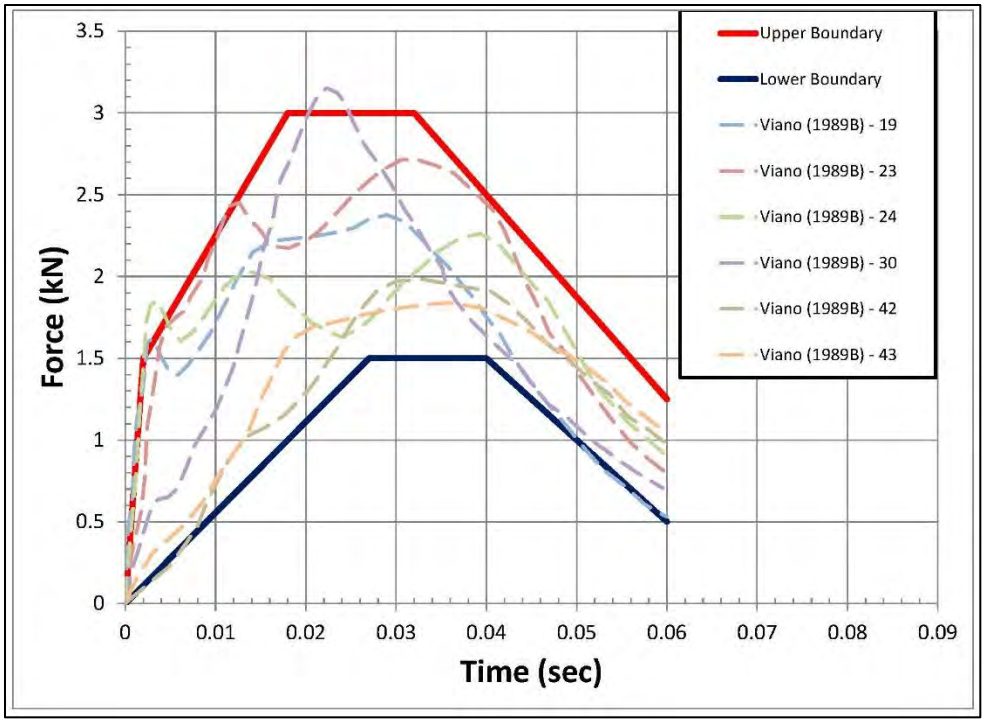

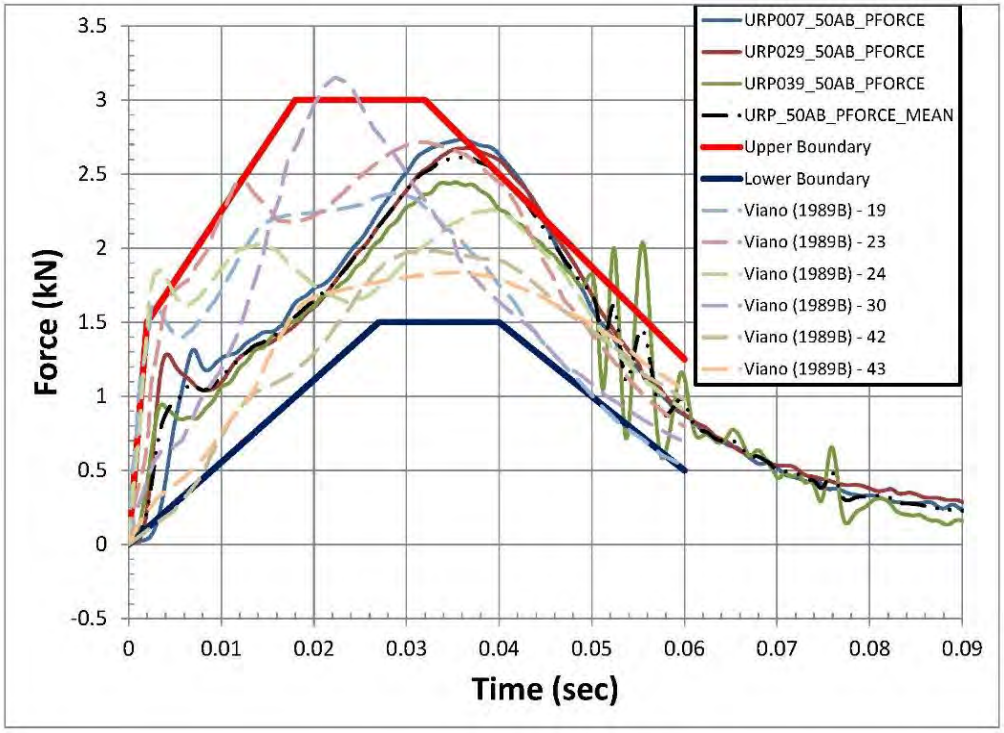

Figure 4.5.5 Comparison of Lateral Pendulum to Abdomen Impact Tests of Human PMHS (Viano et al. (1989B)) to 50th Male PSE (4.8 m/s impact speed)

This study has some important limitations. For instance, although the results were fairly consistent, only three porcine impact tests were conducted for each age level analyzed. Additional testing may be necessary to further quantify any significant variability relative to the presented data.

Weight appears to be an appropriate factor in determining suitable porcine surrogates for human test comparison. However, based on the results of the current study, specifically the fact that the swine torso is stiffer than the human, it is clearly not the only factor. More research needs to be performed to determine if other factors, such as torso stiffness or even swine breed, in combination with weight, can be established for the determination of more suitable swine surrogate models for human pediatric level side impact research. Based on the findings in the current study, further investigation is needed regarding the use of age as a secondary determining factor.

In order to impact the pigs in their upright standing position, a fixture was fabricated to suspend the pigs from chains passed through the swine specimen's dorsal adipose tissue. Multiple impact tests were performed to verify that the chains suspending the swine did not have any significant effect on the response data prior to maximum impact, either from the added mass of the chains or motion limitations during impact. The placement of the three suspension chains and their locations relative to the accelerometers was consistent from pig to pig throughout testing, based on their size. Any significant variation in chain placement could potentially have some effect on swine spinal bending during impact, and therefore, force and acceleration response data.

Any animal model has accompanying limitations in terms of its ability to represent human response. Although relative position of organs are similar, size, location, and

geometry of organs are not entirely comparable from pigs to humans. There are other certain anatomical differences between pigs and humans that can have an effect on the limitations of the current study's findings. For instance, pigs are quadrupedal compared to humans, who are bipedal. As quadrupedal mammals, porcine thoracic and abdominal organs are forced anteriorly (ventrally) due to gravity, whereas a human's organs are forced inferiorly. It should be noted that research performed by Pope et al. (1979) illustrated that influences due to unnatural positioning of the swine could affect impact response results to the thorax and abdomen. Therefore, it was decided to position the pigs in their natural standing position for current study testing and evaluation.

This author is not aware of any current or past thoracic or abdominal lateral impact research performed on human child PMHS. The only known human child PMHS research to date was performed in an anterior-posterior impact direction to the thoracic or abdominal region and was performed by Kent et al. (2006, 2009, 2011) and Ouyang et al. (2006). Ramanchandra et al. (2016) recently performed similar anterior-posterior loading to the abdomen with a transverse oriented seatbelt on adult human PMHS.

Ouyang et al. (2006) performed pneumatic ram loading anterior-posterior to the chest of child PMHS ages 2 to 12. A 2.5 kg impacting mass was used for child PMHS ages 2 to 4, and a 3.5 kg impacting mass was used for child PMHS ages 5 to 12. Impact speeds ranged from 5.9 to 6.4 m/s and resulted in peak impact forces ranging from 0.74 to 1.1 kN. Peak thoracic impact force magnitudes for the 3 to 10-year-old PSE in the current study range from 0.45 to 1.5 kN. The Ouyang et al. (2006) research appears, at least in force magnitude, to be consistent with the magnitude ranges of the current study 3 to 10-year-old PSE as well as the scaled 3 to 10-year-old thoracic impact response

corridors with respect to human lateral impact from Irwin et al. (2002).

Kent et al. (2006, 2009, 2011) showed that quasi-static and dynamic anterior-posterior loading to the abdomen by a transversely oriented seatbelt to their established 6-year-old PSE model abdomen, based on age and weight, was similar in response to the 6-year-old human PMHS abdomen. Belt forces at dynamic loading rates between 1.5 m/s and 7.8 m/s were found to be between 4 to 5 kN. This study also showed that load varied as a function of belt depth penetration into the abdomen and load rate. Ramanchandra et al. (2016) showed abdominal adult PMHS tested with seatbelt load rates ranging from 3.4 to 5.2 m/s and resulting in peak belt forces of 2.86 to 4.76 kN. The Kent et al. (2006, 2009, 2011) and Ramachandra et al. (2016) studies with respect to abdominal force magnitude appear to be greater than what was observed in the PSE abdominal pendulum impact force tests in the current study as well as the scaled 3 to 10-year-old abdomen impact response corridors suggested by van Rantingen et al. (1997) with respect to human lateral impact testing.

4.6 – Conclusions

The primary contributions of this study were to establish age equivalent PSE for the human 3, 6, 10-year-old, and the 50th percentile male; test the thoracic and abdominal regions of the PSE in lateral pendulum impact testing; and compare the results of the PSE lateral pendulum impact testing to established adult human and scaled child lateral impact response corridors for the thorax and abdomen.

The overall findings of the current study confirm that lateral impact force response of the thorax and abdomen of appropriate weight porcine surrogates established for human-equivalent-age 3-year-old, 6-year-old, 10-year-old, and 50th adult male are

consistent with the ISO human scaled lateral impact response corridors presented in Irwin et al. (2002) and van Rantingen et al (1997). Peak PSE thoracic and abdomen pendulum impact force magnitudes essentially fell within the ISO human impact response corridors for all ages. PSE thorax pendulum impact force pulse durations were shorter than the human impact response corridors by approximately 10 msec, whereas the PSE abdominal pendulum impact force pulse durations tended to be within or slightly longer than the human impact response corridors.

Based on the statistical analysis performed, there is a significant linear correlation with respect to peak impact pendulum force and age for porcine thoracic and abdominal test data compared to the ISO human scaled impact response corridors. As for the thoracic T1 acceleration, no significant correlation was found with respect to the thoracic T1 acceleration response data of the pigs when compared to human scaled T1 acceleration response corridors.

The results of the current study confirm that the current ISO scaling laws are applicable and correspond well with PSE ages 3 to adult lateral impact force versus time data at the thorax and abdominal regions. Due to the scarcity of child PMHS data for research in occupant safety in vehicle crashes, animal testing, and particularly porcine thorax and abdomen testing, provides the most applicable and definitive surrogate model to human force response at all equivalent age levels. Porcine surrogate testing in lateral impact can prove to be a powerful research means with regard to vehicle safety.

Further investigation is needed to better understand and interpret the higher magnitude accelerations experienced at T1 for all age PSE compared to scaled human impact response corridors in order to be able to incorporate this data into research

capabilities as well. It appears, from the current study, that T1 acceleration data during thorax impact testing is roughly two times greater in magnitude and slightly less in time pulse duration than corresponding human scaled corridors at all age levels tested.

CHAPTER 5 – ESTABLISHMENT OF SWINE RIB ELASTIC BENDING MODULUS AND COMPARISON TO HUMAN EQUIVALENTS (SPECIFIC AIMS 3-4)

5.1 – A Review of Experimental Studies for the Established Rib Elastic Bending Modulus Using both Human and Animal Surrogates

Child ATDs have been developed over the years based principally by scaling human adult male PMHS test data down to the size of the child. Various scaling methods have been utilized to factor in differences in child versus adult geometry, material properties, or a combination of the two. However, it is a challenge to scale adult tissue properties to pediatric properties because the majority, if not all of the scaling techniques used have never been fully validated against pediatric tissue or cadaver tests (Franklyn, 2007). Research continues in order to establish up-to-date pediatric, adult, and animal surrogate geometry and material properties to aid in validating scaling techniques. One material property of interest in lateral impacts is rib elastic bending modulus.

Berteau et al. (2012) performed a study to provide elastic property values as a function of human growth for cortical bone by analyzing fibula long bone surgical waste (bone transplantation). Eighteen bone samples, from children ages 4 to 16, were tested to obtain young's modulus of elasticity data through three-point microbending. Specimens were loaded under displacement control at a rate of 0.1 mm/min until they failed. An average young's modulus of elasticity of 9.1 GPa was found for the child long bone samples tested. This finding is more than the 6.6 GPa elastic modulus used by Irwin and Mertz (1997) for their human response corridor scaling technique which was based on pediatric parietal bone test data.

Agnew et al. (2013) researched 44 pediatric rib specimens obtained during autopsy from 12 specimens, ages 5 months to 9 years old, to characterize the elastic

properties of human pediatric ribs. The pediatric rib segments were subjected to three-point bending tests simply supported and loaded at their central points. Specimens were loaded under displacement control at a quasi-static rate of 2.5 mm/min until they passed the point of gross failure. An average young's modulus of elasticity of 4.86 GPa was found for the pediatric rib segments tested. This finding is less than the 6.6 GPa elastic modulus used by Irwin and Mertz (1997). A young's modulus of elasticity of 3.4 GPa and 8.0 GPa were measured for the two 3-year-old specimens, 5.65 GPa was measured for the 6-year-old specimen, and 9.8 GPa was measured for the 9-year-old specimen. Rib bending properties from the Agnew et al. (2013) study were compared in the study to other pediatric and adult rib bending property experimental studies known at the time and are provided in Table 5.1.1, below. The analysis of adult rib properties by Yoganandan and Pintar (1998) produced the closest test comparison, in terms of rate and test type (3-point bending), to the Agnew et al. (2013) rib property study, resulting in an average young's modulus of elasticity for the adult rib of approximately 2.32 GPa.

Table 5.1.1 Agnew et al. (2013) Pediatric Rib Bending Comparative Values for Measured Properties from Other Relevant Three-Point Bending Tests on Anterior or Lateral Rib Sections or Coupons

	Current study	Theis[53]	Yoganandan and Pintar[60]	Kemper *et al.*[27]	Stitzel *et al.*[50]	Granik and Stein[25]
Sample	Pediatric (<9 years)	Pediatric (<14 years)	Adult	Adult	Adult	Adult
N, *n*	12, 44	–, 3	30, 120	6, 48	4, 92	10, –
Element	Rib section	Rib section	Rib section	Rib section	Rib coupon	Rib section
Rate (mm/s)	0.042	Quasi-static	0.042	172	356	–
F_P (N)	65.97	240	153	–	–	–
M_P (Nm)	1.025	4.7*	3.8	5.5	–	–
K (N/mm)	29.81	–	–	132.3	–	–
E (GPa)	4.86	–	2.32	20.02	9.68	11.5
σ_Y (MPa)	76	–	–	–	62.25	–
σ_P (MPa)	87.4	–	–	184.7	135.1	106.2

Missing values (–) were not reported in the original cited manuscript. For studies that utilized both lateral and anterior specimens, reported results are averaged between them.
N number of subjects, *n* number of specimens.
* This value is based on other assumed metrics, so should be interpreted with caution.

Bradley et al. (2013) analyzed the 6th ribs of one-day-old domestic pig models (*Sus scrofa*) in three test scenarios (dried, fresh, frozen-then-thawed) to study rib fracture

mechanics and the force limit at which fracture occurs in peri- and post-mortem states. A 500 N load cell was used in combination with a 10 mm/min cross-head speed and 10 mm loading span width with 30 mm support span setup for 4-point force/displacement bending. Since conventional 4-point bending testing uses specimens of beam shapes having rectangular cross-sections, the ribs strength and modulus results of this study were converted to be representative of the ribs' more circular/elliptical shape. The mean elastic bending modulus was found to be 8.41 GPa for fresh rib specimens, 20.34 GPa for dried rib specimens, and 8.99 GPa for thawed rib specimens.

Keiser et al. (2013) analyzed the 5th ribs of freshly slaughtered one-year-old male domestic pig models (*Sus scrofa*) with hanging weights of 85 to 115 kg in two test scenarios (fresh ribs with retained periosteum and dried ribs) to study rib fracture mechanics in bending and the force limit at which fracture occurs in peri- and post-mortem states. A 50 kN load cell was used in combination with a 10 mm/min cross-head speed and 20 mm loading span width with 100 mm support span setup for 4-point force/displacement bending. Rib strength and modulus results of this study were converted to be representative of the ribs' more circular/elliptical shape. The effective elastic bending modulus was found to be 4.7 GPa for fresh rib specimens and 4.92 GPa for the dried rib specimens.

Large variations in biomechanical response were observed in the reported literature, particularly with respect to rib elastic modulus. Load rates, sample preparation, sample size, and test methods (3-point bending versus 4-point bending) used in studying human pediatric and adult rib mechanical properties, including elastic bending modulus) compared to pig rib fracture models are different, and therefore, it is difficult to compare

them directly here.

5.2 – A Brief Review of Pig and Human Skeletal Maturation

Reiland (1978) documented the skeletal development and growth rate of healthy domestic pigs in the form of weight curves, longitudinal bone growth, closure of growth plates, and development of teeth. Domestic swine sexual maturation has been found to occur at approximately 5 to 6 months of age based on: (1) an inflection point of the weight curve with respect to age, (2) the occurrence of sperm in male pig ejaculate, and (3) the timeframe when female pigs come into heat (Reiland, 1978). The weight versus age curve established in Reiland (1978) is similar the weight versus age curve established in Kent et al. (2006). Swine growth plate closure, provided in Table 5.2.1 below, was determined based on radiographic and anatomic observations (Reiland, 1978). Size and shape of domestic swine have evolved over time due to the desire of the farmer to establish more economic characteristics such as rapid growth, low feed consumption, low fat composition, and larger muscle volume (Reiland, 1978). This may make it difficult to establish skeletal growth and maturation characteristics as a function of age and weight for swine test subjects.

Table 5.2.1 Reiland (1978) Swine Growth Plate Closure Ages

Growth Plate Closure Site	Domestic Pig Age (months)	Domestic Pig Age (days)
Phalanges	4	122
Metacarpals/Metatarsals	12 to 14	360 to 420
Distal Radius & Ulna	20	608
Proximal Radius & Ulna	10	304
Proximal Humerus	18	548
Distal Tibia	12	365
Proximal Tibia	20	608
Distal Femur	20	608
Femoral Head	18	548
Ischeatic Tuberosity	20	608
Vertebrae	30 to 36	900 to 1080
Rib Head Region	N/A	N/A

Scheuer and Black (2004) documented the skeletal development and growth of the healthy human juvenile skeleton. Human male and female sexual maturation has been found to occur at approximately 10 to 16 years of age (Scheuer and Black, 2004). Human juvenile growth plate closure at various body regions, is provided in Table 5.2.2 below.

Table 5.2.2 Scheuer and Black (2004) Human Juvenile Growth Plate Closure Ages

Growth Plate Closure Site	Human Male Age (Years)	Human Female Age (Years)
Phalanges	15 to 16	13 to 15
Metacarpals/Metatarsals	15 to 20	14 to 17
Distal Radius & Ulna	16 to 20	14 to 17
Proximal Radius & Ulna	13 to 17	11.5 to 14
Proximal Humerus	16 to 20	13 to 17
Distal Tibia	16 to 20	14 to 18
Proximal Tibia	15 to 19	13 to 17
Distal Femur	16 to 20	14 to 18
Femoral Head	14 to 19	12 to 16
Ischeatic Tuberosity	16 to 18	16 to 18
Vertebrae	10 to Early 20's	10 to Early 20's
Rib Head Region	17 to 25	17 to 25

No known correlation has been established with respect to rib elastic bending modulus as a function of age of swine rib material properties compared to human rib material properties. In order to develop a scaling technique using animal surrogate test data relative to the human pediatric level, particularly in side impact, further scaling parameters in addition to the ones already determined above need to be established.

5.3 – Methods

Porcine Surrogate Rib Section Bending Elastic Modulus

Quantification of rib section elastic bending modulus for the determined 3-year-old, 6-year-old, 10-year-old, and 50th percentile adult human male PSE was performed in order to establish test scaling parameters for the porcine thorax and abdomen as provided in Mertz (1984), Irwin and Mertz (1997) and Irwin et al. (2002) for the human. Gross dissection was performed of the non-struck whole rib 6-7 segments of the thoracic pendulum impacted swine specimens, post testing, allowing for a one-to-one correspondence with the struck side response and material property data. The rib sections were wrapped in saline gauze, placed in a zip lock bag, and stored in a freezer at -20 degrees C until testing.

The methods for testing, described herein, are similar to those utilized in the rib material property research performed by Agnew et al. (2013) and Stitzel et al. (2003). Dynamic three-point bending as per ASTM Standard D790-00 (ASTM International, 2010) was used to measure the material properties of the rib segments where the ribs were simply supported and a load applied by an actuator through its central point. An adjustable aluminum 3-point bending fixture was fabricated to accommodate various length rib specimens. All contact surfaces on the fixture were rounded to a diameter of 10 mm (0.4

in) per the ASTM D790 standard (Standard Test Methods for Flexural Properties of Unreinforced and Reinforced Plastics and Electrical Insulating Materials) in order to confirm that supports and the impacting surface of the actuator were adequately rounded to reduce stress concentrations during testing.

For testing, rib sections, previously harvested and stored as discussed above, were removed from the freezer and allowed to thaw to room temperature. All rib specimens were kept moist throughout testing. All possible soft tissue, excluding the periosteum, was detached from the rib segment specimens.

Each rib specimen was measured from the notch on the rib just lateral of the costochondral juncture to the start of the acute angle of the rib near its attachment to the spine (see Figure 5.3.1). Half of this measured distance was used to determine the actuator load location which was consistent with the struck side rib region impacted during the pendulum impact testing. Ribs were loaded with the actuator on the convex side of the rib, consistent with lateral impact to the rib cage. The rib cross section was measured at this actuator load placement location using digital calipers and measuring the cross-section in the direction of the applied load.

Span lengths for tested rib segments were determined such that the ratio of the rib length (beam length) to rib cross-section was suitable for simple bending analysis (span length/cross-section depth>5) such that maximum shear stress was negligible (Boresi and Schmidt (2003)). This was achieved by taking the measured distance from the notch on the rib just lateral of the costochondral juncture to the start of the acute angle of the rib near its attachment to the spine and subtracting 10 percent of that length from either side (per ASTM D790 standard). This method accomplished the requirement of negligible

shear stress loads and established a consistent method for determining span length across various sized rib specimens. This span length determination method was chosen to provide the widest possible span length for each tested rib in order to assure the best opportunity for rib response similar to the pendulum impact testing.

The top portion of the 3-point bending fixture was securely attached to an Instron Testing System (Norwood, MA) and was used to apply a 5 N pre-load through the superior actuator to the convex rib segment in order to guarantee the rib specimen was secure prior to testing. Rib segments were tested quasi-statically with a controlled actuator displacement rate of 2.5 mm/min, similar to the displacement rate used in Agnew et al. (2013) as well as Yoganandan and Pintar (1998). Displacement was allowed past the point of rib fracture. The force of the superior actuator was recorded using a load cell. The force and displacement data for the loading superior actuator was recorded by the Instron Testing System at a sampling rate of 2,000 Hz for each rib segment tested. A sample of the setup for each rib section and rib loaded to fracture are shown in Figure 5.3.1, below.

Prior to rib bending testing, the ribs segments were CT scanned using a Siemens Inveon Hybrid Micro-PET/CT scanner. Rib specimens were scanned over a 4-cm length, approximately 2 cm either side of the actuator load location. CT scans were collected at 0.04 mm intervals using a scanning resolution of 3072 x 2048. The CT scan nearest the actuator load location for each rib tested was imported into ImageJ (Rasband (1997-2014)) software to determine total subperiosteal cross-sectional area (Tt. Ar.), area moments of inertia (I), and section moduli (Z) by utilizing the MomentMacro plug-in (Ruff (2015)). Cortical bone cross-sectional area (Ct. Ar.), was determined by subtracting the

sub-endosteal cross-sectional area from the total subperiosteal cross-sectional area. A CT scan of one of the tested ribs is provided in Figure 5.3.2 below.

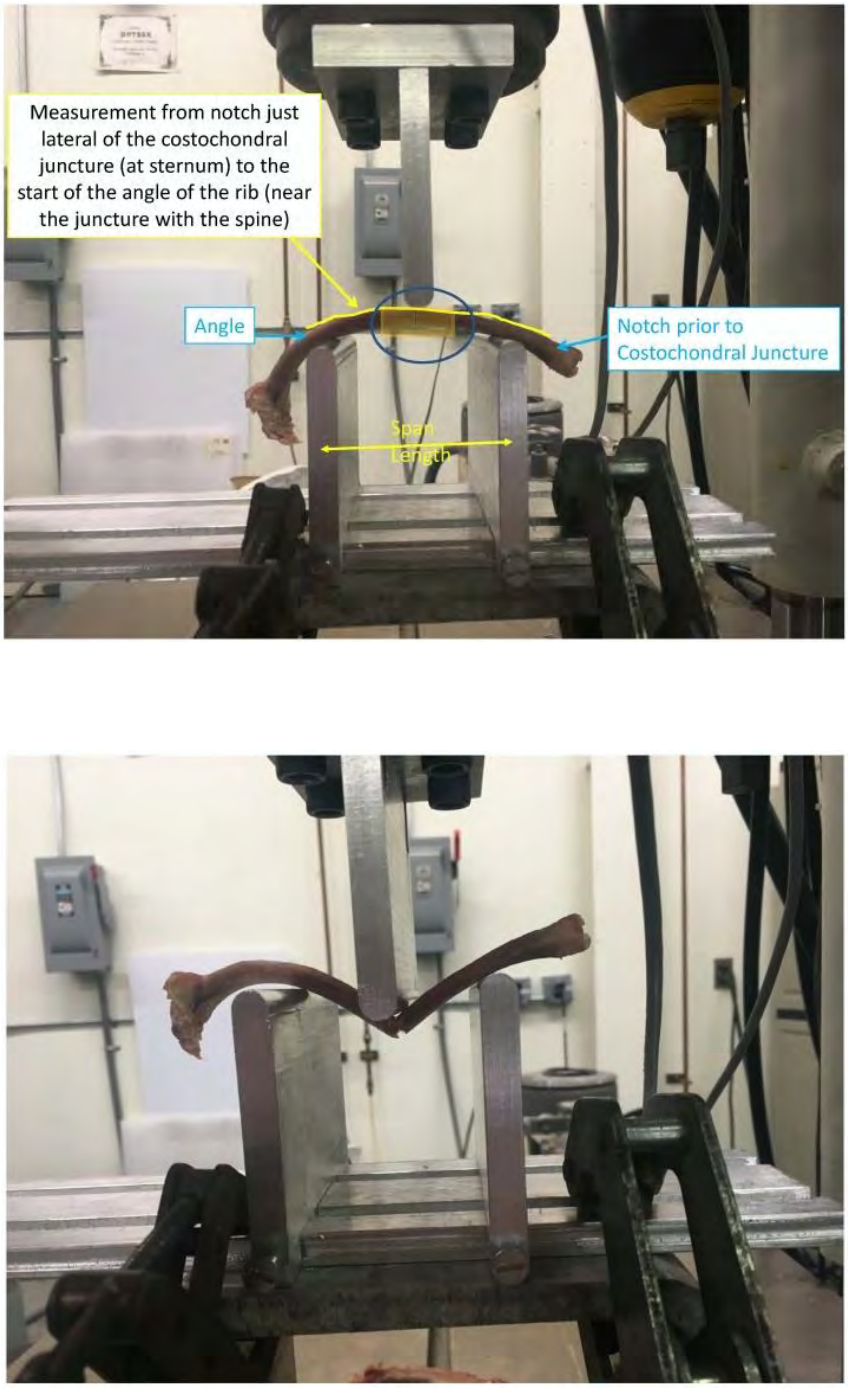

Figure 5.3.1 Rib Specimen 3-Point Bending Fixture, Setup, and Load to Fracture

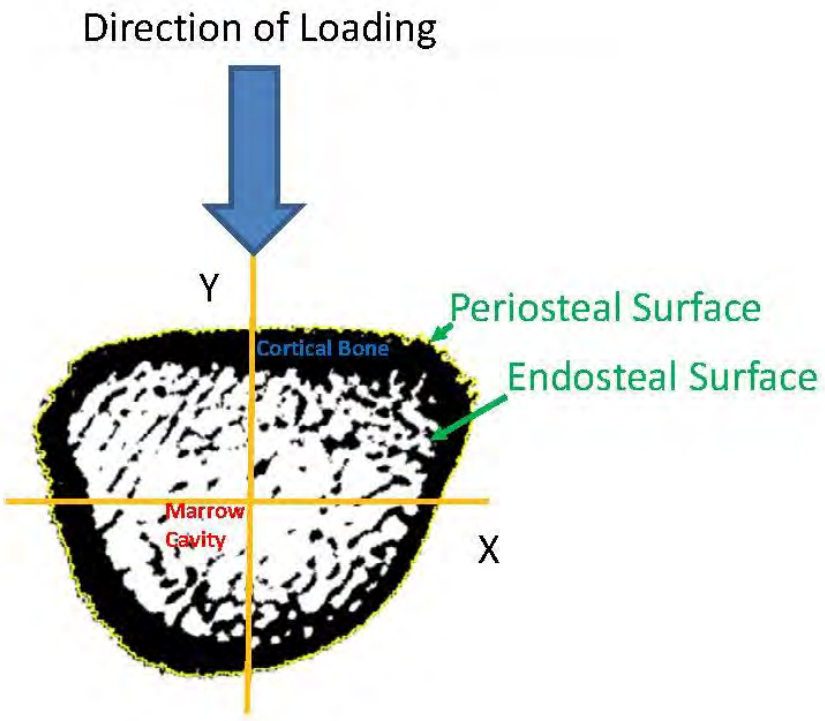

Figure 5.3.2 Rib CT Scan Used to Determine Cross-Sectional Properties

Material properties of the PSE rib segments tested were calculated using a series of simple beam bending analysis equations. Bending moment can be determined using the reaction force from one of the two outer simple rib segment mount supports and one-half the rib segment span length (L/2). The equation to calculate the bending moment is simply (Eq. 1):

$$M = \frac{FL}{4} \qquad (1)$$

Where:

M = Bending Moment

F = Applied Actuator Force

L = Span Length

Maximum displacement of the rib segment can be characterized based on a simple

point-load at the center of a beam simply-supported at both ends as (Eq. 2):

$$\delta = \frac{FL^3}{48EI} \qquad (2)$$

Where:

δ = Rib Segment Displacement

F = Applied Actuator Force

L = Span Length

E = Young's Modulus

I = Area Moment of Inertia

The maximum displacement equation (Eq. 2) is rearranged in order to determine Young's Modulus (elastic bending modulus) (Eq. 3) as:

$$E = \frac{FL^3}{48\delta I} \qquad (3)$$

The effective stiffness of the rib segment, K, is determined by taking the slope of the Force-Displacement curve, through (Eq. 4):

$$K = \frac{F}{\delta} \qquad (4)$$

In order for the analysis using the above equations to be valid, the following assumptions were made:

- The above equations relative to 3-point bending are valid prior to rib material yielding.
- The rib is straight such that the ratio of the radius of curvature to depth of

beam is greater than 5 (Boresi et al. (2003)).

- The ratio of the span length to cross-section of the rib is greater than 5 to minimize effects of shear stresses (Boresi et al. (2003)).
- The material is homogeneous and isotropic.

The force data recorded by the load cell from the superior actuator was plotted against the displacement of the actuator. The end of the linear (or elastic) portion of the force-deflection curve was defined by identifying where its average slope deviated below the mean of all preceding calculated average slopes by more than one standard deviation. This process is illustrated in Figure 5.3.3 below for Rib 6 of one of the 6-year-old PSE.

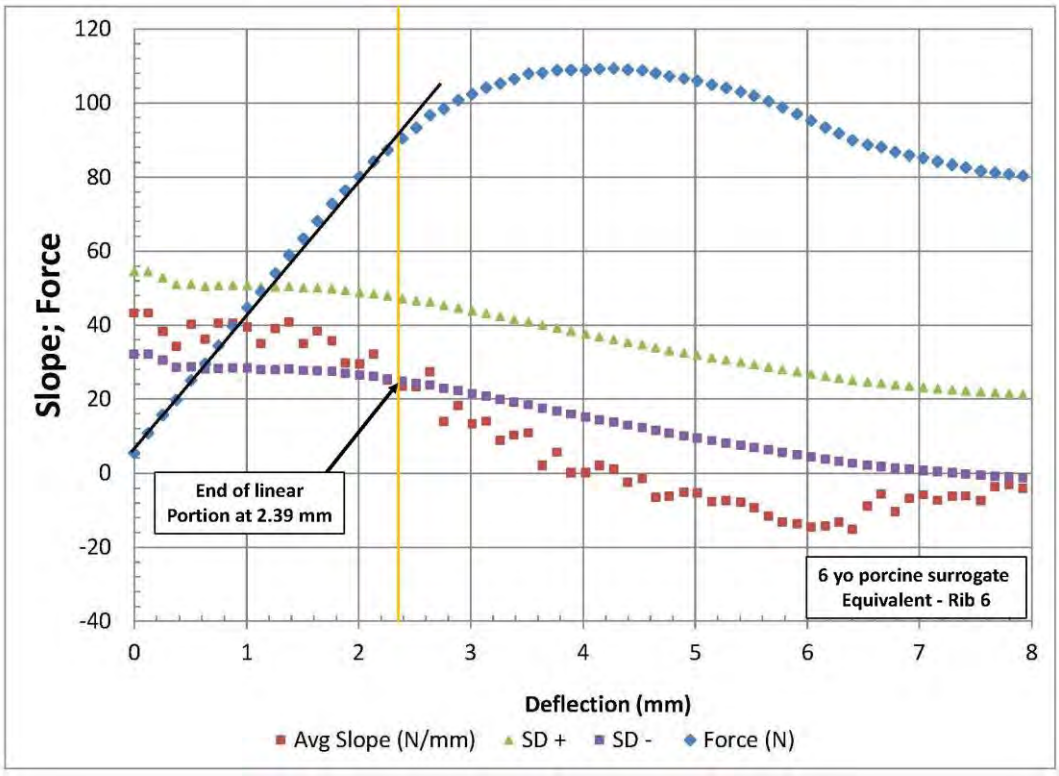

Figure 5.3.3 Average Slope Exceeds the Slopes one STD, Defining the Linear Region of the Force-Deflection Curve

The stiffness, K, was defined as the slope of the defined linear portion of the force-deflection curve. Once the linear portion of the force-deflection curve was defined, this

data was fit with a linear regression equation. A power curve was then fitted to the plastic region (non-linear portion) of the force-deflection curve from 90% of the maximum force level to maximum force. The yield force of the rib specimen was defined as the force at which the linear fit and power fit of the force-deflection curve intersected. This method was adopted from that developed by Pfefferle et al. (2007). This process is illustrated in Figure 5.3.4 below for Rib 6 of one of the 6-year-old PSE.

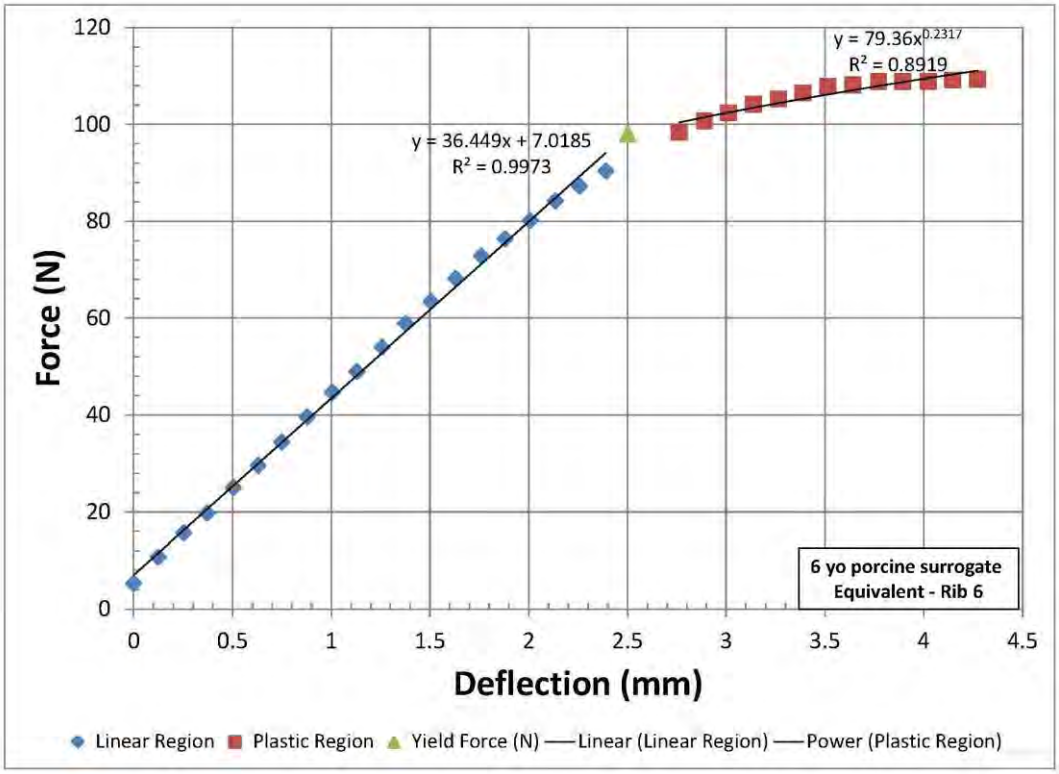

Figure 5.3.4 Rib Testing Linear Region Stiffness and Yield Force Determination

In addition to their intended use for the current study, the calculated material properties of the tested PSE rib segments were compared to past research related to swine and human rib segment material properties.

5.4 – Results

Force-deflection curves from the swine rib 3-point bending tests performed on the

3-year-old, 6-year-old, 10-year-old, and 50th percentile adult human male PSE are provided in Figures 5.4.1 through 5.4.4, respectively. All force-deflection curves from the swine rib 3-point bending tests performed are provided in Figures 5.4.5, below.

As shown in Figure 5.4.5, the amount of force the swine rib can sustain increases with age. Rib stiffness (slope of the increasing portion of the force-displacement curve) is higher from the 3-year-old equivalent age to the 6-year-old equivalent age but was comparable between the 6-year-old and 10-year-old equivalent ages. Rib stiffness increased again from the 10-year-old equivalent age to the adult equivalent age

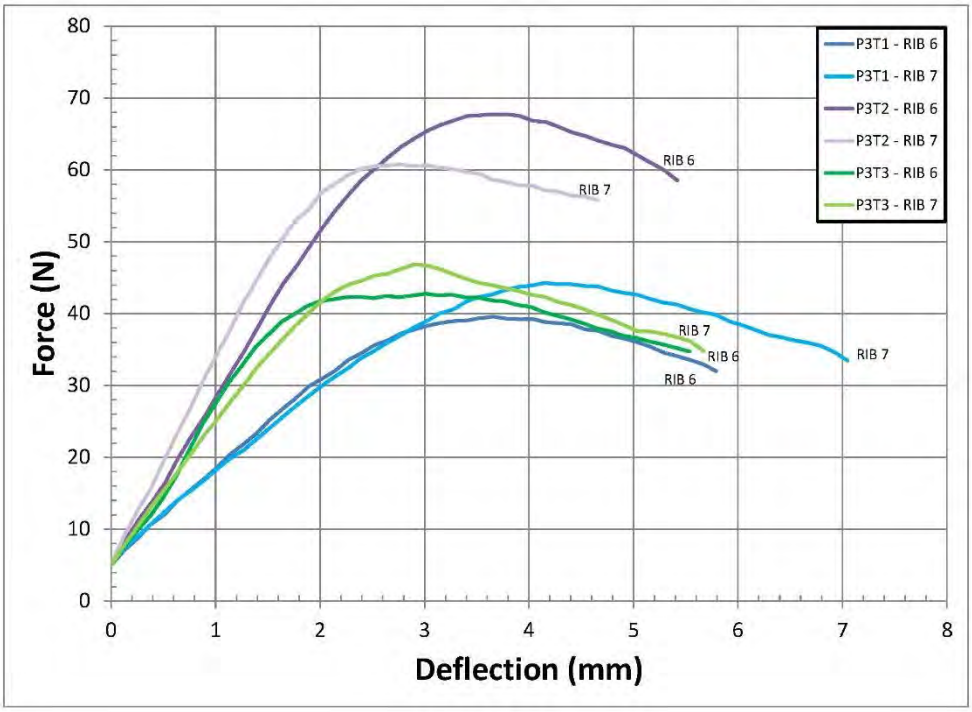

Figure 5.4.1 3-Year-Old Human PSE Rib 3-Point Bending Test Force-Displacement Curves

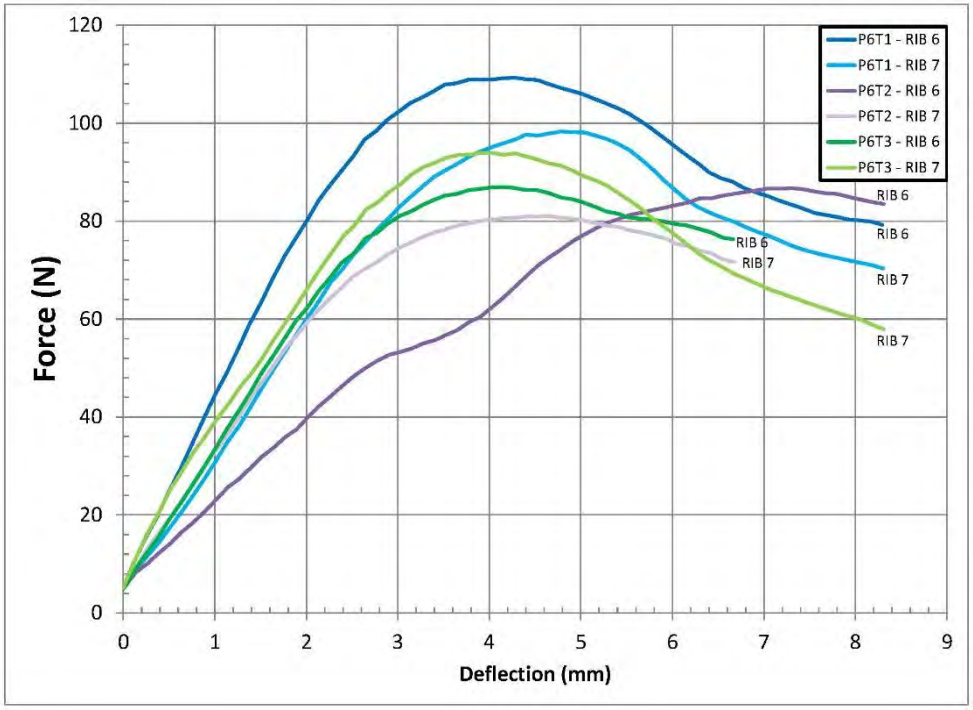

Figure 5.4.2 6-Year-Old Human PSE Rib 3-Point Bending Test Force-Displacement Curves

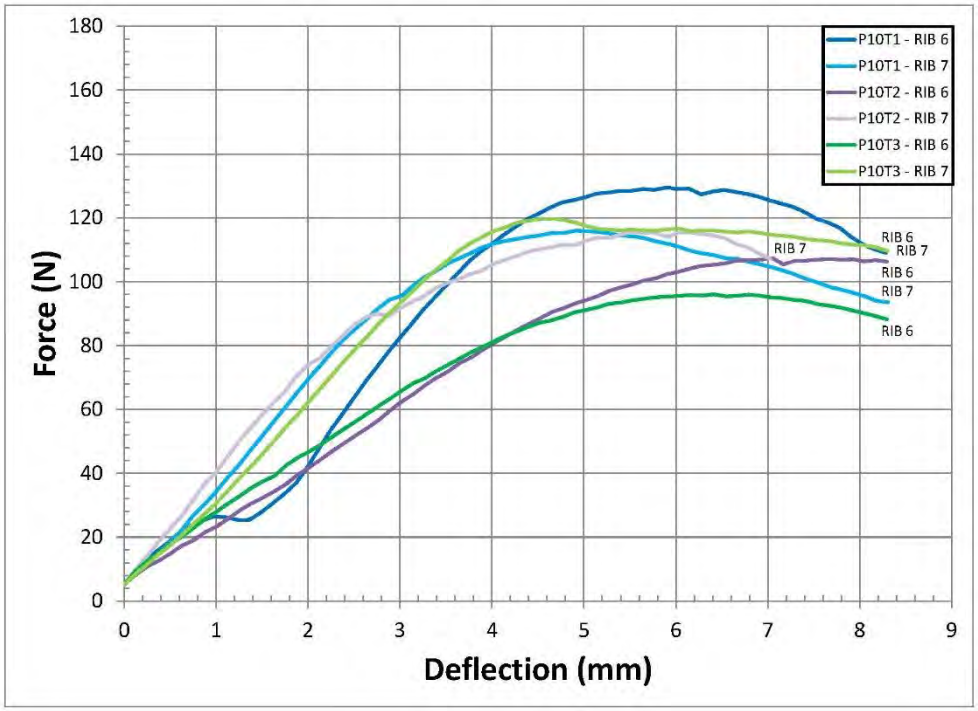

Figure 5.4.3 10-Year-Old Human PSE Rib 3-Point Bending Test Force-Displacement Curves

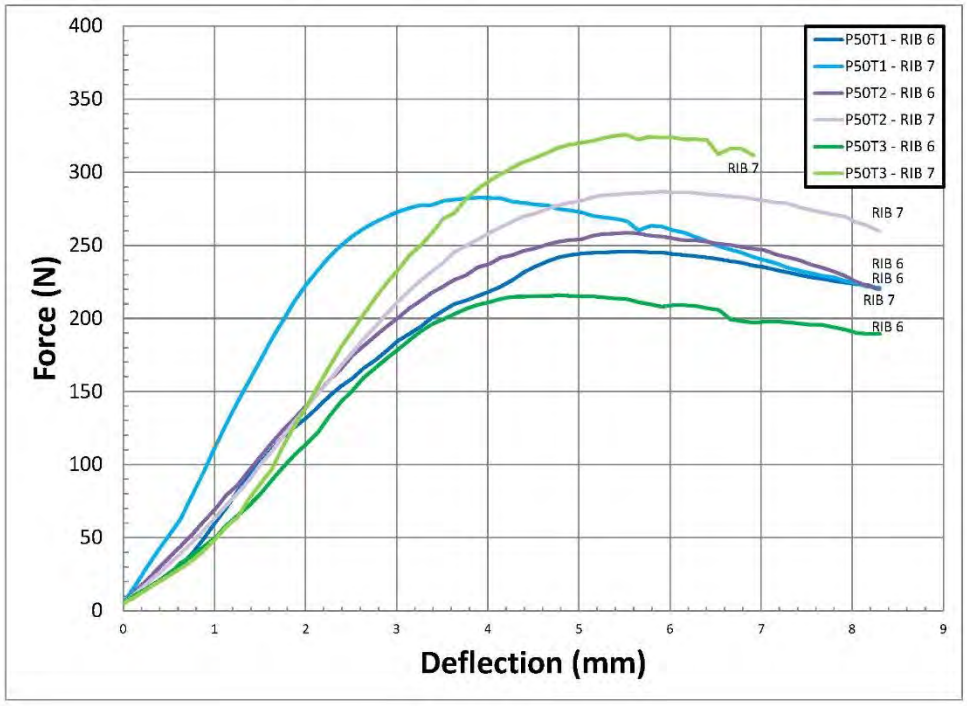

Figure 5.4.4 50th Percentile Human Male PSE Rib 3-Point Bending Test Force-Displacement Curves

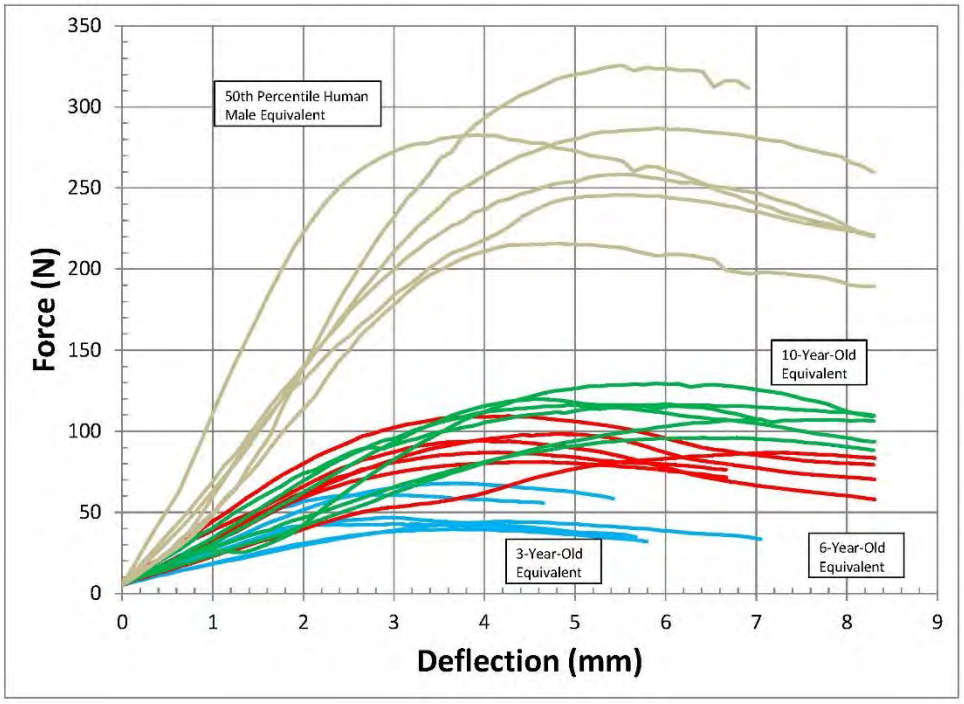

Figure 5.4.5 All PSE Rib 3-Point Bending Test Force-Displacement Curves

.

Table 5.4.1 summarizes the cross-sectional data for each rib specimen while Table 5.4.2 summarizes the mechanical properties for each rib specimen tested.

Table 5.4.1 Summary of Tested Swine Rib Specimens Cross-Sectional Properties

ID	Rib Level	Eq. Age	L (mm)	Tt. Ar. (mm^2)	Ct. Ar. (mm^2)	I (mm^4)	Z (mm^3)
P3T1	6	3 yr	59.84	31.41	14.53	29.87	12.17
P3T1	7	3 yr	61.12	28.89	12.65	28.80	11.02
P3T2	6	3 yr	57.84	36.84	13.08	33.04	11.85
P3T2	7	3 yr	59.76	42.38	19.11	58.93	19.53
P3T3	6	3 yr	58.88	30.46	12.11	34.13	13.28
P3T3	7	3 yr	59.84	29.17	12.85	34.12	12.72
AVERAGE			59.55	33.19	14.05	36.48	13.43
P6T1	6	6 yr	56.00	47.53	25.71	111.93	29.26
P6T1	7	6 yr	58.08	42.16	24.13	98.86	25.02
P6T2	6	6 yr	61.92	37.94	22.08	74.89	20.95
P6T2	7	6 yr	62.48	32.40	18.69	61.44	16.54
P6T3	6	6 yr	62.00	48.12	31.47	104.03	28.56
P6T3	7	6 yr	65.60	37.22	21.85	73.37	20.84
AVERAGE			61.01	40.89	23.99	87.42	23.53
P10T1	6	10 yr	74.24	51.11	20.93	132.44	34.55
P10T1	7	10 yr	74.56	49.85	28.36	127.72	33.04
P10T2	6	10 yr	75.28	72.36	39.98	190.84	45.29
P10T2	7	10 yr	74.72	62.30	24.84	187.68	42.25
P10T3	6	10 yr	75.20	59.50	27.70	172.40	39.44
P10T3	7	10 yr	75.36	49.03	25.72	136.99	32.16
AVERAGE			74.89	57.36	27.92	158.01	37.79
P50T1	6	50th male	91.12	132.11	53.04	757.85	119.26
P50T1	7	50th male	88.00	110.26	45.87	634.56	95.51
P50T2	6	50th male	88.00	129.24	57.01	599.03	111.80
P50T2	7	50th male	91.68	99.99	46.56	481.77	85.19
P50T3	6	50th male	91.84	127.75	31.41	381.84	66.95
P50T3	7	50th male	88.00	112.80	37.81	530.49	90.74
AVERAGE			89.77	118.69	45.29	564.26	94.91

Table 5.4.2 Summary of Tested Swine Rib Specimens Mechanical Properties

ID	Rib Level	Eq. Age	d_P (mm)	F_P (N)	d_Y (mm)	$Force_Y$ (N)	M_Y (N-mm)	E (Gpa)	K (N/mm)	σ_Y (MPa)	σP (MPa)
P3T1	6	3 yr	3.65	39.58	2.28	35.07	524.65	1.94	12.98	43.11	48.66
P3T1	7	3 yr	4.15	44.27	2.73	38.20	583.70	1.95	11.78	52.98	61.40
P3T2	6	3 yr	3.66	67.76	2.32	59.47	859.94	2.87	23.50	72.54	82.65
P3T2	7	3 yr	2.77	60.77	1.75	54.49	814.08	2.11	28.00	41.69	46.49
P3T3	6	3 yr	3.01	42.80	1.56	39.70	584.38	2.85	22.90	44.00	47.43
P3T3	7	3 yr	2.90	46.84	1.94	42.10	629.82	2.45	18.71	49.53	55.11
AVERAGE			3.36	50.34	2.10	44.84	666.09	2.36	19.65	50.64	56.96
P6T1	6	6 yr	4.27	109.28	2.50	98.10	1373.40	1.19	36.45	46.93	52.28
P6T1	7	6 yr	4.78	98.27	2.98	85.80	1245.82	1.13	27.45	49.79	57.03
P6T2	6	6 yr	7.30	86.70	3.99	73.88	1143.66	1.13	17.10	54.59	64.06
P6T2	7	6 yr	4.65	81.00	2.32	68.28	1066.53	2.23	26.92	64.49	76.51
P6T3	6	6 yr	4.14	86.90	2.52	76.90	1191.95	1.36	28.49	41.73	47.16
P6T3	7	6 yr	4.03	93.90	2.69	85.29	1398.76	2.26	28.19	67.12	73.90
AVERAGE			4.86	92.68	2.83	81.38	1236.69	1.55	27.43	54.11	61.82
P10T1	6	10 yr	5.90	129.49	4.01	117.54	2181.54	2.35	36.47	63.13	69.55
P10T1	7	10 yr	4.90	115.95	3.06	103.06	1921.04	2.22	32.81	58.14	65.42
P10T2	6	10 yr	7.05	107.44	4.04	80.75	1519.72	0.87	18.76	33.56	44.65
P10T2	7	10 yr	6.03	115.66	2.53	93.81	1752.39	1.62	34.95	41.48	51.14
P10T3	6	10 yr	6.40	96.04	3.99	85.11	1600.07	1.00	19.39	40.57	45.78
P10T3	7	10 yr	4.65	119.68	3.61	110.55	2082.76	1.95	29.98	64.77	70.12
AVERAGE			5.82	114.04	3.54	98.47	1842.92	1.67	28.73	50.28	57.78
P50T1	6	50th male	5.65	245.65	3.14	208.34	4745.99	1.41	67.68	39.80	46.92
P50T1	7	50th male	3.89	282.60	2.27	254.25	5593.50	2.51	112.02	58.57	65.10
P50T2	6	50th male	5.52	258.53	3.29	226.06	4973.32	1.60	67.62	44.49	50.87
P50T2	7	50th male	5.90	286.86	3.68	256.49	5878.75	2.36	70.69	69.01	77.18
P50T3	6	50th male	4.78	215.87	3.38	199.31	4576.16	2.55	60.41	68.35	74.03
P50T3	7	50th male	5.52	325.59	3.70	290.10	6382.20	2.37	88.59	70.34	78.94
AVERAGE			5.21	269.18	3.24	239.09	5358.32	2.13	77.84	58.42	65.51

5.5 – Discussion

Table 5.5.1, below, provides a summary of the average rib material properties from the current study as well as from other swine and human rib bending material properties research. Those studies highlighted in blue in the table were run at quasi-static load rates and the studies in white were run at dynamic load rates. All dynamic load rate testing generated higher Modulus of Elasticity results than the quasi-static testing, with the exception of the Granik and Stein (1973) testing, which produced an average Modulus of Elasticity of 11.5 GPa from its quasi-static rib 3-point bending test research.

Table 5.5.1 Comparative Values for Material Properties from Other Relevant Human and Swine Rib Bending Research

Author	Loading Type	No. of Specimens	Specimen Age Range (year)	Rib Level	L (mm)	Load Rate (mm/sec)	F_P (N)	K (N/mm)	E (Gpa)	σ_P (MPa)
Human										
Granik and Stein (1973)	3-point bending	15 cadavers	Adult	6,7	101.6	0.042			11.5	160
Yoganandan and Pintar (1998)	3-point bending	120	Adult	7	100	0.042	158		2.3	
				7	100	0.042	137		1.9	
Stitzel et al. (2003)	3-point bending (coupon)	80	Adult	1-12, Anterior	20	356			7.5	116
				1-12, Lateral	20	356			11.8	153
				1-12, Posterior	20	356			10.7	127
Kemper et al. (2005)	Tensile coupon test	117	Adult	1-12, Anterior and Posterior		0.5 strain/sec			14	120
Kemper et al. (2007)	Tensile coupon test	46	Adult	4-7, anterior and Lateral	82.55	0.5 strain/sec		57.99-225.71	13.3-15.1	110-140
	3-point bending	48		4-7, anterior and Lateral		1778 mm/sec (0.7 strain/sec)				
Sandoz et al. (2007)	3-point bending	31	Adult	4,5,6,7,9	100	250	230			
				4,5,6,7,9	100	100	210			
				4,5,6,7,9	100	0.033	150			
Subit et al. (2011)	Tensile coupon test	10	Adult	6,7		0.01-0.02			13.5	112
						24				94-1550
Agnew et al. (2013)	3-point bending	11	0	5,6,7	33 to 109	0.042	42.98	23.33	3.54	81.63
		8	1	6,7,8		0.042	44.74	18.77	3.12	82.58
		11	2	5,6,7		0.042	70.7	37.08	3.49	74
		8	3	6,7		0.042	84.62	37.52	5.765	94.115
		2	6	5,6		0.042	110.7	44.11	5.65	119.6
		4	9	6,7		0.042	90.44	20.05	9.8	87.4
Kalra et al. (2015)	3-point bending	82	Adult		100	0.169	188			
Schultz et al. (1974)	Whole Rib Bending - Frontal Load	5	Adult	2,4,6,8,9,10		Incremental loading with 2.45 N	7.35			
Li et al. (2010)	Whole Rib Bending - Frontal Load	3	Adult	2,4,10		2	41.2-57.1			
						500-1000	87.4-123.4			
Schafman (2016)	Whole rib bending - Frontal Load	184	4 to 99			1000-2000	17-300	0.4-13.1		
Porcine			Human Equivalent Age (Years)							
Bradley et al. (2013)	4-point bending**	8 thawed	0	6	80	0.167	17.98		8.99	
Kieser et al. (2013)	4-point bending**	20 wet	Adult	5	100	0.167	350		4.7	
Current Study	3-point bending	6	3	6,7	59.55	0.04	50.34	19.65	2.36	56.96
		6	6	6,7	61.01	0.04	92.68	29.50	1.55	61.82
		6	10	6,7	74.89	0.04	114.04	28.73	1.67	57.78
		6	Adult	6,7	89.77	0.04	269.18	77.84	2.13	65.51

* Age was adjusted for developmental age as in Pfefferle et al. (2007)
** Material Properties were adjusted for comparison with 3-point bending testing results

Comparable quasi-static load rate testing to the current study includes human

pediatric rib material properties research by Agnew et al. (2013) and human adult rib material properties research by Yoganandan and Pintar (1998) and Granik and Stein (1973). It should be noted that rib material properties for both human and swine are limited for comparison purposes. Due to the scarcity of pediatric PMHS for research, the number of pediatric rib specimens tested in 3-point bending for various age levels is lower than what was tested during the current study. For instance, after adjustment of the rib specimens in Agnew et al. (2013) based on developmental age as opposed to biological age of the pediatric PMHS, there were only two rib specimens used to determine the 6-year-old human rib material properties and only four rib specimens generating the 10-year-old human rib material properties. Much research has been performed with human adult ribs; however, the majority of the research has been performed at dynamic testing levels which is not directly comparable to the current study since faster load rates typically result in higher forces sustained over shorter distances and time, as demonstrated in Sandoz et al. (2007). The only direct comparison of 3-point bending quasi-static load rate research performed on human adult ribs known is the work performed by Yoganandan and Pintar (1998) and Granik and Stein (1973). Only two adult rib specimens were tested in the Yoganandan and Pintar (1998) study. Ribs 6 and 7 from ten normal cadavers (20 rib specimens) were tested in the Granik and Stein (1973) study. Next to the current study testing performed, the only porcine rib material properties research found, which was performed at somewhat higher load rates, was by Kieser et al. (2013) and Bradley et al. (2013). The material properties comparison values based on the comparable quasi-static load rate testing is provided in Table 5.5.2, below.

Table 5.5.2 Comparative Values for Material Properties from Comparable Quasi-Static Load Rate Human and Swine Rib Bending Research

Author	Loading Type	No. of Specimens	Specimen Age Range (year)	Rib Level	L (mm)	Load Rate (mm/sec)	F_P (N)	K (N/mm)	E (Gpa)	σ_P (MPa)	Tt. Ar. (mm^2)	Ct. Ar. (mm^2)	I (mm^4)
Human													
Granik and Stein (1973)	3-point bending	15 cadavers	Adult	6,7	101.6	0.042			11.5	160			
Yoganandan and Pintar (1998)	3-point bending	120	Adult	7	100	0.042	158		2.3				
				7	100	0.042	137		1.9				
Agnew et al. (2013)	3-point bending	11	0*	5,6,7	33 to 109	0.042	42.98	23.33	3.54	81.63	15.06	7.72	9.43
		8	1*	6,7,8		0.042	44.74	18.77	3.12	82.58	17.92	10.11	9.98
		11	2*	5,6,7		0.042	70.7	37.08	3.49	74	26.6	12.23	29.4
		8	3*	6,7		0.042	84.62	37.52	5.765	94.115	33.35	15.215	36.265
		2	6	5,6		0.042	110.7	44.11	5.65	119.6	33.61	17.88	56.03
		4	9	6,7		0.042	90.44	20.05	9.8	87.4	39.98	18.41	56.82
Porcine			**Human Equivalent Age (Years)**										
Bradley et al. (2013)	4-point bending**	8 thawed	0	6	80	0.167	17.98		8.99				1.22
Kieser et al. (2013)	4-point bending**	20 wet	Adult	5	100	0.167	350		4.7				
Current Study	3-point bending	6	3	6,7	59.55	0.042	50.34	19.65	2.36	56.96	33.19	14.05	36.48
		6	6	6,7	61.01	0.042	92.68	29.50	1.55	61.82	40.89	23.99	87.42
		6	10	6,7	74.89	0.042	114.04	28.73	1.67	57.78	57.36	27.92	158.01
		6	Adult	6,7	89.77	0.042	269.18	77.84	2.13	65.51	118.69	45.29	564.26

* Age was adjusted for developmental age as in Pfefferle et al. (2007)
** Material Properties were adjusted for comparison with 3-point bending testing results

Comparison of values between human and pigs for each material property was performed for each age group and a percent difference between human rib and porcine rib material property values was calculated. In addition, each material property was compared between the human and porcine ribs at each equivalent age level to determine if there was any correlation between the two for each material property. Figure 5.5.1 displays the comparison of human and all swine tested rib specimen peak force versus age. A power curve through the current study porcine rib testing displays a correlation of 93.81 percent with respect to peak force versus equivalent age. As shown in Figure 5.5.2, although there is a slight decrease in peak force seen from the 6-year-old to the 10-year-old human rib strength, the general trend is that peak force is higher with age for both humans and pigs. The 3-year-old human ribs display a 50.8 percent higher peak force versus the 3-year-old PSE ribs. The 6-year-old human ribs display a 17.7 percent higher peak force versus the 6-year-old PSE ribs. In contrast, the 10-year-old and adult human ribs display a 23.1 percent and 58.6 percent lower peak force, respectively, when

compared to the 10-year-old and 50th percentile adult male PSE ribs.

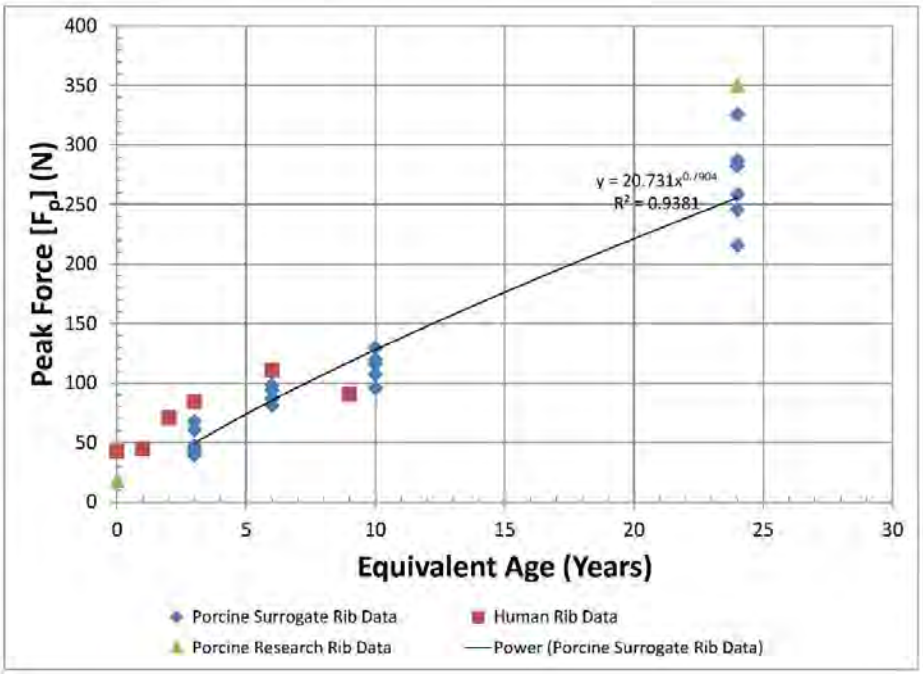

Figure 5.5.6 Peak Force v. Equivalent Age - Human and Swine Ribs

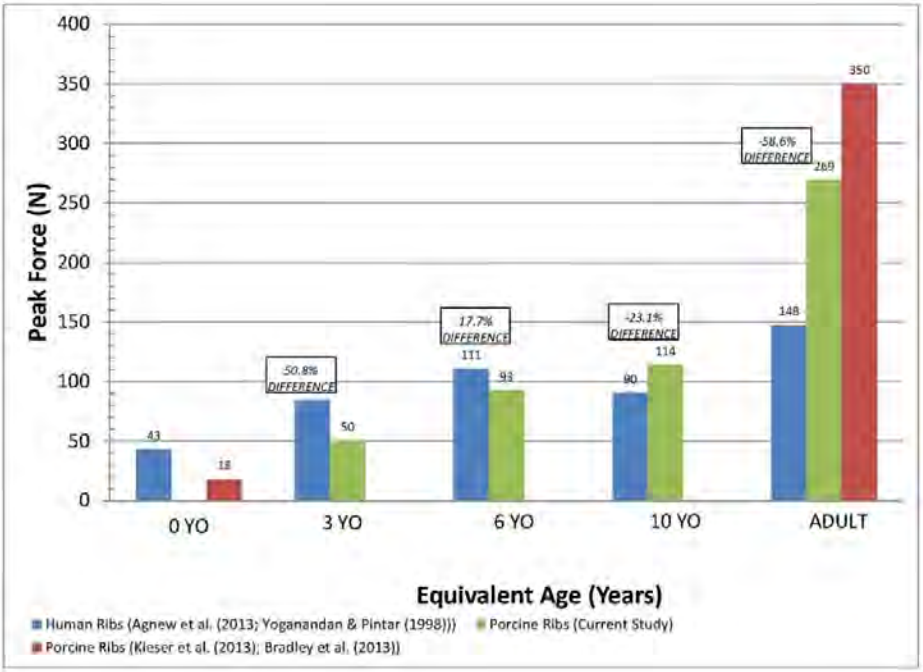

Figure 5.5.2 Peak Force v. Age - Human and Swine Ribs (Average of Specimens)

An 85.75 percent linear correlation is displayed in Figure 5.5.3 when comparing human rib peak force and the current study porcine rib peak force relative to equivalent age. It should be noted that due to the small sample sizes for both human and porcine ribs tested, significance level of the correlation was not calculated.

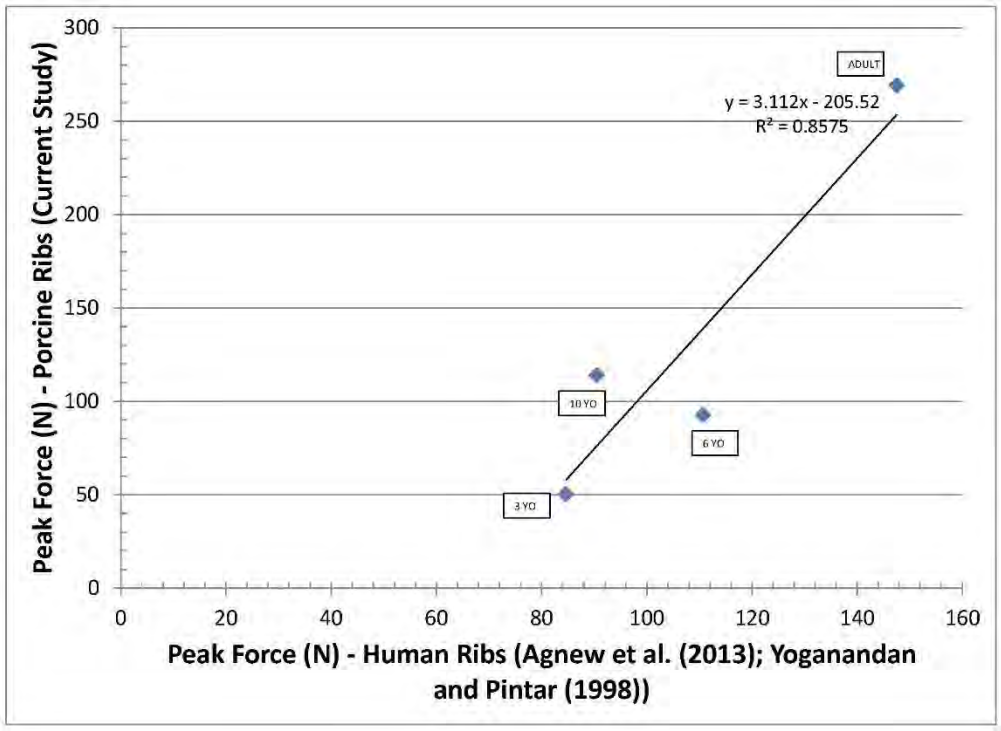

Figure 5.5.3 Peak Force Porcine Ribs versus Peak Force Human Ribs at Equivalent Age Levels

Human and all current study swine tested rib specimens were compared with respect to cortical cross-sectional area versus equivalent age and the results are displayed in Figure 5.5.4, below. A power curve through the current study porcine rib testing displays a correlation of 79.63 percent with respect to cortical bone cross-sectional area versus equivalent age. The current study porcine rib testing displays a higher cortical bone cross-sectional area with equivalent age. The human rib cortical bone cross-sectional area increases relative to equivalent age up to 6 years of age. Average cortical

bone cross-sectional area for the 9-year-old human was very similar to that of the 6-year-old resulting in a leveling off of the human rib cortical bone cross-sectional area with increase in age.

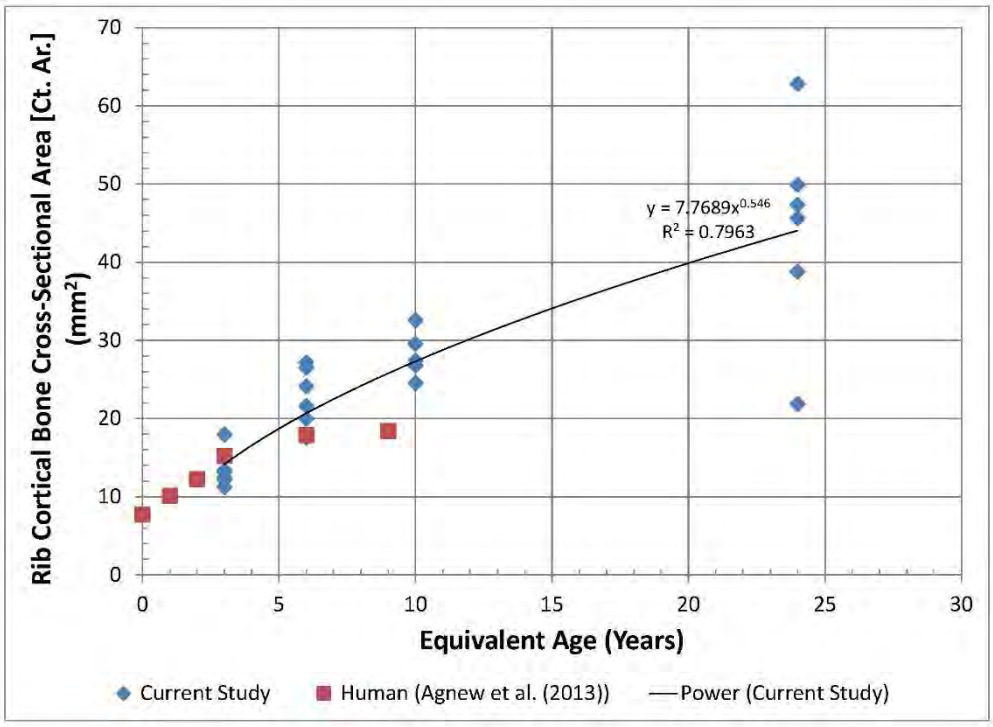

Figure 5.5.4 Rib Cortical Bone Cross-Sectional Area v. Equivalent Age - Human and Porcine Ribs

Figure 5.5.5 again shows the increase in cortical bone cross-sectional area versus equivalent age for the current study porcine rib testing and the similar cross-sectional area for the human 6-year-old and 10-year-old rib data. The 3-year-old human rib data displays a 7.9 percent higher cortical bone cross-sectional area versus the 3-year-old PSE rib data. The 6-year-old and 10-year-old human rib data displays a 29.2 percent decrease and a 41.1 percent decrease in cortical cross-sectional area, respectively, versus the PSE rib data. No data was available for the adult human rib data for comparison to the current study porcine rib data for this material property.

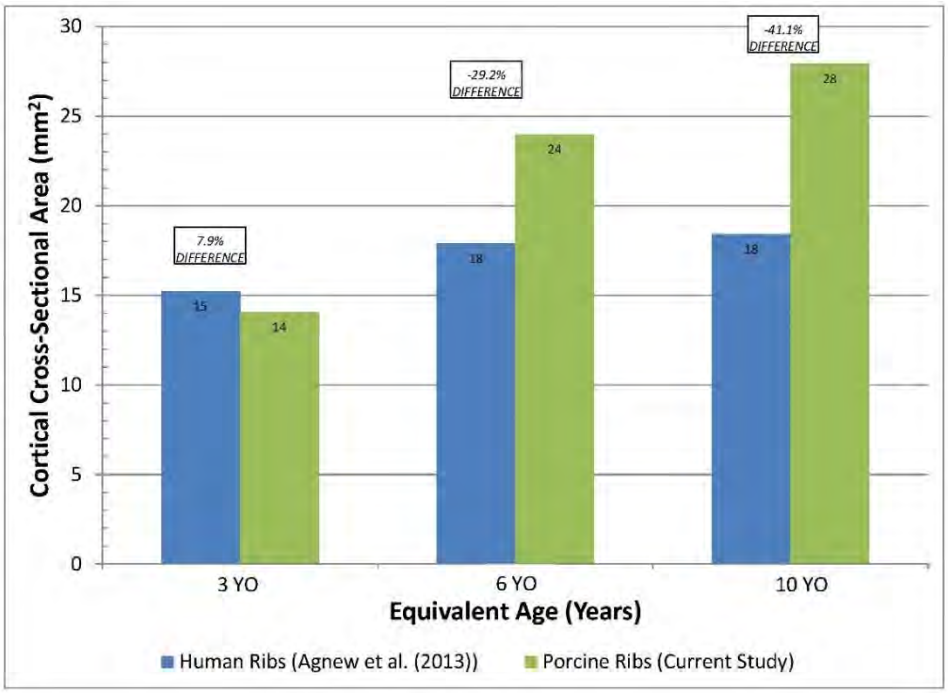

Figure 5.5.5 Cortical Bone Cross-Sectional Area v. Age - Human and Porcine Ribs (Average of Specimens)

A 98.48 percent linear correlation is displayed in Figure 5.5.6 when comparing human cortical bone cross-sectional area and the current study porcine rib cortical bone cross-sectional area relative to equivalent age.

The current study porcine rib specimens tested and human rib data were also compared with respect to moment of inertia versus equivalent age and the results are displayed in Figure 5.5.7, below. A power curve through the current study porcine rib testing displays a correlation of 95.53 percent with respect to porcine rib moment of inertia versus equivalent age. The current study porcine rib testing displays higher area moment of inertia with an increase in equivalent age. The human rib area moment of inertia increases slightly relative to equivalent age up to 6 years of age. Area moment of inertia for the 9-year-old human was very similar to that of the 6-year-old resulting in a leveling off of the moment of inertia with increase in age.

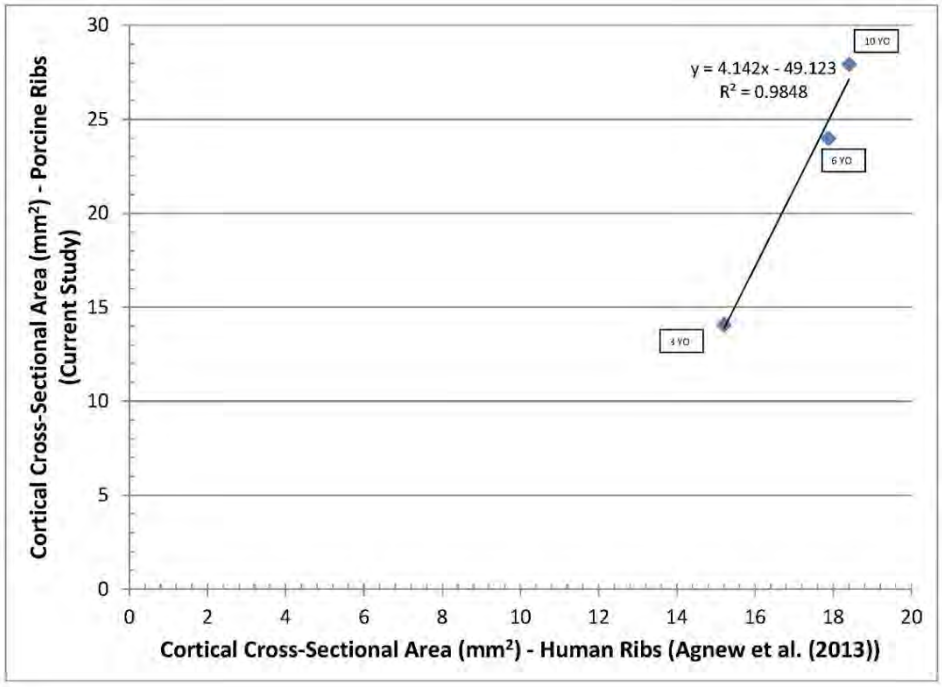

Figure 5.5.6 Cortical Bone Cross-Sectional Area of Porcine Ribs versus Cortical Bone Cross-Sectional Area of Human Ribs at Equivalent Age Levels

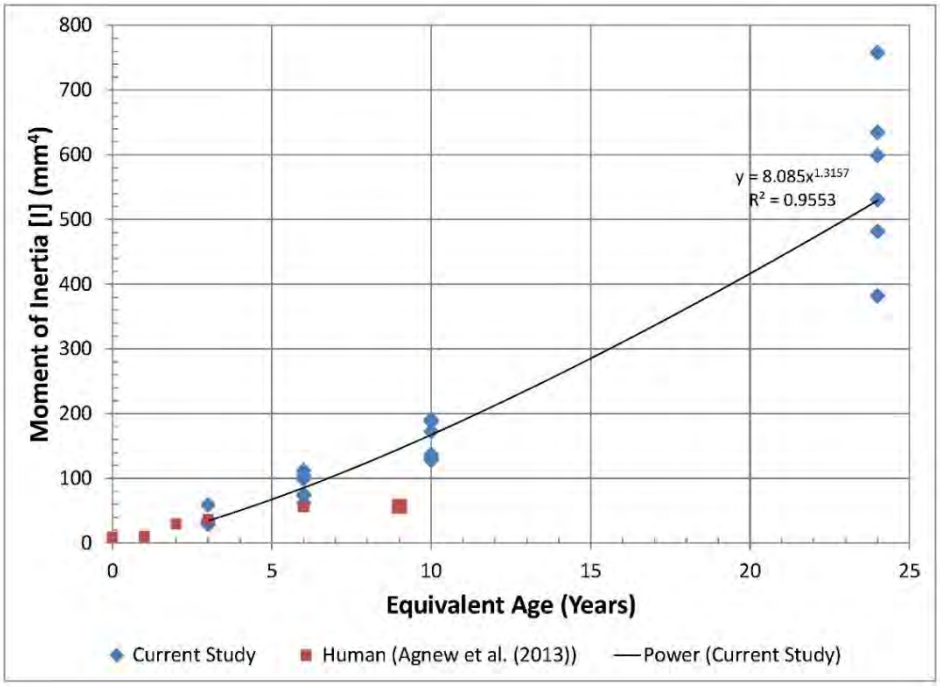

Figure 5.5.7 Moment of Inertia v. Equivalent Age - Human and Porcine Ribs

Figure 5.5.8 shows the higher moment of inertia versus equivalent age for the

current study porcine rib testing and how the moment of inertia for the human 6-year-old and 10-year-old rib data is similar in value. The 3-year-old human rib data shows a 0.6 percent lower moment of inertia versus the 3-year-old PSE rib data. The 6-year-old and 10-year-old human rib data displays a 43.8 % lower and a 98.2 % lower moment of inertia, respectively, versus the PSE rib data. No data was available for the adult human rib data for comparison to the current study porcine rib data for this material property.

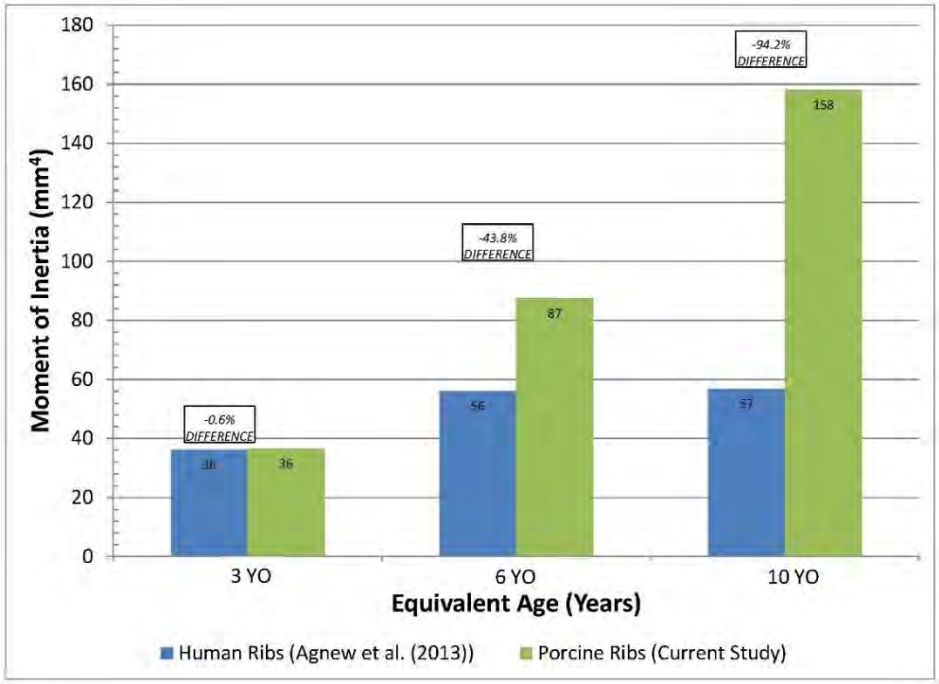

Figure 5.5.8 Area Moment of Inertia v. Age - Human and Porcine Ribs (Average of Specimens)

A 69.71 percent correlation is displayed in Figure 5.5.9 when comparing human area moment of inertia and the current study porcine rib moment of inertia values relative to equivalent age.

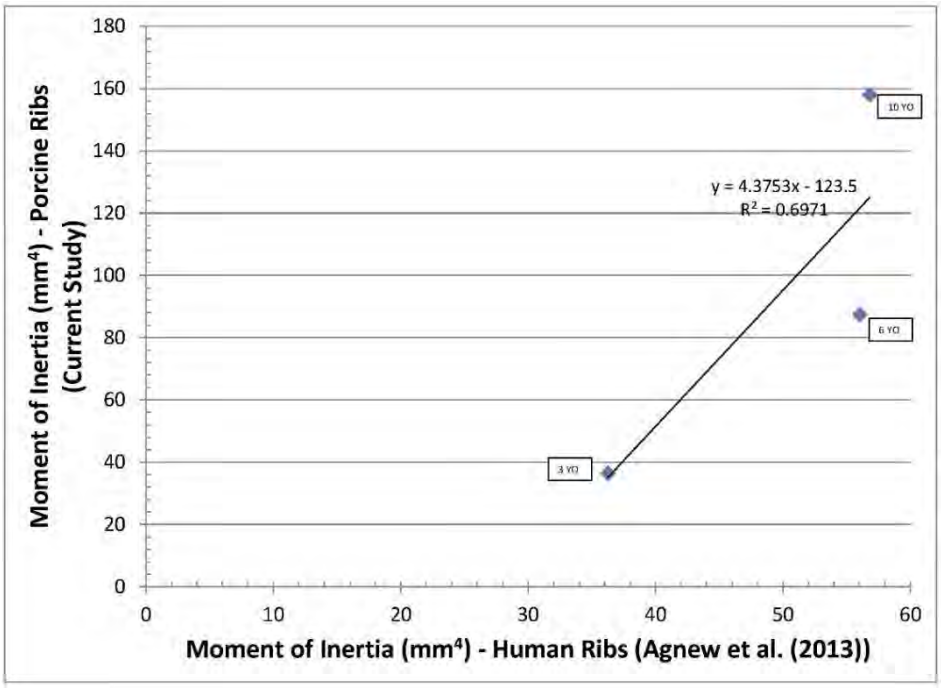

Figure 5.5.9 Area Moment of Inertia of Porcine Ribs versus Area Moment of Inertia of Human Ribs at Equivalent Age Levels

The current study porcine tested rib specimens and human rib specimens were also compared with respect to stiffness versus equivalent age and the results are displayed in Figure 5.5.10, below. A power curve through the current study swine rib testing displays a correlation of 71.68 percent with respect to rib stiffness relative to equivalent age. The current study porcine rib testing shows an increase in rib stiffness from the 3-year-old equivalent to the 6-year-old equivalent specimens, a similar stiffness level between the 6-year-old and the 10-year-old equivalent specimens and then a higher stiffness level for the adult equivalent specimens. The human rib stiffness levels demonstrate an irregular pattern with respect to equivalent age with a lower stiffness level from ages 0 to 2, and higher stiffness level from ages 2 to 6, and then a lower stiffness level from age 6 to age 9. It also shown in Figure 5.5.10 that the human rib stiffness levels are higher than the porcine rib stiffness levels from equivalent ages 2 to 6.

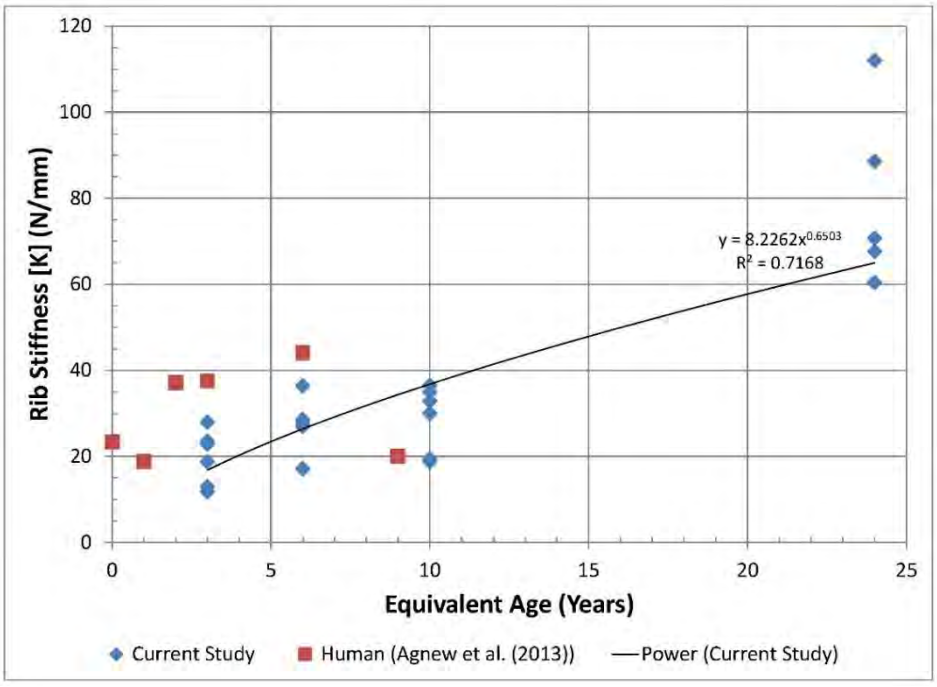

Figure 5.5.10 Rib Stiffness v. Equivalent Age - Human and Porcine Ribs

Figure 5.5.11 better illustrates the higher human rib stiffness levels compared to the current study porcine rib stiffness levels at equivalent ages 3 and 6 but a lower rib stiffness level for the human ribs compared to the porcine ribs at the 10-year-old equivalent age. The 3-year-old human rib data shows a 62.5 percent higher rib stiffness versus the 3-year-old PSE rib data. The 6-year-old human rib data demonstrates a 39.7 percent higher rib stiffness versus the 6-year-old PSE rib data. The 10-year-old human rib data, however, is 35.6 % lower in rib stiffness compared to the PSE rib data. No data was available for the adult human rib data for comparison to the current study porcine rib data for this material property.

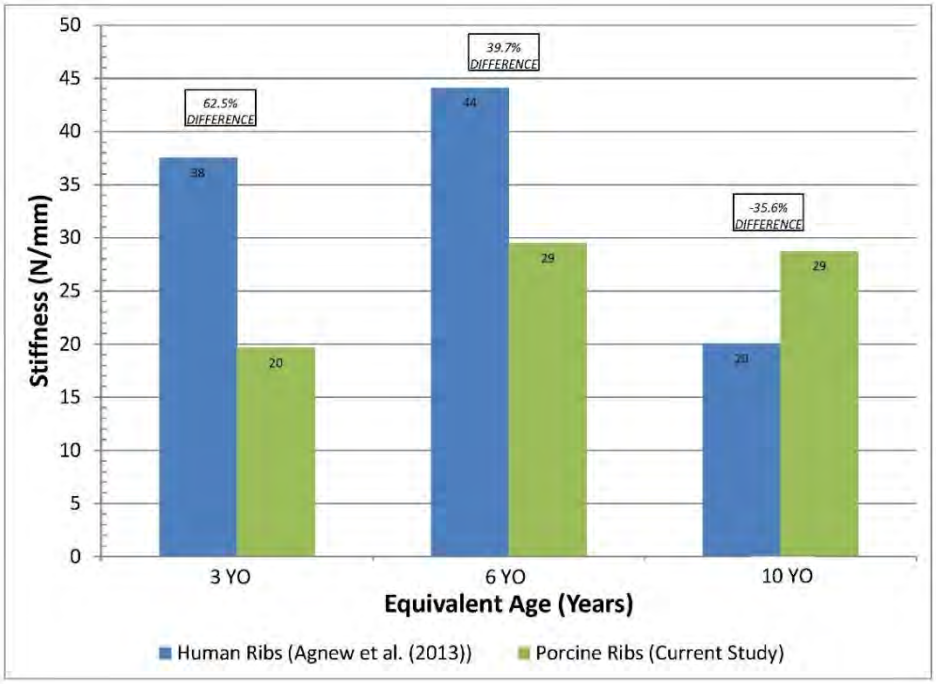

Figure 5.5.11 Rib Stiffness v. Age - Human and Porcine Ribs (Average of Specimens)

There was no correlation found when comparing human rib stiffness and the current study porcine rib stiffness relative to equivalent age, as illustrated in Figure 5.5.12, below. This lack of correlation should be considered with caution. At least fourteen equivalent years of data relative to rib material properties for both human and swine have not been accounted for in research from equivalent age 10 to adult. This age range for humans encompasses puberty and would be considered a time of substantial skeletal changes. More research is necessary, where this data is lacking, to be able to appropriately determine data trends and correlation of rib stiffness and material properties from pediatric to adult.

Finally, the current study porcine tested rib specimens and human rib specimens were compared with respect to modulus of elasticity in bending versus equivalent age

and the results are displayed in Figure 5.5.13, below. The current study porcine rib testing data displays a slight decrease in modulus of elasticity from the 3-year-old equivalent to the 6-year-old equivalent specimens and the modulus of elasticity tends to remain at a fairly consistent value from the 6-year-old to the 10-year-old PSE, and is higher from the 10-year-old to the adult equivalent age specimens. The higher elastic modulus of the 3-year-old PSE ribs is most probably due to the fact that the 3-year-old PSE ribs are only slightly shorter in length (of the linear rib portion) than the 6-year-old PSE, but the 3-year-old PSE rib has a smaller cross-section than the 6-year-old PSE rib. The human rib elastic modulus is higher than the porcine rib data from ages 3 through 10 and then is at similar values to the porcine rib data at the adult equivalent age. Swine rib modulus of elasticity from the Bradley et al. (2013) and Kieser et al. (2013) studies demonstrate higher levels than both the current study swine rib and human rib modulus of elasticity in bending.

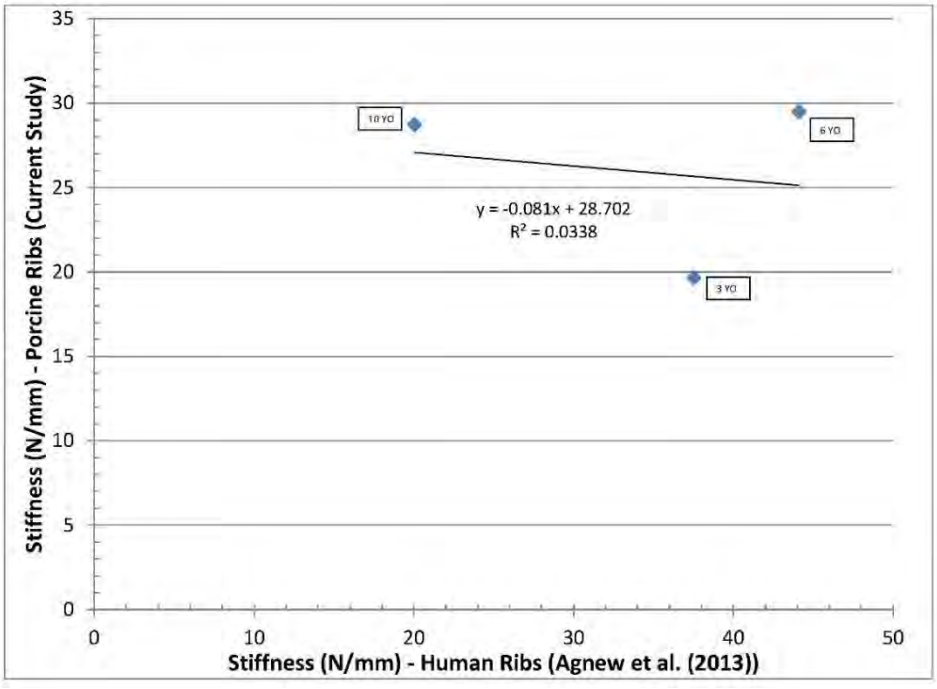

Figure 5.5.12 Porcine Rib Stiffness versus Human Rib Stiffness at Equivalent Age Levels

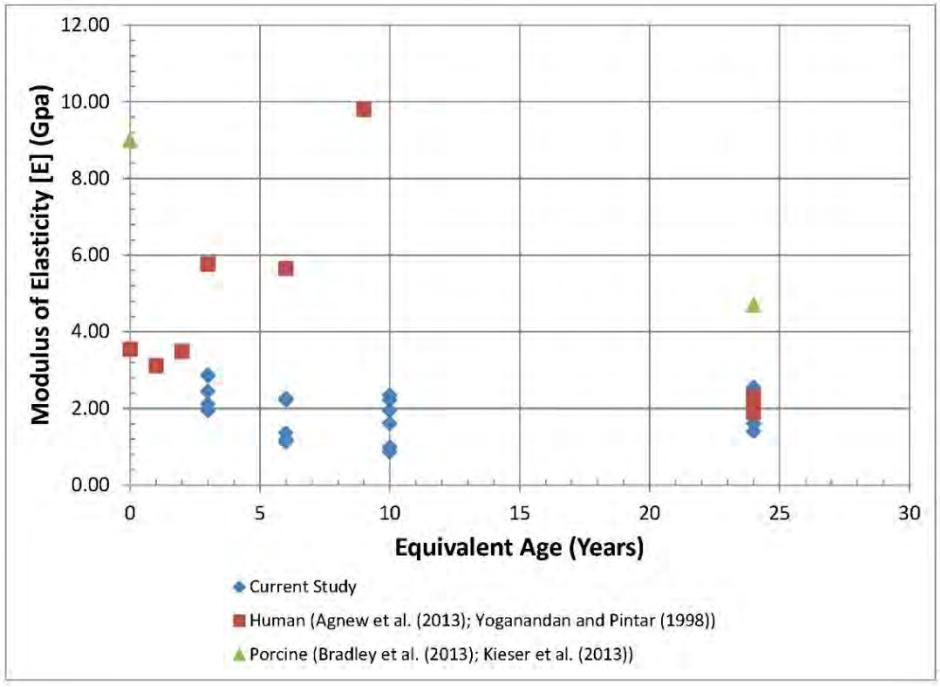

Figure 5.5.13 Modulus of Elasticity in Bending versus Equivalent Age - Human and Porcine Ribs

Figure 5.5.14 better illustrates the higher human rib modulus of elasticity values compared to the current study swine rib modulus of elasticity values at equivalent ages 3 through 10 but similar modulus of elasticity values for the human ribs compared to the porcine ribs at the adult equivalent age. The 3-year-old human rib data shows an 83.8 percent higher rib modulus of elasticity versus the 3-year-old PSE rib data. The 6-year-old human rib modulus of elasticity data demonstrates a 113.9 percent higher value than the 6-year-old PSE rib data. The 10-year-old human rib data displays a 141.8 percent higher rib modulus of elasticity compared to the PSE rib data. The adult age human rib data displays only a 1.54 percent higher rib modulus of elasticity compared to the PSE

rib data.

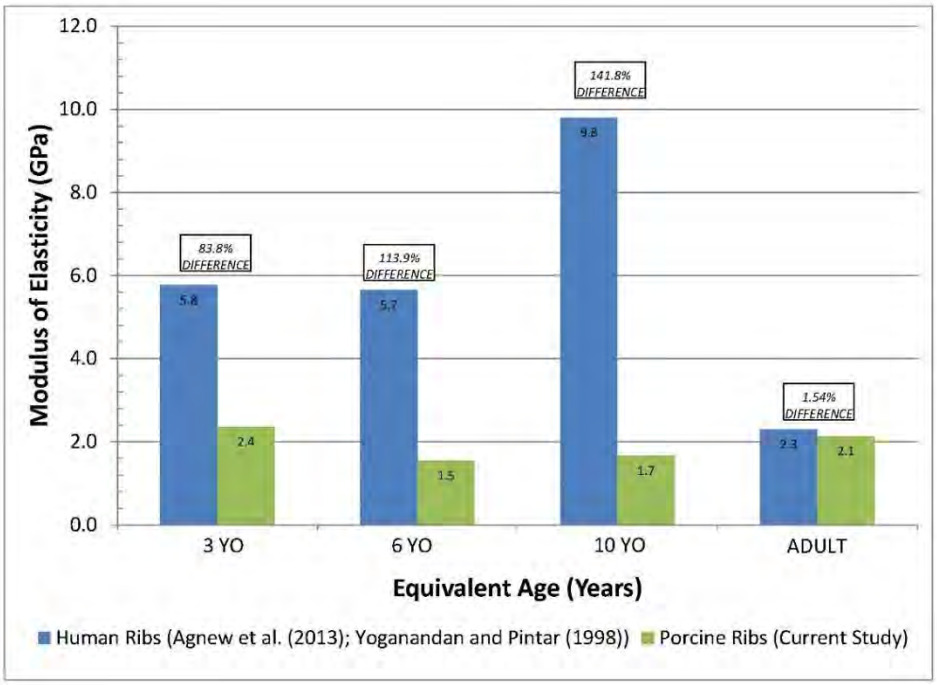

Figure 5.5.14 Modulus of Elasticity in Bending versus Age - Human and Porcine Ribs (Average of Specimens)

There was no correlation found when comparing human rib modulus of elasticity and the current study swine rib modulus of elasticity relative to equivalent age, as illustrated in Figure 5.5.15, below.

Quasi-static 3-point bending porcine rib testing was performed in the current study on six rib specimens for each of four human age equivalent levels for a total of twenty-four rib specimens tested. Force and displacement data was recorded during testing in order to develop force-displacement curves for each of the tested rib specimens. Swine rib specimens at each of the four human age equivalent levels were found to respond similarly to the applied load at the set load rate relative to other rib specimens tested in their comparable age equivalent groups. Sustained force levels before rib fracture

occurred were found to increase with increasing equivalent age. Rib stiffness was also found to increase with equivalent age although stiffness levels were similar for the 6-year-old and 10-year-old equivalent age levels.

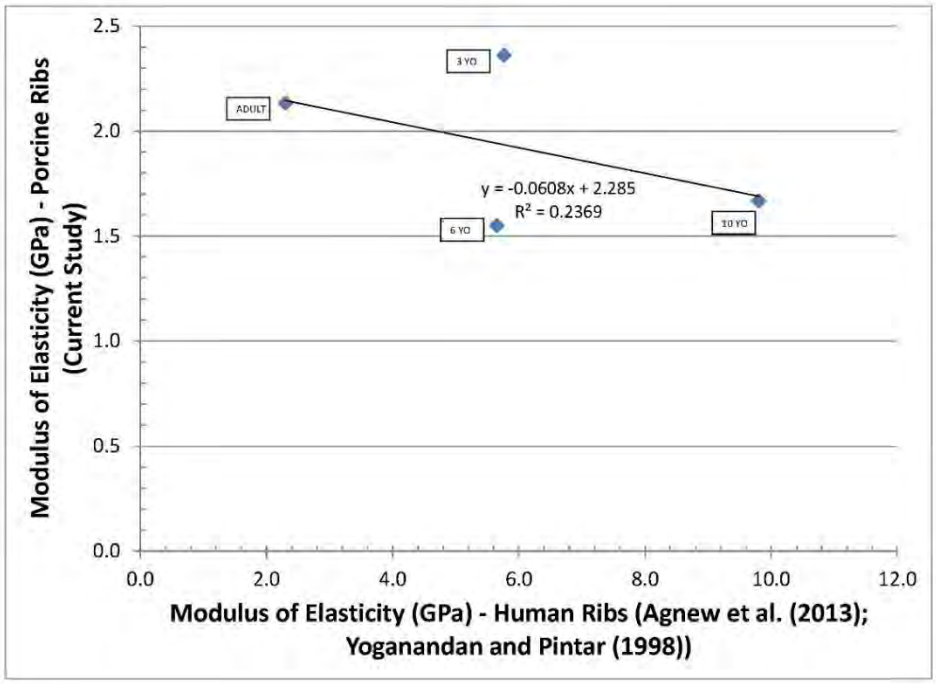

Figure 5.5.15 Swine Rib Modulus of Elasticity in Bending versus Human Rib Modulus of Elasticity in Bending at Equivalent Age Levels

Modulus of elasticity in bending was calculated from the material properties obtained from CT cross-sections of the tested porcine ribs and their force-displacement data for use in the ATD scaling laws analysis presented in Chapter 6 of this current study. It was found that calculated modulus of elasticity for the current study porcine ribs decreased somewhat from 2.4 GPa at the 3-year-old equivalent age to 1.5 GPa at the 6-year-old equivalent age and then increased from the 6-year-old equivalent age to 2.1 GPa at the adult equivalent age. The change in modulus of elasticity observed with equivalent age in the current study may be a function of the span length determination technique used. Measured lengths of the 3-year-old and 6-year-old rib specimens were similar,

resulting in similar span lengths for these two equivalent age groups. The moment of inertia and effective rib stiffness properties determined for the 3-year-old ribs were found to be less than the 6-year-old equivalent age group. Since the calculation of the modulus of elasticity property of the rib is a function of the product of effective stiffness and span length cubed over moment of inertia, lower moment of inertia and longer span lengths will have an effect on increasing modulus of elasticity, as was the case for the 3-year-old PSE ribs in the current study.

The modulus of elasticity for the 50th male PSE ribs in the current study was found to be less than the 6.6 GPa elastic modulus based on human pediatric parietal bone test data used by Irwin and Mertz (1997) in establishing the adult to child ATD scaling laws.

This study is subject to some important additional limitations. For instance, although the results were fairly consistent, only six ribs per equivalent age group were tested in 3-point bending. Additional testing may be necessary to further quantify any significant variability relative to the presented data.

Structural and material-level responses of rib using the 3-point bending testing and simple beam theory assumptions have been shown to be appropriate through research performed by Cormier et al. (2005); however, this testing is performed at a quasi-static load rate. Rib material and structural properties would be expected to be different at higher load rates and deformation. More recent rib property studies have incorporated the Charpail et al. (2005) methodology in which the rib specimen extremities were potted in caps by polyester cement with a hardener and placed in a test apparatus where one cap was fixed to the apparatus with a pin joint and the second cap was allowed to rotate along the same axis and to translate along the anterior-posterior axis. This methodology

has only been observed by this author in anterior-posterior rib loading research. It is unclear how this methodology could be used for lateral rib testing, that determination was not part of the current study's focus, and therefore this methodology was not used. This may be a focus, however, of future studies in order to establish an improved method of determining rib structural and material properties in lateral rib impact testing.

The swine rib elastic bending moduli determined in the current study are similar in values to the adult human rib elastic bending modulus determined by Yoganandan and Pintar (1998). The values in the current study, however, are not consistent with any other human or swine rib elastic bending modulus property study performed (see Table 5.5.1 for reference and comparison). Other studies, with the exception of Yoganandan and Pintar (1998), resulted in higher rib elastic bending modulus values compared to the current study, regardless of the variance in test parameters with respect to the different studies.

The lower and fairly constant swine rib elastic modulus values observed in the current study, across all equivalent ages, when compared to previous research, was an unexpected result. It would be expected that rib bone would be more flexible at the younger equivalent age levels, becoming more calcified with age as bones material properties change and ossification occurs. Calculations of rib elastic modulus in the current study were based on assumptions of simple beam bending analysis in an attempt to correlate the current study data to human pediatric and adult rib materials calculated using the same assumptions. This approach has limitations. For instance, it is assumed that the swine and human ribs are straight. The swine rib cage is fairly circular in shape, and therefore the swine's ribs are not straight but are curved. This can play a role in

overall mechanical properties. Past studies have assumed the rib cross-section is circular for ease in cross-sectional material property calculations. That technique was not used in the current study. The current study used CT scans of the rib specimen's cross sections for more accurate cross-sectional material property calculations. Despite this approach, simple beam bending analysis assumes that the cross-section remains constant throughout the length of the specimen, which is not the case for the tested ribs. Span length determination for rib 3-point bending testing requires simple beam bending assumptions in order to use this approach. Using test coupons from the rib as opposed to rib bending testing would prove more repeatable in test results by reducing or eliminating some of the assumptions necessary in 3-point bending, and perhaps resulting in more expected rib material property results.

Kalra et al. (2015) analyzed characteristics of adult human rib biomechanical responses due to 3-point bending in quasi-static loading. Variations in adult human rib elastic modulus observed in previous research were analyzed. It was concluded that using reverse engineering from thickness of bone contours in medical images to determine rib bending moment of inertia for the determination of rib elastic bending modulus was more appropriate and eliminated the use of cross sectional areas. Further research with respect to porcine surrogate equivalent rib elastic bending modulus using this approach or rib coupon testing should be considered in future research to determine if any differences in swine elastic bending modulus with human-equivalent-age is observed compared to the current study's results.

There was a discernable gap in the data analyzed in the current study from age 10 to adult. As discussed previously, calcification of bones and growth plate closures occur

during this age range in humans. More research is necessary to verify the trends in material properties relative to age through this age range are consistent with those observed in the current study.

Any animal model has accompanying limitations in terms of its ability to represent human response. For instance, the size and shape of porcine ribs are not the same as human ribs at any age level, porcine ribs do not angle the same direction as human ribs, nor do porcine ribs attach to the rib cage in a similar manner as human ribs.

To this author, there are presently no known lateral bending rib structural and material property analyses over the equivalent ages presented in the current study for either humans or PSE. Rib material properties, in lateral bending, for both humans and pigs are limited for comparison purposes due to the minimal number of rib specimens tested at these age levels and comparable load rates among sample data. General comparison was made, however, between the limited human rib material properties data to the current study porcine rib material properties. Modulus of elasticity for the current study porcine ribs was found to be much lower than the modulus of elasticity calculated for the human pediatric ribs from age 3 to age 10 studied by Agnew et al. (2013). Modulus of elasticity for the current study adult equivalent age porcine ribs was found, however, to be comparable to the adult human rib modulus of elasticity determined through similar quasi-static 3-point bending rib testing performed by Yoganandan and Pintar (1998). One possible reason for this difference may be the low number of human rib specimens tested at these individual ages, particularly for the 6 to 10-year-old age levels, even though adjustment for developmental versus biological age was made for the tested specimens. Another possible reason for this difference may be the smaller cortical bone cross-

sectional area and moment of inertias for the human ribs compared to the porcine ribs.

5.6 – Conclusions

The primary contributions of this study were to establish lateral bending structural and material rib properties for PSE to the 3-year-old, 6-year-old, 10-year-old and 50th male human, and compare the results to known human rib properties. In addition, calculation of the elastic bending modulus of the porcine ribs was calculated in order to use these material properties to calculate scaled corridors for swine lateral impact testing, compare it to the PSE ages studied, and determine if the scaling laws are appropriate.

The overall findings of the current study confirm a positive correlation between swine peak bending force, rib stiffness, rib cortical cross-sectional area, and moment of inertia with age. There was no positive correlation found in the current study between swine rib modulus of elasticity and age.

Further investigation is needed to better understand the lack of positive correlation for swine rib modulus of elasticity with age. In addition, further investigation is needed regarding the understanding of how the material and structural properties of ribs change with age for both humans and pigs, both quasi-statically and dynamically. Further understanding of rib material and structural properties, as well as thoracic material and structural properties as a unit would be useful in the design and establishment of more biofidelic ATDs at all age levels.

CHAPTER 6 – RESPONSE RATIO DEVELOPMENT FOR LATERAL PENDULUM IMPACT PORCINE THORAX AND ABDOMEN SURROGATE EQUIVALENTS (SPECIFIC AIM 5)

6.1 – A Brief Overview of Pediatric PMHS and Animal Surrogate Thorax and Abdomen Testing Comparisons

There has been recent research progress over the past 10 years comparing 6-year-old thoracic and abdominal response of pediatric volunteers, pediatric PMHS, animal surrogates, and 6-year-old ATDs.

For instance, Kent et al. (2009) performed a series of frontal loading tests on a 7-year-old PMHS and compared it to the test data obtained for the 6-year-old porcine model presented in Kent et al. (2006). The PMHS data was also used to analyze the efficacy of various scaling techniques used for scaling existing adult thoracic response data to the child as well as to analyze and confirm the porcine abdominal model. Results showed that the pediatric PMHS lower abdominal response was similar to the porcine model and the upper abdomen and thorax being slightly stiffer. Four different scaling techniques, including mass scaling (Eppinger et al., 1984), SAE (Mertz et al., 1989, and Irwin and Mertz, 1997), ISO 9790 (Irwin et al., 2002), and Parallel Springs (Kent et al. 2004, and Kent, 2008) were used in the scaling analysis. It was determined that none of the four scaling techniques effectively predicted the PMHS response. All scaling techniques were found to reduce the stiffness of the adult response even though the pediatric PMHS response was found to be as stiff as or slightly more stiff than published adult response corridors.

Lamp et al. (2010) expanded on the analysis performed by Kent et al. (2009) by including an additional abdominal test series from a 6-year-old PMHS in order to further evaluate the efficacy of the Kent et al. (2006) porcine model. It was found that the two

pediatric PMHS were similar in abdominal stiffness behavior both by level (upper and lower) as well as rate.

Kent et al. (2011) again expanded on previous research by analyzing a series of frontal impact load tests on a 6, 7, and 15-year-old PMHS in order to analyze the efficacy of scaling of existing adult thoracic response data for application to the child and evaluate the validity of the porcine model. This study provided useful information to help support the concept that thoracic stiffness is not a linear relationship relative to age, and therefore, existing scaling techniques do not properly represent this relationship. The pediatric response data follow a general trend in which pediatric and elderly PMHS have similar thoracic stiffness in dynamic diagonal belt frontal loading whereas late adolescents and young adults tend to possess a greater thoracic stiffness behavior.

Although progress has been made to guide scaling of adult to pediatric thorax and abdomen data, further effort is needed, particularly with respect to lateral and oblique impacts.

The objective of this study was to develop scaling and response ratios using the ISO 9790 method provided in Irwin et al. (2002) for the 3-year-old, 6-year-old, 10-year-old, from 50th adult male PSE lateral pendulum impact testing of the thorax and abdomen. The swine scaling and response ratios were then used to scale the established 50th adult male PSE lateral impact response corridors obtained from test data at this age equivalent level to develop scaled impact response corridors for the younger age PSE. These scaled response corridors were then compared to the actual test data obtained from lateral pendulum impacting testing of the younger age PSE to determine if current scaling laws used in the development of younger ATDs apply for PSE.

6.2 – Methods

Lateral impact response corridors were created from the phase shifted and normalized 50th adult male PSE pendulum lateral impact T1, T14, and L6 accelerations, pendulum impact force, and rib deflection parameter time histories for the thorax and abdomen testing performed in Specific Aim 3 using the technique identified in Rhule et al. (2013). Using this technique, the set of three impact runs for each parameter recorded were averaged point by point to obtain a mean response curve. The mean response curve was then bracketed with plus and minus one standard deviation curves in order to generate the impact response corridors for each parameter recorded. To avoid "necking" of the standard deviation curves where original curves had points similar in value, a single standard deviation value was obtained by averaging point by point standard deviation values, and using that single average standard deviation value to bracket the mean curve.

The ISO 9790 scaling technique using length, mass, and elastic modulus scale factor formulas provided in Irwin et al. (2002) were used in conjunction with the swine measured scale parameters obtained in Specific Aims 3 and 4 (Chapters 4 and 5) to calculate scale factors for the PSE. Relevant scale factor formulas applicable to this research are included in Table 6.2.1 below. It should be noted that in Irwin et al. (2002), elastic bending modulus of bone data and corresponding scale factors were established using values of the elastic modulus of skull bone by interpolating from child and adult data. The current study uses the rib elastic bending modulus data established in Chapter 5 from the PSE.

Table 6.2.1 Formulas for Length, Mass, and Elastic Modulus Scale Factors used by Irwin et al. (2002)

Torso	$\lambda_{z_{torso}} = \frac{(ESH)_i}{(ESH)_{50th}}$ Total Body: $\lambda_{m_{total}} = \frac{(m_t)_i}{(m_t)_{50th}}$ $\lambda_{x_{torso}} = \lambda_{y_{torso}} = \sqrt{\frac{\lambda_{m_{total}}}{\lambda_{z_{torso}} \lambda_\rho}}$ Upper Torso: $\lambda_{m_{ut}} = \frac{(m_{ut})_i}{(m_{ut})_{50th}}$ Where ESH = erect seated height, m = total body mass, m_{ut} = upper torso mass, $\lambda_\rho =$ mass density = 1.000
Elastic (Young's) Modulus	$\lambda_{E_{bone}} = \frac{E_i}{E_{50th}}$ Where E = elastic bending modulus of bone
Torso Stiffness	Thorax & Abdomen: $\lambda_{K_{torso}} = \lambda_{E_{bone}} \lambda_{z_{torso}}$

In addition to calculation of pertinent scale factors, pertinent test scale factors, also known as response ratios, for the pendulum impact tests were calculated using the formulas utilized in Irwin et al. (2002). Relevant test response ratio formulas applicable to this research are included in Table 6.2.2 below.

Table 6.2.2 Formulas for Impact Response Ratios used by Irwin et al. (2002)

	Pendulum Tests
Force	Torso Forces: $R_F = \lambda_v \sqrt{\lambda_{me}\lambda_{K_{torso}}}$
Displacement	Torso Displacement: $R_d = \lambda_v \sqrt{\frac{\lambda_{me}}{\lambda_{K_{torso}}}}$
Acceleration	Torso Acceleration: $R_{at} = \lambda_v \frac{\sqrt{\lambda_{me}\lambda_{K_{torso}}}}{\lambda_{m_{total}}}$
Time	Torso Period: $R_t = \sqrt{\frac{\lambda_{me}}{\lambda_{K_{torso}}}}$

Where:

$\lambda_v = \frac{\lambda_i}{\lambda_{50th}}$ is the Velocity Scale Factor for the test condition

$\lambda_{me} = \frac{(\lambda_{m_{total}}\lambda_{mp})}{\lambda_{ms}}$ is the Equivalent Mass Scale Factor, λ_{me} , for pendulum tests, and

$\lambda_{mp} =$ ratio of pendulum mass used

$\lambda_{ms} =$ ratio of sums of masses

For shoulder & thorax: $\lambda_{ms} = \frac{(m_{ut} + m_p)_i}{(m_{ut} + m_p)_{50th}}$

m_p = mass of pendulum

The scaling factors and response ratios determined for the porcine surrogates were compared to the already established ISO human pendulum impact response ratios provided in Irwin et al. (2002) to determine whether there was a consistent pattern over the age levels for the two sets of data.

Once the PSE pendulum impact scaling and response ratios were calculated, the values were used to scale the 50th adult male PSE lateral impact response corridors for each of the recorded parameter time histories to produce the scaled impact response corridors for the younger age PSE. Using the 3-year-old PSE as an example, the 50th male PSE response corridors were determined for each parameter (T1, T14, L6 acceleration, pendulum force). The time history for the 50th male PSE response corridor for a given parameter was then scaled based on the determined time response ratio for the 3-year-old, and the 50th male response corridor data for a given parameter of interest (acceleration, force, or displacement) would be scaled by its corresponding 3-year-old PSE calculated response ratio.

The scaled response corridors were then compared to the actual test data obtained during swine pendulum lateral impact testing at each corresponding age level to determine if current scaling laws using the porcine parameters mimicked human scaled response corridors and whether scaling laws using swine rib elastic bending modulus are applicable.

In addition, known pediatric human response data will be compared to known adult human response data and young swine impact response data to older swine response data of the thorax and abdomen in lateral impact to determine if any relationship exists.

6.3 – Results

Based on the formulas for length, mass, and elastic modulus scale factors provided previously in Table 6.2.1, the calculated scale factors for the PSE and used in the current study are provided in Table 6.3.1 below. The parameters in the table highlighted in green

were measured or calculated (in terms of Young's Modulus and Effective Stiffness) from the swine specimens used in the pendulum lateral impact testing and used to develop the scale factors provided in the bottom portion of the table.

Table 6.3.1 Swine Length, Mass, and Elastic Modulus Scale Factors

SCALING PARAMETERS	50th Male PSE	10-Year-Old PSE	6-Year-Old PSE	3-Year-Old PSE
Pendulum Mass [kg]	23.28	6.5	2.89	1.7
Erect Seated Height (ESH) [mm]	1244.6	962	835.7	755.7
Total Body Mass [kg]	73.8	30.9	21.3	13.6
Upper Torso Mass [kg]	37.2	14.8	10.3	7.4
Young's Modulus [N/mm^2]]	2130	1670	1550	2360
Effective Stiffness [N/mm]	77.84	28.73	29.5	19.65
λ z torso	1.000	0.773	0.671	0.607
λ m total	1.000	0.419	0.289	0.184
λ x torso = λ y torso	1.000	0.736	0.656	0.551
λ m UT	1.000	0.398	0.277	0.199
λ mass density	1.000	1.000	1.000	1.000
λ E bone	1.000	0.784	0.728	1.108
λ K torso (torso stiffness)	1.000	0.606	0.489	0.673
λ p (pendulum mass ratio)	1.000	0.279	0.124	0.073
λ ms (mass sums ratio)	1.000	0.352	0.218	0.150
λ me (equivalent mass scale factor)	1.000	0.332	0.164	0.089

The equivalent human ISO lateral pendulum impact response corridor scale factors, provided in Irwin et al. (2002) are listed in Table 6.3.2 for reference.

Table 6.3.2 Human Length, Mass, and Elastic Modulus Scale Factors

SCALING PARAMETERS	50th Male	10-Year-Old	6-Year-Old	3-Year-Old
Pendulum Mass [kg]	23.28	6.89	2.89	1.7
Erect Seated Height (ESH) [mm]	907	719	635	546
Total Body Mass [kg]	78.2	32.4	20.86	14.5
Upper Torso Mass [kg]	17.2	7.11	4.59	3.2
Young's Modulus [N/mm^2]]	9900	8450	6600	4700
λ z torso	1.000	0.793	0.700	0.602
λ m total	1.000	0.414	0.267	0.185
λ x torso = λ y torso	1.000	0.723	0.617	0.555
λ m UT	1.000	0.413	0.267	0.186
λ mass density	1.000	1.000	1.000	1.000
λ E bone	1.000	0.854	0.667	0.475
λ K torso (torso stiffness)	1.000	0.677	0.467	0.286
λ p (pendulum mass ratio)	1.000	0.296	0.124	0.073
λ ms (mass sums ratio)	1.000	0.346	0.185	0.121
λ me (equivalent mass scale factor)	1.000	0.355	0.179	0.112

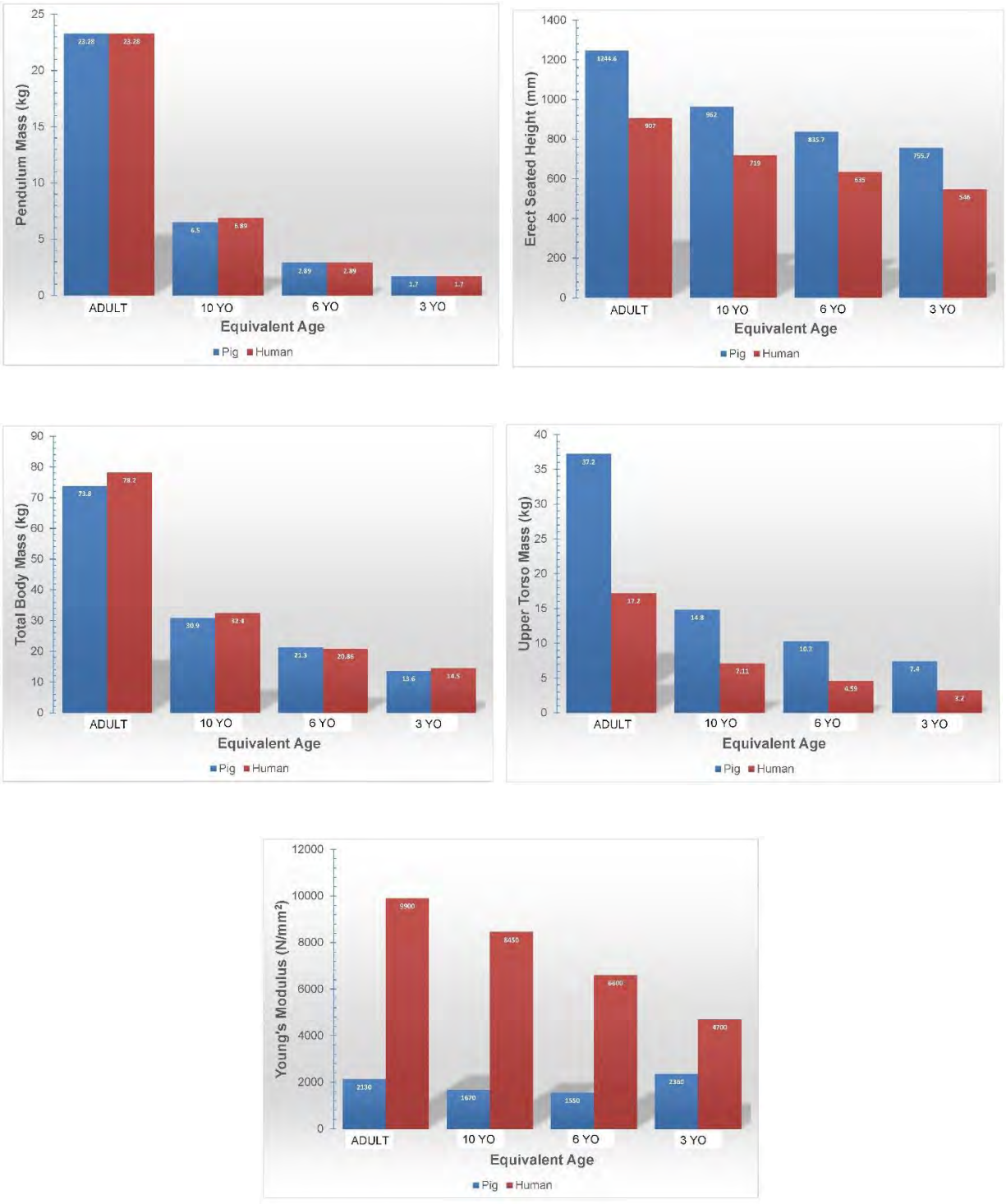

Figure 6.3.7 Human and Swine Material Properties for Each Age Level Used to Generate Scale Factors - Pendulum Mass (upper left); Erect Seated Height (upper right); Total Body Mass (second row left); Upper Torso Mass (second row right); Young's Modulus (bottom)

Comparison of the swine and human material properties, including pendulum mass, erect seating height, total body mass, upper torso mass, and Young's Modulus used to develop the scaling factors are provided in bar chart format in Figure 6.3.1, above, for additional reference below.

Comparison of the swine and human calculated scale factors are also provided in bar chart format in Figures 6.3.2 through 6.3.5 for reference.

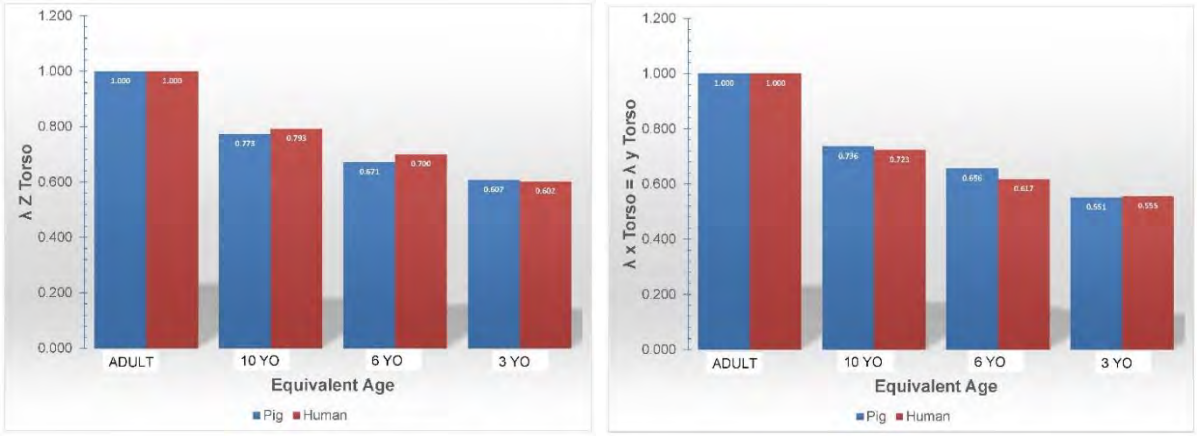

Figure 6.3.2 Human and Swine Calculated Scale Factors for Each Age Level - λ z Torso (left); λ x torso = λ y torso (right)

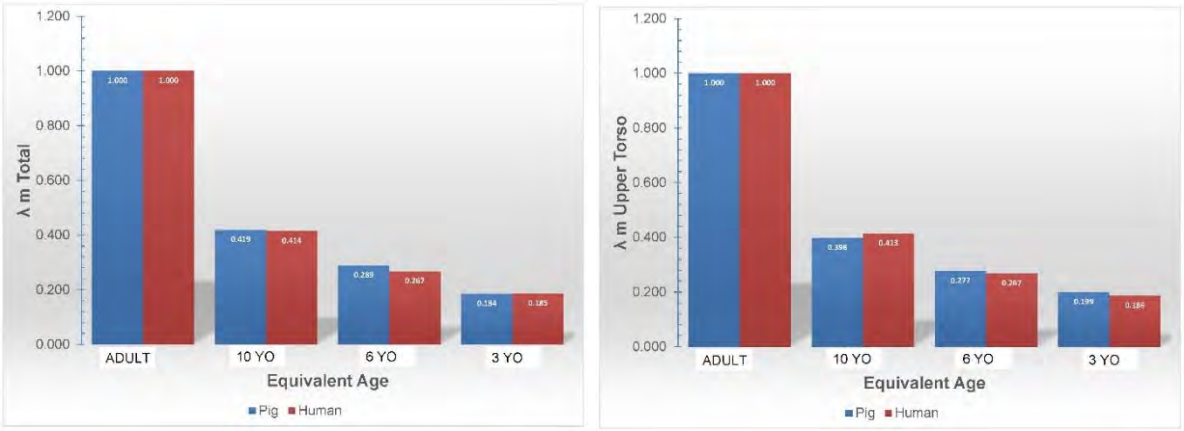

Figure 6.3.3 Human and Swine Calculated Scale Factors for Each Age Level - λ m Total (left); λ x torso = λ m Upper Torso (right)

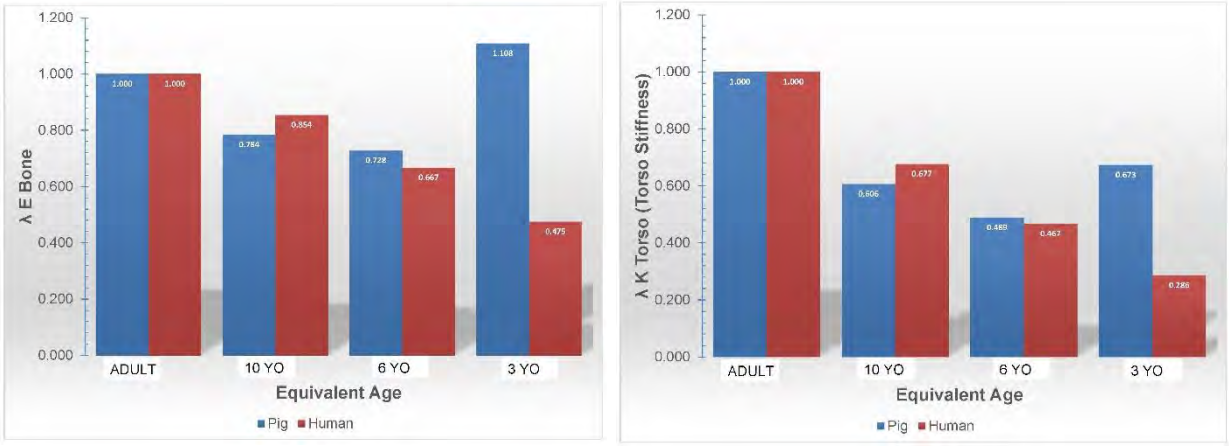

Figure 6.3.4 Human and Swine Calculated Scale Factors for Each Age Level - λ E Bone (Young's Modulus) (left); λ K Torso (Torso Stiffness) (right)

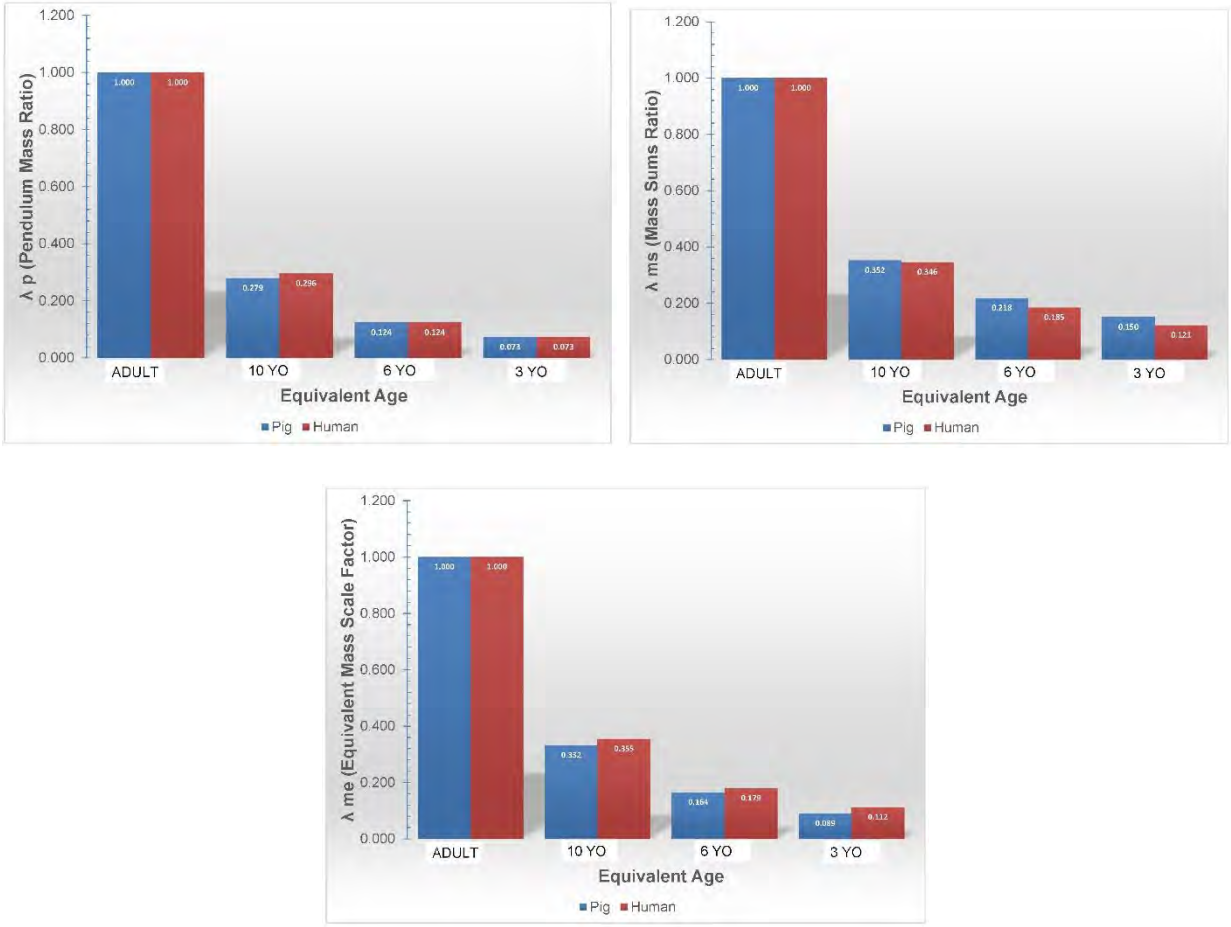

Figure 6.3.5 Human and Swine Calculated Scale Factors for Each Age Level - λ p (Pendulum Mass Ratio) (upper left); λ ms (Mass Sums Ratio) (upper right); λ me (Equivalent Mass Scale Factor) (bottom)

The main difference between the PSE scale factors and the human scale factors for each age level is the elastic bending modulus of bone scale factors, recalling that Young's Modulus used for the pigs was derived from the porcine ribs in the research performed in Chapter 5, whereas the human Young's modulus data is derived from human child and adult skull bone. The other scale factor difference that stand out is the difference in the torso stiffness for the 3-year-old age level.

The scale factors provided in Table 6.3.1 were used with the equations in Table 6.2.2 to obtain the impact response ratios for the 3, 6, and 10-year-old PSE relative to the 50th male PSE, given in Table 6.3.3 below. The equivalent human ISO (per Irwin et al. (2002)) and van Rantingen et al. (1997) lateral pendulum impact response ratios are provided in Table 6.3.4 for comparative reference.

Table 6.3.3 Response Ratios for the Swine- Force, Deflection, Acceleration, Time Period Relative to the 50th Male PSE

Impact Response Ratios - Pendulum Tests	50th Male PSE	10-Year-Old PSE	6-Year-Old PSE	3-Year-Old PSE
ABDOMEN				
Abdomen Force (Rf)	1.000	0.465	0.295	0.254
Abdomen Displacement (Rd)	1.000	0.768	0.604	0.377
Abdomen Acceleration (Rat)	1.000	1.111	1.023	1.376
Abdomen Period - Time (Rt)	1.000	0.740	0.580	0.365
Velocity Scale Factor AB (λ v)	1.000	1.037	1.042	1.034
THORAX				
Torso Force (Rf)	1.000	0.447	0.283	0.241
Torso Displacement (Rd)	1.000	0.737	0.580	0.359
Torso Acceleration (Rat)	1.000	1.067	0.982	1.309
Torso Period - Time (Rt)	1.000	0.740	0.580	0.365
Velocity Scale Factor TH (λ v)	1.000	0.996	1.000	0.983

Table 6.3.4 Response Ratios for Humans - Force, Deflection, Acceleration, Time Period

Impact Response Ratios - Pendulum Tests	50th Male	10-Year-Old	6-Year-Old	3-Year-Old
ABDOMEN				
Abdomen Force (Rf)	1.000	0.490	0.301	0.179
Abdomen Displacement (Rd)	1.000	0.724	0.646	0.626
Abdomen Acceleration (Rat)	1.000	1.182	1.130	0.964
Abdomen Period - Time (Rt)	1.000	0.724	0.620	0.626
Velocity Scale Factor AB (λ v)	1.000	1.000	1.042	1.000
THORAX				
Torso Force (Rf)	1.000	0.490	0.289	0.179
Torso Displacement (Rd)	1.000	0.724	0.620	0.626
Torso Acceleration (Rat)	1.000	1.182	1.084	0.964
Torso Period - Time (Rt)	1.000	0.724	0.620	0.626
Velocity Scale Factor TH (λ v)	1.000	1.000	1.000	1.000

Comparison of the swine and human calculated abdominal impact response ratios are provided in bar chart format in Figures 6.3.6 and 6.3.7 for reference.

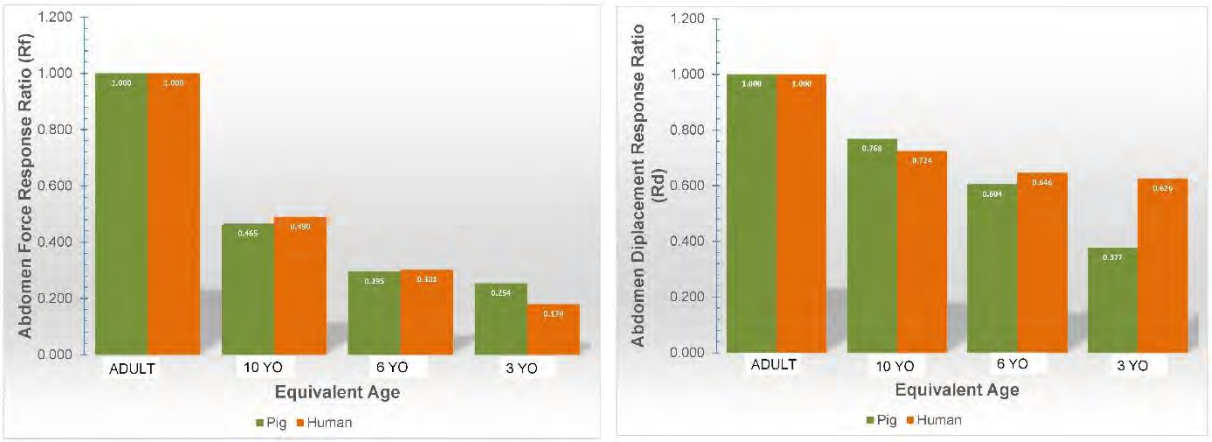

Figure 6.3.6 Human and Swine Calculated Impact Response Ratios (IRR) at Each Age Level – Abdomen Force IRR (left); Abdomen Displacement IRR (right)

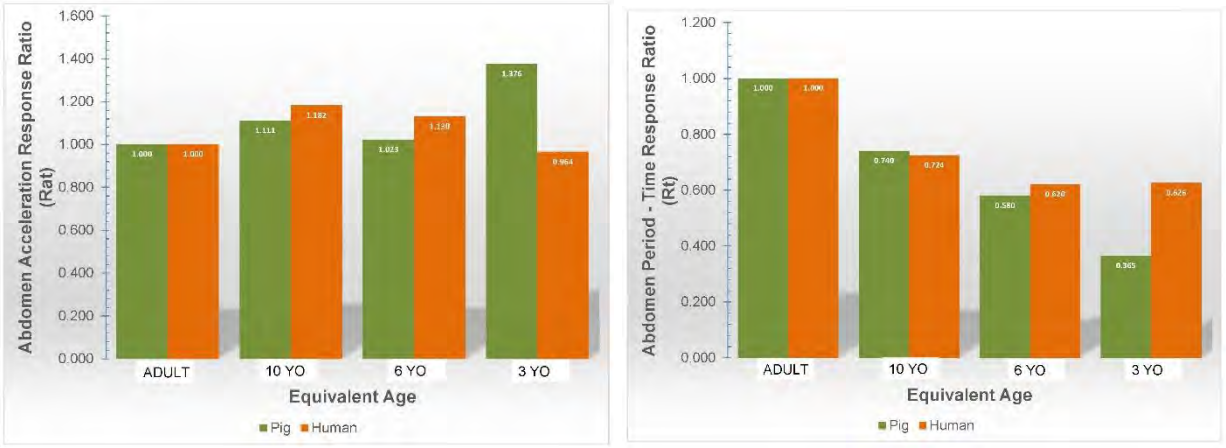

Figure 6.3.7 Human and Swine Calculated Impact Response Ratios at Each Age Level – Abdomen Acceleration IRR (left); Abdomen Time IRR (right)

Comparison of the swine and human calculated thorax impact response ratios are also provided in bar chart format in Figures 6.3.8 and 6.3.9 for reference below.

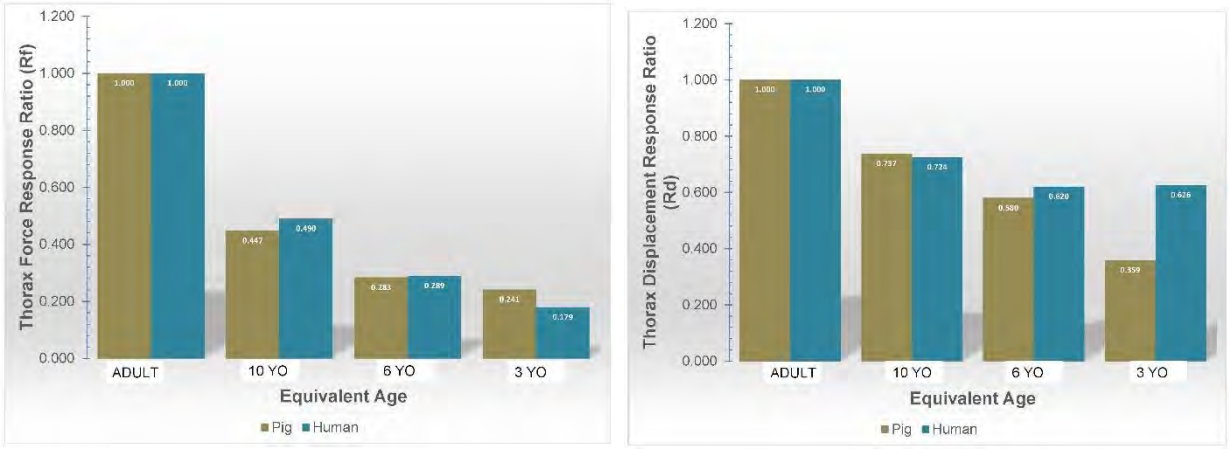

Figure 6.3.8 Human and Swine Calculated Impact Response Ratios at Each Age Level – Thorax Force IRR (left); Thorax Displacement IRR (right)

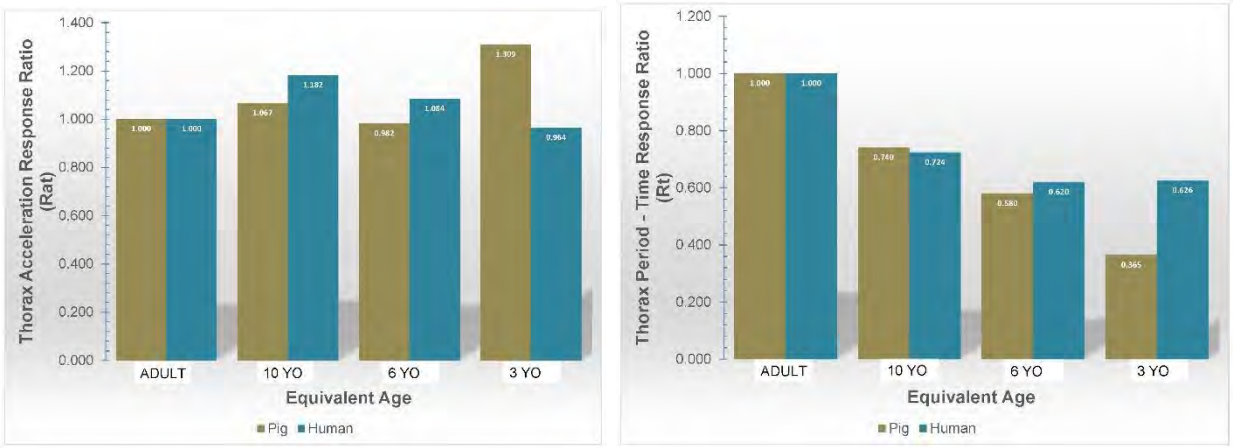

Figure 6.3.9 Human and Swine Calculated Impact Response Ratios at Each Age Level – Thorax Acceleration IRR (left); Thorax Time IRR (right)

The main differences between the PSE response ratios and the human response ratios for each age level are the acceleration and time response ratios. Additionally, substantial difference in response ratios from swine to human are seen for all 3-year-old parameters.

The impact response ratios provided in Table 6.3.3 were applied to the 50th male PSE response corridors to develop scaled response corridors for the 3, 6, and 10-year-old PSE, as described previously. Pendulum impact response data for the PSE tested were compared to the corresponding PSE scaled corridors for the 3-year-old, 6-year-old, and 10-year-old PSE.

Abdomen

Figure 6.3.10 illustrates the comparison of the 3, 6, 10-year-old, and 50th male PSE tested pendulum abdominal impact force traces versus time to the response corridors scaled from the 50th male PSE based on the calculated response ratios, respectively.

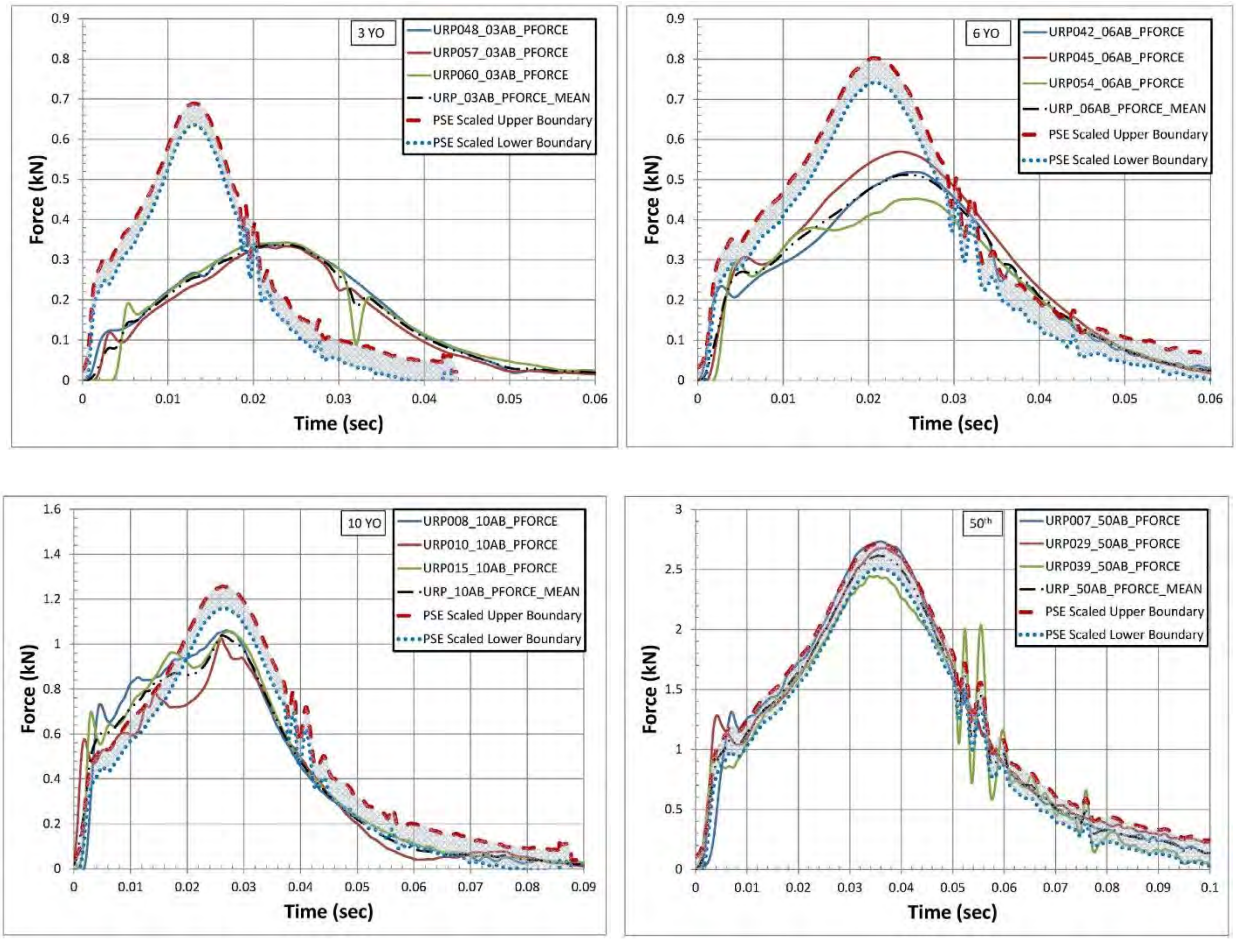

Figure 6.3.10 PSE Pendulum Lateral Abdominal Impact Force v. Time Actual Test Data Comparison to Scaled Response Corridors from 50th Male PSE (3-year-old (upper left); 6-year-old (upper right); 10-year-old (lower left); 50th male (lower right))

Scaled corridors in Figure 6.3.10 for abdominal force versus time show a trend of being higher in magnitude and shorter in duration at the 3-year-old level, higher in magnitude but similar in time duration at the 6-year-old level, and higher in magnitude and somewhat longer in duration at the 10-year-old level when compared to the actual test data.

Figure 6.3.11 establishes the comparison of the 3, 6, 10-year-old, and 50th male PSE tested pendulum abdominal impact T1 resultant acceleration traces versus time to the response corridors scaled from the 50th male PSE, respectively.

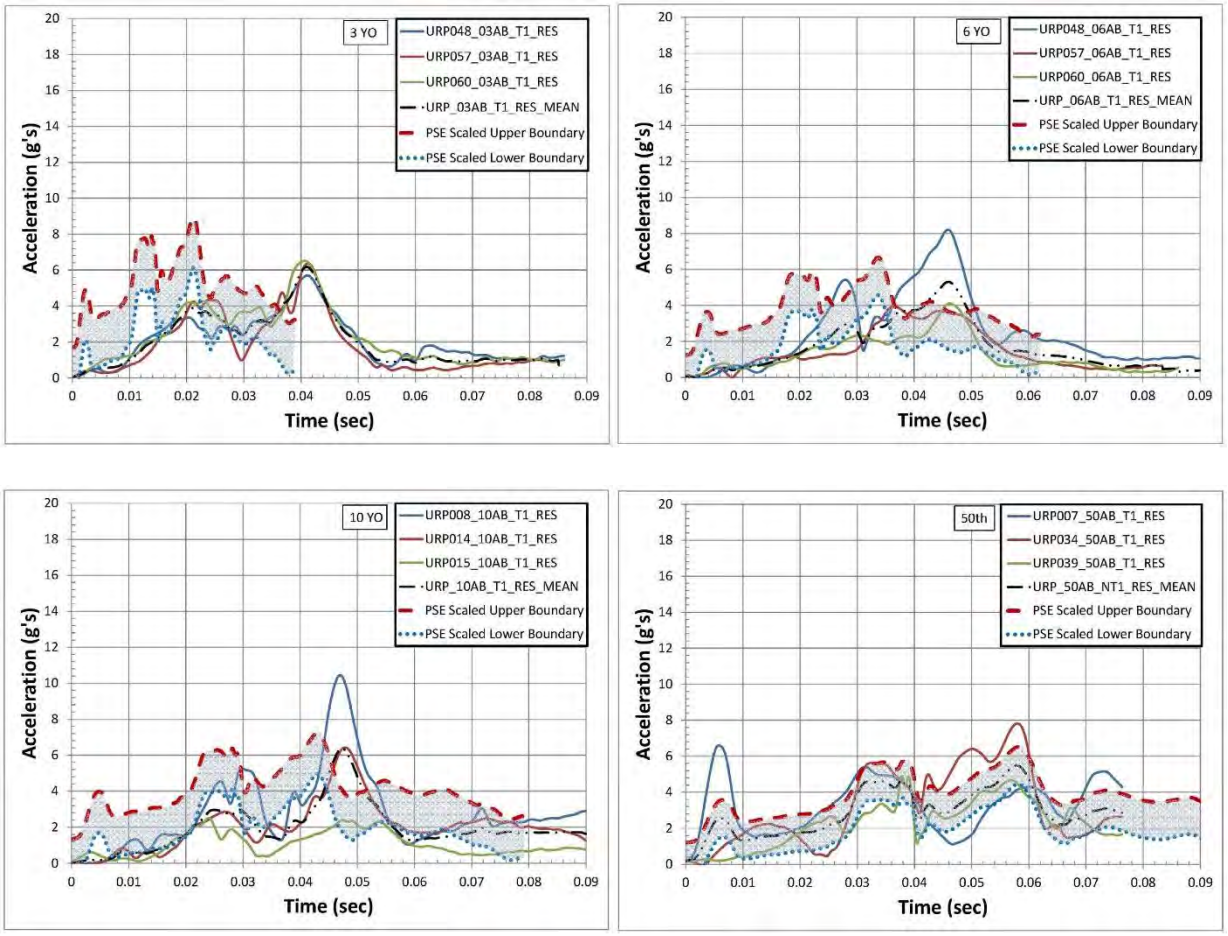

Figure 6.3.11 PSE Pendulum Abdominal Lateral Impact T1 Acceleration v. Time Actual Test Data Comparison to Scaled Response Corridors from 50th Male PSE (3-year-old (upper left); 6-year-old (upper right); 10-year-old (lower left); 50th male (lower right))

Scaled corridors in Figure 6.3.11 for T1 acceleration versus time from the abdominal impact testing show a trend of being somewhat higher in magnitude and shorter in duration at the 3-year-old level, and similar in magnitude and time duration at the 6 and 10-year-old levels compared to the actual test data.

Figure 6.3.12 illustrates the comparison of the 3, 6, 10-year-old, and 50th male PSE tested pendulum abdominal impact T14 resultant acceleration traces versus time to the response corridors scaled from the 50th male PSE, respectively.

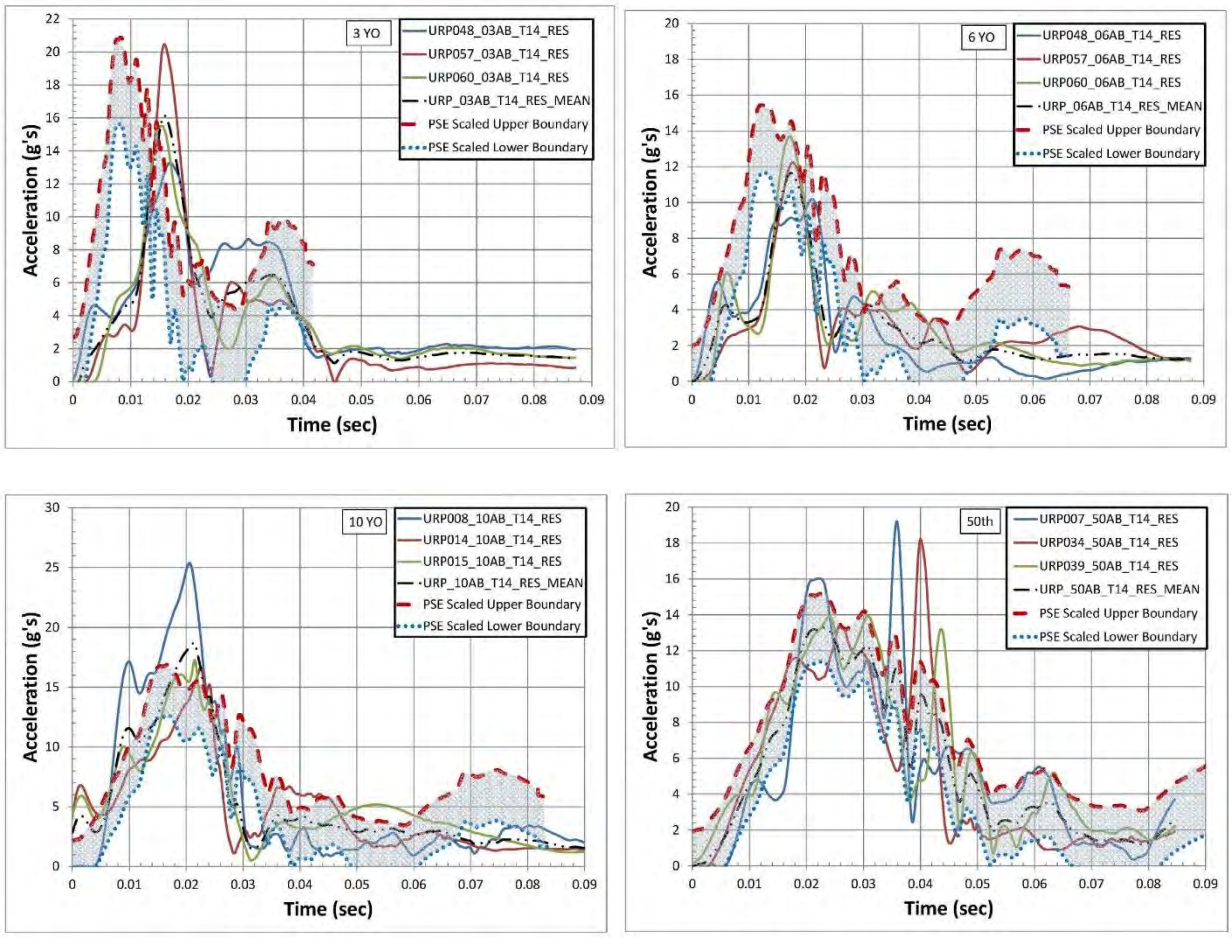

Figure 6.3.12 PSE Pendulum Abdominal Lateral Impact T14 Acceleration v. Time Actual Test Data Comparison to Scaled Response Corridors from 50th Male PSE (3-year-old (upper left); 6-year-old (upper right); 10-year-old (lower left); 50th male (lower right))

Scaled corridors in Figure 6.3.12 for T14 acceleration versus time from the abdominal impact testing display a trend of being somewhat higher in magnitude and shorter in duration at the 3-year-old level, similar in magnitude and time duration at the 6 and 10-year-old levels compared to the actual test data.

Figure 6.3.13 shows the comparison of the 3, 6, 10-year-old, and 50th male PSE tested pendulum abdominal impact L6 resultant acceleration traces versus time to the response corridors scaled from the 50th male PSE, respectively.

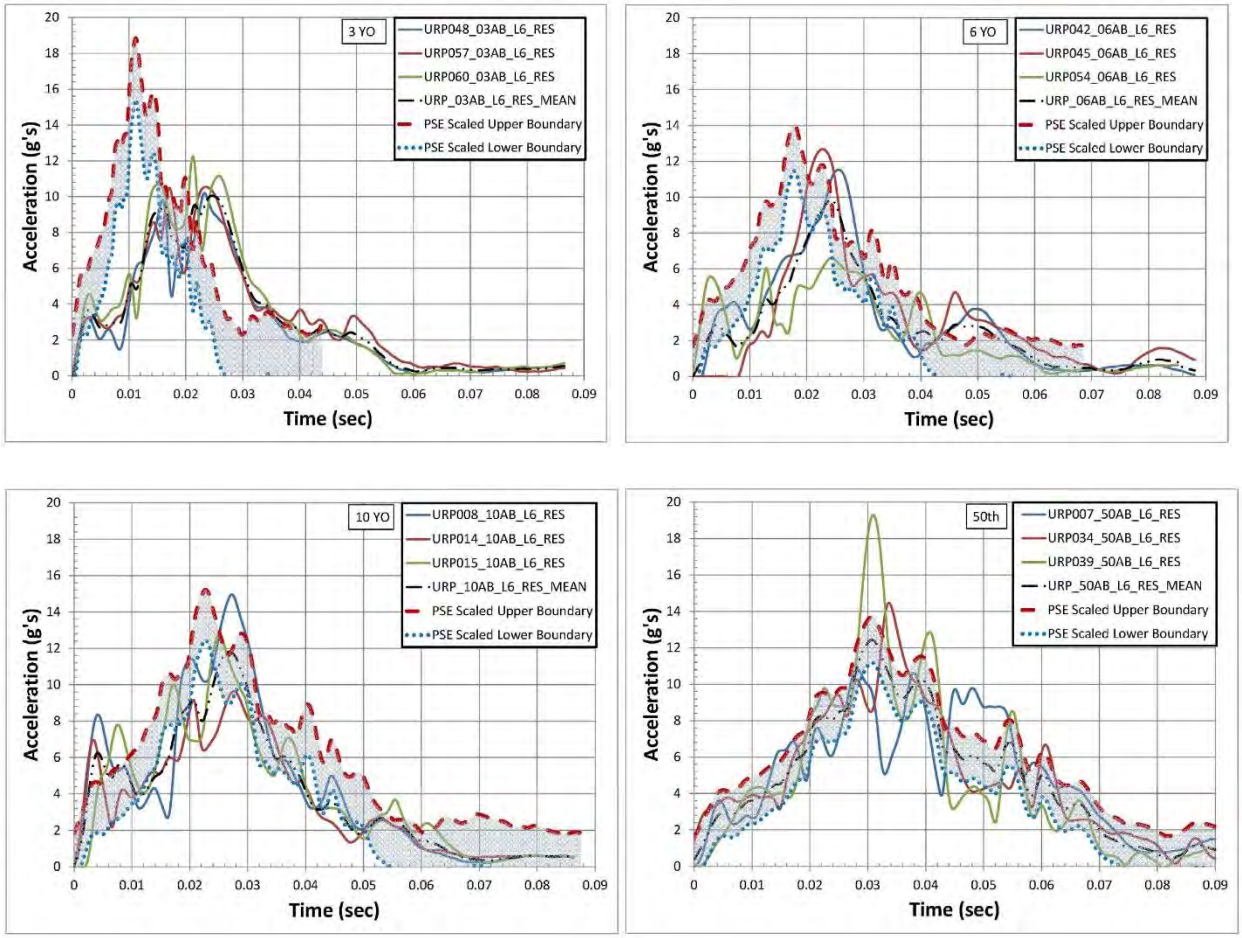

Figure 6.3.13 PSE Pendulum Abdominal Lateral Impact L6 Acceleration v. Time Actual Test Data Comparison to Scaled Response Corridors from 50th Male PSE (3-year-old (upper left); 6-year-old (upper right); 10-year-old (lower left); 50th male (lower right))

Scaled corridors in Figure 6.3.13 for L6 acceleration versus time from the abdominal impact testing exhibits a trend of being somewhat higher in magnitude and shorter in duration at the 3-year-old level, and similar in magnitude and time duration at the 6 and10-year-old levels compared to the actual test data.

Thorax

Figure 6.3.14 illustrates the comparison of the 3, 6, 10-year-old, and 50th male PSE tested pendulum thorax impact force traces versus time to the response corridors scaled from the 50th male PSE, respectively.

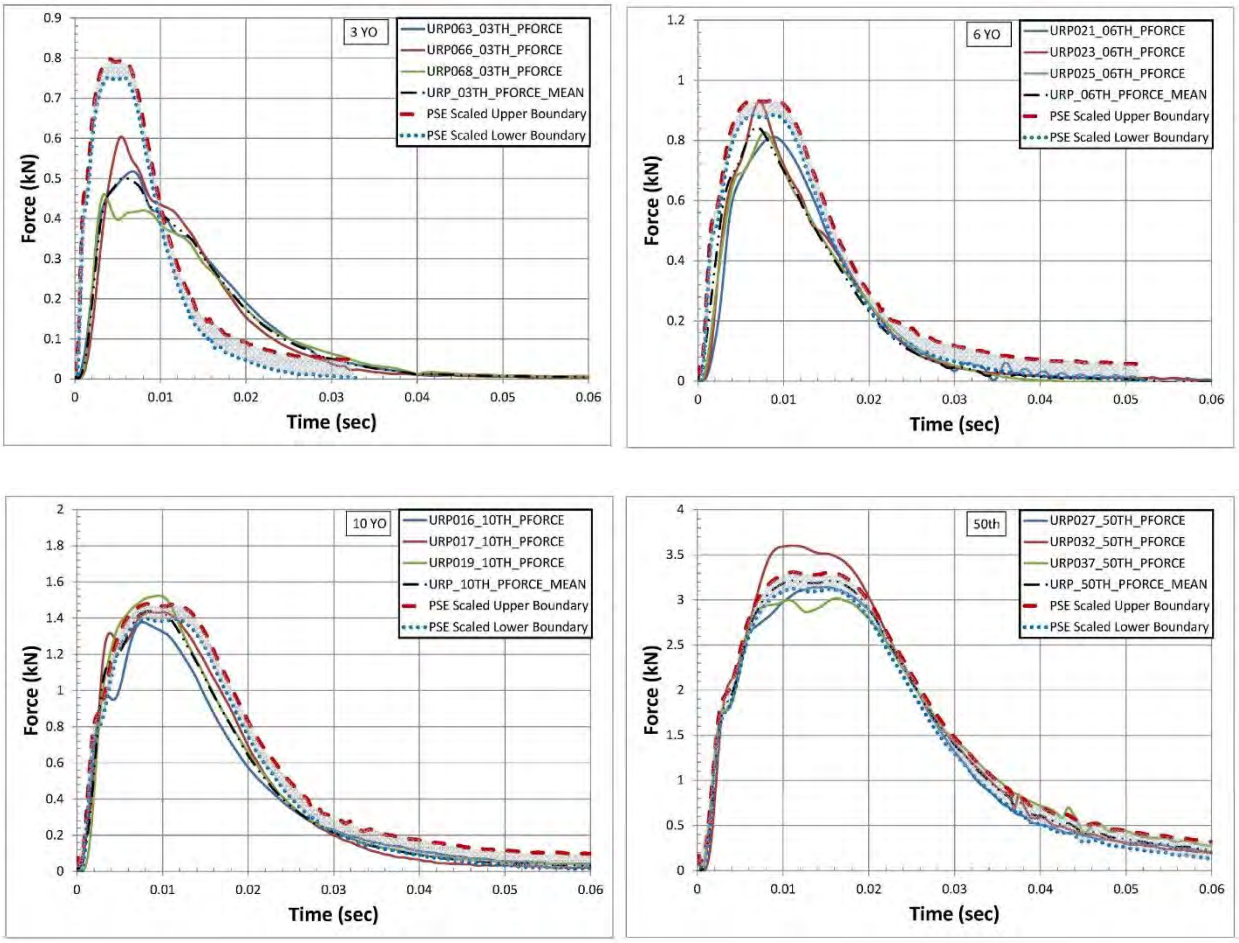

Figure 6.3.14 PSE Pendulum Lateral Thoracic Impact Force v. Time Actual Test Data Comparison to Scaled Response Corridors from 50th Male PSE (3-year-old (upper left); 6-year-old (upper right); 10-year-old (lower left); 50th male (lower right))

Scaled corridors in Figure 6.3.14 for thoracic force versus time show a trend of being higher in magnitude and shorter in duration for the 3-year-old and similar in magnitude and time duration at the 6 and 10-year-old levels when compared to the actual test data.

Figure 6.3.15 shows the comparison of the 3, 6, 10-year-old, and 50th male PSE tested pendulum thorax impact T1 lateral acceleration traces versus time to the response corridors scaled from the 50th male PSE, respectively.

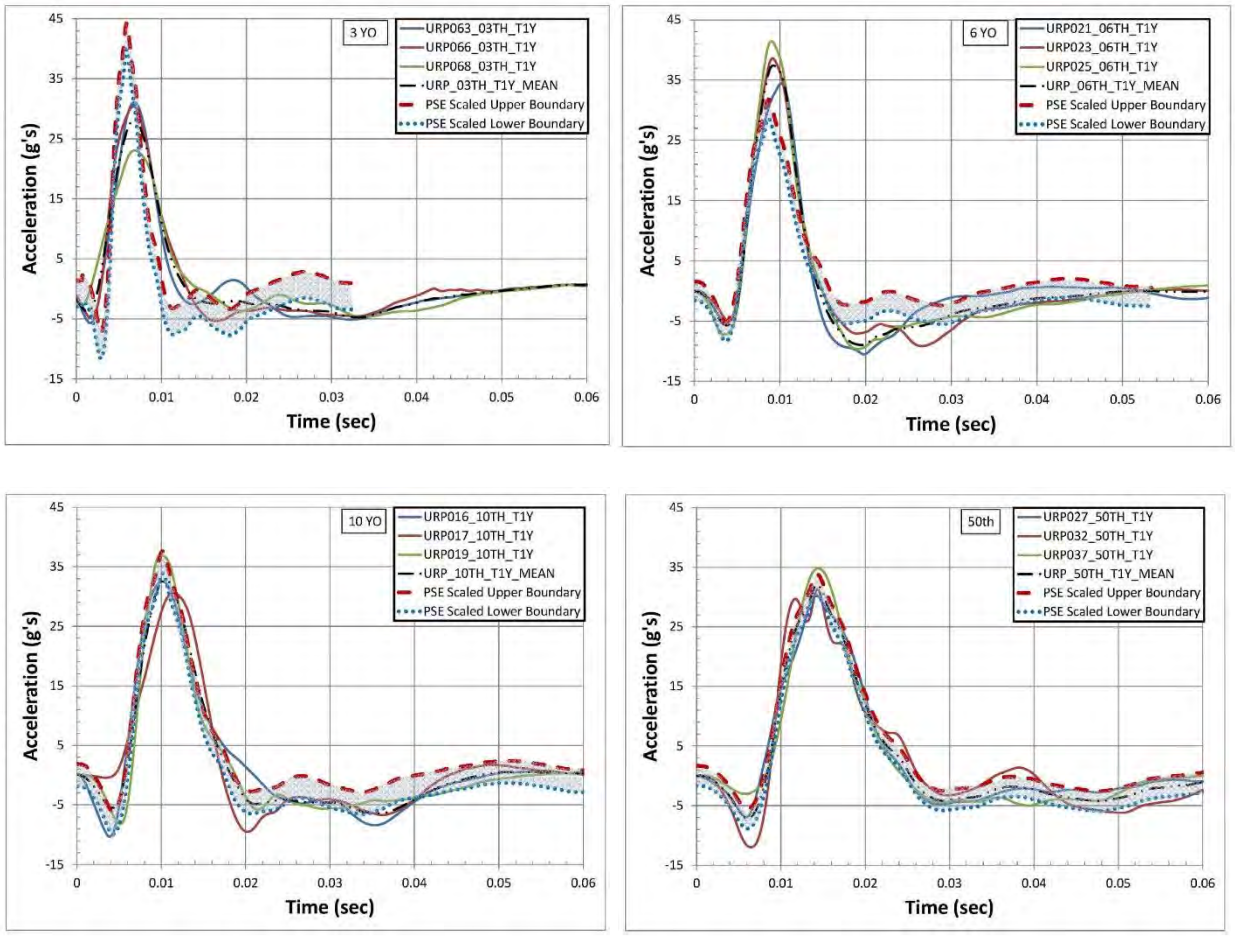

Figure 6.3.15 PSE Pendulum Thoracic Lateral Impact T1 Acceleration v. Time Actual Test Data Comparison to Scaled Response Corridors from 50th Male PSE (3-year-old (upper left); 6-year-old (upper right); 10-year-old (lower left); 50th male (lower right))

Scaled corridors in Figure 6.3.15 for T1 acceleration versus time from the thorax impact testing show a trend of being higher in magnitude and shorter in duration at the 3-year-old level, somewhat lower in magnitude and similar in time duration at the 6-year-old level, and similar in magnitude and time duration at the 10-year-old level compared to the actual test data.

Figure 6.3.16 provides the comparison of the 3, 6, 10-year-old, and 50th male PSE tested pendulum thorax impact T14 lateral acceleration traces versus time to the response corridors scaled from the 50th male PSE, respectively.

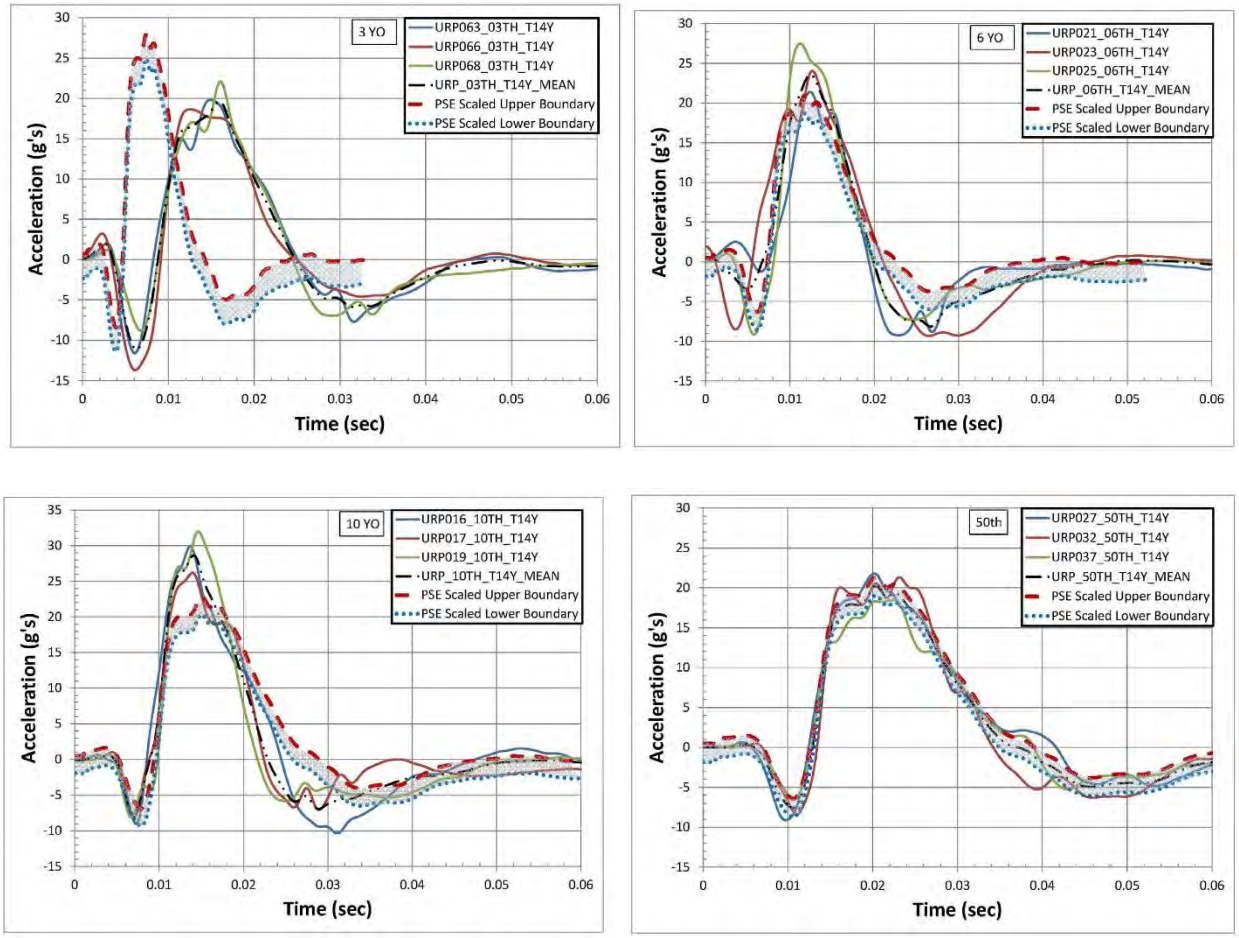

Figure 6.3.16 PSE Pendulum Thoracic Lateral Impact T14 Acceleration v. Time Actual Test Data Comparison to Scaled Response Corridors from 50th Male PSE (3-year-old (upper left); 6-year-old (upper right); 10-year-old (lower left); 50th male (lower right))

Scaled corridors in Figure 6.3.16 for T14 acceleration versus time from the thorax impact testing display a trend of being higher in magnitude and shorter in duration at the 3-year-old level and similar in magnitude and time duration at the 6 and 10-year-old levels compared to the actual test data.

Figure 6.3.17 illustrates the comparison of the 3, 6, 10-year-old, and 50th male PSE tested pendulum thorax impact L6 lateral acceleration traces versus time to the response corridors scaled from the 50th male PSE, respectively.

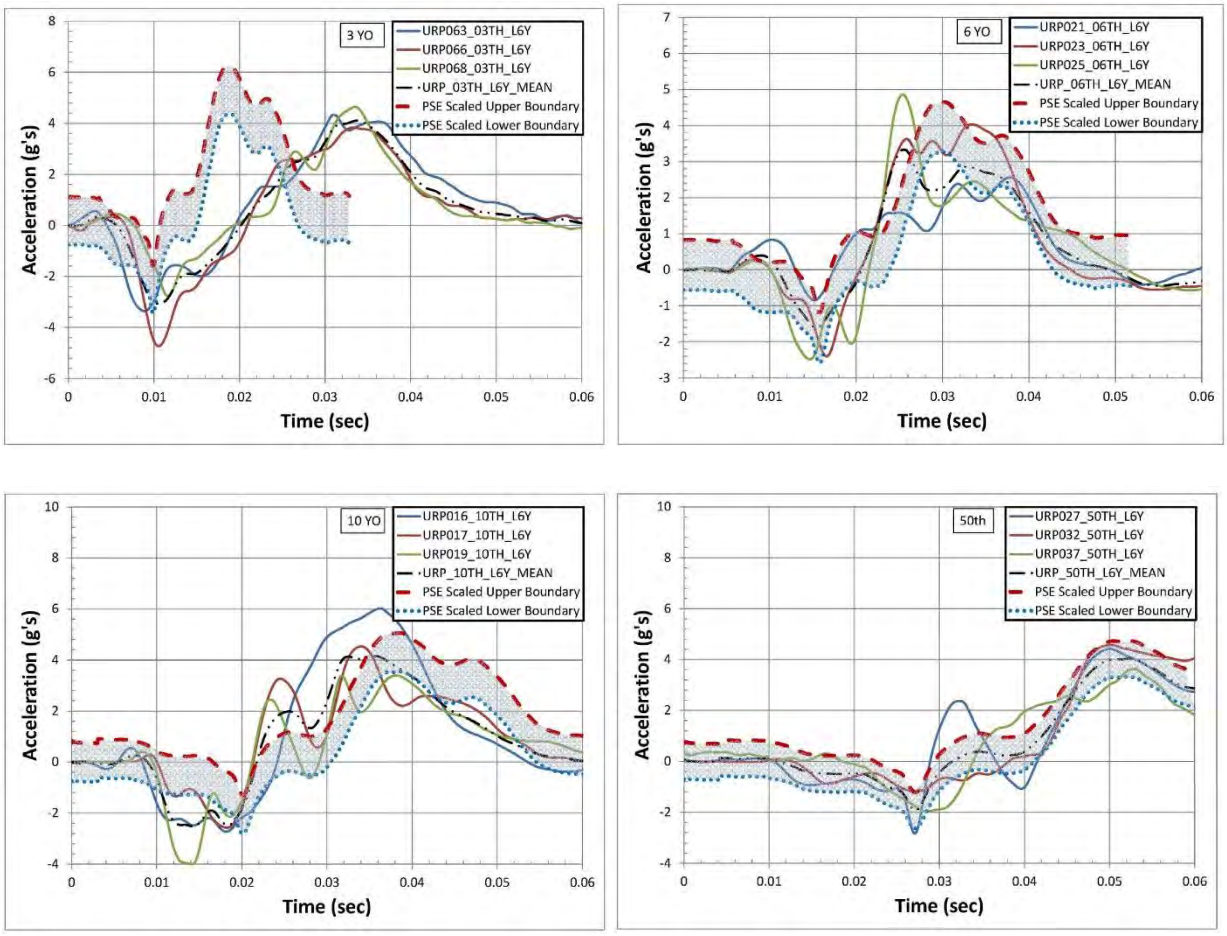

Figure 6.3.17 PSE Pendulum Thoracic Lateral Impact L6 Acceleration v. Time Actual Test Data Comparison to Scaled Response Corridors from 50th Male PSE (3-year-old (upper left); 6-year-old (upper right); 10-year-old (lower left); 50th male (lower right))

Scaled corridors in Figure 6.3.17 for L6 acceleration versus time from the thorax impact testing display a trend of being higher in magnitude and shorter in duration at the 3-year-old level and similar in magnitude and time duration at the 6 and 10-year-old levels compared to the actual test data

Figure 6.3.18 shows the comparison of the 3, 6, 10-year-old, and 50th male PSE tested pendulum thorax impact full chest impact force traces versus chest displacement. Thorax impact force versus full chest displacement displays an increase in force with age and an increase in chest displacement up to the 10-year-old age level. The current data

shows a similar chest displacement at the 10-year-old level as the 50th male PSE age.

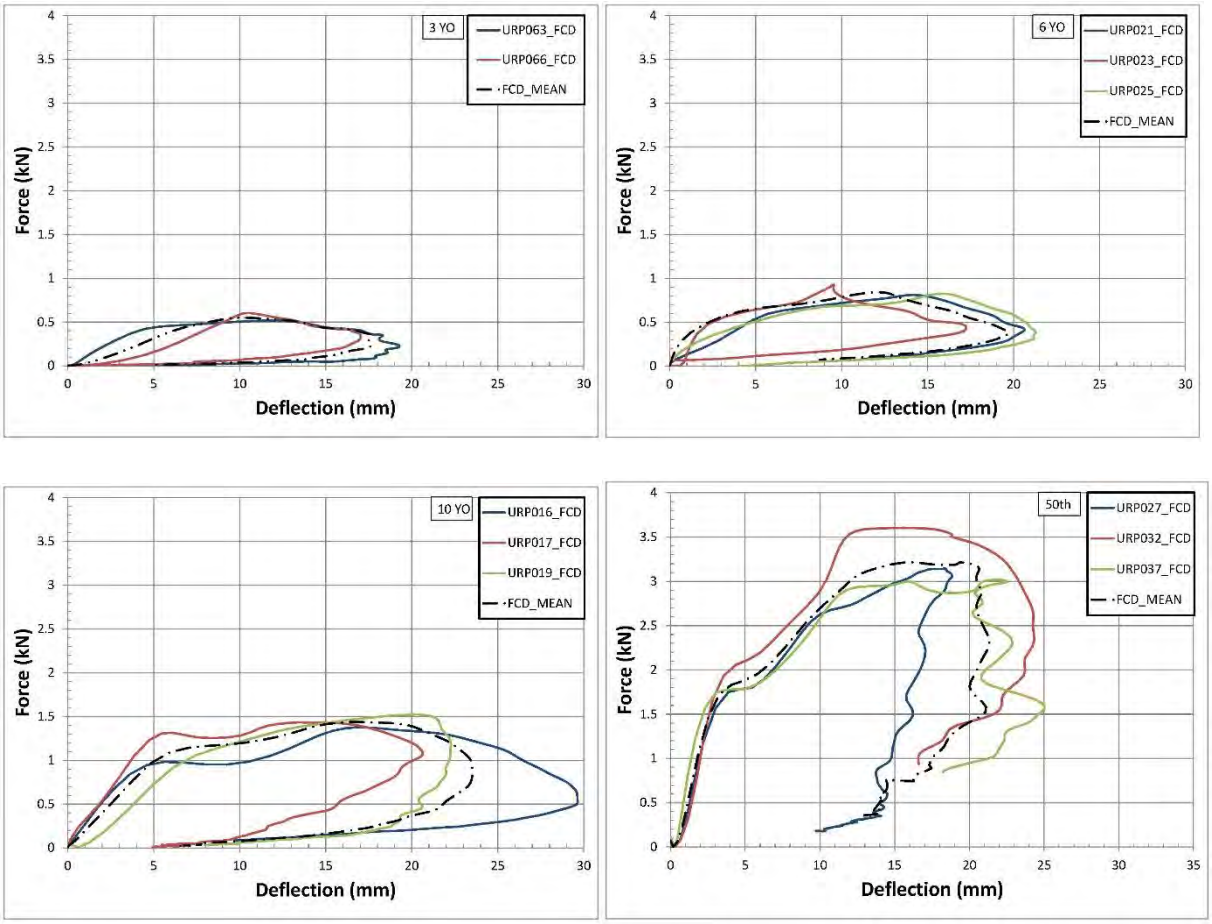

Figure 6.3.18 PSE Pendulum Thoracic Lateral Impact Force v. Full Chest Displacement Data Comparison (3-year-old (upper left); 6-year-old (upper right); 10-year-old (lower left); 50th male (lower right))

Figure 6.3.19 illustrates the comparison of the 3, 6, 10-year-old, and 50th male PSE tested pendulum thorax impact full chest displacement versus time. These graphs more readily show the increase in chest displacement with age up to the 10-year-old age level and a similar chest displacement at the 10-year-old level as the 50th male PSE age. Peak chest displacement occurs at approximately 15 msec for all age levels.

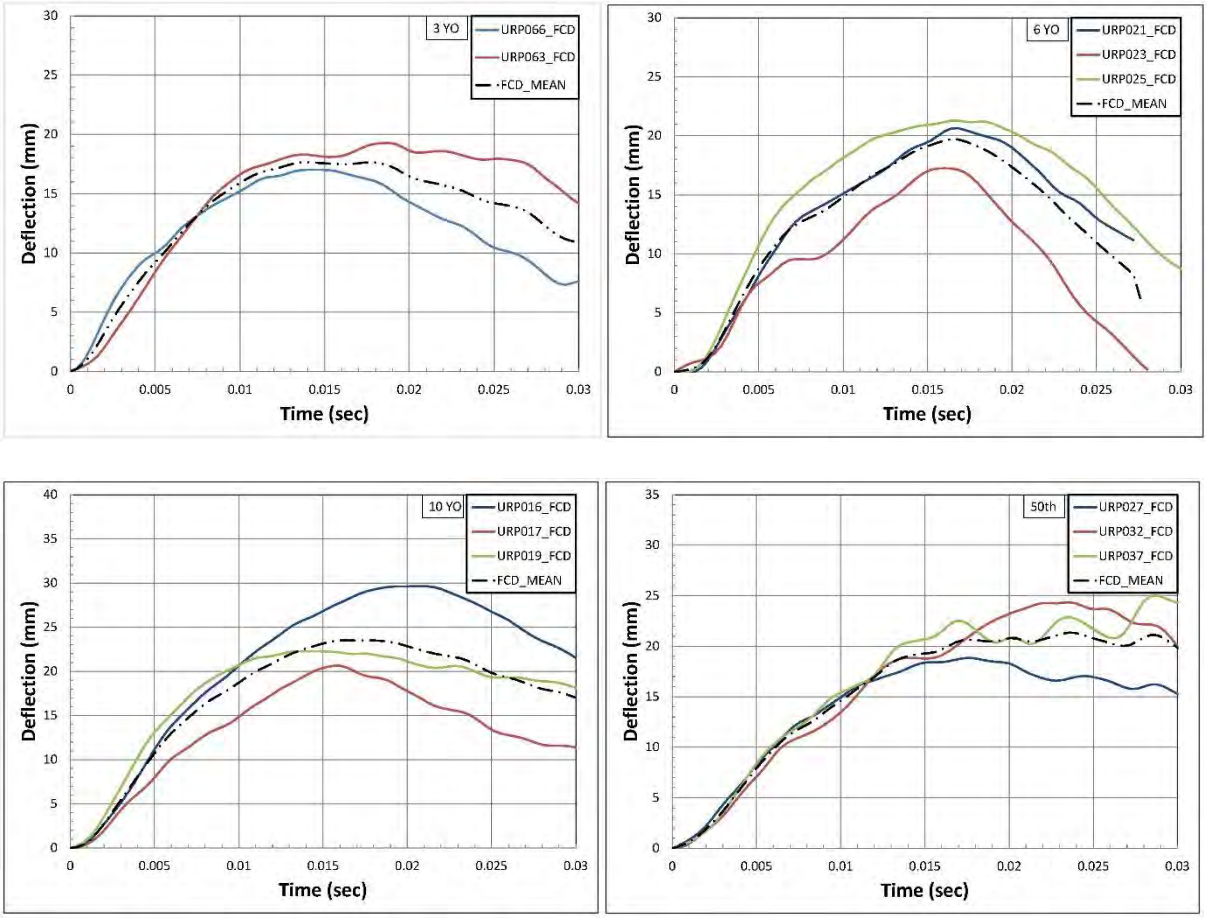

Figure 6.3.19 PSE Pendulum Thoracic Lateral Impact Full Chest Displacement v. Time Data Comparison (3-year-old (upper left); 6-year-old (upper right); 10-year-old (lower left); 50th male (lower right))

6.4 – Discussion

The general trend observed when comparing scaling response corridors from the 50th male PSE to the younger ages for all parameters tested was that all 3-year-old PSE impact response corridors did not match, and were found to be greater in magnitude and shorter in time duration than the actual data. The main factors that make up the response ratio calculations (provided in Table 6.2.2) are the mass equivalent and torso stiffness scale factors. The torso stiffness calculation, in turn, is determined using the scale factor for elastic bending modulus of bone and the length scale factor which is based on the

erect seated height of the various aged pigs. The main difference between the PSE scale factors and the human scale factors for each age level is the Young's Modulus of bone scale factors. The elastic bending modulus of bone scale factor for the 10-year-old human was determined to be 0.854, but was calculated to be 0.784 for the 10-year-old PSE. The elastic bending modulus of bone scale factor for the 6-year-old human age level was determined to be 0.667, and calculated to be 0.728 for the 6-year-old PSE. The elastic bending modulus of bone scale factor for the 3-year-old human age level was documented to be 0.475, but was calculated to be 1.108 for the 3-year-old PSE.

The human scale factors for elastic bending modulus of bone, derived from extrapolation of child and adult skull bone, and provided in Irwin et al. (2002) increase with age. The elastic bending modulus of bone scale factors used in the current study for the PSE were derived from the swine rib bending testing of the individual ribs harvested from the non-impacted side of the test specimens at each equivalent age level. As documented in Chapter 5, Young's Modulus values for the porcine ribs were found to decrease from the 50th male PSE to the 10-year-old age level, decrease slightly more from the 10-year-old to the 6-year-old PSE age levels, and then increase from the 6-year-old to the 3-year-old PSE age levels. This pattern observed with the elastic bending modulus values for swine ribs carried over to the calculated elastic bending modulus scale factors which in turn were used in determining the torso stiffness scale factors for the pigs.

The torso stiffness scale factor is used in the denominator of the time response ratio calculation and in the numerator for the force and acceleration response ratio calculations (see Table 6.2.2 for reference). Therefore, the larger torso stiffness scale

factor value calculated for the 3-year-old PSE, as a function of its higher rib elastic bending modulus value, results in impact response corridors that have a shorter time duration and a greater magnitude than those observed for the 6-year-old and 10-year-old PSE age levels. This is not the pattern the actual data possesses, however.

The actual lateral impact pendulum data, for both thoracic and abdominal regions, increases in magnitude and time duration from the 3-year-old PSE up to the 50th male PSE. This increasing magnitude and time duration is comparable to the human response corridors developed based on an impulse-momentum analysis and the elastic bending modulus derived from skull bone. This pattern was observed in the comparison of the porcine data to the human impact response corridors in Chapter 4 as well as from the response ratio values presented in Table 6.3.4 above.

In an attempt to appreciate the effect the elastic modulus has on the formation of the impact response corridors, the human elastic modulus values established in Irwin et al. (2002) were used to develop the swine scaling corridors instead of the swine rib elastic bending moduli. Data and scale factors used to develop the updated swine impact response ratios, are provided in Table 6.4.1, below. Calculated swine impact response ratio updated values are provided in Table 6.4.2.

Table 6.4.1 Swine Length, Mass, and Updated Elastic Modulus Scale Factors

SCALING PARAMETERS	50th Male PSE	10-Year-Old PSE	6-Year-Old PSE	3-Year-Old PSE
Pendulum Mass [kg]	23.28	6.5	2.89	1.7
Erect Seated Height (ESH) [mm]	1244.6	962	835.7	755.7
Total Body Mass [kg]	73.8	30.9	21.3	13.6
Upper Torso Mass [kg]	37.2	14.8	10.3	7.4
Young's Modulus [N/mm^2]]	9900	8450	6600	4700
Effective Stiffness [N/mm]	77.84	28.73	29.5	19.65
λ z torso	1.000	0.773	0.671	0.607
λ m total	1.000	0.419	0.289	0.184
λ x torso = λ y torso	1.000	0.736	0.656	0.551
λ m UT	1.000	0.398	0.277	0.199
λ mass density	1.000	1.000	1.000	1.000
λ E bone	1.000	0.854	0.667	0.475
λ K torso (torso stiffness)	1.000	0.660	0.448	0.288
λ p (pendulum mass ratio)	1.000	0.279	0.124	0.073
λ ms (mass sums ratio)	1.000	0.352	0.218	0.150
λ me (equivalent mass scale factor)	1.000	0.332	0.164	0.089

Table 6.4.2 Updated Response Ratios for the Swine- Force, Deflection, Acceleration, Time Period Relative to the 50th Male PSE

Impact Response Ratios - Pendulum Tests	50th Male PSE	10-Year-Old PSE	6-Year-Old PSE	3-Year-Old PSE
ABDOMEN				
Abdomen Force (Rf)	1.000	0.485	0.283	0.166
Abdomen Displacement (Rd)	1.000	0.736	0.631	0.576
Abdomen Acceleration (Rat)	1.000	1.159	0.979	0.901
Abdomen Period - Time (Rt)	1.000	0.709	0.606	0.557
Velocity Scale Factor AB (λ v)	1.000	1.037	1.042	1.034
THORAX				
Torso Force (Rf)	1.000	0.466	0.271	0.158
Torso Displacement (Rd)	1.000	0.707	0.606	0.548
Torso Acceleration (Rat)	1.000	1.113	0.940	0.857
Torso Period - Time (Rt)	1.000	0.709	0.606	0.557
Velocity Scale Factor TH (λ v)	1.000	0.996	1.000	0.983

Figure 6.4.1 illustrates the comparison of the 3, 6, 10-year-old, and 50th male PSE tested pendulum abdominal impact force versus time traces to the updated response corridors based on the human skull bone elastic modulus and scaled from the 50th male PSE.

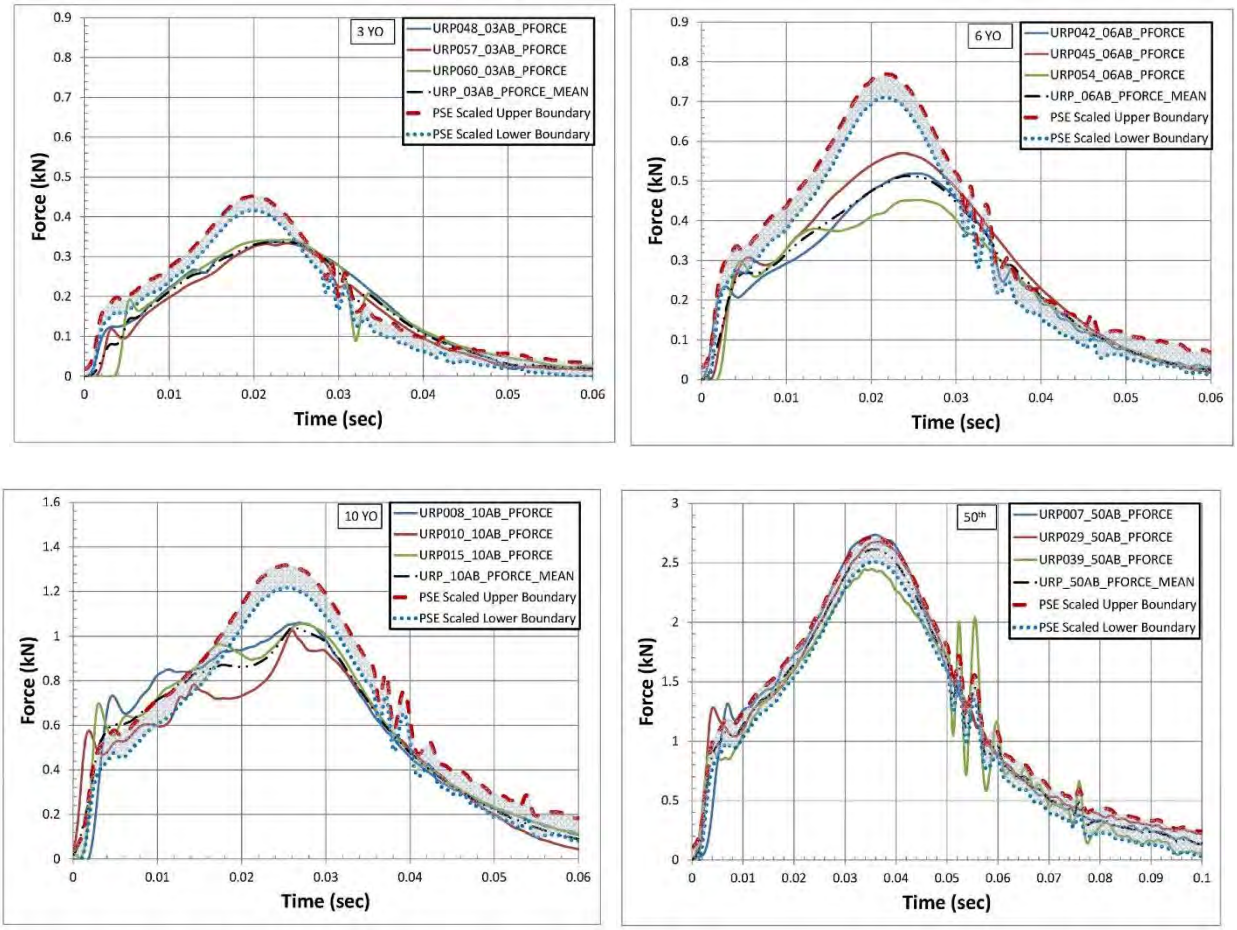

Figure 6.4.1 PSE Pendulum Lateral Abdominal Impact Force v. Time - Actual Test Data Comparison to Updated Scaled Response Corridors from 50th Male PSE (3-year-old (upper left); 6-year-old (upper right); 10-year-old (lower left); 50th male (lower right))

The updated scaled corridors in Figure 6.4.1 for abdominal force versus time based on using the elastic modulus from Irwin et al. (2002) shows a compatible pulse duration and an improved match in magnitude for all age levels when compared to the actual porcine test data. This is an enhancement over the scaled corridors for pendulum impact force versus time based on swine rib elastic modulus provided earlier in Figure 6.3.1.

Figure 6.4.2 establishes the comparison of the 3, 6, 10-year-old, and 50th male PSE tested pendulum abdominal impact T1 resultant acceleration traces versus time to the updated response corridors scaled from the 50th male PSE, respectively.

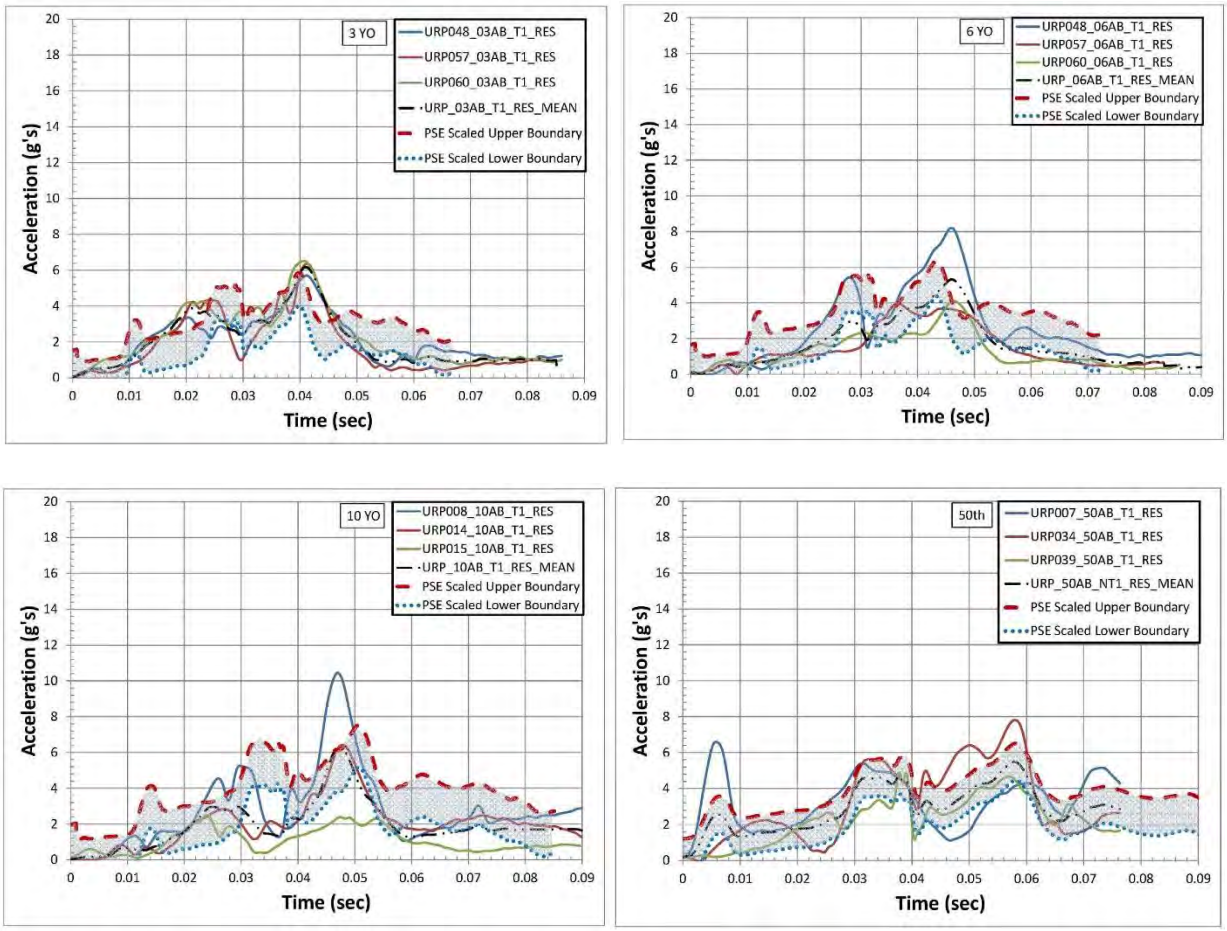

Figure 6.4.2 PSE Pendulum Abdominal Lateral Impact T1 Acceleration v. Time - Actual Test Data Comparison to Updated Scaled Response Corridors from 50th Male PSE (3-year-old (upper left); 6-year-old (upper right); 10-year-old (lower left); 50th male (lower right))

Updated scaled corridors in Figure 6.4.2 for T1 acceleration versus time from the abdominal impact testing shows a compatibility both in magnitude and pulse duration at all age levels compared to the actual test data. This is an improvement over the scaled corridors for T1 acceleration versus time based on swine rib elastic modulus provided earlier in Figure 6.3.2.

Figure 6.4.3 illustrates the comparison of the 3, 6, 10-year-old, and 50th male PSE tested pendulum abdominal impact T14 resultant acceleration traces versus time to the updated response corridors scaled from the 50th male PSE, respectively.

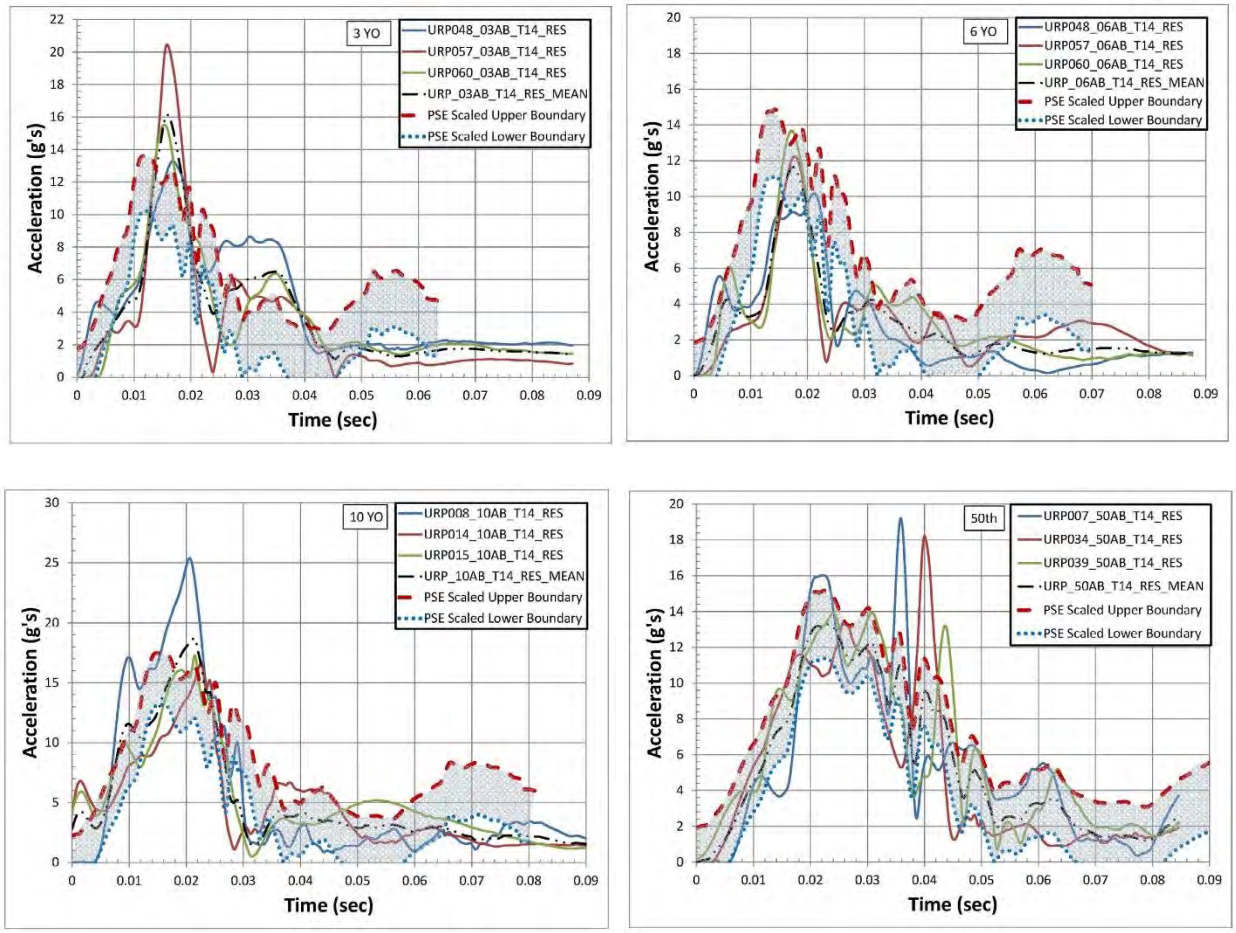

Figure 6.4.3 PSE Pendulum Abdominal Lateral Impact T14 Acceleration v. Time Actual Test Data Comparison to Updated Scaled Response Corridors from 50th Male PSE (3-year-old (upper left); 6-year-old (upper right); 10-year-old (lower left); 50th male (lower right))

Updated scaled corridors in Figure 6.4.3 for T14 acceleration versus time from the abdominal impact testing shows a compatibility both in magnitude and pulse duration at all age levels compared to the actual test data. This is a vast improvement over the scaled corridors for T14 acceleration versus time based on swine rib elastic modulus provided

earlier in Figure 6.3.3.

Figure 6.4.4 shows the comparison of the 3, 6, 10-year-old, and 50th male PSE tested pendulum abdominal impact L6 resultant acceleration traces versus time to the updated response corridors scaled from the 50th male PSE, respectively.

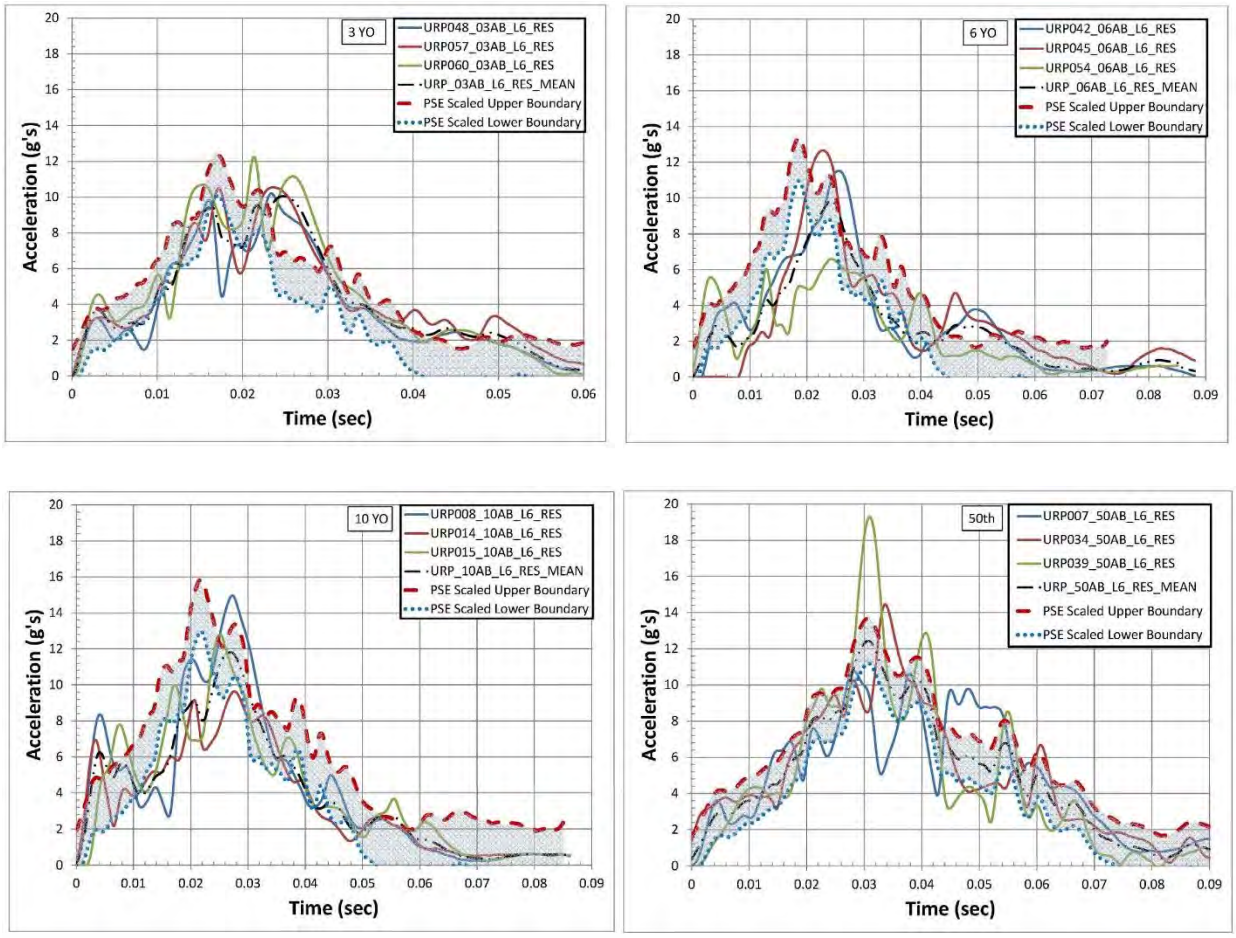

Figure 6.4.4 PSE Pendulum Abdominal Lateral Impact L6 Acceleration v. Time Actual Test Data Comparison to Updated Scaled Response Corridors from 50th Male PSE (3-year-old (upper left); 6-year-old (upper right); 10-year-old (lower left); 50th male (lower right))

Updated scaled corridors in Figure 6.4.4 for L6 acceleration versus time from the abdominal impact testing shows a compatibility in both magnitude and pulse duration for the 3-year-old, higher magnitude and shorter time duration for the 6-year-old, and

compatible magnitude and time duration for the 10-year-old compared to the actual test data. This is an improvement over the scaled corridors for L6 acceleration versus time based on swine rib elastic modulus provided earlier in Figure 6.3.4.

Thorax

Figure 6.4.5 illustrates the comparison of the 3, 6, 10-year-old, and 50th male PSE tested pendulum thorax impact force traces versus time to the updated response corridors scaled from the 50th male PSE, respectively.

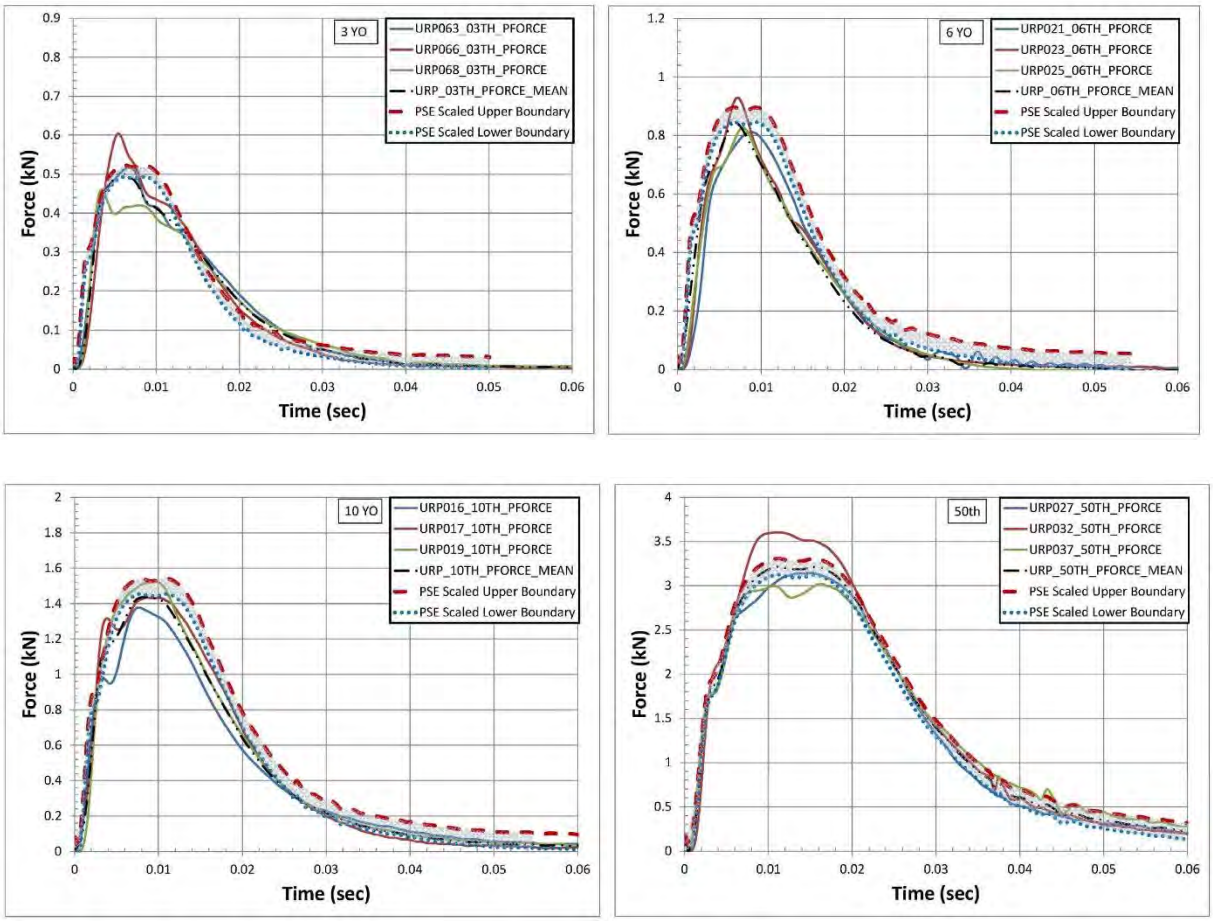

Figure 6.4.5 PSE Pendulum Lateral Thoracic Impact Force v. Time Actual Test Data Comparison to Updated Scaled Response Corridors from 50th Male PSE (3-year-old (upper left); 6-year-old (upper right); 10-year-old (lower left); 50th male (lower right))

Updated scaled corridors in Figure 6.4.5 for thoracic pendulum impact force versus

time shows a compatibility in both magnitude and pulse at all age levels compared to the actual test data. This is a vast improvement over the force versus time scaled corridors based on swine rib elastic modulus (Figure 6.3.5).

Figure 6.4.6 shows the comparison of the 3, 6, 10-year-old, and 50th male PSE tested pendulum thorax impact T1 lateral acceleration traces versus time to the updated response corridors scaled from the 50th male PSE, respectively.

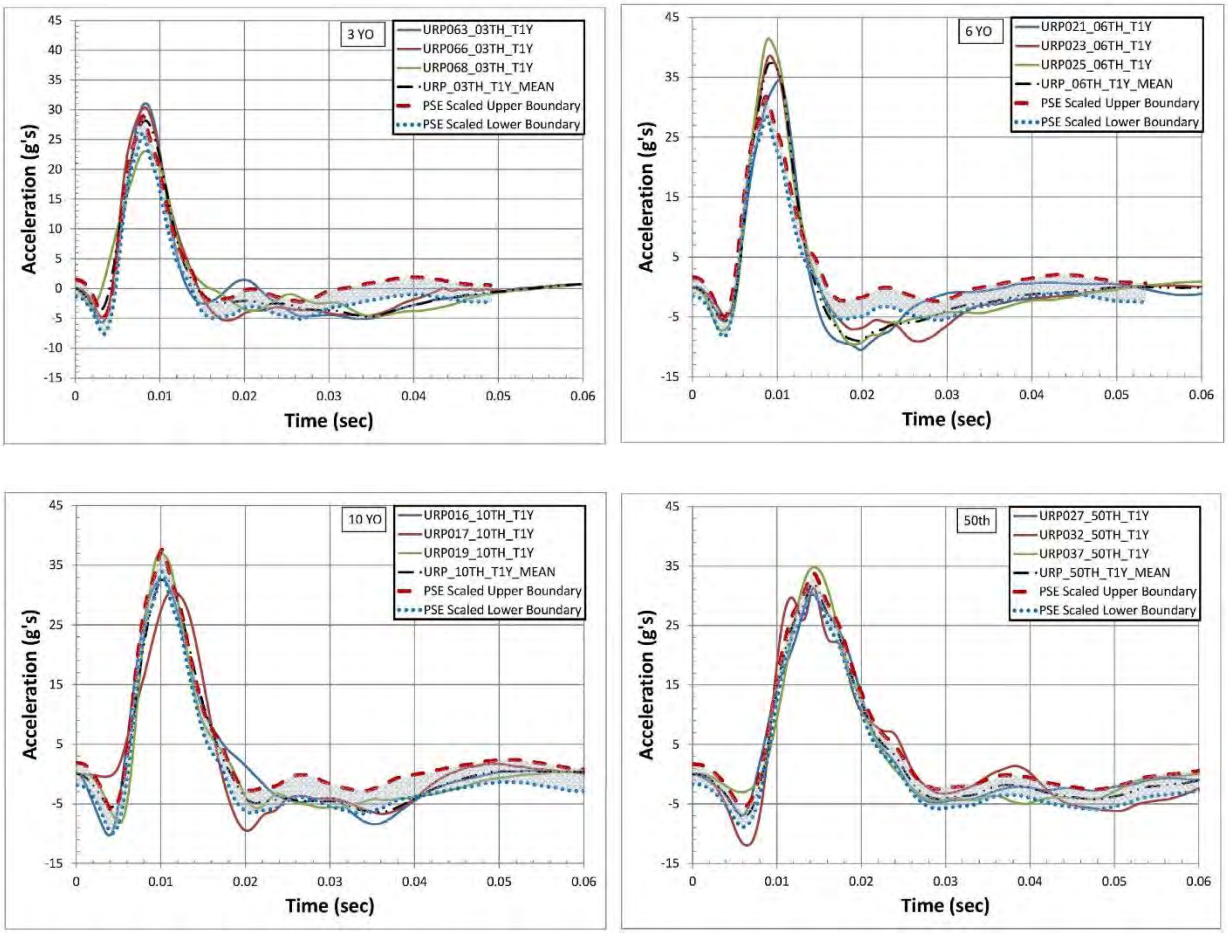

Figure 6.4.6 PSE Pendulum Thoracic Lateral Impact T1 Acceleration v. Time Actual Test Data Comparison to Updated Scaled Response Corridors from 50th Male PSE (3-year-old (upper left); 6-year-old (upper right); 10-year-old (lower left); 50th male (lower right))

Updated scaled corridors in Figure 6.4.6 for thoracic T1 acceleration versus time

shows a compatibility in both magnitude and pulse at all age levels except at the 6-year-old age level where the magnitude is lower compared to the actual test data. This is an improvement over the T1 acceleration versus time scaled corridors based on swine rib elastic modulus (Figure 6.3.6).

Figure 6.4.7 provides the comparison of the 3, 6, 10-year-old, and 50th male PSE tested pendulum thorax impact T14 lateral acceleration traces versus time to the updated response corridors scaled from the 50th male PSE, respectively.

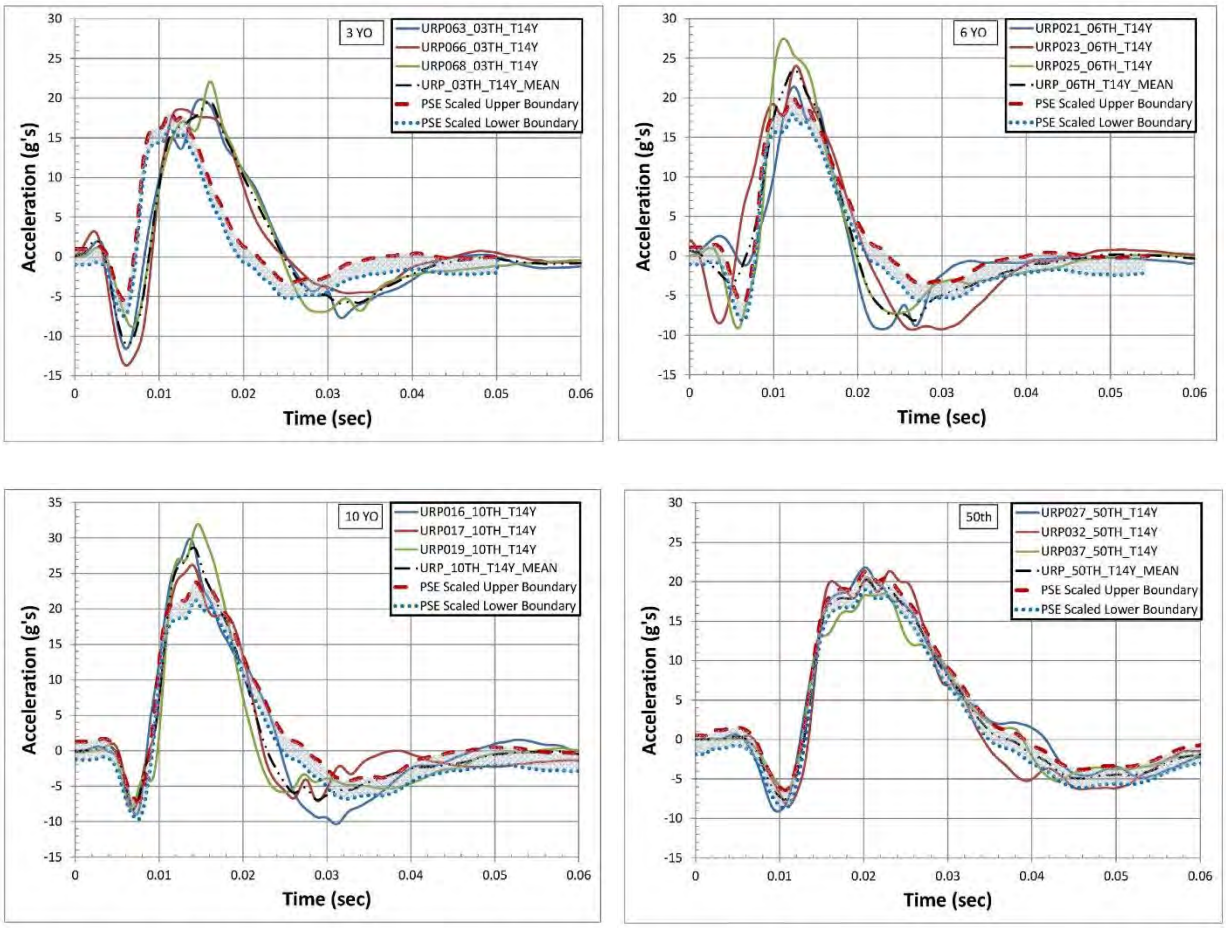

Figure 6.4.7 PSE Pendulum Thoracic Lateral Impact T14 Acceleration v. Time Actual Test Data Comparison to Updated Scaled Response Corridors from 50th Male PSE (3-year-old (upper left); 6-year-old (upper right); 10-year-old (lower left); 50th male (lower right))

Updated scaled corridors in Figure 6.4.7 for thoracic T14 acceleration versus time demonstrates compatibility in both magnitude and pulse duration at the 3-year-old age level, no significant change at the 6-year-old age level, and a compatibility in the pulse duration at the 10-year-old age compared to the actual test data. This is an improvement over the T14 acceleration versus time scaled corridors based on swine rib elastic modulus (Figure 6.3.7).

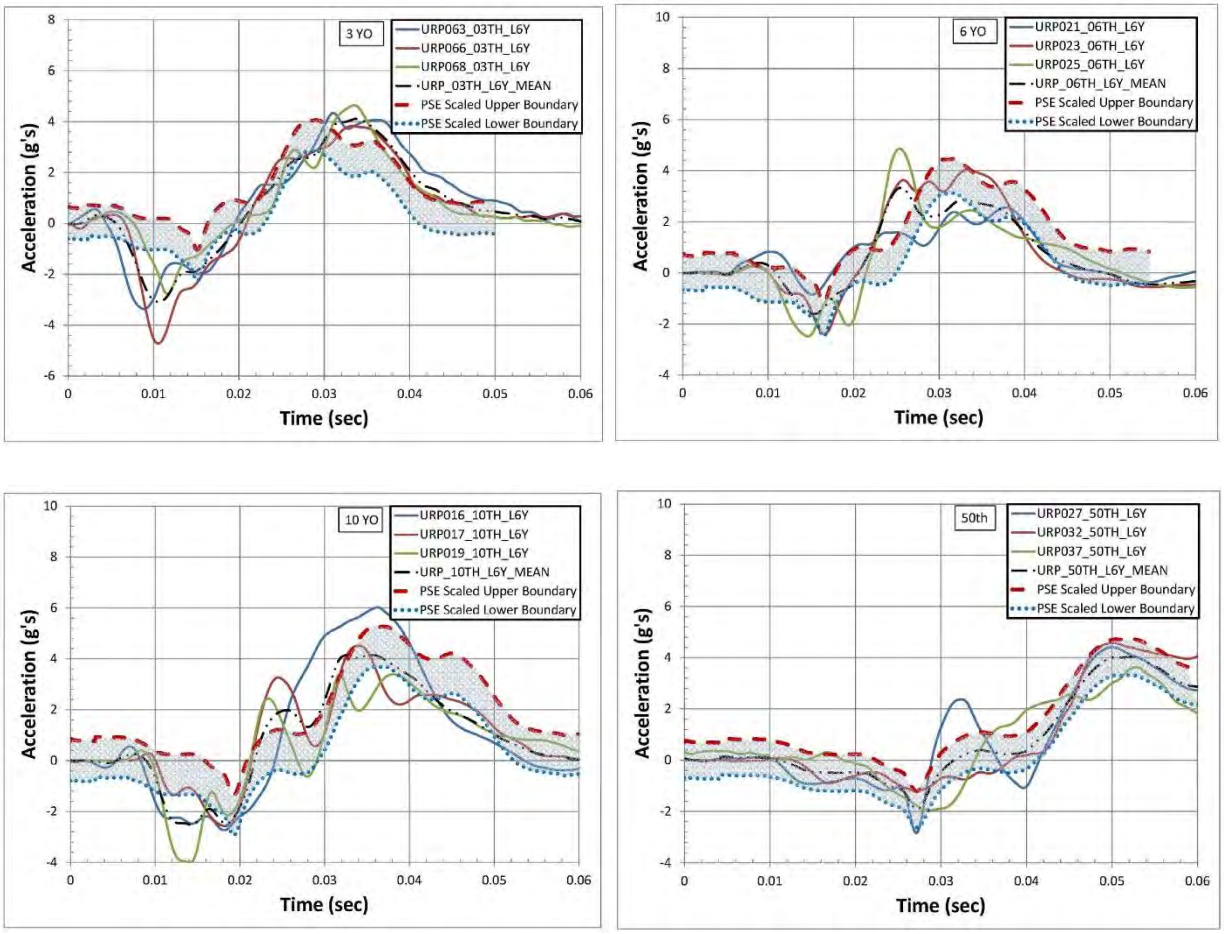

Figure 6.4.8 PSE Pendulum Thoracic Lateral Impact L6 Acceleration v. Time Actual Test Data Comparison to Updated Scaled Response Corridors from 50th Male PSE (3-year-old (upper left); 6-year-old (upper right); 10-year-old (lower left); 50th male (lower right))

Figure 6.4.8, above, illustrates the comparison of the 3, 6, 10-year-old, and 50th male PSE tested pendulum thorax impact L6 lateral acceleration traces versus time to the updated response corridors scaled from the 50th male PSE, respectively.

Updated scaled corridors in Figure 6.4.8 for thoracic L6 acceleration versus time shows compatibility in both magnitude and pulse for all age levels compared to the actual test data. This is again an improvement over the L6 acceleration versus time scaled corridors based on swine rib elastic modulus (Figure 6.3.8).

Based the current study's findings, when utilizing the elastic modulus of human skull bone presented in Irwin et al. (2002), thoracic and abdominal lateral pendulum impact response of PSE follows the general scaling laws, based on the impulse-momentum spring-mass model developed by Mertz (1984). The thoracic and abdominal lateral pendulum impact response of PSE also follows the ISO human scaled impact response corridors for lateral pendulum impact testing presented in Irwin et al. (2002).

Full chest force versus displacement and full chest displacement versus time were also documented during the thoracic pendulum lateral impact tests and were presented previously in Figures 6.3.9 and 6.3.10, respectively. The force-deflection response defines the compliance of the rib cage in lateral impact and the area under the curve designates the amount of energy absorbed through body deformation. Comparison of the current study 50th male PSE full chest force versus deflection data to the human and swine impact results presented for the 4.3 m/s testing performed by Viano et al. (1989B; 1989C), indicates the current study porcine thorax is less compliant that either the human or swine specimens studied by Viano et al. in 1989 (Figure 6.4.9). That is to say, the current study 50th male PSE achieved a higher impact force over a shorter rib cage

deformation which is representative of a stiffer rib cage. The difference in rib cage stiffness of the current study and that performed by Viano et al. (1989B; 1989C) is potentially due to the method used to determine deflection. The current study utilized a superior view high speed camera, a carbon-fiber rod secured to the impacted rib which passed laterally through the thoracic region to the non-impacted side of the pig, and tracking markers (one located on the end of the carbon fiber rod secured to the impacted side of the thorax and one located on the end of a rod secured to the non-impacted side). Viano et al. (1989B; 1989C) also used high speed video analysis to determine displacement, but it is unclear whether any sort of tracking markers were used.

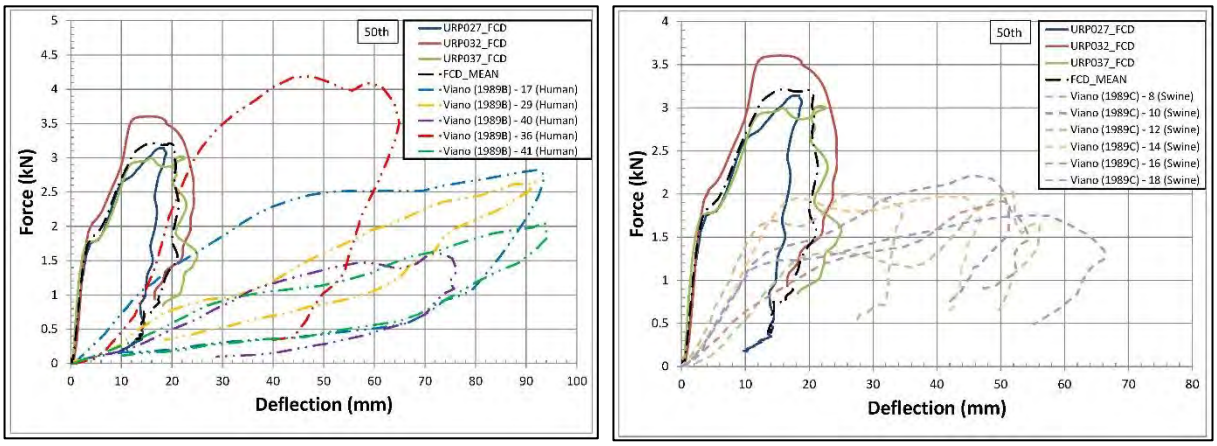

Figure 6.4.9 Comparison of Current Study 50th Male PSE Full Chest Force versus Deflection to Human (left) and Swine (right) Lateral Impact Testing in Viano et al. (1989B; 1989C) at a 4.3 m/s Pendulum Impact Speed

Kent et al. (2009), through their research of pediatric thoracoabdominal biomechanics in anterior-posterior belt loading and CPR analyses of children and adults suggested that a non-linear relationship may exist between age and thoracic stiffness, with peak thoracic stiffness occurring during the young adult phase of life and decreased thoracic stiffness for young children and the elderly. This study further suggested that current scaling methods may not adequately capture this behavior. Based on thoracic

lateral impact force-displacement results for the PSE evaluated in the current study, there appears to be an increase in thoracic stiffness with age up to the 50th male adult equivalent. In addition, the current study, at least from a human-equivalent-age from 3 to adult, follows the scaling laws currently established. Unlike the Kent et al. (2009) study, the current study does not take into consideration thoracic stiffness of PSE at an elderly human adult age level. Further investigation and study of PSE representing elderly humans would be needed to evaluate this hypothesis.

This study is subject to limitations. For instance, the current testing only evaluated whether current ISO lateral pendulum impact scaling laws are applicable for child ATD biofidelic design of the thorax and abdominal regions. The current study confirms that scaling laws are applicable for the human adult to the 3-year-old child and appropriate weight and breed pigs are appropriate surrogate models for biofidelic evaluation in this age range. The current study, however, does not evaluate whether scaling laws are applicable for any other test method such as dynamic sled testing or drop tests. The current study does not evaluate any other body region beyond the thorax and abdomen. In addition, the current study does not evaluate whether scaling laws are appropriate for human children under age 3 or the elderly.

Any animal model has accompanying limitations in terms of its ability to represent human response. For instance, not every domestic swine grows at the same rate or has the same structural makeup as the swine used in the current study. The current study used only Hampshire/Yorkshire Cross domestic pigs throughout testing and analysis. Further investigation should be made to determine how results may be effected by other swine breeds.

The impulse-momentum normalization model Mertz (1984) developed, which was analyzed in this study, uses mass and stiffness ratios along with assumptions of lumped mass and spring models. Young's Modulus was used in the calculation of the stiffness scaling factor. The stiffness scaling factor, based on this model is used to calculate the force, acceleration, displacement, and time impact response ratios. The stiffness ratio is directly proportional to force and acceleration in the impact response ratio calculations, but inversely proportional in the time and displacement impact response ratio calculations (see Tables 6.2.1 and 6.2.2 for reference). The force and acceleration magnitudes as well as impact pulse durations increased with age in the actual measured response data for the swine in the current study. In order for the impact response corridor scaling model to work, the corridors need to also increase in force, acceleration, and time duration with age at a similar rate. This is accomplished by the stiffness scale parameter, and therefore, Young's Modulus, increasing at a similar rate with age. The porcine rib elastic bending modulus calculated in the current study remained fairly similar with increase in age resulting in large bone modulus and stiffness scaling factors for the lower age groups, particularly the 3-year-old PSE. Due to the inverse proportionality the stiffness scaling factor has on the time response ratio, this produced shorter time duration corridors than the actual data. Similarly, the direct proportionality the stiffness scale factor has with force and acceleration response ratio calculations yielded corridors higher in magnitude than actual data for the 3-year-old PSE. The human parietal bone elastic bending modulus used by Irwin and Mertz (1997) was of proper magnitude for the adult and decreased appropriately in magnitude with decrease in age. This trend is similar to the PSE actual data, therefore resulting in a better correlation match to the PSE data than using the

determined swine rib elastic bending modulus for the torso stiffness scale factor More research into the determination of human-equivalent-age swine rib material properties using reverse engineering methods, further direct testing using accurate cross-sectional measurements, as well as dynamic material properties of the swine and human thorax in lateral impact could provide more appropriate torso scaling parameter data.

6.5 – Conclusions

The primary contributions of this study were to determine if existing human ISO lateral pendulum impact scaling laws for the thorax and abdomen are applicable from the mid-male adult down to the 3-year-old human. In addition, contributions of this study were also to determine if weight appropriate porcine surrogates could be used as models for humans at various age equivalent levels to assist in the advancing child safety in lateral impacts.

The overall findings of the current study confirm, through actual swine testing of appropriate weight surrogates that scale laws are applicable from the mid-male adult down to the 3-year-old age level. There is presently no known study that attempts to validate the existing scaling laws at various age levels to this author. Scarcity of human child PMHS limits such an analysis. In addition, existing scaling laws can be applied to porcine surrogates, using human skull elastic modulus values established and provided in Irwin et al. (2002), to provide a viable and powerful impact test model alternative for child safety research in lateral impacts.

CHAPTER 7 – CONCLUSIONS

Based on the research testing presented, the following observations were made:

- The majority of side and oblique impacts occurred in either the 2 o'clock or 10 o'clock PDOF directions. The majority of child occupants, age 4 through 10, involved in side and oblique impacts were reported as being restrained to some extent; however, only a small percentage of those reported as restrained were identified as using a child seat.
- The vast majority of injuries identified in the current study using the NASS-CDS database (49.2%) occurred at the head and face regions of child occupants involved in side and oblique impacts. Upper and lower extremities were also identified as being regions of the body frequently injured (11.2% and 13.3% of the total injuries, respectively). Thorax (6.7%) and abdomen (8.8%) body regions were also recognized as significant injury locations in side and oblique vehicle impacts for the child occupants.
- When considering only injured thorax and abdomen body regions, the primary sources of injury were documented as the vehicle interior or the belt restraint/buckle.
- In order to continue to advance child safety technologies and protect child occupants in lateral vehicle impacts, more innovative and biofidelic child anthropometric test devices (ATDs) need to be designed.
- In lateral impact, none of the three 6-year-old ATDs (HIII, Q6, and Q6s) would be considered good tools for assessing side impact occupant protection.

- Lateral impact force response of the thorax and abdomen of appropriate weight porcine surrogates established for human-equivalent-age 3-year-old, 6-year-old, 10-year-old, and 50th adult male are consistent with the ISO human scaled lateral impact response corridors presented in Irwin et al. (2002) and van Rantingen et al (1997).
- There is a significant linear correlation with respect to peak impact pendulum force and age for porcine thoracic and abdominal test data compared to the ISO human scaled impact response corridors. As for the thoracic T1 acceleration, no significant correlation was found for swine compared to human response corridors.
- Further investigation is needed to better understand and interpret the higher magnitude accelerations experienced at T1 for all age PSE compared to scaled human impact response corridors in order to be able to incorporate this data into research capabilities. It appears that T1 acceleration data during thorax impact testing is roughly two times greater in magnitude and slightly less in pulse duration than corresponding human scaled corridors at all tested age levels. This is most likely due to the difference in shape of the pig and human thorax, with the pig rib cages tending to be thinner in breadth and longer in depth than the human rib cage (Sack, 1982).
- A positive correlation exists between porcine peak bending force, rib stiffness, rib cortical cross-sectional area, and moment of inertia with age. There was no positive correlation between human and porcine rib elastic modulus and age.
- Swine testing of appropriate weight surrogates confirm that scaling laws are applicable from the mid-male adult down to the 3-year-old age level.

- Existing scaling laws can be applied to appropriate weight and breed porcine surrogates, using human skull elastic modulus values established and provided in Irwin et al. (2002), to provide a viable and powerful impact test model alternative for child safety research in lateral impacts.

APPENDIX: ATD Biofidelity Response Graphs and Tables

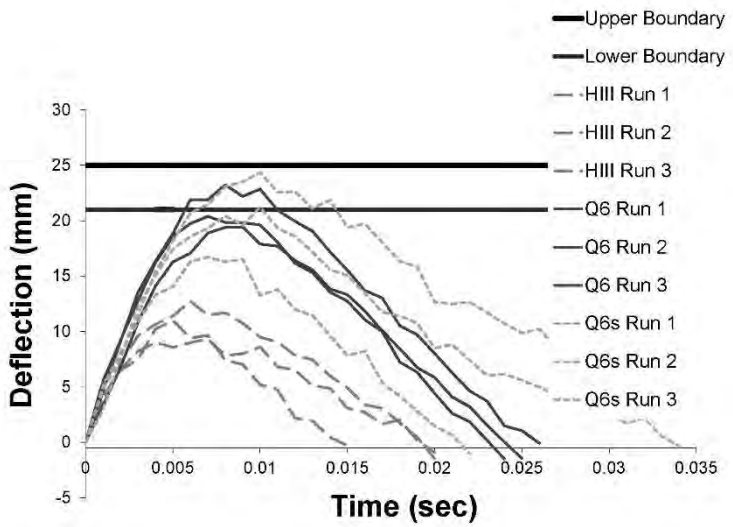

Figure A1: ISO 9790 – Lateral Pendulum Shoulder Impact – Deflection v Time (4.5 m/s)

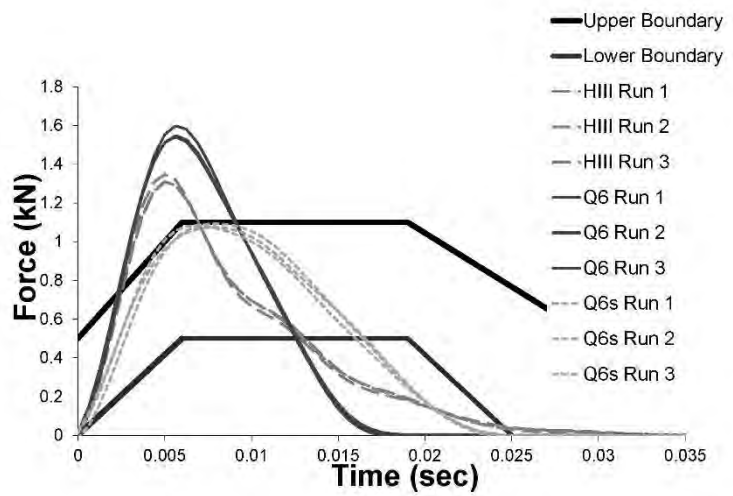

Figure A2: ISO 9790 – Lateral Pendulum Thorax Impact - Force v Time (4.3 m/s)

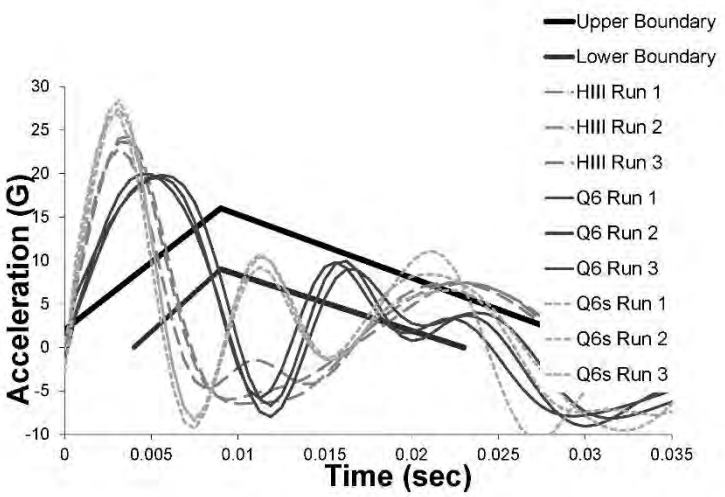

Figure A3: ISO 9790 – Lateral Pendulum Thorax Impact - Upper Spine T1 Acceleration v Time (4.3 m/s)

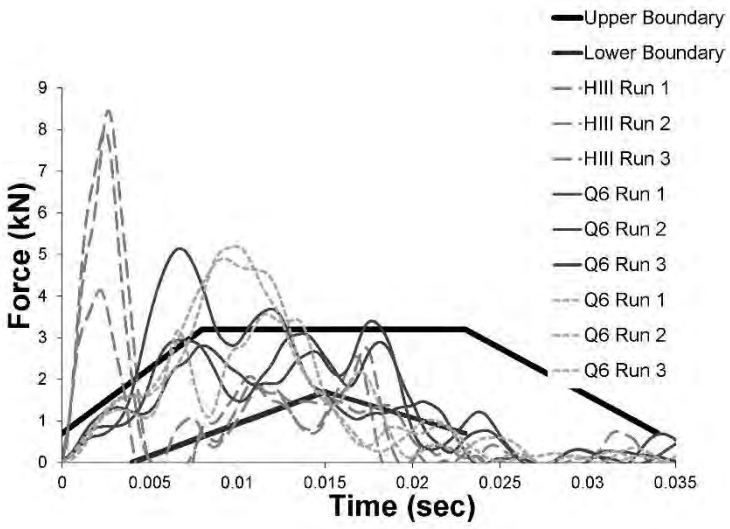

Figure A4: ISO 9790 – 1.0 Meter Drop Test – Thorax Plate Impact Force v Time

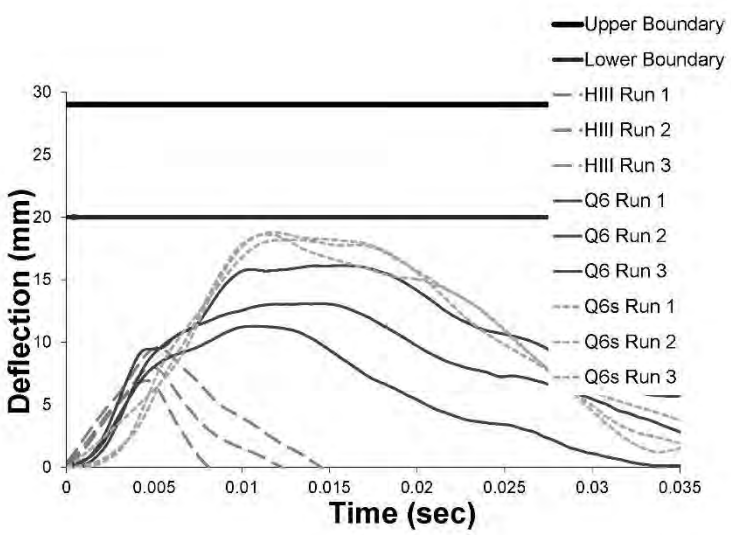

Figure A5: ISO 9790 – 1.0 Meter Drop Test – Peak Deflection of Impacted Rib v Time

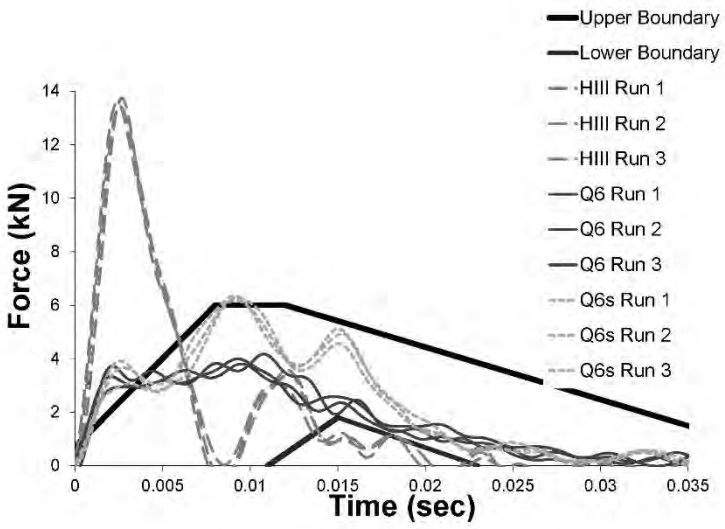

Figure A6: ISO 9790 – WSU Rigid Sled Test – Thorax/Shoulder Plate Impact Force v Time (6.8 m/s)

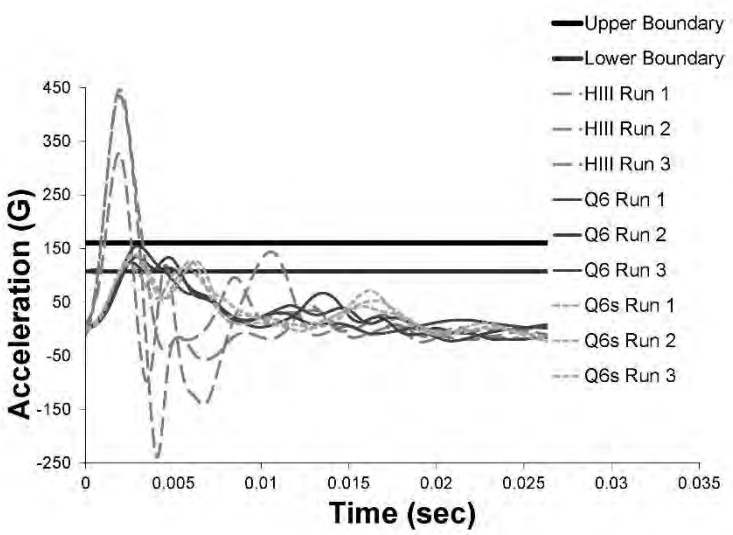

Figure A7: ISO 9790 – WSU Rigid Sled Test – Peak Upper Spine T1 Lateral Acceleration v Time (6.8 m/s)

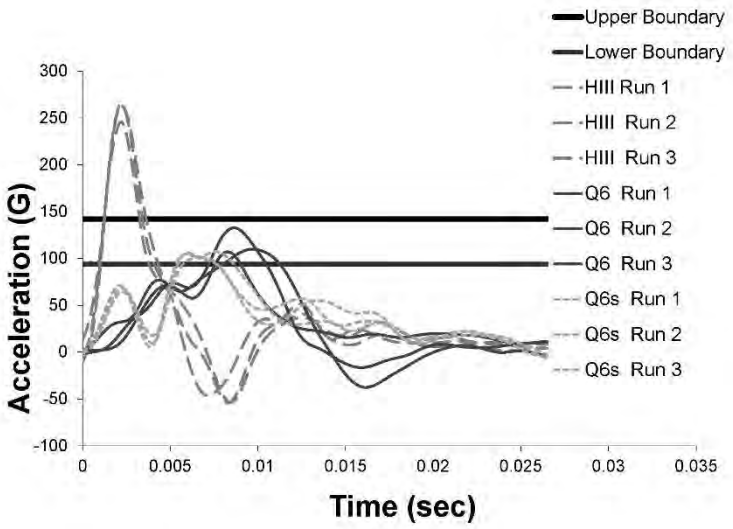

Figure A8: ISO 9790 – WSU Rigid Sled Test – Peak Lower Spine T12 Lateral Acceleration v Time (6.8 m/s)

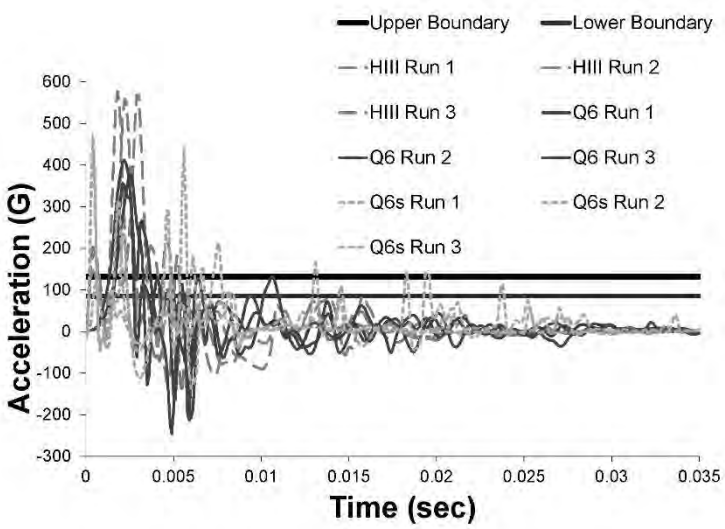

Figure A9: ISO 9790 – WSU Rigid Sled Test – Peak Lateral Acceleration of Impacted Rib v Time (6.8 m/s)

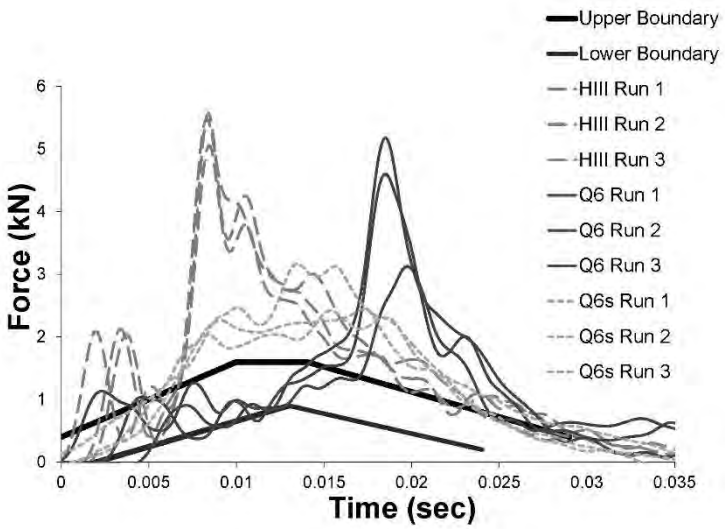

Figure A10: ISO 9790 – 1.0 Meter Drop Test – Armrest/Abdomen Impact Force v Time

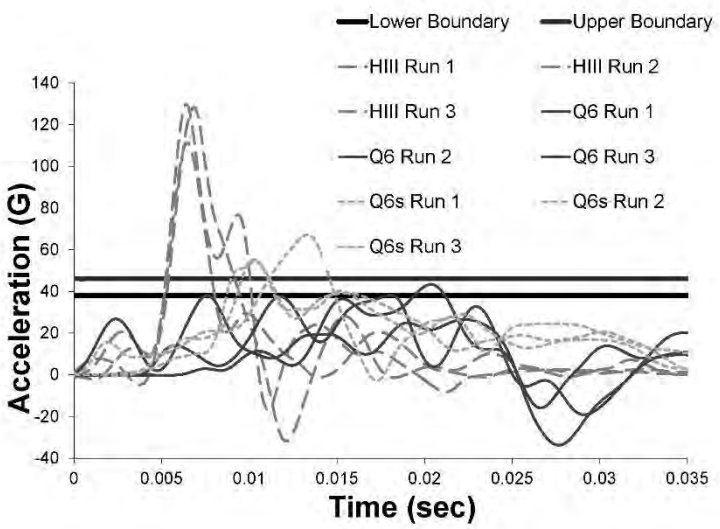

Figure A11: ISO 9790 – 1.0 Meter Drop Test – Peak Lower Spine T12 Acceleration v Time

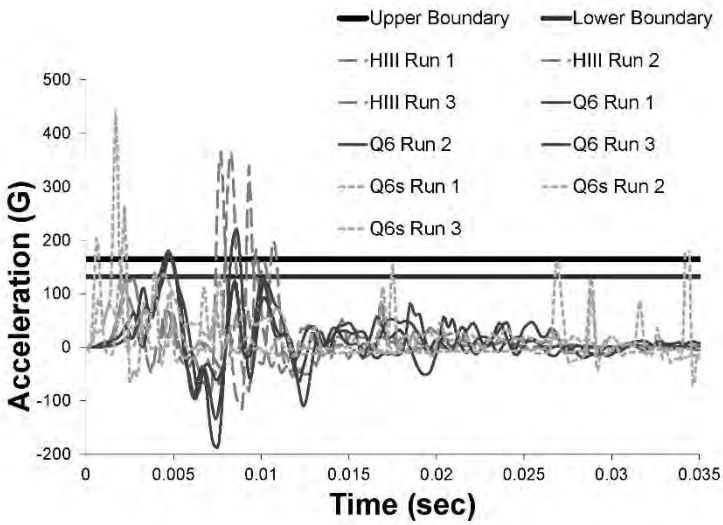

Figure A12: ISO 9790 – 1.0 Meter Drop Test – Peak Acceleration of Impacted Rib v Time

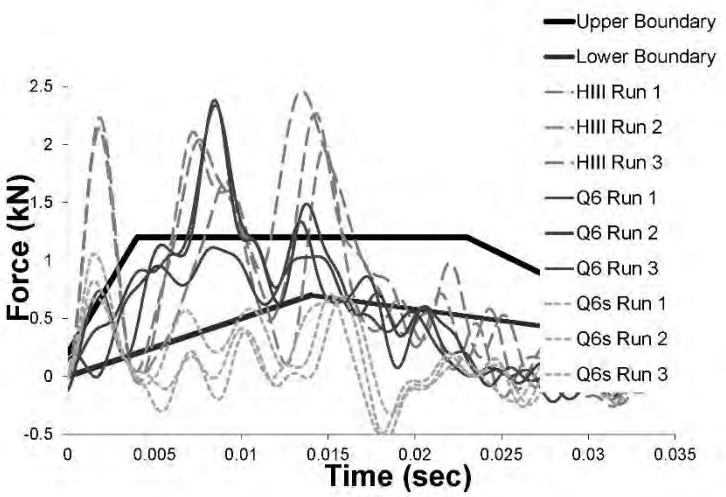

Figure A13: ISO 9790 – WSU Rigid Sled Test – Abdomen Plate Impact Force v Time (6.8 m/s)

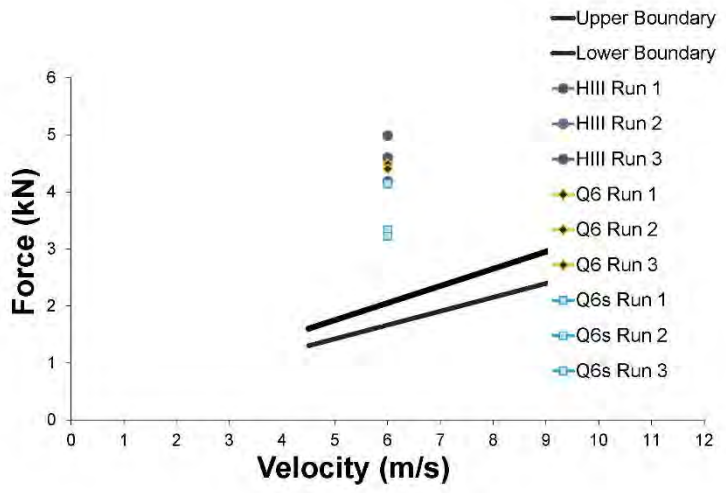

Figure A14: ISO 9790 – Lateral Pendulum Pelvis Impact Force v Time (6/0 m/s)

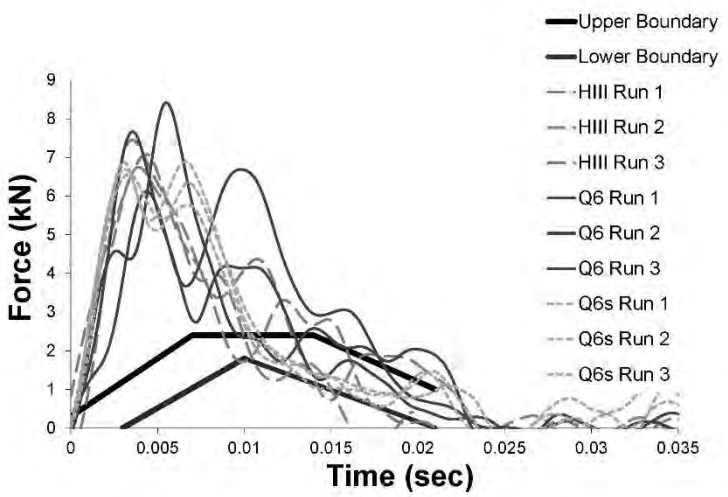

Figure A15: ISO 9790 – WSU Rigid Sled Test – Pelvis Plate Impact Force v Time (6.8 m/s)

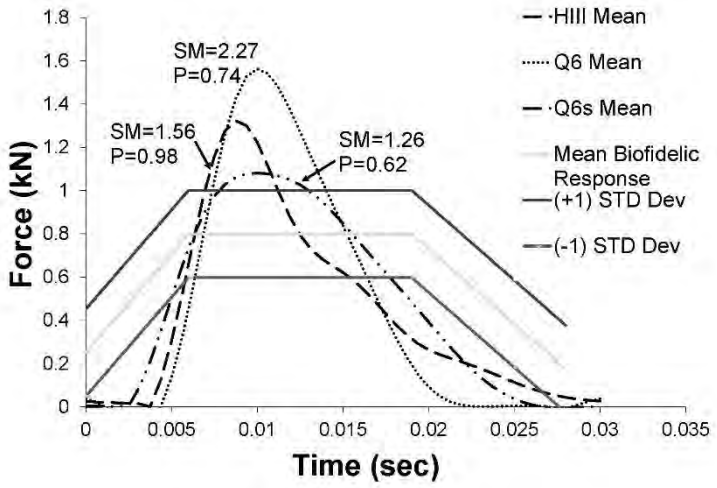

Figure A16: BRS – Lateral Pendulum Thorax Impact Force v Time (4.3 m/s)

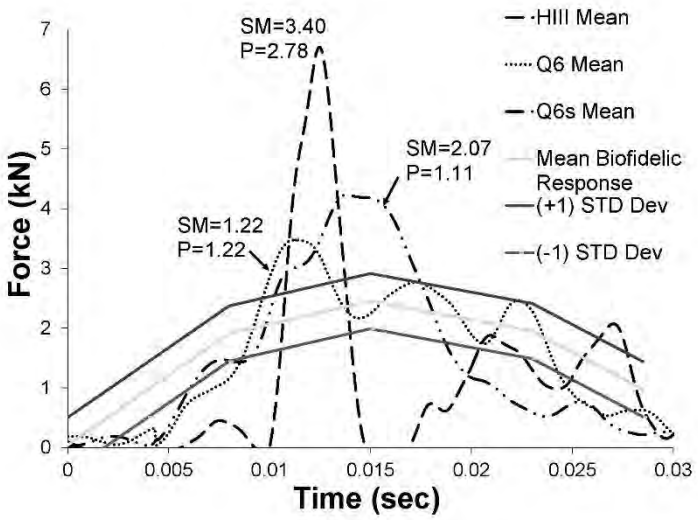

Figure A17: BRS – 1.0 Meter Drop Test – Thorax Plate Impact Force v Time

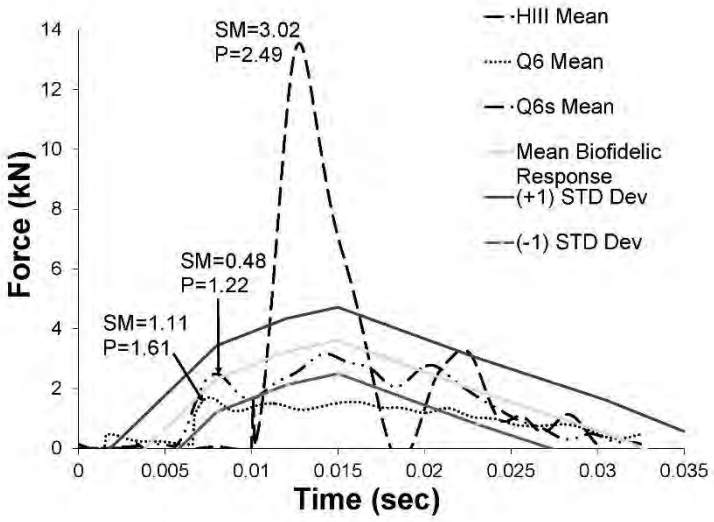

Figure A18: BRS – WSU Rigid Sled Test – Thorax/Shoulder Plate Impact Force v Time (6.8 m/s)

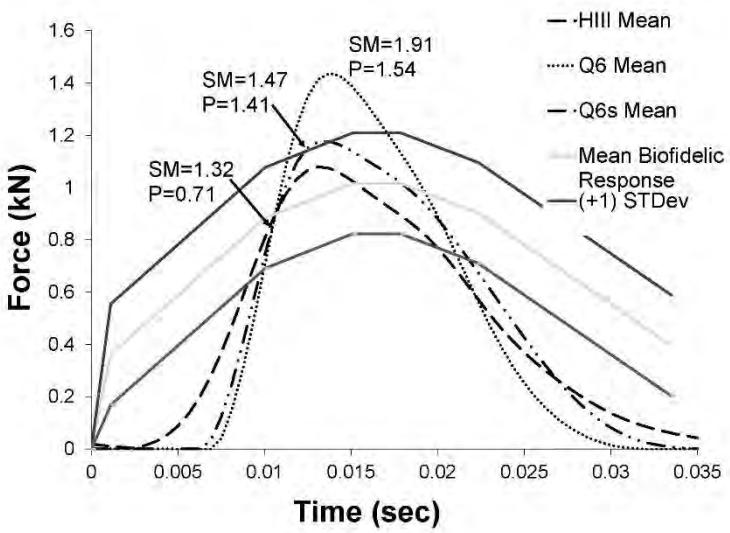

Figure A19: BRS – Lateral Pendulum Shoulder Impact Force v Time (4.3 m/s)

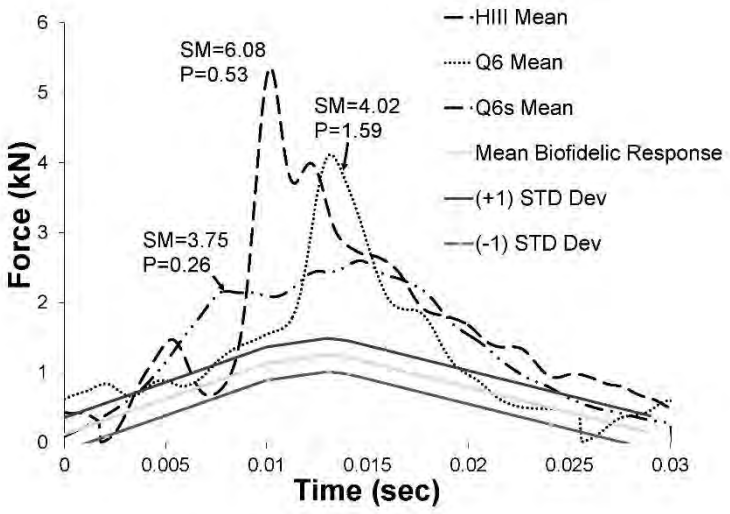

Figure A20: BRS – 1.0 Meter Drop Test – Armrest/Abdomen Impact Force v Time

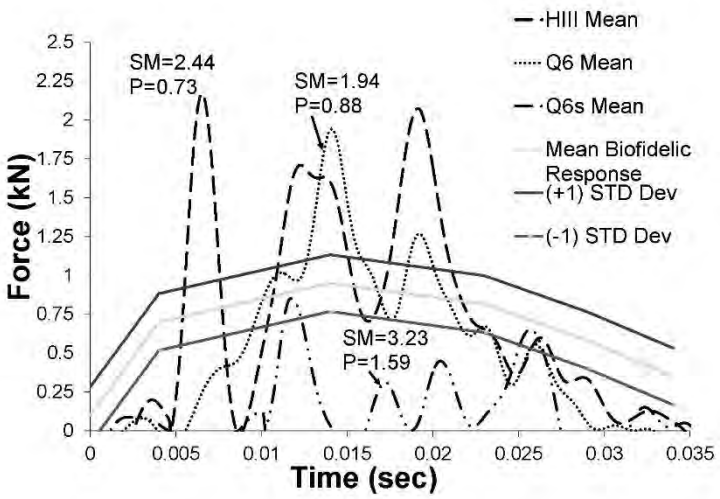

Figure A21: BRS – WSU Rigid Sled Test – Abdomen Plate Impact Force v Time (6.8 m/s)

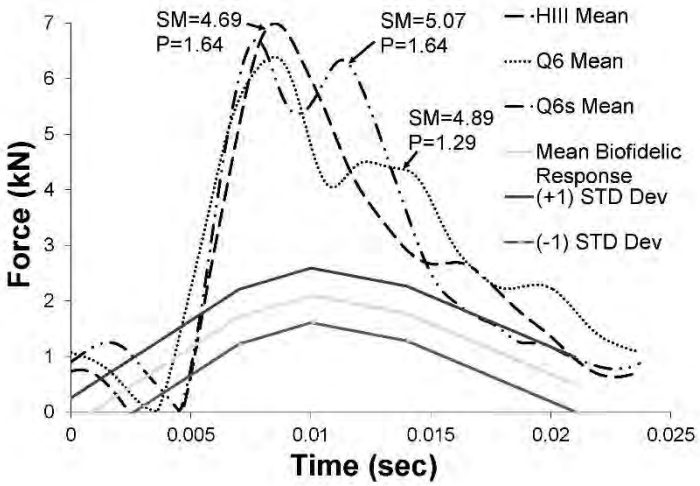

Figure A22: BRS – WSU Rigid Sled Test – Pelvis Plate Impact Force v Time (6.8 m/s)

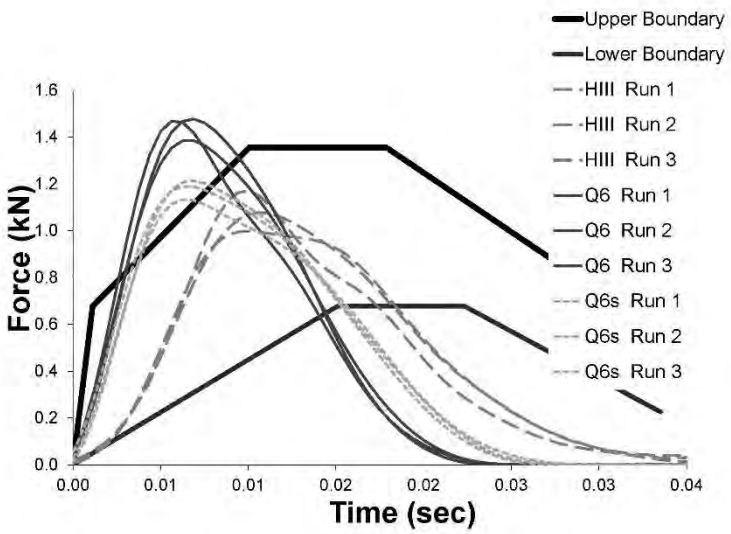

Figure A23: van Rantingen Response Corridors – Lateral Pendulum Oblique Abdomen Impact Force v Time (4.8 m/s)

Table A1: ISO 9790 Biofidelity Rating – HIII ATD

Weighting Factors For Impact Conditions and Responses Defined for the Shoulder						
Impact Condition	Weighting Factors (V3,j)	Response Measurements	Weigiting Factors (W3,j,k)	Weighting Factors (R3,j,k)	j	k
Shoulder Test 1, 4.5 m/s Pendulum	6	Pendulum Force	8	0	1	1
	6	Peak Shoulder Deflection	6	0	1	2

Weighting Factors For Impact Conditions and Responses Defined for the Thorax						
Impact Condition	Weighting Factors (V4,j)	Response Measurements	Weighting Factors (W4,j,k)	Weighting Factors (R4,j,k)	j	k
Thorax Test 1, 4.3 m/s Pendulum	9	Pendulum Force	9	5	1	1
	9	Upper Spine Lateral Acceleration	7	0	1	2
Thorax Test 3, 1.0 Meter Drop	6	Thorax Plate Force	8	0	3	1
	6	Peak Deflection of the Impacted Rib	8	0	3	2
Thorax Test 5, 6.8 m/s Rigid Sled	7	Thorax/Shoulder Plate Force	8	0	5	1
	7	Peak Lateral Acceleration of Upper Spine	7	0	5	2
	7	Peak Lateral Acceleration of Lower Spine	7	0	5	3
	7	Peak Lateral Acceleration of Impacted Rib	6	0	5	4

Weighting Factors For Impact Conditions and Responses Defined for the Abdomen						
Impact Condition	Weighting Factors (V5,j)	Response Measurements	Weighting Factors (W5,j,k)	Weighting Factors (R5,j,k)	j	k
Abdomen Test 1, 1.0 Meter Drop	7	Armrest Force	9	0	1	1
	7	Peak Acceleration of Lower Spine	6	0	1	2
	7	Peak Acceleration of Impacted Rib	4	5	1	3
Abdomen Test 3, 6.8 m/s Rigid Sled	3	Abdomen Plate Force	9	1.67	3	1

Weighting Factors For Impact Conditions and Responses Defined for the Pelvis						
Impact Condition	Weighting Factors (V6,j)	Response Measurements	Weighting Factors (W6,j,k)	Weighting Factors (R6,j,k)	j	k
Pelvis Test 1, 6.0 m/s Pendulum Impact	8	Pendulum Force	9	0	1	1
Pendulum Test 10, 6.8 m/s Rigid Sled	3	Pelvic Plate Force	9	0	10	1

Body Region	Ui
Shoulder	5
Thorax	10
Abdomen	8
Pelvis	8

Body Region	BR Subscript
Shoulder	3
Thorax	4
Abdomen	5
Pelvis	6

Body Region Biofidelity Ranking	
B3 - Shoulder	0.00
B4 - Thorax	0.75
B5 - Abdomen	1.25
B6 - Pelvis	0.00
B HIII	0.56

Table A2: ISO 9790 Biofidelity Rating – Q6 ATD

Weighting Factors For Impact Conditions and Responses Defined for the Shoulder						
Impact Condition	Weighting Factors (V3,j)	Response Measurements	Weigiting Factors (W3,j,k)	Weighting Factors (R3,j,k)	j	k
Shoulder Test 1, 4.5 m/s Pendulum	6	Pendulum Force	8	0	1	1
	6	Peak Shoulder Deflection	6	6.67	1	2

Weighting Factors For Impact Conditions and Responses Defined for the Thorax						
Impact Condition	Weighting Factors (V4,j)	Response Measurements	Weighting Factors (W4,j,k)	Weighting Factors (R4,j,k)	j	k
Thorax Test 1, 4.3 m/s Pendulum	9	Pendulum Force	9	5	1	1
	9	Upper Spine Lateral Acceleration	7	0	1	2
Thorax Test 3, 1.0 Meter Drop	6	Thorax Plate Force	8	8.33	3	1
	6	Peak Deflection of the Impacted Rib	8	5	3	2
Thorax Test 5, 6.8 m/s Rigid Sled	7	Thorax/Shoulder Plate Force	8	10	5	1
	7	Peak Lateral Acceleration of Upper Spine	7	10	5	2
	7	Peak Lateral Acceleration of Lower Spine	7	10	5	3
	7	Peak Lateral Acceleration of Impacted Rib	6	0	5	4

Weighting Factors For Impact Conditions and Responses Defined for the Abdomen						
Impact Condition	Weighting Factors (V5,j)	Response Measurements	Weighting Factors (W5,j,k)	Weighting Factors (R5,j,k)	j	k
Abdomen Test 1, 1.0 Meter Drop	7	Armrest Force	9	0	1	1
	7	Peak Acceleration of Lower Spine	6	10	1	2
	7	Peak Acceleration of Impacted Rib	4	6.67	1	3
Abdomen Test 3, 6.8 m/s Rigid Sled	3	Abdomen Plate Force	9	3.33	3	1

Weighting Factors For Impact Conditions and Responses Defined for the Pelvis						
Impact Condition	Weighting Factors (V6,j)	Response Measurements	Weighting Factors (W6,j,k)	Weighting Factors (R6,j,k)	j	k
Pelvis Test 1, 6.0 m/s Pendulum Impact	8	Pendulum Force	9	0	1	1
Pendulum Test 10, 6.8 m/s Rigid Sled	3	Pelvic Plate Force	9	0	10	1

Body Region	Ui
Shoulder	5
Thorax	10
Abdomen	8
Pelvis	8

Body Region	BR Subscript
Shoulder	3
Thorax	4
Abdomen	5
Pelvis	6

Body Region Biofidelity Ranking	
B3 - Shoulder	2.86
B4 - Thorax	6.19
B5 - Abdomen	4.17
B6 - Pelvis	0.00
B Q6	3.53

Table A3: ISO 9790 Biofidelity Rating – Q6s ATD

Weighting Factors For Impact Conditions and Responses Defined for the Shoulder						
Impact Condition	Weighting Factors (V3,j)	Response Measurements	Weigiting Factors (W3,j,k)	Weighting Factors (R3,j,k)	j	k
Shoulder Test 1, 4.5 m/s Pendulum	6	Pendulum Force	8	0	1	1
	6	Peak Shoulder Deflection	6	8.33	1	2

Weighting Factors For Impact Conditions and Responses Defined for the Thorax						
Impact Condition	Weighting Factors (V4,j)	Response Measurements	Weighting Factors (W4,j,k)	Weighting Factors (R4,j,k)	j	k
Thorax Test 1, 4.3 m/s Pendulum	9	Pendulum Force	9	10	1	1
	9	Upper Spine Lateral Acceleration	7	0	1	2
Thorax Test 3, 1.0 Meter Drop	6	Thorax Plate Force	8	6.67	3	1
	6	Peak Deflection of the Impacted Rib	8	5	3	2
Thorax Test 5, 6.8 m/s Rigid Sled	7	Thorax/Shoulder Plate Force	8	10	5	1
	7	Peak Lateral Acceleration of Upper Spine	7	10	5	2
	7	Peak Lateral Acceleration of Lower Spine	7	10	5	3
	7	Peak Lateral Acceleration of Impacted Rib	6	0	5	4

Weighting Factors For Impact Conditions and Responses Defined for the Abdomen						
Impact Condition	Weighting Factors (V5,j)	Response Measurements	Weighting Factors (W5,j,k)	Weighting Factors (R5,j,k)	j	k
Abdomen Test 1, 1.0 Meter Drop	7	Armrest Force	9	3.33	1	1
	7	Peak Acceleration of Lower Spine	6	3.33	1	2
	7	Peak Acceleration of Impacted Rib	4	6.67	1	3
Abdomen Test 3, 6.8 m/s Rigid Sled	3	Abdomen Plate Force	9	5	3	1

Weighting Factors For Impact Conditions and Responses Defined for the Pelvis						
Impact Condition	Weighting Factors (V6,j)	Response Measurements	Weighting Factors (W6,j,k)	Weighting Factors (R6,j,k)	j	k
Pelvis Test 1, 6.0 m/s Pendulum Impact	8	Pendulum Force	9	0	1	1
Pendulum Test 10, 6.8 m/s Rigid Sled	3	Pelvic Plate Force	9	0	10	1

Body Region	Ui
Shoulder	5
Thorax	10
Abdomen	8
Pelvis	8

Body Region	BR Subscript
Shoulder	3
Thorax	4
Abdomen	5
Pelvis	6

Body Region Biofidelity Ranking	
B3 - Shoulder	3.57
B4 - Thorax	6.72
B5 - Abdomen	4.35
B6 - Pelvis	0.00
B Q6s	3.87

Table A4: BRS Biofidelity Ranking – HIII ATD

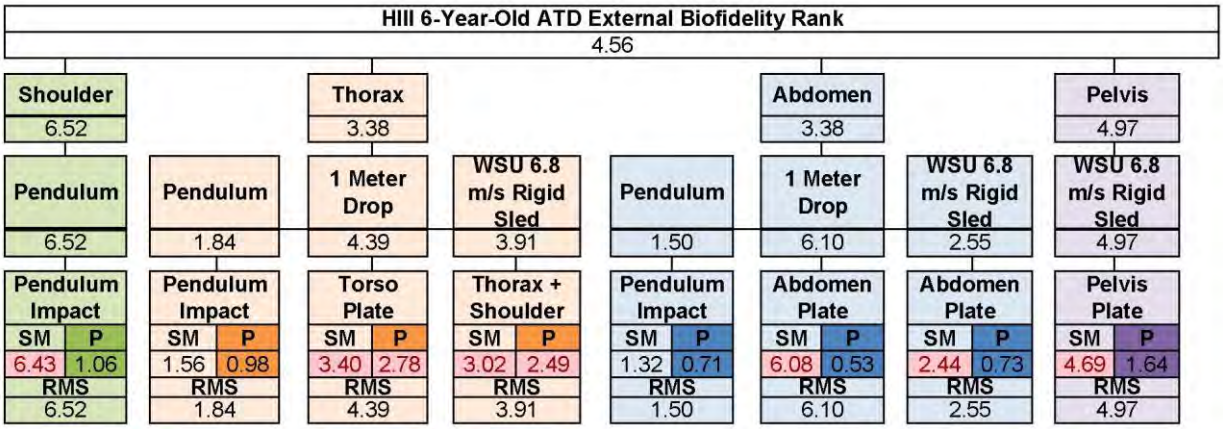

Table A5: BRS Biofidelity Ranking – Q6 ATD

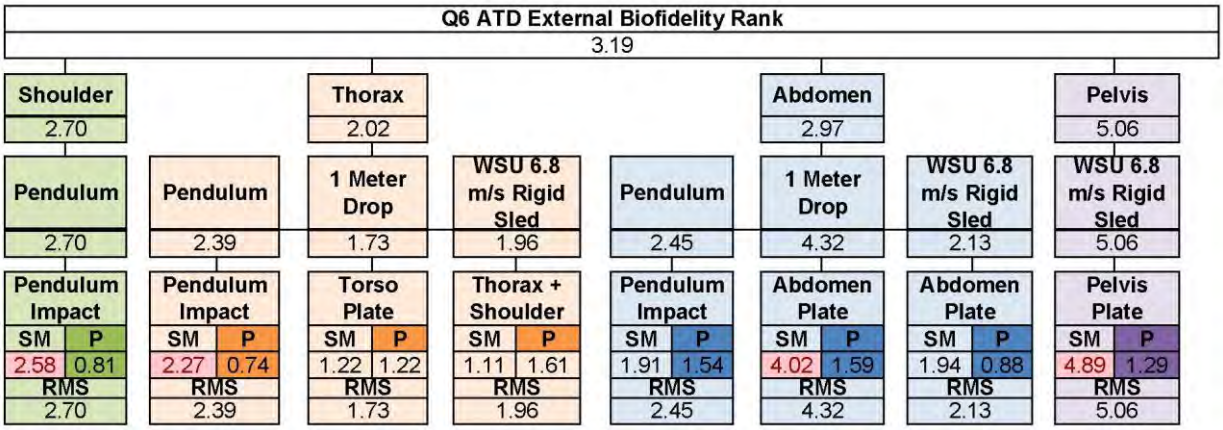

Table A6: BRS Biofidelity Ranking – Q6s ATD

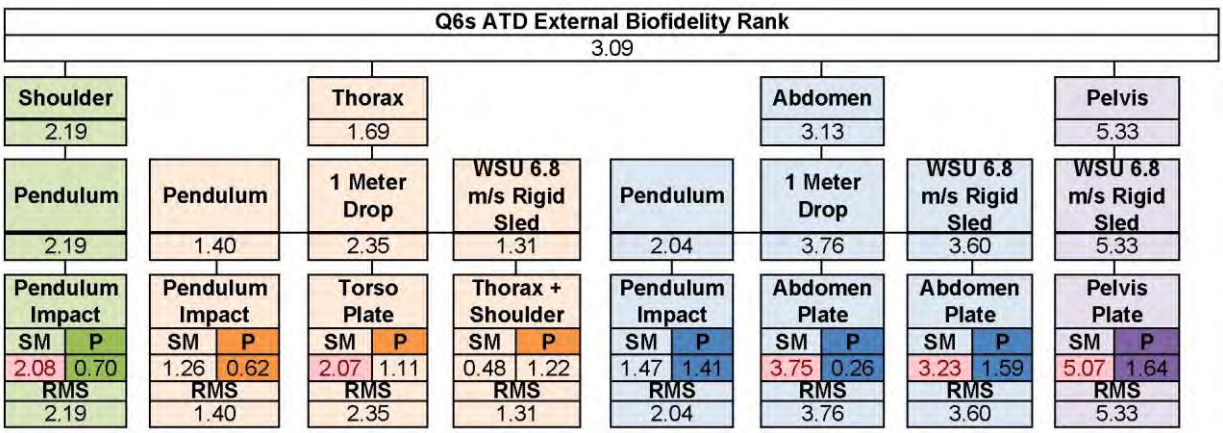

REFERENCES

AGNEW, A.M., MOORHOUSE, K, KANG, Y.S., et al. (2013). The Response of Pediatric Ribs to Quasi-static Loading: Mechanical Properties and Microstructure. *Ann Biomed Eng*, Vol 41, No. 12, pp. 2501-2514.

ARBOGAST, K.B., MOLL, E.K., MORRIS, S.D., ANDERKO, R.L., DURBIN, D.R., WINSTON, F.K., (2001). Factors influencing pediatric injury in side impact collisions. J Trauma, 51(3), 469-77.

ARBOGAST, K.B., MARI-GOWDA, S., KALLAN, M.J., et al., (2002). Pediatric pelvic fractures in side impact collisions. Stapp Car Crash J 46:285-296.

ARBOGAST, K.B., KALLAN, M.J., DURBIN, D.R., (2005). Effectiveness of high back and backless belt-positioning booster seats in side impact crashes. Annu Proc Assoc Adv Automot Med 49:201-213.

ARBOGAST, K.B., JERMAKIAN, J.S., KALLAN, M.J., (2009). Effectiveness of belt positioning booster seats: an updated assessment. Pediatrics 124:1281-1286.

ASTM Standard D790-00, (2010). Standard Tests Methods for Flexural Properties of Unreinforced and Reinforced Plastics and Electrical Insulating Materials. ASTM International West Conshohocken, PA.

BORESI, A.P., SCHMIDT, R.J., Bending of Straight Beams. In: *Advanced Mechanics of* 6th ed. Hoboken, NJ: John Wiley & Sons, Inc.; 2003: 263-294.

BERTEAU, J., BARON, C., PITHIOUX, M., CHABRAND, P., LASAYGUES, P., (2012). Mechanical properties of children cortical bone: a bimodal characterization. hal.archives-ouvertes.fr. Nantes, France, pp.1-5.

BRADLEY, A.L., SWAIN, M.V., WADDELL J.N., DAS, R, ATHENS, J, KIESER, J.A., (2013). A Comparison Between Rib Fracture Patterns in Peri- and Post-mortem

Compressive Injury in a Piglet Model. Journal of the Mechanical Behavior of Biomedical Materials.

CARLSON, M., BURLEIGH, M., BARNES, A., WAAGMEESTER, K., VAN RATINGEN, M., (2007). Q3S 3 Year old side impact dummy development. 20th ESV Conference, Paper No. 07-205.

CAVANAUGH, J.M., WALILKO, T.J., MALHOTRA, A., ZHU, Y., KING, A.I. (1990). Biomechanical response and injury tolerance of the pelvis in twelve sled side impacts, Proc. 34th Stapp Car Crash Conference, Paper No. 902305.

CDC. Web-based Injury Statistics Query and Reporting System [online]. National Center for Injury Prevention and Control, Centers for Disease Control and Prevention (producer). [2015 Apr 05].

CHARPAIL, E., TROSSEILLE, X., PETIT, P., LAPORTE, S., LAVASTE, F., VALLANCIEN, G., (2005) Characterization of PMHS ribs: a new test methodology. *Stapp Car Crash J. 49:1-16.*

CHENGULAR, S.N., RODGERS, S.H., BERNARD, T.E., (2005). Normal Growth and Development in Pediatric Orthopaedics. Kodak's Ergonomic Design for People at Work (2nd Edition), *Ergonomic Design Philosophy* (Table 1.5, pp. 48-49). Hoboken, N.J.: John Wiley & Sons, Inc.

CHING, R.P., NUCKLEY, D.J., HERSTED, S.M, ECK, M.P., MANN, F.A., SUN, E.A., (2001). Tensile Mechanics of the Developing Cervical Spine. *45th Stapp Car Crash Conference.* 2001-22-0015.

CODE OF FEDERAL REGULATIONS, Test Conditions and Instrumentation, Title 49, Section 572.36 (1998).

CORMIER, J.M., STITZEL, J.D., DUMA, S.M., MATSUOKA, F., (2005). Regional

variation in the structural response and geometric properties of human ribs. *Annu Proc Assoc Adv Automot. Med.* 49, 153-170.

DONNELLY, B.R., MOORHOUSE, K., (2012). Moorhouse K. Optimized phasing of PMHS response curves for biofidelity targets. Paper presented at: IRCOBI Conference. IRC-12-51.

ELHAGEDIAB, A.M., HARDY W.N., ROUHANA, S.W., (2006). Advancements in the rate-sensitive abdomen for the Hybrid III family of dummies. Journal of Biomechanics. 39, Suppl. 1, page S158.

EPPINGER, R., (1976). Prediction of Thoracic Injury Using Measureable Experimental Parameters. In: *Proc. 6th International ESV Conference,* Washington, DC. NHTSA, pp 770-779.

EUROPEAN ENHANCED VEHICLE-SAFETY COMMITTEE (EEVC). *Q-Dummies* Report: Advanced Child Dummies and Injury Criteria for Frontal Impact. Working Group 12 and 18 Report, Doc. No. 514. Obtained from: www.eevc.org , April 2008.

FOSTER J.K., KORTGE, J.O., WOLANIN, M.J., (1977). Hybrid III – A Biomechanically Based Crash Test Dummy. *Society of Automotive Engineers*. 770938.

FRANKLYN, M., (2007). Pediatric material properties: a review of human child and animal surrogates. Critical Reviews in Bioengineering. 35 (3/4), 197.

FRICK, S.L., (2005). Normal Growth and Development in Pediatric Orthopaedics. In JP Dormans (1st Ed.), *Pediatric Orthopaedics: Core Knowledge in Orthopaedics* (pp. 9 -10). Philadelphia: Elsevier Mosby, Inc.

GOGLER, E., BEST, A., BRAESS, H., BURST, E., LASCHET, G., (1977)., Biomechanical Experiments with Animals on Abdominal Tolerance Levels. *21st*

Stapp Car Crash Conference. #770931.

HANNA, R., (2010). Children Injured in Motor Vehicle Traffic Crashes, NHTSA Report No. DOT HS 811 325. NHTSA Washington, DC.

Hybrid III 6-Year-Old User Manual. First Technology Safety Systems, Inc.; 2009.

Hybrid III 50th Male User Manual. Humanetics Innovative Solutions; 2012.

HOWARD, H., ROTHMAN, L., MOSES MCKEAG, A., PAZMINO-CANIZARES, J., MONK, B., COMEAU, J.L., MILLS, D., BLAZESKI, S., HALE, I., GERMAN, A. (2004). Children in side-impact motor vehicle crashes: seating positions and injury mechanisms. J Trauma. 56, 1276–1285.

INSURANCE INSTITUTE FOR HIGHWAY SAFETY, Highway Loss Data Institute. (2017). <http://www.iihs.org/iihs/topics/laws/safetybeltuse?topicName=child-safety>.

IRWIN, A.L., MERTZ, H.J., (1997). Biomechanical Basis for the CRABI and Hybrid III Child Dummies. *Society of Automotive Engineers*. 973317.

IRWIN, A.L., MERTZ, H.J., ALI, M., ELHAGEDIAB, A.M., MOSS, S., (2002). Guidelines for Assessing the Biofidelity of Side Impact Dummies of Various Sizes and Ages. *Stapp Car Crash Journal*, Vol. 46, Paper No. 2002-22-0016, 297-319.

IRWIN, A.L., MERTZ, H.J., (2010). Rationale for and dimensions of impact surfaces for biofidelity tests of different sizes of frontal and side impact dummies. Stapp Car Crash Journal; 54, Paper No. 2010-22-0002, 19-35.

ISO/TR 9790 TECHNICAL REPORT. Road Vehicles - Anthropometric Side Impact Dummy - Lateral Impact Response Requirements to Assess the Biofidelity of the Dummy. First Edition 1999-12-01.

ITA, M., KANG, Y., SEACRIST, T., DAHLE, E., BOLTE, J., (2014). Comparison of Q3s

ATD biomechanical responses to pediatric volunteers. Traffic Injury Prevention Journal. 15: 215-222.

KALLIERIS, D., BARZ, J., SCHMIDT, G., et al., (1976). Comparison Between Child Cadavers and Child Dummy by Using Child Restraint Systems in Simulated Collisions. SAE Paper 760815:513-542.

KALRA, A., SAIF, T., SHEN, M., et al., (2015). Characterization of Human Rib Biomechanical Responses due to Three-Point Bending. Stapp Car Crash J 59: 113-130.

KEISER, J.A., WELLER, S., SWAIN, M.V., WADDELL, J.N., DAS, R., (2013). Compressive Rib Fracture: Peri-mortem Trauma Patterns in a Pig Model. Legal Medicine, Vol. 15, pp. 193-201.

KEMPER, A.R., MCNALLY, C., KENNEDY, E.A., et al., (2005). Material Properties of Human Rib Cortical Bone From Dynamic Tension Coupon Testing. Stapp Car Crash J 49: 199-230.

KEMPER, A.R., MCNALLY, C., PULLINS, C.A., et al., (2007). The Biomechanics of Human Ribs: Material and Structural Properties From Dynamic Tension and Bending Tests. Stapp Car Crash J 51: 235-273.

KENT, R., STACEY, S., KINDIG, M., et al., (2006). Biomechanical Response of the Pediatric Abdomen, Part 1: Development of an Experimental Model and Quantification of Structural Response to Dynamic Belt Loading. *Stapp Car Crash Journal*. Vol. 50, pp. 1-26.

KENT, R., SALAZAR, R., KERRIGAN, J., et al., (2009). Pediatric Thoracoabdominal Biomechanics. Stapp Car Crash J 53:373-402.

KENT, R., LOPEZ-VALDES, F.J., LAMP, J., et al. (2011). Characterization of the

Pediatric Chest and Abdomen Using Three Post-Mortem Human Subjects. 22nd Enhanced Safety of Vehicles Conference, Paper No. 11-00394.

KLINICH, K.D., REED, M.P., MANARY, M.A., ORTON, N.R., (2010). Development and testing of a more realistic pelvis for the Hybrid III 6-year-old ATD. Traffic Injury Prevention Journal. 11: 606-612.

LAMP, J.F., SALZAR, R., KERRIGAN, J., et al., (2010). Expansion and Evaluation of Data Characterizing the Structural Behavior of the Pediatric Abdomen. *Annals for Advances in Automotive Medicine.* Vol. 54.

LAST, J.M., editor. (2001). Dictionary of Epidemiology. 4th ed. New York: Oxford University Press. p. 61.

LESIRE, P., GRANT, R., HUMMEL, T., (2001). The CREST project accident database. 17th International Technical Conference on the Enhanced Safety of Vehicles (ESV), Amsterdam, The Netherlands.

LI, Z., KINDIG, M.W., KERRIGAN, J.R., et al., (2010). Rib Fractures Under Anterior-Posterior Dynamic Loads: Experimental and Finite-Element Study. J Biomech 42(2): 228-234.

LUCK, J.F., NIGHTINGALE, R.W., LOYD, A.M., et al., (2008). Tensile Mechanical Properties of the Perinatal and Pediatric PMHS Osteoligamentous Cervical Spine. *Stapp Car Crash Conference Journal.* Vol. 52: pp 107-134.

McGRAW, M.A., MEHLMAN, C.T., LINDSELL, C.J., KIRBY, C.L., (2009). Postnatal Growth of the Clavicle: Birth to Eighteen Years of Age. *J Pediatr Orthop.* 29(8): 937-943.

MALTESE, M.R., LOCEY, C.M., JERMAKIAN, J.S., et al., (2007). Injury causation scenarios in belt-restrained nearside child occupants. *Stapp Car Crash J*

51:299-311.

MERTZ, H., (1984). A Procedure for Normalizing Impact Response Data. *Society of Automotive Engineers.* 840884.

MERTZ, H.J., IRWIN, A.L., MELVIN, J.W., STALNAKER, R.L., BEEBE, M.S., (1989). Size, Weight and Biomechanical Impact Response Requirements for Adult Size Small Female and Large Male Dummies. *Society of Automotive Engineers.* 890756.

MILLER, M., (1989). The Biomechanical Response of the Lower Abdomen to Belt Restraint Loading. *The Journal of Trauma.* 29(11), 1571-1584.

MOLINA, K.D., DIMAIO, V.M. (2012). Normal Organ Weights in Men Part II – The Brain, Lungs, Liver, Spleen, and Kidneys. Am J Forensic Med Pathol. Dec: 33 (4):368-72.

MOORE, K.L., AGUR, A.M.R., (2007). Essential Clinical Anatomy (3rd Edition), *Pelvis and Perineum* (p. 205). Baltimore: Lippincott Williams & Wilkins.

MOORE, K.L., DALLEY, A.F., AGUR, A.M.R., (2010). *Clinical Oriented Anatomy*. 6th ed. Philadelphia, Pa: Lippincott Williams & Wilkins.

MOORHOUSE, K., (2013). An improved normalization methodology for developing mean human response curves. 23rd Enhanced Safety of Vehicles Conference. Paper No. 13-0192.

NASA-STD-3000. Man-Systems Integration Standards. Volume 1, Section 3 – Anthropometry and Biomechanics. Revision B, July, 1995.

NATIONAL HIGHWAY TRAFFIC SAFETY ADMINISTRATION. (2004). Federal Motor Vehicle Safety Standards; Side Impact Protection; Side Impact Phase-In Reporting Requirements, 47 CFR Part 571, Document Number 04-10931.

NATIONAL HIGHWAY TRAFFIC SAFETY ADMINISTRATION. (2011). NHTSA's Biomechanics Research Plan, 2011-2015. Washington D.C: U.S. Department of Transportation. DOT HS 811 474.

NATIONAL HIGHWAY TRAFFIC SAFETY ADMINISTRATION. (2014A). Traffic Safety Facts 2012: Children. Washington D.C: U.S. Department of Transportation. DOT HS 812 011.

NATIONAL HIGHWAY TRAFFIC SAFETY ADMINISTRATION. (2014B). New Proposed Rule-Making (NPRM) Federal Motor Vehicle Safety Standards; Child Restraint Systems, 47 CFR Part 571, Docket No. NHTSA-2014-0012, RIN 2127-AK95.

ORZECHOWSKI, K.M., EDGERTON, E.A., BULAS, D.I., MCLAUGHLIN, P.M., EICHELBERGER, M.R., (2003). Patterns of injury to restrained children in side impact motor vehicle crashes: the side impact syndrome. J Trauma, 54(6), 1094-101.

OUYANG, J., ZHU, Q., ZHAO, W., XU, Y., CHEN, W., ZHONG, S., (2003). Experimental Cadaveric Study of Lateral Impact of the Pelvis of Children. *Di Yi Jun Yi Da Xue Xue Bao.* Vol. 23: pp 397-401.

OUYANG, J., ZHU, Q., ZHAO, W., XU, Y., CHEN, W., ZHONG, S., (2005). Biomechanical Assessment of the Pediatric Spine Under Bending and Tensile Loading. *SPINE.* Vol. 30: pp E716-E723.

OUYANG, J., ZHAO, W., et al., (2006). Thoracic impact testing of pediatric cadaveric subjects. The Journal Of Trauma 61(6): 1492.

PETITJEAN, A., TROSEILLE, X., YOGANANDAN, N., PINTAR, F., (2015). Normalization and Scaling for Human Response Corridors and Development of

Injury Risk Curves. In: YOGANANDAN, N., NAHUM, A.M., MELVIN, J.W., ed. *Accidental Injury*. New York: Springer Chapter 26.

PFEFFERLE, K.L., LITSKY, A., DONNELLY, B., BOLTE IV, J., (2007). Biomechanical Properties of the Excised Pediatric Human Rib. *NHTSA's 35th International Workshop on Human Subject for Biomechanical Research.*

PINTAR, F.A., MAYER, R.G., YOGANANDAN, N., SUN, E., (2000). Child Neck Strength Characteristics Using an Animal Model. *44th Stapp Car Crash Conference.* 2000-01-SC06.

POPE, M.E., KROELL, C.K., VIANO, D.C., WARNER, C.Y., ALLEN, S.D., (1979). Postural Influences on Thoracic Impact. *23rd Stapp Car Crash Conference.* 791028.

PRASAD, P, DANIEL, RP. (1984). A Biomechanical Analysis of Head, Neck, and Torso Injuries to Child Surrogates Due to Sudden Torso Acceleration. *Society of Automotive Engineers*. 8401656.

Q3s User Manual. Humanetics Innovative Solutions; 2012.

Q6 (ADVANCED 6 YEAR OLD CHILD) USER MANUAL. (2012). Humanetics Innovative Solutions.

RAMACHANDRA, R., KANG, Y., BOLTE, J.H., HAGEDORN, A., HERRIOTT, R., STAMMEN, J.A., MOORHOUSE, K., (2016). Biomechanical Responses of PMHS Subjected to Abdominal Seatbelt Loading. *Stapp Car Crash Journal.* Vol. 60: pp. 58-87.

RASBAND, W.S., (1997-2014). ImageJ, U. S. National Institutes of Health, Bethesda, Maryland, USA, http://imagej.nih.gov/ij/.

REED, M.P., LEHTO, M.M., SCHNEIDER, L.W., (2001). Development of

Anthropometric Specifications for the Six-Year-Old OCATD. *Society of Automotive Engineers*. 2001-01-1057.

REED, M.P., EBERT-HAMILTON, S.M., MANARY, M.A., KLINICH, K.D., SCHNEIDER, L.W., (2005). A New Database of Child Anthropometry and Seated Posture for Automotive

REILAND, S., (1978). Growth and Skeletal Development of the Pig. Acta Radiological. Supplemental Vol. 358, pp. 15-22.

RHULE, H., MALTESE, M., DONNELLY, B.R., EPPINGER, R.H., BRUNNER, J., BOLTE, J.H., (2002). Development of a new biofidelity ranking system for anthropometric test devices. Proceedings from the 46th Stapp Car Crash Conference. Vol. 462.

RHULE, H., DONNELLY, B., MOORHOUSE, K., KANG, Y.S., (2013). A methodology for generating objective targets for quantitatively assessing the biofidelity of crash test dummies. Presented at: 23rd Enhanced Safety of Vehicles Conference. 2013; Paper No. 13-0138.

ROUHANA, S.W., FOSTER, M.E., (1985). Lateral Impact – An Analysis of the Statistics in the NCSS. Proc. 29th Stapp Car Crash Conference, SAE 851727, Washington D.C.

ROUHANA, S.W., KROELL, C.K., (1989). The effect of door topography on abdominal injury in lateral impact. Proc. 33rd Stapp Car Crash Conference, SAE 892433, Warrendale, PA.

ROUHANA, S.W., ELHAGEDIAB, A.M., CHAPP, J.J., (1998). A High-Speed Sensor for Measuring Chest Deflection in Crash Test Dummies. Paper presented at: 16th Enhanced Safety of Vehicles Conference. Paper No. 98-S9-O-15.

ROUHANA, S.W., (2006). Abdominal impact injury research – a review. Journal of Biomechanics. 39, Suppl. 1, S157.

RUFF, C., (2015). MomentMacroJ program [Internet]. Available from: http://www.hopkinsmedicine.org/fae/mmacro.htm. Accessed March 4, 2015.

SACK, W.O., (1982). *Essentials of Pig Anatomy.* Ithaca, NY: Veterinary Textbooks.

SAE International Surface Vehicle Recommended Practice. Instrumentation for Impact Test - Part 1 - Electronic Instrumentation. SAE Standard J211 -1; 2003.

SANDOZ, B., LAPORTE, S., CHARPAIL, E., TROSSEILLE, X., LAVASTE, F., (2007). Influence of the Velocity in Human Rib Response. J Biomech 40: S215.

SCHAFMAN, M.A., KANG, Y.S., MOORHOUSE, K., WHITE, S.E., BOLTE, J.H., AGNEW, A.M., (2016). Age and Sex Alone are Insufficient to Predict Human Rib Structural Response to Dynamic A-P Loading. J Biomech 49: 3516-3522.

SCHEUER, L., BLACK, S., (2004). *The Juvenile Skeleton*. London, U.K.: Elsevier Academic Press.

SCHULTZ, A.B., BENSON, D.R., HIRSCH, C., (1974). Force-Deformation Properties of Human Ribs. J Biomech 7: 303-309.

SEACRIST, T., LOCEY, C.M., MATHEWS, E.A., JONES, D.L., BALASUBRAMANIAN, S., MALTESE, M.R., ARBOGAST, K.B., (2014). Evaluation of pediatric ATD as compared to child volunteers in low-speed far-side oblique and lateral impacts. Traffic Injury Prevention Journal. 15: sup1, S206-S214.

SHERWOOD, C.P., FERGUSON, S.A., et al., (2003). Factors leading to crash fatalities to children in child restraints. Annu Proc Assoc Adv Automot Med 7:343-359.

SILBER, J., FLYNN, J., (2002). Changing patterns of pediatric pelvis fractures with skeletal maturation: implications for classification and management. J Pediatr

Orthop 22:22-26.

STARNES, M., EIGEN, A.M., (2002). Fatalities and Injuries to 0-8 Year Old Passenger Vehicle Occupants based on Impact Attributes, NHTSA Report No. DOT HS 809 410. NHTSA Washington, DC.

STITZEL, J.D., CORMIER, J.M., BARETTA, J.T. et al., (2003). Defining Regional Variation in the Material Properties of Human Rib Cortical Bone and Its Effect on Fracture Prediction. *Stapp Car Crash Journal.* 2003-22-0012, pp. 243-265.

SUBIT, D., DE DOIS, E.D.P, VALAZQUEZ-AMEIJIDE, J., ARREGUI-DELMASES, C., CRANDALL, J., (2011). Tensile Material Properties of Human Rib Cortical Bone Under Quasi-static and Dynamic Failure Loading and Influence of the Bone Microstructure on Failure Characteristics. arXiv: 1108.0390.

SUNTAY, B., MOORHOUSE, K., BOLTE, J., (2011). Characterization of the pediatric shoulder's resistance to lateral loading conditions. Paper presented at: 22nd Enhanced Safety of Vehicles Conference. Paper No. 11-0038.

TYLKO, S., CHARLEBOIS, D., BUSSIERES, A., (2009). In-vehicle crash testing for the development of a child side impact test protocol. Presented at: 7th Conference "Protection of Children in Cars", Munich, Germany.

VAN RATINGEN, M., TWISK, D., SCHROOTEN, M., BEUSENBERG, M., (1997). Biomechanically based design and performance targets for a 3-Year-Old child crash dummy for frontal and side impact. *Proc. 41st Stapp Car Crash Conference,* 243-260.

VIANO, D.C., WARNER, C.Y., HOOPES, K., MORTENSON, D., WHITE, R., ARTINIAN, C.G., (1978). Sensitivity of Porcine Thoracic Responses and Injuries to Various Frontal and a Lateral Impact Site. *Society of Automotive Engineers.*

Paper No. 780890.

VIANO, D.C., (1989A). Biomechanical Responses and Injuries In Blunt Lateral Impact. *Proc. Of the 33rd Stapp Car Crash Conference*, SAE 892432.

VIANO, D.C., LAU, I.V., ASBURY, C., KING, A.I., BEGEMAN, P., (1989B). Biomechanics of the Human Chest, Abdomen, and Pelvis in Lateral Impact. *Accid. Anal. & Prev.*, 21(6), 553-574.

VIANO, D.C., LAU, I.V., ANDRZEJAK, D.V., ASBURY, C., (1989C). Biomechanics of Injury in Lateral Impacts. *Accid. Anal. & Prev.*, 21(6), 535-551.

VIANO, D.C., PARENTEAU, C.S., (2008). Fatalities of children 0-7 years old in the second row. Traffic Inj Prev., 9(3), 231-237.

WENGER, D.R., PRING, M.E., (2005). Children Are Not Just Small Adults. In: DR Wenger and ME Pring (3rd Ed.), *Rang's Children's Fractures* (pp. 1-2). Philadelphia: Lippincott, Williams & Wilkins.

YOGANANDAN, N., PINTAR, F.A., (1998). Biomechanics of Human Thoracic Ribs. *Journal of Biomechanical Engineering.* Vol. 120, pp. 100-104.

YOGANANDAN, N., NAHUM, A.M., MELVIN, J.W., (2015). *Accidental Injury: Biomechanics and Prevention: 3rd Edition*. New York: Springer Science+Business Media

ABSTRACT

BIOFIDELITY ASSESSMENT OF 6-YEAR-OLD ANTHROPOMETRIC TEST DEVICES (ATDs) AND SCALING LAWS IN LATERAL IMPACT

by

JENNIFER L. YAEK

December 2017

Advisors: Dr. John C. Cavanaugh; Dr. Steve W. Rouhana

Major: Biomedical Engineering

Degree: Doctor of Philosophy

There is a clear need to further develop the design and biofidelity of the 6-Year-Old ATDs for future child safety research and child occupant protection in side impacts. Due to the scarcity of pediatric PMHS impact testing, specifically in the lateral direction, alternative means of obtaining relevant data for pediatric models need to be considered.

In this first portion of this study, assessment of the mechanical behavior and biofidelity of existing 6-Year-Old ATDs in lateral impact were performed. None of the three 6-year-old ATDs (HIII, Q6, and Q6s) tested were found to be considered good tools for assessing side impact occupant protection.

In the second portion of this study, evaluation of material properties and thorax and abdominal region biofidelity response in lateral impact for porcine subjects that were matched for age and torso size to the human 3-Year-Old, 6-Year-Old, 10-Year-Old, and 50th Percentile Adult male was performed. Lateral impact force response of the porcine surrogate equivalents thorax and abdomen regions were found to be consistent with the ISO human scaled lateral impact response corridors presented in

Irwin et al. (2002) and van Rantingen et al (1997).

In the third portion of this study, test response ratios for force, deflection, acceleration, and time for the 3-year-old, 6-year-old, 10-year-old, and 50th adult male porcine surrogate equivalents from the thorax and abdomen lateral pendulum impacts were obtained, and 50th adult male swine impact response corridors were scaled to the 10-year-old, 6-year-old, and 3-year-old swine to assess current scaling laws. It was determined that scaling laws can be applied to appropriate weight and breed porcine surrogates, using human skull elastic modulus values established and provided in Irwin et al. (2002), to provide a viable and powerful impact test model alternative for child safety research in lateral impacts.

AUTOBIOGRAPHICAL STATEMENT

Jennifer L. Yaek

Education

Ph.D. Biomedical Engineering, Wayne State University, Detroit, MI, 2017

M.S. Biomedical Engineering, Wayne State University, Detroit, MI, 2012

M.S. Mechanical Engineering, University of Michigan, Ann Arbor, MI, 1996

B.S. Mechanical Engineering, Michigan Technological University, Houghton, MI, 1994

Experience

Principal Engineer, Exponent, Incorporated, 2017-present

Senior Managing Engineer, Exponent, Incorporated, 2012-2016

Partner and Consultant, M.P. Holcomb Engineering Corporation, 2004-2012

Consultant, M.P. Holcomb Engineering Corporation, 2000-2004

Engineer, M.P. Holcomb Engineering Corporation, 1996-2000

Engineering Intern, M.P. Holcomb Engineering Corporation, 1995-1996

Publications

Yaek JL, Li Y, Lemanski PJ, Begeman PC, Rouhana SW, Cavanaugh JM. Biofidelity assessment of the 6-Year-Old ATDs in lateral impact. DOI: 10.1080/15389588.2015.1101080, Traffic Injury Prevention, 2015.
Yaek JL, Curry BA, Goertz AR. Review and comparison of published rollover test results. Paper Number 2010-01-0057, Society of Automotive Engineers, 2010.
Goertz AR, **Yaek JL**, Compton CP. Accident statistical distributions from NASS CDS. Paper Number 2010-01-0139, Society of Automotive Engineers, 2010.

Invited Presentations

Yaek JL, Biofidelity assessment of the 6 Year Old ATDs in side impact. Ohio State University Injury Biomechanics Symposium, 2014.
Yaek JL, Newberry W. Introduction to accident investigation, accident reconstruction, and the biomechanics of motor vehicle accidents. Wisconsin Defense Counsel Young Lawyers Section Event, 2013.
Yaek JL, Newberry W. Introduction to accident investigation, accident reconstruction, and the biomechanics of motor vehicle accidents - Webinar. Ohio Association of Civil Trial Attorneys, 2013.
Yaek JL, Curry BA, Goertz AR. Review and comparison of published rollover test results. Paper Number 2010-01-0057, Society of Automotive Engineers, 2010.
Goertz AR, **Yaek JL**, Compton CP. Accident statistical distributions from NASS CDS. Paper Number 2010-01-0139, Society of Automotive Engineers, 2010.
Yaek JL, Using science and accident reconstruction effectively at trial. Women Drive Results in Transportation Law National Program, Tort Trial & Insurance Practice Section - American Bar Association, 2008.
Yaek JL, Basics of accident reconstruction and occupant motion. Michigan Association of Traffic Accident Investigators, Training Conference, 2003.